RIGA TECHNICAL UNIVERSITY

Jingzhi Fan

METABOLĪTU IZMANTOŠANA BIOMATERIĀLOS KAULAUDU REĢENERĀCIJAI

Promocijas darbs

METABOLITE INCORPORATION IN BIOMATERIALS FOR BONE TISSUE REGENERATION

Doctoral Thesis

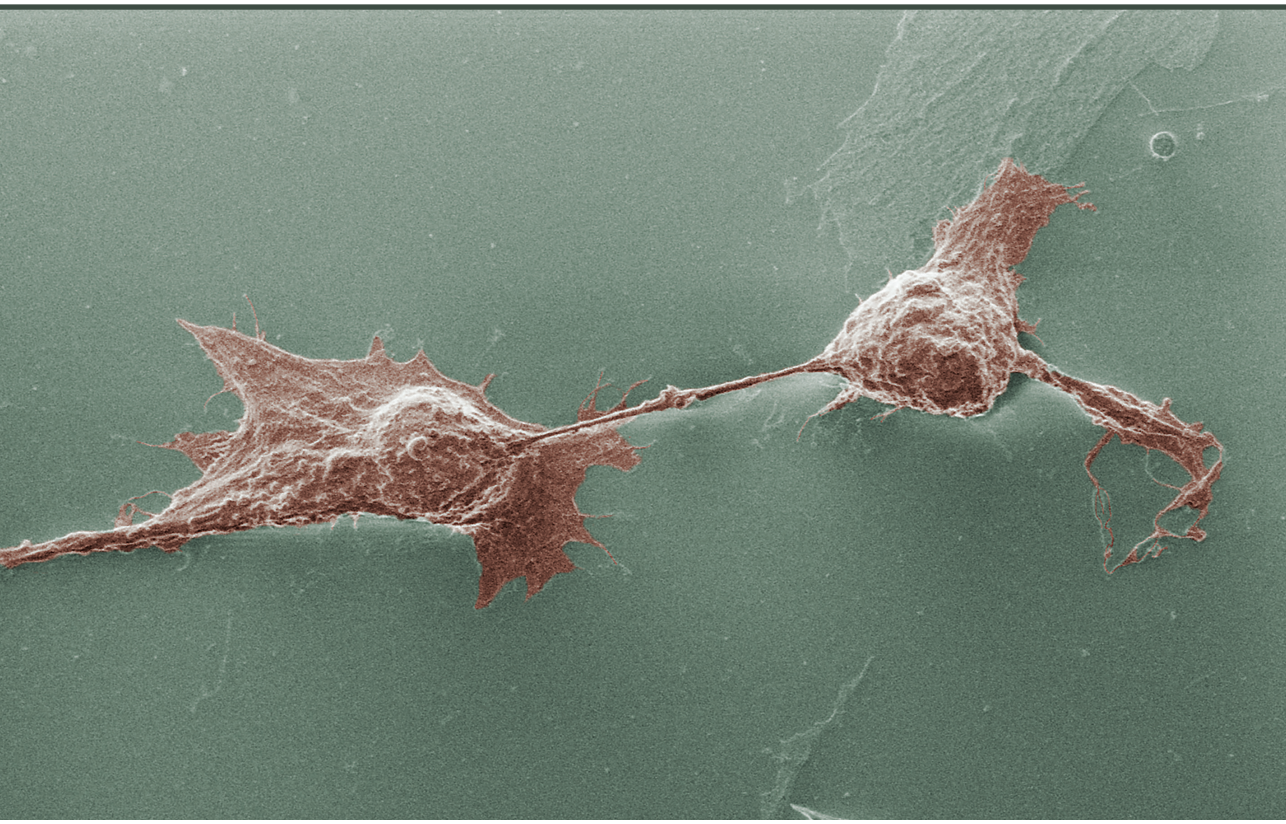

RTU Izdevniecība
RTU Press
Rīga 2025

RĪGAS TEHNISKĀ UNIVERSITĀTE
Dabaszinātņu un tehnoloģiju fakultāte
Biomateriālu un bioinženierijas institūts

RIGA TECHNICAL UNIVERSITY
Faculty of Natural Sciences and Technology
Institute of Biomaterials and Bioengineering

Jingzhi Fan
Doktora studiju programmas "Ķīmija, materiālzinātne un tehnoloģijas" doktorants
Doctoral Student of the Study Programme "Chemistry, Materials Science and Engineering"

METABOLĪTU IZMANTOŠANA BIOMATERIĀLOS KAULAUDU REĢENERĀCIJAI

Promocijas darbs

METABOLITE INCORPORATION IN BIOMATERIALS FOR BONE TISSUE REGENERATION

Doctoral Thesis

Zinātniskie vadītāji / Scientific supervisors

profesore *Dr. sc. ing.* / Professor Dr. sc. ing
DAGNIJA LOČA

asociētais profesors *Dr. nat.tech.* / Assoc. professor Dr. nat. Tech.
KRISTAPS KĻAVIŅŠ

RTU Izdevniecība / RTU Press
Rīga 2025 / Riga 2025

Fan, J. Metabolītu izmantošana biomateriālos kaulaudu reģenerācijai. Rīga: RTU Izdevniecība, 2025. 184 lpp.

Fan, J. Metabolite incorporation in biomaterials for bone tissue regeneration. Doctoral Thesis. Riga: RTU Press, 2025. 184 p.

Iespiests saskaņā ar promocijas padomes "RTU P-02" 2025. gada 29. septembra lēmumu Nr. 04030- 9.2/7.

Published in accordance with the decision of the Promotion Council "RTU P-02" of 29 September 2025, Minutes No. 04030- 9.2/7.

Acknowledgements

I would like to express my gratitude to Kristaps Kļaviņš for his guidance and support throughout my PhD journey. I am also thankful to Antons Sizovs and Sophie Verrier for their assistance with animal data, and to Abhishek Indurkar for his help with material synthesis. My appreciation extends to Ilijana Kovrlija, Kristaps Rubenis, Theresa Schiemer and all others who contributed to this work.

Finally, I am grateful to my parents for their constant support and to my friends for their companionship. I also acknowledge with respect the sacrifices of the experimental animals used in this study.

This work has been supported by the European Union's Horizon 2020 research and innovation programme "Baltic Biomaterials Centre of Excellence" [No. 857287, BBCE].

PROMOCIJAS DARBS IZVIRZĪTS ZINĀTNES DOKTORA GRĀDA IEGŪŠANAI RĪGAS TEHNISKAJĀ UNIVERSITĀTĒ

Promocijas darbs zinātnes doktora (*Ph. D.*) grāda iegūšanai tiek publiski aizstāvēts 2025. gada 12. decembrī plkst. 14.00 Rīgas Tehniskās universitātes Dabaszinātņu un tehnoloģiju fakultātē, Paula Valdena ielā 3, 272. auditorijā.

OFICIĀLIE RECENZENTI

Prof. *Dr. chem.* Māris Turks
Rīgas Tehniskā universitāte

Asoc. prof. *Dr. sc. ing*. Egils Stalidzāns
Rīgas Stradiņa universitāte, Latvija

Asoc. prof. *Dr*. Gernot Schabbauer
Vīnes Medicīnas universitāte, Austrija

APSTIPRINĀJUMS

Apstiprinu, ka esmu izstrādājis šo promocijas darbu, kas iesniegts izskatīšanai Rīgas Tehniskajā universitātē zinātnes doktora (Ph. D.) grāda iegūšanai. Promocijas darbs zinātniskā grāda iegūšanai nav iesniegts nevienā citā universitātē.

Jingzhi Fan ……. (paraksts)
Datums: ……

Promocijas darbā ir ievads un četras nodaļas. Darbā iekļauti 58 attēli, četras tabulas un viens pielikums. Darbā izmantoti 167 bibliogrāfiskie avoti. Kopējais darba apjoms ir 184 lappuses.

DOCTORAL THESIS PROPOSED TO RIGA TECHNICAL UNIVERSITY FOR THE PROMOTION TO THE SCIENTIFIC DEGREE OF DOCTOR OF SCIENCE

To be granted the scientific degree of Doctor of Science (Ph. D.), the present Doctoral Thesis has been submitted for the defense at the open meeting of the RTU Promotion Council on 12 December, 2025 at 14:00, at the Faculty of Natural Sciences and Technology of Riga Technical University, 3 Paula Valdena Street, Room 272.

OFFICIAL REVIEWERS

Prof. Dr. chem. Māris Turks
Riga Technical University, Latvia

Asoc. prof. Dr. sc. ing. Egils Stalidzāns
Rīga Stradiņš University, Latvia

Asoc. prof. Dr. Gernot Schabbauer
Medical University of Vienna, Austria

DECLARATION OF ACADEMIC INTEGRITY

I hereby declare that the Doctoral Thesis submitted for review to Riga Technical University for promotion to the scientific degree of Doctor of Science (Ph. D.) is my own. I confirm that this Doctoral Thesis has not been submitted to any other university for the promotion to a scientific degree.

Jingzhi Fan ……. (signature)
Date: ……

The Doctoral Thesis has been written in English. It consists of an Introduction, four chapters, Conclusions, 58 figures, four tables, and one appendix; the total number of pages is 184, including the appendixes. The Bibliography contains 167 titles.

General Characteristics of the Thesis

Background

As of September 2025, the most recent comprehensive global data on fractures remains from year 2019, 178 million new fractures and 455 million acute or long-term fracture symptoms were reported globally. Artificial interventions for repairing hard tissue defects are critical for effectively treating patients and improving their quality of life. Today, bone tissue engineering is advancing rapidly, utilizing cutting-edge biomaterials, scaffold designs, and cell-based therapies to develop innovative bone regeneration and repair solutions. Calcium phosphate plays a crucial role in bone tissue engineering as it mimics the mineral composition of natural bone, promoting osteoconduction and osteoinduction. Its biocompatibility allows for seamless integration with surrounding tissues, supporting bone regeneration and healing. Calcium phosphate-based scaffolds are widely used in tissue engineering to provide structural support and enhance cell attachment and proliferation, facilitating effective bone tissue regeneration.

Aims and objectives

The aim of the work was to develop a novel CaP-based biomaterial with an incorporated metabolite that enhances bone regeneration.

To achieve the aim, the following main tasks were proposed during this work:

1. Characterize systemic metabolic alterations during bone regeneration utilizing *in vivo* models, elucidating the dynamic changes in metabolic profiles associated with the healing process.
2. Investigate and characterize alterations in cellular metabolism induced by biomaterial interactions, employing advanced metabolomics techniques to delineate the molecular mechanisms underlying these changes.
3. Identify and validate potential bioactive metabolites integral to bone healing, unraveling specific metabolite signatures indicative of enhanced regenerative processes.
4. Synthesize biomaterials incorporating identified metabolites as a novel system, establishing a link between metabolomic discoveries and material design for enhanced bioengineering applications.

5. Evaluate the synthesized metabolite-loaded biomaterials' *in vitro* performance and physical properties, employing rigorous characterization methods to ascertain their suitability for clinical translation and potential impact on therapeutic outcomes.

The following thesis are proposed for defense:

1. Bone healing in mammals triggers systemic alterations in energy and amino acid metabolism.
2. Calcium phosphate (CaP)-based biomaterials change cellular metabolic microenvironment by enhancing glycolytic activity.
3. Metabolites depleted during bone healing can be integrated into biomaterials to facilitate bone regeneration.

Scientific novelty and main results

1. The progress of bone healing has been widely researched; however, the knowledge of small molecular changes during this process is still vague. The metabolomics profiling from rat calvaria and sheep tibia provided a deeper understanding of systemic metabolome changes during bone regeneration. Notably, serum concentrations of glutamate and glutamine were significantly reduced during bone healing, indicating increased metabolic demand for these amino acids.
2. Cell-material interaction studies in the bioengineering field have mainly ignored the role of endogenous metabolites. This work demonstrated that ceramic biomaterials are capable of adsorbing a broad range of small molecules from their surrounding microenvironment. The results also show that exposure to CaP-based materials affects cellular amino acids and energy metabolism.
3. Utilizing the results from the critical size defect models, amorphous calcium phosphate synthesized from a glutamate source was prepared. The new biomaterial, ACP-Glu (amorphous calcium phosphate incorporating glutamate) was characterized through established osteogenesis assays and metabolomics studies. ACP-Glu behaved excellently in boosting cell energy metabolism and osteogenesis properties. Enhanced energy metabolism, particularly increased tricarboxylic acid (TCA) cycle activity, could compensate for anaerobic glycolysis and supply the energy required for tissue repair. This material could be used as a biomaterial for bone regeneration with a faster healing rate by triggering more efficient in situ energy metabolism.

Practical application of the work

This research presents a metabolomics-based evaluation of animal serum during bone regeneration, providing novel insights relevant to several biomedical disciplines, including nutrition, clinical medicine, rehabilitation, and bioengineering. The study demonstrates that biomaterials can adsorb small molecules from their surrounding environment, which offers valuable guidance for the rational design and functionalization of future biomaterials. The investigation into cell–material interactions further highlight the relevance of metabolic pathways such as anaerobic glycolysis, which is closely associated with chronic inflammation. These findings emphasize the importance of considering cellular metabolic states in developing bioactive materials, potentially opening new avenues for anti-inflammatory biomaterial design. A notable contribution of this work is its integration of metabolomics into biomaterial research—an area where a significant gap exists between material science and bioinformatics. The methodologies and results presented in this thesis can serve as a reference model for future studies aiming to assess the biological performance of materials using omics technologies. The novel biomaterial developed in this study, amorphous calcium phosphate incorporating glutamate (ACP-Glu), has been shown to significantly enhance the activity of bone-forming cells through the modulation of energy metabolism. This material exhibits strong potential to replace conventional, biologically inert bone fillers, offering improved outcomes in bone regeneration. Furthermore, incorporating endogenous metabolites to elicit biological responses represents a safer and more physiologically compatible alternative to commonly used bioactive additives, such as cytokines and growth factors. This metabolite-guided strategy aligns with current trends toward minimally invasive and patient-friendly biomaterial solutions. In conclusion, the primary practical outcome of this thesis is the development of the ACP-Glu biomaterial, which shows promise in promoting faster and more effective bone healing. Its potential clinical translation could contribute to improved patient recovery and enhanced outcomes in orthopedic and regenerative medicine applications.

Structure and volume of the thesis

The thesis consists of an introduction and 4 chapters: literature review in Chapter 1, methodological part (Materials and Methods) in Chapter 2, results and discussions in Chapter 3, and conclusion in Chapter 4. The work also includes a list of figures and tables, and an explanation of abbreviations. The main text of the thesis is presented on 121 pages; the volume

of the work together is 187 pages. The work includes 58 Figures, 4 tables, and 1 appendix. 167 bibliography sources are used in the work.

Publications and Approbation of the Thesis

Publications:

1. **Fan J**, Jahed V, Klavins K. Metabolomics in bone research. Metabolites. 2021 Jul 1;11(7):434. (Scopus, Open Access, IF 3.4, Q2, CiteScore 5.7)
2. **Fan J**, Abedi-Dorcheh K, Sadat Vaziri A, Kazemi-Aghdam F, Rafieyan S, Sohrabinejad M, Ghorbani M, Rastegar Adib F, Ghasemi Z, Klavins K, Jahed V. A review of recent advances in natural polymer-based scaffolds for musculoskeletal tissue engineering. Polymers. 2022 May 20;14(10):2097. (Scopus, Open Access, IF 4.7, Q1, CiteScore 8)
3. **Fan J**, Schiemer T, Vaska A, Jahed V, Klavins K. Cell via Cell Viability Assay Changes Cellular Metabolic Characteristics by Intervening with Glycolysis and Pentose Phosphate Pathway. Chemical Research in Toxicology. 2024 Jan 8;37(2):208-11. (Scopus, Open Access, IF 3.7, Q1, CiteScore 7.9)
4. **Fan J**, Schiemer T, Steinberga V, Vaska A, Metlova A, Sizovs A, Locs J, Klavins K. Exploring the Impact of Calcium Phosphate Biomaterials on Cellular Metabolism. Heliyon. 2024 Nov 30;10(22):e39753. (Scopus, Open Access, IF 3.7, Q1, CiteScore 4.5)

Conferences:

1. **Jingzhi F.**, Abhishek I., Annija V., Diana G., Sophie V., Antons S., Janis L., Kristaps K., Metabolomics-Inspired Biomaterials: Amorphous Calcium Phosphate with Targeted Metabolic Enhancement for Bone Repair, in: 21st Annual International Conference of the Metabolomics Society.
2. **Jingzhi F.**, Abhishek I., Annija V., Diana G., Sophie V., Antons S., Janis L., Kristaps K., Metabolomics-Inspired Biomaterials: Amorphous Calcium Phosphate with Targeted Metabolic Enhancement for Bone Repair, in: The Scandinavian Society for Biomaterials conference 2025. With travel award.
3. **Jingzhi F.**, Abhishek I., Annija V., Diana G., Sophie V., Antons S., Janis L., Kristaps K., Development of Amorphous Calcium Phosphate with Incorporated Metabolites for Enhanced Bone Healing, in: 12th World Biomaterials Congress 2024.

4. **Jingzhi F.**, Vahid J., Liva-Vita K., Annija V., Antons S., Dagnija L., Lilite S., Aija L., Kristaps K., Unraveling the Molecular Mechanisms of Cytotoxicity Induced by Physically Crosslinked Hyaluronic Acid/Poly-L-Lysine Hydrogel, in: 12th World Biomaterials Congress 2024.
5. **Jingzhi F.**, Vahid J., Liva K., Kristaps K., Exploring the mechanism of PLL/HA hydrogel cytotoxicity, in: Materials Science and Applied Chemistry 2023.
6. **Jingzhi F.**, Theresa S., Annija V., Kristaps K., Influence of cell viability assay on cellular metabolisms, in: Tissue Engineering and Regenerative Medicine International Society EU chapter 2023.
7. **Jingzhi F.**, Theresa S., Antons S., Janis L., Kristaps K., Calcium Phosphates Based Biomaterial Influence on Cell Metabolism, in: Nordic Metabolomics Conference 2022. With travel award.
8. **Jingzhi F.**, Theresa S., Antons S., Janis L., Kristaps K., Metabolomics investigation of biomaterial-cell interactions, in: The Scandinavian Society for Biomaterials conference 2022.
9. **Jingzhi F.**, Theresa S., Antons S., Janis L., Kristaps K., Calcium phosphate based biomaterials influence on cell metabolism, in: Tissue Engineering and Regenerative Medicine International Society EU chapter 2022.

Figures

Tables

Contents

Abbreviation

ACP - amorphous calcium phosphate

ACP-GLU – amorphous calcium phosphate with glutamate

ALP - alkaline phosphatase

ANOVA - one-way variance analysis

ATP - adenosine triphosphate

BCP - biphasic calcium phosphate

BET - Brunauer–Emmett–Teller

BMP - bone morphogenetic protein

CaP - calcium phosphate

CaS - calcium sulphate

CCK-8 - Cell Counting Kit-8

CMC - carboxymethyl cellulose

CNT – control group

COl-1 - type I collagen

CSH - calcium sulphate hemihydrate

DBM - demineralized bone matrix

DCPD - dicalcium phosphate dihydrate

DMEM - Dulbecco's Modified Eagle Medium

ECM - extracellular matrix

F6P - fructose-6-phosphate

FBP - fructose 1,6-bisphosphate

G6P - glucose-6-phosphate

GC - gas chromatography

Glu – glutamate

H58 - calcium phosphate with 58% hydroxyapatite and 42% beta-tricalcium phosphate

H95 - calcium phosphate with 95% hydroxyapatite and 5% beta-tricalcium phosphate

HAp - hydroxyapatite

HPLC - High-performance liquid chromatography

HPMC - hydroxypropyl methylcellulose

ICDD - International Center for Diffraction Data

LC - liquid chromatography

LDH - lactate dehydrogenase

MS - mass spectrometry

MSCs - mesenchymal stem cells

NMR - nuclear magnetic resonance

OCN - osteocalcin

OCP - octacalcium phosphate

OPN – osteopontin

PBS - phosphate-buffered saline

PCA - principal component analysis

PFK-1 - phosphofructokinase-1

pH - potential of hydrogen

PLGA - Poly(lactic-co-glycolic acid)

PMMA - polymethyl methacrylate

PS – Polystyrene

PVP - polyvinyl pyrrolidone

RANKL - receptor activator of nuclear factor kappa beta

Runx2 - runt-related transcription factor 2

SEM - scanning electron microscope

TCA - tricarboxylic acid

XRD - X-ray diffraction analysis

β-TCP - beta-tricalcium phosphate

Literature Review

1.1 Tissue engineering and biomaterials

Tissue engineering, first defined by Langer in 1993, is a multidisciplinary field that uses the concepts of engineering and the life sciences to create biological replacements that restore, maintain, or enhance tissue function (1). The importance of tissue engineering is profound and far-reaching. Traditional therapies often fail to address the intricate tissue repair and regeneration dynamics. Organ transplantation, while life-saving, is plagued by scarcity, immune rejection, and lifelong dependence on immunosuppressive drugs (2). Tissue engineering promises to alleviate these challenges by providing patient-specific, tailor-made solutions. Through manipulating cellular behavior and creating three-dimensional structures that mimic native tissue environments, tissue engineers strive to produce functional substitutes that can seamlessly integrate with the patient's body, bypassing the barriers of rejection and minimizing long-term complications (3,4).

Biomaterials serve as the architectural foundation upon which tissue engineering strategies are built. Biomaterials have a long history as an aid in medicine. As a combination of biology, medicine, materials science, and engineering, the progress of biomaterials as a discipline is also swift. Biomaterials nowadays enable the translation of scientific concepts into tangible therapeutic solutions, potentially regenerating damaged or diseased tissues, improving patient outcomes, and revolutionizing medicine. There are many ways to classify biomaterials. Materials can be initially divided into polymers, ceramics, metals, alloys, and composites based on their composition. Considering the source of the materials, it can be divided into natural biomaterials and synthetic biomaterials (5). Divided by biological properties, there are inert biomaterials and bioactive materials (6). Considering the biomaterials used in current medical practice, besides the medical implants for tissue regeneration or replacement purposes, there are also molecular probes and nanoparticles, biosensors, and drug-delivery systems (7). Depending on the application, biomaterials have various performance requirements for tissue engineering purposes. These include biocompatibility, mechanical properties, cell adhesion, migration and proliferation, angiogenesis promotion, bioactive factor delivery or biological functionality, immunomodulation, and so on (3,4,8,9). Balancing these functions while considering the specific requirements of the target tissue type is crucial for designing biomaterials that effectively contribute to successful tissue engineering outcomes. The

interplay between biomaterial properties, cellular behavior, and tissue development is at the heart of creating functional and viable tissue substitutes for various medical applications (10).

1.1.1 Biomaterials for bone tissue engineering

Biomaterials in bone tissue engineering have evolved from early metal and ceramic implants to synthetic polymers and later composites with functional designs (11). The current focus involves biomaterials integrated with cells, growth factors, and additive manufacturing, aiming for active engagement in bone remodeling and enhanced interactions with stem cells for advanced functional bone regeneration (10). Biomaterials for bone tissue engineering have been created mainly to trigger particular biological reactions. Like any bodily tissue, bone consists of characteristic cell types surrounded by an extracellular matrix (ECM), with biologically active molecules integrated into the ECM or produced by the cells. Bone tissue is a natural nanocomposite material with organic proteins (primarily type I collagen), inorganic minerals (mainly calcium phosphate), and various cells located at different places (5) (Figure 1). The structure can be divided into a few levels. There are two types of bones: compact bone and spongy (cancellous) bone. Compact bone is the outer layer of bones that consists of dense bone tissue that provides strength and protection. It forms the hard outer shell of bones and provides most mechanical properties, like support. Spongy bone is a network of trabeculae, or bony struts, creating a porous or cancellous bone structure. This arrangement is lighter than compact bone and helps in shock absorption. Within compact bone, the tissue is organized into cylindrical units called osteons. Each osteon consists of concentric rings of bone matrix called lamellae, surrounding a central (Haversian canal) region containing blood vessels and nerves. At the same time, osteons are interconnected by perforating canals (Volkmann's canals), which allow blood vessels and nerves to reach deeper into the bone. Collagen fibrils embedded with mineral crystals can be found at the nano level. At the molecular level, collagen is observed as the primary organic component of bone, while hydroxyapatite crystals are the inorganic component of bone. Due to this complex structure, the biological conditions of various bone tissues must be considered when designing and developing new biomaterials (5).

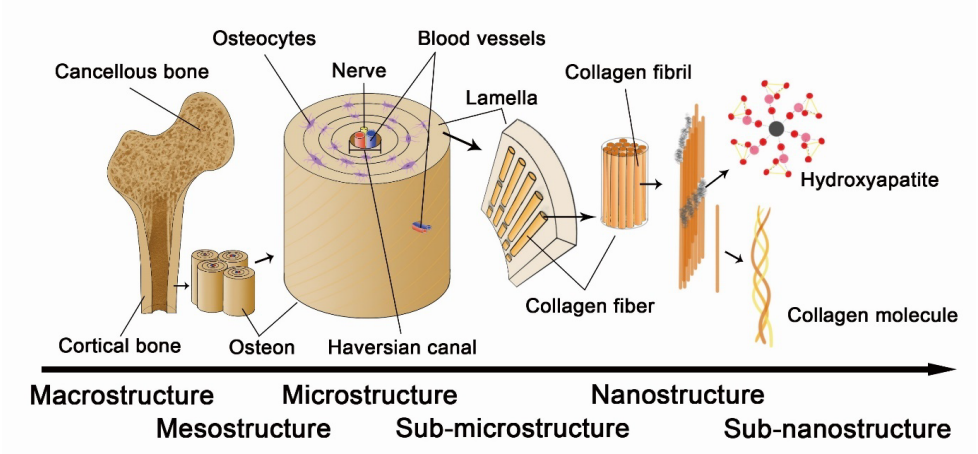

Figure 1 Hierarchical structure of bone, showing macroscopic, microscopic, and nanoscale organisation, including compact and spongy bone, osteons, lamellae, and mineralised collagen fibrils.

Bone defects due to trauma, infection, tumors, surgical debridement of osteomyelitis, and various congenital diseases are prevalent worldwide, causing millions of patients in need of bone grafting operations. Conducting osseous repair with autograft, allograft, and synthetic materials is the most effective treatment for bone defects. In tissue engineering, autogenous bone has been considered the gold standard of bone implants for a long time (12). However, there are a lot of problems in clinical practice, such as the risk of donor site morbidity and the pain to patients after operations (13). Also, doubts are raised about the so-called gold standard (12). Additionally, many companies have developed commercially mature products for bone repair based on demineralized bone matrix (DBM). Although DBM is already widely applied, the risk of disease transmission and supply limitations still impact the stability and safety of products as implantable materials (14).

Artificial materials have shown their advantages in manufacturing and costs compared with implants from biological sources (15). Various materials, such as alloys, polymers, and ceramics, have been used in bone tissue engineering. The family of Ti and its alloys is usually used in load-bearing applications to provide mechanical and structural support in bone replacement operations (16). Such inert materials are permanent in the body and cannot be the ultimate solution for bone repair. Polymers are classified into many types and are widely applied in tissue regeneration. The main disadvantage of polymers is their low mechanical properties. Even with structure designs, load-bearing tissues like bone applications still need improvement (5,17). Bone cements are usually applied as bone fillers during orthopedic surgeries. Commonly seen bone cement is based on polymethyl methacrylate (PMMA), CaP

(calcium phosphate), and CaS (calcium sulphate). However, there are many problems because of PMMA implants. The mechanical compatibility of PMMA could be improved, leading to the risk of subsequent fractures (18). The thermal necrosis due to the heat generated from the polymerization of PMMA during the surgery seriously threatens patients' health (19). In addition, PMMA is not a biodegradable material. The biocompatibility is not perfect, and the phagocytosis of the material particles continuously happens (20). As a result, the risk of inflammation is unavoidable, even though many efforts have been made to modify the properties of PMMA. These limitations have driven the development of ceramic bone fillers (21).

1.1.2 Bioceramic in bone repair

Bioceramics have emerged as pivotal players in bone regeneration, offering innovative solutions for addressing bone defects, fractures, and degenerative conditions.

Ceramics are widely applied in hard tissue engineering. Derived from either natural or synthetic sources, these materials possess high biocompatibility and structural resemblance to bone minerals. With their ability to promote osteogenesis and serve as scaffolds for tissue ingrowth, bioceramics stand at the forefront of modern medicine, propelling advancements in orthopedics and regenerative therapies to restore function and vitality to compromised skeletal structures (22). There are many kinds of ceramics used as bone fillers; the materials that are often used clinically are bioglasses, hydroxyapatite (HAp), beta-tricalcium phosphate (β-TCP), calcium sulphate, zirconia toughened alumina, and so on.

The initial endeavor was to implant laboratory-produced calcium orthophosphate (specifically TCP) as an artificial material to mend surgically induced defects in rabbit bones in 1920. The researchers injected 0.5 or 1 c.c. of 5% TCP slurries in sterilized distilled water into surgically created radial bone gaps of rabbits, preserving the periosteum (11). The first study on crafting biodegradable porous β-TCP scaffolds was reported in 1971 (11). In the 1980s, more and more developments of commercialized hydroxyapatite bioceramics for the orthopedic and dental market showed up (23). Nowadays, the application and research on bioceramics have been focusing on drug delivery, implants, scaffolds, antibacterial, and other tissue engineering strategies. Materials science, tissue engineering, and additive manufacturing advancements have led to more sophisticated and effective bioceramic solutions for biomedical progress.

Commercially available products are in large quantities. A summary of biodegradable commercial bone fillers was prepared (Table 1). To collect product data, the first step was to

search for injectable ceramic bone implant products via various search engines and other methods (e.g., MedicalExpo). Search terms were "bone cement" or "bone substitutes." Then, the product information was gathered by browsing the official websites, product brochures, and instructions provided by producers. The primary supplementary sources were public patents and literature with product information. Publications shown in patents were also referenced. The intended usage or indications of products were collected from the FDA's 510(k) premarket notification database and verified by literature. Products were abandoned when no clinical report could be searched. All the products selected are approved by CE and/or FDA. Analyzing commercial products' main applications can clarify how to design biomaterials that align with market needs and trends. It is worth noting that biodegradable calcium bone filling materials have a variety of clinical application methods, and the same material could also be used in different methods.

Table 1 Calcium-based biodegradable and injectable bone filler products and their information

Company	Product	Main composition	Main application	Strength	Working time/min	Setting time/min	Pore size/μm	Pore rate	Osteoinductivity	Degradation/mon
Acumed	Carlos	CaP, sodium silicate solution	Filler for extremities and cranial	2 times greater than cancellous bone	2-6	4-6				
Biocomposites	Genex	ß–TCP, CSH	Filler in pelvis and spine	3 times greater than cancellous bone		<15				2-3 (CS), 12 (CP)
Biomatlante	In'Oss	HAp, ß–TCP, hydrogel[c]	Bone void filler in extremities, pelvis, spine, and dental	No initial mechanical properties			<10(1/3), 300-600(2/3)	70%		
BONE SUPPORT	CERAMENT	60%CSH, 40%HAp, iohexol mixing solution	Bone void filler in extremities, pelvis, and spine	6-12MPa (after 24h in Ringer solution)	3-5	15				
Exactech	Ossilix	CaP	metaphyseal void filler	2.4 times greater than cancellous bone after 6 months	<5	8-10				50% in 6
Graftys	Graftys QuickSet	78%α-TCP, 5%DCPD, 5%MCPM, 10%Ca-deficient HAp, 2%HPMC[d] Na_2HPO_4 solution,	Bone void filler in extremities and pelvis	13±3MPa	2			63%		
JNJ	ChronOS Inject	42%β-TCP, 21%MCPM, 31%β-TCP, granules, 5%$MgHPO_4 \cdot 3H_2O$	Bone void filler in extremities, pelvis, and spine, carrier of autogenous blood or bone marrow	20MPa	3	6	100			6-18
	Norian	85%α-TCP, $MgSO_4$ 12%$CaCO_3$, 3%MCPM, Na_2HPO_4 solution	Bone void filler in extremities and pelvis	33MPa /35MPa /55MPa[e]	2	3-6	47±2	30-45%		13-24
MIS	4MATRIX	66%CSH/CSD, 33%HAp	Periodontology	No initial mechanical properties	3-5		1-50, 300-800			1-2 (CS)

	BONDBONE	CSH, CSD	Periodontology, binder	No initial mechanical properties	3-5		1-50, 300-800	46%		
	4BONE BCH	60%HAp, 40%TCP	Periodontology	No initial mechanical properties	3-5		<10, 300-600	70%		5-8
Mitsubishi Materials	Biopex	75%α-TCP, 18%TTCP, 5%DCPD, 2%HAp, sodium succinate, sodium chondroitin sulphate	Bone void filler in extremities, pelvis, and spine	80MPa	4-8	2				
OSTEOMED	OsteoVation	ß–TCP, CaS	Filler craniofacial skeleton	50MPa	5	6				6
Straumann	Bone Ceramic	60%HAp, 40%ß–TCP	Periodontology				200-800	80%		
Stryker	BoneSource	73%TTCP, 27%DCPD, Na_2HPO_4/NaH_2PO_4 solution	Cranial defects	36MPa after 24 hours/60-65MPa		10-15	33.4±6.2	45%		
	HydroSet	TTCP, trisodium citrate, PVP[d]	Bone void filler in extremities, pelvis, cranial, and spine	15.9MPa	3.75	4				
Wright	AlloMatrix	DBM (86% by volume), CaS, CMC[d]	Binder, a bone void filler for the skeletal system	No initial mechanical properties	<10				yes	12
	MIIG[f]	α-CSH, saline	Bone void filler in extremities, pelvis, and spine	Low mechanical properties	1		20-250			
	PRO-DENSE	75%CaS, 25%CaP (brushite & granular ß–TCP)	Bone void filler in extremities, pelvis, and spine	40MPa, 3 times greater than autograft after 26 weeks	3-5	20-30				3-24
	PRO-STIM	CaS, CaP, DBM	Bone void filler in extremities, pelvis, and spine	1.4 times greater than autograft after 26 weeks					yes	
ZIMMER BIOMET	Beta-bsm	HAp, carbonated apatite	Bone void filler in extremities, pelvis, and spine	28-32MPa	2	3-5				
	AccuFill	CaP (apatite)	Bone void filler for cancellous bone	10MPa	15	10	1-300	65%		

	Calcibon	61%α-TCP, 26%DCP, 10%$CaCO_3$, 3%HAp, NaH_2PO_4 solution	Bone void filler in extremities, pelvis, and spine	15MPa after 6 hours, 45MPa after 3 days	4	5	20% in 12
	Mimix	TTCP, α-TCP, trisodium citrate	Repair of cranial defects	3300 PSI (23MPa)	2-4	3-4	

Radiopaque ability and handling properties are discussed in the next part of this review.

b Some details like compounds, crystal forms, and proportions were unpublished. The unrevealed parts were presented directly by known materials. The liquid phase or solution was included in this part.

c The ratio of HAp against ß–TCP is 6:4; the ceramic/hydrogel weight ratio was 1:1; the proportion of polysaccharides in the hydrogel was 4%.

d HPMC (hydroxypropyl methylcellulose), CMC (carboxymethyl cellulose), PVP (polyvinyl pyrrolidone)

e Different sources gave different results on compressive strength.

f MIIG® has different product variants. Here, it only shows basic substances and data.

1.1.2.1 Hydroxyapatite (HAp)

HAp is a mineral form of calcium apatite with the formula $Ca_{10}(PO_4)_6(OH)_2$, and is widely used in dentistry and orthopedics. As a naturally occurring mineral component of bone and teeth, HAp exhibits a remarkable affinity for biological systems, positioning it as a prime material for promoting successful bone healing and regeneration. HAp mimics the mineral composition of native bone, allowing for seamless integration with surrounding tissues. As a result, it can serve as a biocompatible scaffold. There is a long history of using HAp as a bone filler in orthopedics (24).

The application of HAp ranges from bone grafts and implant coatings to three-dimensional scaffolds. These scaffolds provide a supportive environment for cells to colonize and remodel, guiding the formation of new tissue. Moreover, HAp's ability to act as a carrier for bioactive factors and drugs enables controlled release, influencing cell behavior and tissue regeneration dynamics (25). As a drug carrier, HAp, especially nano-HAp, is commonly used for bone-related therapies and is loaded with drugs such as growth factors, antibiotics, or anti-inflammatory agents (26). Because of its excellent biocompatibility and comprehensive research, HAp can also be used as a drug carrier in cancer treatments (27). HAp is also often used as a coating layer to enhance the implant's ability to bond with the host bone (osseointegration) (28). HAp can improve the effects of bone repair and reduce long-term inflammation compared with metallic implants. There are many methods to coat HAp, such as plasma spray coating, electrochemical deposition, electrophoretic deposition, physical vapor deposition, sol-gel method, and so on (29–31). Each method has advantages and limitations, and researchers often select the most appropriate technique based on the desired outcome and the characteristics of the coated material.

1.1.2.2 β-tricalcium phosphate

β-TCP is also a bioceramic material widely recognized for its significance in bone tissue engineering and regenerative medicine. As a classic bone graft material, it serves as a scaffold to support the growth of new bone tissue (32). One of the features of β-TCP is its controlled biodegradability. Over time, β-TCP undergoes gradual degradation, providing temporary mechanical support as new bone tissue forms. The calcium and phosphate ions released during degradation can benefit local bone mineralization and support natural healing. Compared with HAp, β-TCP has a more open crystal structure and is less dense than hydroxyapatite (Table 2). It crystallizes in a monoclinic or rhombohedral structure. Because of the faster degradation

process, β-TCP is particularly useful when rapid bone healing and regeneration are desired. β-TCP is generally less mechanically stable and more brittle than HAp. These mechanical differences also make the application of β-TCP different from HAp (33).

Table 2 List of commercially used CaP and CaS with their properties

Name	Formula	Ca/P ratio	Crystallography	Symbol
Tetracalcium phosphate monoxide	$Ca_4(PO_4)_2O$	2	Monoclinic	TTCP
Hydroxyapatite	$Ca_{10}(PO_4)_6(OH)_2$	1.67	Hexagonal	HAp
α-Tricalcium phosphate	α-$Ca_3(PO_4)_2$	1.5	Monoclinic	α-TCP
β-Tricalcium phosphate	β-$Ca_3(PO_4)_2$	1.5	Rhombohedral	β-TCP
Dicalcium phosphate	$CaHPO_4$	1	Triclinic	DCP
Dicalcium phosphate dihydrate	$CaHPO_4 \cdot 2H_2O$	1	Monoclinic	DCPD
Monocalcium phosphate monohydrate	$Ca(H_2PO_4)_2 \cdot H_2O$	0.5	Triclinic	MCPM
α-Calcium sulphate hemihydrate	α-$CaSO_4 \cdot 0.5H_2O$	-	[a]	α-CSH
β-Calcium sulphate hemihydrate	β-$CaSO_4 \cdot 0.5H_2O$	-	[a]	β-CSH
Calcium sulphate dihydrate	$CaSO_4 \cdot 2H_2O$	-	Monoclinic	CSD

a The crystal forms of α-CSH and β-CSH are controversial (58).

Additionally, β-TCP is a valuable component in composite biomaterials, combining its properties with other materials like polymers or growth factors to enhance their effectiveness (34,35). β-TCP particles or fibers can act as reinforcing agents within the polymer matrix, improving the composite's mechanical properties. There are many methods to process β-TCP, such as polyurethane-foam replica, sol-gel, 3D printing, gelatin-freeze casting, and so on (36). The potential of β-TCP combined with other engineering strategies benefits the development of bone tissue engineering.

1.1.2.3 Amorphous calcium phosphate

Amorphous calcium phosphate (ACP) is a biomaterial with significant promise in various fields, notably dentistry, bone tissue engineering, and drug delivery. Unlike its crystalline counterparts, ACP lacks a well-defined atomic arrangement in a disordered and non-crystalline state (37). It plays a role as a precursor phase of synthetic hydroxy-carbonate apatite, which is a critical component of bone and dentin mineralization. In natural bone formation, ACP forms as an intermediary precursor phase that eventually transforms into crystalline hydroxyapatite, contributing to the strengthening of bone tissue (38). Also, ACP is more soluble than crystalline CaPs, giving the microenvironment a higher concentration of calcium and phosphate ions. ACP is also more active than crystalline forms. This reactivity makes it an ideal material for drug delivery systems (39). Various forms of ACP exhibit thermal instability, rendering them unable

to withstand calcination or sintering processes. Upon heating, precipitated ACPs primarily undergo a water loss, encompassing two distinct phases: the release of loosely bound water molecules adhering to the surface of ACP agglomerates and the removal of more tightly bound internal water molecules. The former is reversible, while the latter is typically irreversible (40,41). ACP is easy to convert into crystalline apatite, especially in aqueous media. During such conditions, pH, temperature, and the presence of foreign ions all play important roles. Stabilization of ACP becomes essential at acidic conditions, where the amorphous phase is unstable, and other phases like OCP (octacalcium phosphate) or brushite may form (42). Furthermore, it has been shown that a sufficient quantity of Mg^{2+}, F^-, carbonate, pyrophosphate, diphosphonates, or polyphosphorylated metabolites or nucleotides will prevent the transformation of synthetic ACP to HAp (43–45). Adding Si or Zr elements during the low-temperature synthesis of the ACP can increase the remineralizing potential of the final biomaterial. By delaying the ACP to HAp conversion, Si- and Zr-ACPs prolonged the time that mineral ions were released (46). As mentioned, high-energy coatings like plasma-sprayed HAp coatings are well-established in the industry. These coatings primarily consist of HAp, but ACP phases may also be present, significantly affecting their mechanical properties, including adhesion to metals and biological performance (47).

ACP has been applied as a solid phase for CaP cements and coatings and in composite development for biomaterial applications (48). Due to the instability of ACP, maintaining its structure during its production has become a key area of research. Studies have shown that ACP has been evidenced to have better *in vivo* osteoconductivity than hydroxyapatite and better biodegradability than beta-tricalcium phosphate (40). ACP is also presented as ACP-filled polymeric composites in hard tissue engineering (49,50). Among these, poly(d,l-lactic acid) is often used. The ACP/poly(d,l-lactic acid) composites usually show fast mineralization and good cytocompatibility (48,49). Liao et al. applied ACP in tendon-bone regeneration with adenosine triphosphate, which enhanced osteogenesis and angiogenesis results both *in vitro* and *in vivo* (51). Because of their excellent biocompatibility and mechanical properties, ACP has become increasingly significant in orthopedics and dentistry.

1.1.2.4 Cold sintering of bioceramics

Sintering is a process of bonding, densification, and recrystallization of powder compacts. Traditionally, solid state, liquid phase, and pressure-assisted sintering are used to process ceramics at high temperatures, usually over 1000 degrees Celsius (52). Sintering involves

enduring chemical and physical transformations that decrease porosity through grain growth and bonding. Larger grains grow at the expense of smaller ones, increasing the average size while reducing the number of grains. This can lead to undesirable effects like grain growth, phase transformation, and increased energy consumption.

Cold sintering is an innovative materials processing technique that consolidates ceramic materials at significantly lower temperatures (room temperature or often below 300 degrees Celsius) than traditional sintering methods (52,53). Cold sintering offers a more energy-efficient and controlled alternative. Many advanced ceramics and composite materials are sensitive to high temperatures, which can lead to phase changes or chemical reactions. Cold sintering enables the fabrication of such materials without compromising their properties. Cold sintering also allows for rapid ceramics manufacturing, reducing lead times in temperature-changing processes and enabling quicker iterations in development and engineering applications. Besides these, cold sintering technology provides a platform for researchers to explore new material compositions and properties, benefiting the development of advanced materials (53). Because of these features, many materials, not only biomaterials but also electrical conductors, have been manufactured by cold sintering. For example, NaCl microwave dielectric ceramics were successfully fabricated by cold sintering (54). Cold sintering was also applied to densify the ceramics. Guo et al. developed a one-step low-temperature reactive cold-sintering approach to synthesize and densify $BaTiO_3$ ceramics with nanograins. They found that densification was achieved through pressure-induced particle rearrangement, deposition of the reaction product at grain boundaries, and grain coarsening (55).

A standardized protocol for the cold sintering process, particularly regarding temperature and pressure application, has yet to be established (53). Previous approaches involve mixing a solvent with ceramic powder to ensure good contact. The resulting ceramic paste is placed in a steel die, typically cylindrical, and compressed using hydraulic or mechanical force. A heating system, like a jacket or hot plate, can control the temperature if the room temperature is not favored (Figure 2).

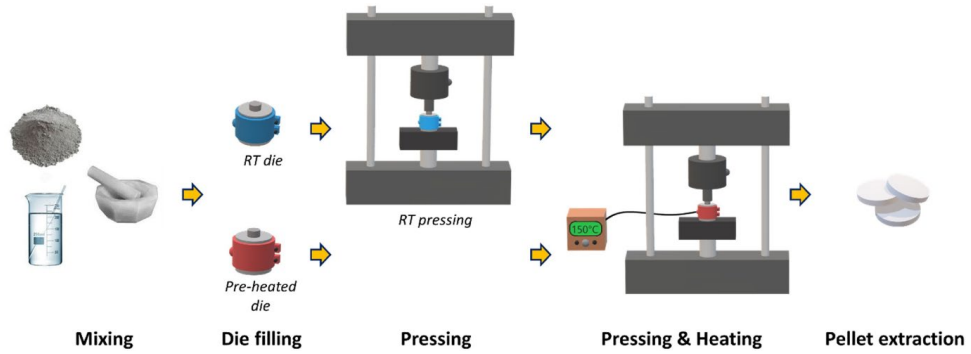

Figure 2 Scheme of the cold sintering route (53)

One of the most prominent features of cold sintering is that it can maintain the original amorphous state of ceramic materials. Due to the unique properties of ACP, cold sintering can benefit the processes of manufacturing ACP (56). Studies have shown that ACP maintains the same amorphous phases under different pressures after the room temperature cold sintering process (57). Cold sintering has also been applied to some amorphous ceramic-based materials. In dielectric ceramics, the complex microstructure of the grain boundary and limited grain growth obtained from cold sintering can change the electrical properties of materials. Optimizing the cold sintering process for various applications in ceramics, composites, and advanced materials can significantly benefit the development of application materials and engineering.

1.1.3 Materials characterization

Material characterization is crucial in biomaterial research as it provides detailed insights into materials' structural, chemical, and physical properties, ensuring their suitability for specific biomedical applications. Accurate characterization enables researchers to understand how biomaterials interact with biological systems, influencing biological performance.

1.1.3.1 X-ray diffraction analysis (XRD)

XRD is an analytical technique used in materials science, engineering, and other fields to determine crystalline substances' atomic and molecular structure. It relies on the principle of X-ray diffraction, which occurs when X-rays strike a crystalline material and are scattered at specific angles due to the regular arrangement of atoms within the crystal lattice (59). By measuring the angles and intensities of these scattered X-rays, XRD provides valuable information about the crystal structure, including lattice parameters, unit cell dimensions, and

the identification of crystalline phases. The XRD results are presented by feature peaks. These peaks represent the diffraction of X-rays by crystal planes within the material. Each peak's position (2θ angle) is characteristic of the spacing between these crystal planes. Because of the amorphous characteristics of ACP, sharp and well-defined peaks in the XRD patterns should not be observed in such amorphous materials (44).

1.1.3.2 Scanning electron microscope (SEM)

In SEM, a beam of high-energy electrons is focused onto the sample's surface using electromagnetic lenses, interacting with the atoms in the sample (60). SEM is used to study biomaterials' surface features and topography, including the texture and roughness of implants, scaffolds, and tissue engineering constructs. SEM helps researchers examine the microstructure of biomaterials, such as the arrangement of fibers in polymers or the porosity of ceramics (61). This information is crucial for assessing the materials' biocompatibility and interaction with biological tissues, and also benefits in optimizing material properties in medical devices and implants. SEM analysis can also investigate how cells interact with the material's surface, which is linked with cell-material interaction (2.2) (62). SEM aids in designing materials that promote cell adhesion, proliferation, and differentiation. SEM can not only be applied to materials but also to cells. With the surface morphology and topography information, we can evaluate the adhesion and cell-material interaction (63).

1.1.3.3 Porosity of biomaterials

Porosity is a critical parameter in biomaterials, specifically for implantable biomedical materials, and it plays a crucial role in the design, performance, and functionality of biomaterials across various biomedical applications. Traditionally, the pore scale is defined as macroporous if it exceeds 50 nm, mesoporous between 2 and 50 nm, and microporous when less than 2 nm (64). Porosity allows cells to infiltrate and populate the biomaterial, promoting tissue regeneration and integration with host tissues. Cells can migrate into the pores, deposit extracellular matrix (ECM), and establish connections with surrounding tissues, facilitating tissue repair and growth (65). Besides cell migration, pores can also provide nutrient and oxygen transport channels. At the same time, the waste products produced by cells can also be transported out by pores. Nowadays, scaffold design values the importance of porosity, especially for bone tissue engineering, to achieve better osteogenesis results (66).

1.2 Cell-material interaction

The field of biomaterials has undergone a transformative evolution, propelled by a deep understanding of the intricate interplay between living cells and engineered materials. Cell-material interaction is a dynamic and multifaceted dialogue with immense significance in diverse disciplines, ranging from regenerative medicine and tissue engineering to medical device development and drug delivery systems (67). These interactions are pivotal determinants of the success or failure of biomaterial implants, scaffolds, and devices when introduced into the body. From the moment a biomaterial comes into contact with living tissues, a cascade of events is set in motion that influences cell behavior, tissue regeneration, inflammation, and overall biological response (68). Conversely, biomaterial surface characteristics, such as roughness, topography, chemistry, and charge, significantly influence cell behaviors (69).

1.2.1 Material characteristics

Surface roughness at the nanoscale and microscale levels can significantly impact cell adhesion, migration, proliferation, and differentiation (67,70). Cells exhibit distinct preferences for different roughness profiles; some may thrive on smoother surfaces, while others may respond favorably to rougher textures. Different roughness can also change the immune states, either pro-inflammation or anti-inflammation (69,71).

Topography, which refers to the three-dimensional features of a surface, guides cell behavior by influencing cell attachment and spreading. Nanostructured or microstructured topographies can guide cell alignment, enhance extracellular matrix production, and even modulate gene expression, offering tailored control over tissue regeneration (67). Many studies create different patterns to modulate the immune response, predominantly neutrophils and macrophages, by material surfaces (69,72,73). Changes in different dimensions will subject cells to different forces. The resulting cytoskeleton and cell membrane stress stimulation changes will further affect cell functions.

Porosity plays a significant role in influencing cell-material interactions in tissue engineering and biomaterial applications. Porous biomaterials typically have a larger surface area than non-porous materials with the same volume. This increased surface area provides more sites for cell adhesion. The interconnectivity of pores can also support cell migration and nutrient delivery. A polypore structure also benefits angiogenesis, accelerating the formation of blood vessels.

The minimum requirement for pore size is approximately 100 micrometers due to cell size, migration requirements, and transport. However, pore sizes greater than 300 micrometers are recommended due to enhanced new bone formation and the formation of capillaries (66).

In cell-material interaction, protein adsorption and cell attachment are often studied to determine the fate of biomaterials within biological systems. Protein adsorption involves the spontaneous binding of proteins from surrounding body fluids onto the surface of a biomaterial. This knowledge has led to a better understanding of the regenerative capabilities of biomaterials, aiding their design with improved functionalities (74). CaPs, such as octacalcium phosphate and amorphous calcium phosphate, have shown excellent protein adoption ability (75,76). Such characteristics can directly influence the cellular behaviors that occur at the interface.

1.2.2 Cellular behaviors

Cell-material interaction studies comprehensively assess various cellular behaviors to understand how biomaterials influence cell responses. Usually, cell behaviors evaluated in these studies include cell adhesion, reflecting the initial binding of cells to the material surface (77); cell spreading, indicating cell interaction and extension on the substrate; cell proliferation, tracking cell growth and division over time (78); cell migration and cell differentiation (79); ECM deposition, examining the production and arrangement of surrounding matrix components (78); cell signaling, cytokine, and growth factor secretion, investigating how materials impact intracellular pathways and gene expression and the release of signaling molecules (80); immune responses, studying interactions with immune cells and inflammatory reactions. These assessments reveal how materials influence cellular behavior, vital for enhancing biomaterials in tissue engineering and regenerative medicine.

In CaPs for complex tissue engineering, besides the regular proliferation assessment, the evaluation of osteoinduction, osteoconduction, and osseointegration is vital for developing hard tissues like bone or dentin (81). Osteoinduction triggers osteogenesis and recruits immature cells to become preosteoblasts, crucial in bone healing. Osteoconduction involves bone growth on a surface, often seen in implants. Osseointegration is a stable implant anchorage through direct bone-to-implant contact, particularly successful in craniofacial implantology. Its significance in primary arthroplasties remains debated, as bone ingrowth in porous-coated prostheses may or may not constitute osseointegration (15,81). Meeting more performance requirements is what advanced bone repair materials need to have.

Many studies on biomaterials in regenerative medicine and tissue engineering have traditionally focused on protein activity and gene expression. This focus is often driven by the need to understand the molecular and cellular processes underlying tissue regeneration and the interaction between biomaterials and cells. However, there is a growing interest in incorporating metabolomics and considering the role of metabolites and metabolism in biomaterial-related research. While protein activity and gene expression are crucial aspects of cell behavior and tissue regeneration, metabolomics provides a more comprehensive view of cellular processes (82). Metabolites represent the end products of gene expression and enzymatic activity, reflecting the actual metabolic state of cells. Studying metabolites can offer insights into how biomaterials affect cellular metabolism, energy production, and biochemical pathways, which will be discussed in Section 2.4. Metabolomics can reveal changes in metabolic pathways that are affected by the presence of biomaterials. This information can help identify metabolic signatures associated with successful tissue regeneration and the potential impact of biomaterials on those pathways (83). While biomaterial research has traditionally focused on gene expression and protein activity, there is a growing interest in integrating metabolomics to gain a more holistic understanding of how biomaterials impact cellular metabolism and tissue regeneration. This multidisciplinary approach can enhance our ability to design biomaterials for regenerative medicine applications and improve patient outcomes.

1.3 Bone regeneration

Bone has impressive natural regenerative abilities. It allows scarless healing and restores mechanical function, even in challenging scenarios like advanced age and metabolic or immunological degenerative diseases (84). Nevertheless, many bone injuries still result in unsatisfactory healing outcomes. Bone undergoes continuous renewal, with approximately one-fifth of the skeleton undergoing remodeling annually. This dynamic process, termed bone remodeling, requires precise coordination between bone formation and resorption, orchestrated by various cell types within the bone multicellular unit and tightly regulated signaling pathways to maintain bone balance (10,85). Fracture healing involves communication among diverse cell types, such as endothelial cells, nerve cells, osteoblasts, osteoclasts, and osteoprogenitor cells, via the release of soluble factors (Figure 3). Figure 3 presents the progress of bone repair (85). Metabolic phases (blue bars) in fracture healing coincide with biological stages (brown bars), consisting of anabolic and catabolic phases within three critical biological stages: inflammation, endochondral bone formation, and coupled remodeling. The chart highlights key cell types and

their durations in each stage, aligned with the timeline for mouse femur fracture healing using an intramedullary rod.

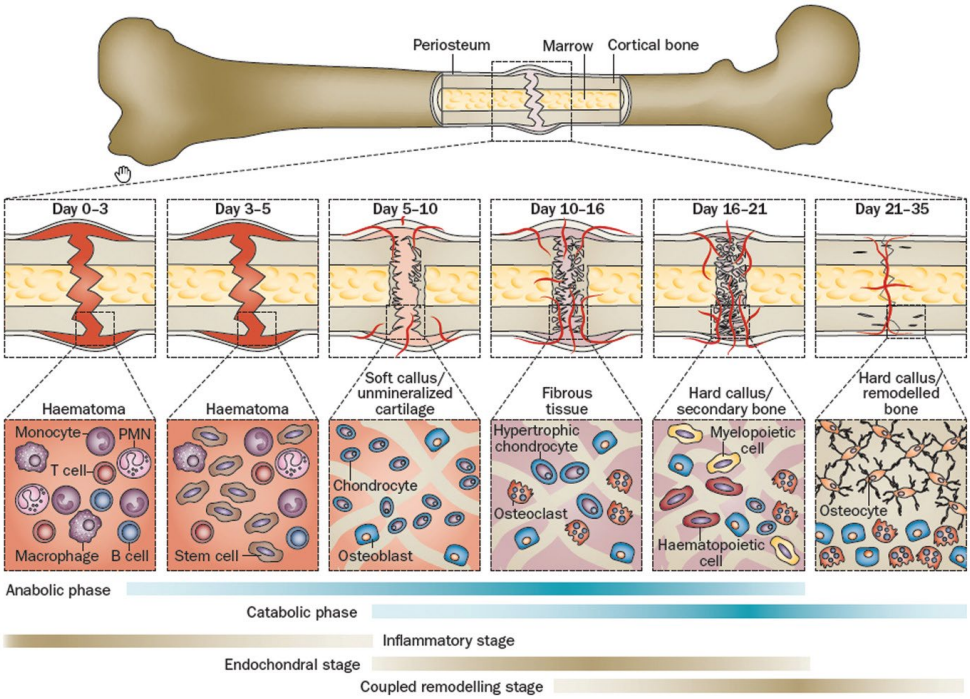

Figure 3 Femur fracture repair (85). *(Reprint promised)*

1.3.1 Osteoblasts

Osteoblasts are specialized cells responsible for bone formation and mineralization in the human body. They are one of the key cell types involved in the dynamic process of bone remodeling, which is essential for maintaining the strength and integrity of the skeletal system (10). Osteoblasts are derived from mesenchymal stem cells (MSCs), which are multipotent cells capable of differentiating into various cell types, including osteoblasts. These MSCs are found in the bone marrow and periosteum (the membrane covering bones) (Figure 4). The differentiation of MSCs into osteoblasts is regulated by various signaling pathways and factors, including bone morphogenetic proteins (BMPs), Wnt signaling, and runt-related transcription factor 2 (Runx2) (86). That differentiation can be triggered by various factors (87).

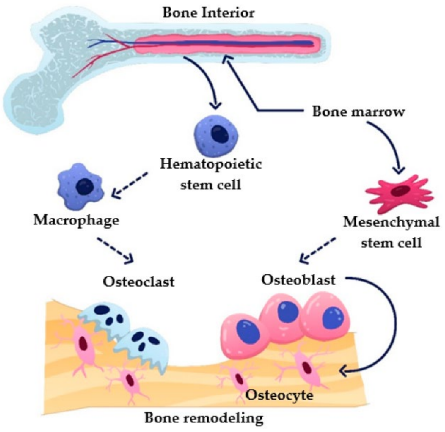

Figure 4 The functions of bone cells (82)

Osteoblasts generate the organic bone matrix called osteoid, which is later mineralized in a poorly understood process. Upon completing their biosynthetic role, osteoblasts transform into osteocytes, remaining dormant within the ECM. Osteoblasts respond to various hormones and growth factors, including parathyroid hormone, calcitonin, vitamin D, and bone morphogenetic proteins. These factors influence osteoblast activity and bone remodeling (88). Because osteoblasts initiate the mineralization of the bone matrix by depositing hydroxyapatite crystals, researchers usually study the mineralization process to ensure the development of a mineralized bone-like tissue. Gene expression and protein activity are typically combined to evaluate the osteogenesis level. The often-used ones are osteocalcin, Runx2, and ALP (alkaline phosphatase). For example, Shuai et al. considered ALP, type I collagen (COL-1), osteocalcin (OCN), and Runx2 gene expression to characterize their manufactured magnetically actuated bone scaffold. Those factors that can trigger MSC differentiation are also detected in the biomaterials. Zheng et al. developed ruthenium (II) functional selenium nanoparticles for osteogenic transcription and attenuating adipogenic transcription. They successfully differentiated MSCs into osteoblasts and verified this by flow cytometry. After 14 days of incubation, the Alizarin Red staining indicated stronger osteogenesis from this nanoparticle (89). The differentiation into osteoblasts is also a core research spot in microchip developments. Altmann et al. demonstrated that a 3D microenvironment created with a fibronectin-coated PMMA/PC-based microchip enhances the differentiation of primary human osteoblasts. This is evident through the formation of densely packed 3D bone cell clusters and the expression of biomarkers signifying osteoblast differentiation (90). They detected higher gene expression of OCN, osteonectin, and ALP. The function of osteoblasts can also be influenced by

immune cells such as macrophages, and this feature is also utilized in the bone tissue engineering field (91). As osteoblasts play a significant role in producing bone matrix, characterizing osteoblasts is very common and essential in evaluating biomaterials for bone regeneration.

1.3.2 Osteocytes

Osteocytes are the most abundant and long-lived cells within bone tissue and are essential for bone health. Osteocytes are embedded within the mineralized bone matrix and are found in small, fluid-filled cavities called lacunae. These cavities are interconnected by tiny canaliculi (Figure 1).

Osteocytes communicate with each other and with other bone cells, such as osteoblasts and osteoclasts. Osteocytes are mechanosensor cells that control the activity of osteoblasts and osteoclasts within a basic multicellular unit. This kind of communication is crucial in coordinating bone remodeling and repair. Besides the connection with other bone cells, osteocytes can also release calcium into the bloodstream when needed to maintain calcium homeostasis in the body (92). Under the fluid stimuli, Mastuzaka et al. developed a system that can manipulate osteoblast arrangement by osteocyte mechanoresponse (93). Bernhardt et al. conducted a triple culture of primary human osteoblasts, osteoclasts, and osteocytes to study the interaction between each bone cell. They further evaluated the markers and morphology. OCN level was hugely increased in this triculture model (94).

Like osteoblasts, osteocytes are widely used in biomaterials characterization and cell-biomaterial interaction, especially for hard tissue engineering. Osteocytes in peri-implant bone physically communicate with implant surfaces through canaliculi and respond to mechanical loading, influencing osteocyte numbers and morphology. Specific implant design features help maintain a more youthful osteocyte phenotype, even as the extracellular matrix matures (95).

Daily activities transmit whole-body mechanics to the organ, tissue, and cellular levels, which is also highly relevant to the skeletal system. In bone tissue, osteocytes are essential mechanosensitive cells (96). Evidence of their function comes from studies showing that mice with osteocyte ablation fail to respond to unloading-induced bone loss (97). Osteocytes within the mineralized extracellular matrix experience multiple biophysical stimuli, including strain, stress, shear, osmotic pressure, fluid flow, streaming potentials, and acceleration. Among these, fluid flow-induced shear stress is the primary force stimulating osteocytes (98). During various

illnesses, osteocytes can also be influenced. Altered mechanical stimulation of osteocytes in osteoporosis results from changes in the extracellular environment, including modified mineralization and lacunar-canalicular architecture (99). Because of this mechanical sensitivity, osteocytes were also widely applied in studies that utilized bioreactors. Studies have shown that hydrostatic pressure could stimulate osteocytes and further enhance the differentiation of the murine macrophage cell line into osteoclast-like cells (100). They revealed that the arrangement worked through soluble molecular interactions, with prostaglandin E2 identified as a novel determinant for oriented collagen/apatite organization of bone matrix.

As our understanding of the role of osteocytes in bone health deepens, their inclusion in biomaterial design and tissue engineering strategies is likely to become increasingly important for developing effective and long-lasting solutions for bone-related conditions and injuries.

1.3.3 Osteoclasts

Osteoclasts are specialized cells responsible for bone resorption, a crucial bone remodeling and maintenance process. Bone remodeling is a natural outcome of ongoing cellular processes that enhance survival. It involves essential tasks for renewing bone structural units by basic multicellular units (101). Osteoclasts play a central role in breaking down bone tissue, allowing for the removal of old or damaged bone and the subsequent formation of new bone (102). Osteoclasts originate from hematopoietic stem cells primarily found in the bone marrow (Figure 3). These stem cells give rise to myeloid lineage cells, including monocytes and macrophages (82). Osteoclasts specialize in breaking down the mineralized and organic components of bone tissue. They release enzymes and acids that dissolve the hydroxyapatite (mineral) and degrade the organic matrix, primarily composed of collagen fibers. This remodeling activity is tightly regulated by various factors, such as cytokines and hormones (101). Beyond their role as "bone eaters," osteoclasts significantly contribute to bone remodeling, angiogenesis, osteoimmunology, and the establishment of hematopoietic niches. Osteoporosis occurs when there is an imbalance between bone resorption (the removal of old or damaged bone) and bone formation. Osteoclasts are the primary cells responsible for bone resorption, and their overactivity or increased lifespan can contribute to osteoporosis's loss of bone density (102). The over-resorption of bone tissue has become a severe medical problem. Various factors, such as hormones and age, can influence the bone resorption of osteoclasts (103). Osteoporosis treatment strategies often focus on reducing osteoclastic activity, stimulating osteoblastic activity, or both. Recently, a new bone cell type originating from

osteoclasts was found. Researchers revealed that RANKL (receptor activator of nuclear factor kappa beta) stimulated osteoclasts possess an alternative cell fate involving fission into daughter cells known as osteomorphs. Inhibition of RANKL hindered this cellular recycling, leading to osteomorph accumulation. Single-cell RNA sequencing demonstrated that osteomorphs exhibit distinctive gene expression profiles, differing from osteoclasts and macrophages. When deleted in mice, they express several non-canonical osteoclast genes associated with structural and functional bone phenotypes (104). Understanding the role of osteoclasts in all kinds of biological progress is essential for developing effective therapies.

In tissue engineering, *in vitro* assays can be used to assess the ability of osteoclasts to resorb bone or biomaterials. These assays involve culturing osteoclasts on bone slices or synthetic materials and measuring the extent of resorption (105). Furthermore, osteoclasts and osteoblasts can be co-cultured for deeper evaluation. Kowal et al. synthesized new bioactive glass scaffolds with exceptional qualities; they applied osteoblasts and per-osteoclasts co-culture and evaluated the osteogenesis from the per-osteoblasts and immunofluorescence images from the osteoclasts (106).

1.3.4 Bone healing process

Bone formation occurs through two distinct processes: intramembranous ossification and endochondral ossification. In intramembranous ossification, osteoblasts directly differentiate within mesenchymal tissue, forming flat bones like the skull, mandible, maxilla, clavicles, and patella (84). In endochondral ossification, bone forms indirectly, with an initial cartilaginous template remodeled into bone, creating long bones like the femur, tibia, and humerus. Because the patient's recovery process is complicated, developing biomaterials for hard tissue engineering is primarily focused on the endochondral route of bone healing (10).

Inflammation is one of the significant issues that troubles both patients and researchers. Both the short-term and long-term inflammation would result in pain. At the same time, it serves as the body's initial response to injury and plays several crucial roles in the early stages of bone healing. One phase of the inflammation is involved in hemostasis, including the formation of blood clots to stop bleeding. Platelets and coagulation factors are activated to create a temporary seal at the fracture site, preventing excessive blood loss (107). Furthermore, the injury caused by a fracture exposes the body to potential pathogens, and there is a risk of infection. Inflammation initiates an immune response, recruiting white blood cells, particularly neutrophils and macrophages, to the injury site (71). These immune cells help remove any

foreign materials, bacteria, or debris that may have entered the wound, reducing the risk of infection (108). These removal stages remove the broken tissues, foreign materials, and bacteria (109). The regulation of inflammation is also a significant issue for implant design.

Aging also influences the progress of bone healing. In elderly murine models, periosteal MSCs exhibited diminished chondrogenic potential and reduced cartilage matrix deposition during initial fracture healing stages. This delays the eventual conversion of cartilage to bone at the fracture site (110).

The role of implanted bioceramics in bone tissue regeneration is to serve as scaffolds that provide structural support and promote the healing process. They mimic the properties of natural bone, such as biocompatibility and osteoconductivity, allowing them to integrate with host tissue (10). Bioceramics facilitate cell attachment, proliferation, and differentiation while enabling the formation of new bone tissue. Over time, the bioceramic scaffold is gradually resorbed and replaced by newly formed bone, restoring bone structure and function.

1.4 Metabolomics

Metabolomics is a rapidly evolving field of scientific research focusing on the comprehensive study of small molecules, known as metabolites, within cells, tissues, and biological fluids. These metabolites are the end products of cellular processes, reflecting the dynamic interplay of genes, proteins, and environmental factors. It seeks to analyze and quantify the diverse metabolites in a biological system to gain insights into the metabolic processes that govern cellular functions (111). By providing a holistic snapshot of an organism's metabolic state, metabolomics holds immense potential in various fields, including medicine, nutrition, environmental science, and drug discovery. In recent years, metabolomics has gained increasing interest in all biomedical fields, including tissue-related research, enhancing our comprehension of cellular processes in health and disease (82). The development of metabolomics as a discipline has been driven by advancements in analytical technologies and data science and a growing recognition of its potential applications in academic research.

There are two leading platforms of metabolomics analysis: mass spectrometry (MS) and nuclear magnetic resonance (NMR) spectroscopy. Of these, the joint separation techniques in MS technology are liquid chromatography (LC) and gas chromatography (GC) columns (112). Metabolite detection employs specific techniques, followed by raw signal pre-processing for data formatting (data pre-processing). Normalization reduces bias. Spectral data identifies metabolites (data processing). Univariate and multivariate stats pinpoint significant ones

(statistical analysis). Enrichment and pathway analysis provide biological context (functional analysis). Integrating metabolomics with other omics data, such as gene expression and protein activity, enhances understanding of pathophysiological processes (Omics data integration). The workflow is concluded in Figure 5 (111).

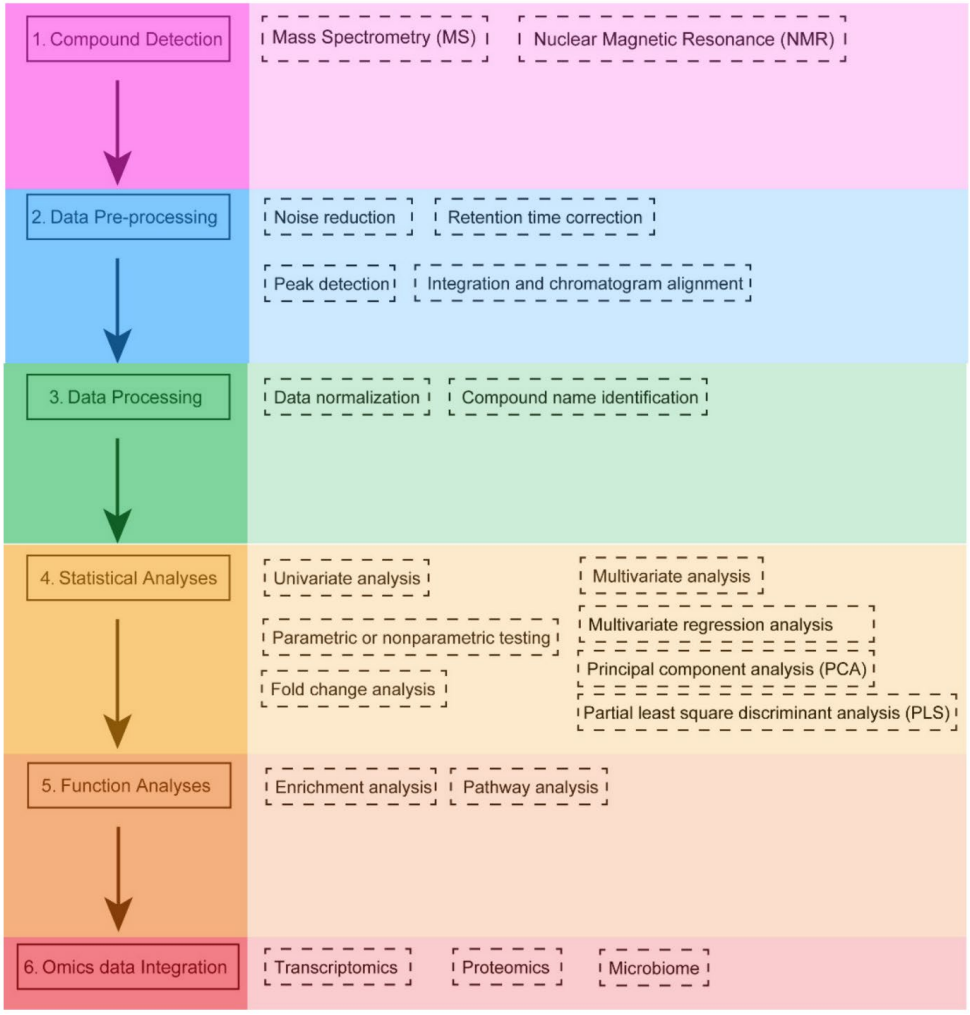

Figure 5 Typical workflow of metabolomics analysis.

As a complex bioinformatic subject, the analysis takes a significant part of the metabolomics study. The analysis is usually divided into statistical analysis and pathway analysis.

Based on the context, different data mining and statistical approaches are used in metabolomics research. Methods like fold change analysis, t-tests, and volcano plots are applied to two-group

data. For multi-group data, one-way variance analysis of variance (ANOVA) and related post hoc and correlation analyses are commonly used. For multivariate analysis, in addition to cluster analysis similar to classic principal component analysis (PCA), more and more studies have brought machine learning, such as random forest, into metabolomics research (113,114). PCA and random forest can also assess the clustering or scattering of quality control samples to identify any variability, which may indicate issues with assay quality. A Spanish group used metabolomics and other experimental approaches to understand the biochemical alterations induced by free and polymer-conjugated chemotherapeutic agents (115). The PCA plots from two types of drugs presented different profiles, with 35 other intracellular metabolites (115). Another study also demonstrated PCA in 3 dimensions to compare multiple groups of titanium nanotopographies in the skeletal stem cell physiology (116).

Screened metabolites are connected to their biological context through pathway and enrichment analysis. Pathway analysis in metabolomics is crucial in understanding the complex network of metabolic processes within a biological system. It involves identifying and interpreting the biological pathways and molecular interactions that underlie the observed changes in metabolite concentrations (111). This function analysis helps researchers extract meaningful insights from large metabolomics datasets and can be particularly useful in identifying potential biomarkers, understanding disease mechanisms, and gaining a deeper understanding of cellular metabolism. Mei et al. applied enrichment pathway analysis to prove the function of their antibacterial materials. The results showed a significant downregulation of the TCA cycle (117).

The combination of statistical and pathway analysis can present a comprehensive view of biological progress in various research fields.

1.4.1 Metabolomics in bone research

Metabolomics offers a comprehensive and unbiased approach to studying the intricate metabolic processes that underlie bone development, maintenance, and pathology. Metabolomics can provide valuable insights into the metabolic markers associated with healthy bone development and maintenance. Blood plasma or serum hosts various macromolecules that can coincide with peaks from small molecule metabolites, particularly in specific physiological or pathological conditions. The significant metabolites in blood plasma or serum garner growing interest for their potential in diagnosing human diseases (118). Bellissimo et al. applied metabolomics to determine plasma metabolic pathways and targeted metabolites related to bone resorption and formation markers in adults. They found that some

macronutrient-related pathways were highly associated with bone turnover markers, procollagen type I N-terminal propeptide, and C-terminal telopeptides of type I collagen (119). Awareness of metabolic changes in the patient can lead to early diagnosis of bone-related diseases, especially osteoporosis and bone injuries (120–122). Metabolomics can also accommodate a design of appropriate drugs to control the progression of the disease by following the decrease or increase of an effective biomarker in a disease (123).

Metabolomics has also been successfully used to study disease-induced metabolic changes and identify potential biomarkers *in vitro* and *in vivo*. Additionally, as demonstrated by multiple animal model studies, metabolomics is a valuable tool to predict the therapeutic effect of a bone protective agent on the recovery of bone diseases or its side effects on the normal function of bone. So far, several drugs have been designed to improve bone function, but their effectiveness can be challenged in further metabolomics studies (124). Furthermore, future metabolomics studies could help pinpoint the molecular targets for a therapeutic strategy.

1.4.2 Metabolomics in biomaterials research

Using metabolomics to explore biomaterials for the biomedical field is a novel and fascinating area of research. Trials had been made with MSCs on dynamic surfaces by Roberts et al. The difference in carbohydrate metabolism stood out, with detailed records of MSC growth and targeted differentiation footprints (125). Such fundamental studies can provide clues for further understanding cell-material interaction.

Existing literature demonstrates that biomaterial cues, including ions, oxygen, and regulatory metabolites, influence cell metabolism, potentially altering metabolic pathways and regeneration outcomes. Zhu et al. conducted metabolomics and lipidomics with their PLGA-based biomaterials. The omics result showed that the material effectively regulated multiple metabolites and more than 20 excessive metabolic pathways in osteonecrosis (126). Chen et al. applied metabolomics analysis for medium supernatant in functional ductal organoids at different time points (127). Their results showed that the metabolic influence caused by organoids was strong at the beginning (day 1) and decreased through time. Different analysis methods from metabolomics were also used differently among the biomaterials research fields. Li et al. developed an antitumor platform based on graphene-family nanomaterials, and the metabolomics characterization they conducted was shown by correlation pattern search. This analysis concluded that glycine/serine/threonine metabolism was upregulated, and alanine/aspartate/glutamate metabolism was downregulated by blood-treated graphene (128).

Combining the bio information from bone research and integrating metabolomics with osteogenesis confirmation assays, such as polymerase chain reaction, immunohistochemistry, and bone matrix mineralization, could provide a robust approach for guiding and assessing engineered biomaterials with desired properties (82). In recent years, researchers have noticed the potential of metabolomics to be applied in materials science. An increasing number of interdisciplinary studies are being published. Research in this area can provide a deeper understanding of the various principles of cells after encountering biological materials. In turn, metabolomics can guide researchers in the design of advanced functional materials.

2 Materials and Methods

2.1 Serum analysis of the animal model

2.1.1 Ethical aspects of the rat experiment

The Latvian Institute of Organic Synthesis animal facility corresponds to EU animal care regulations, and all manipulations were performed by FELASA C-certified personnel. The proposed animal experiments were designed following 3R principles and approved by the Food and Veterinary Service of the Republic of Latvia (ethics permit No. 123/2021).

2.1.2 Rat calvaria critical size defect model

In the *in vivo* assessment of the metabolic changes during bone healing, we employed a well-established critical-size calvaria defect model in rats (see Figure 6), renowned for its reproducibility and reliability in biomaterial evaluation. This model obviates the need for mechanical fixation and stimulation, allowing a direct assessment of biomaterial effectiveness. Calvarial defects, each 8 mm in diameter, were generated through trepanation of the calvarium in male Wistar rats aged 8-12 weeks, constituting a critical-size defect.

In one group (n=6), the defect site was left untreated, denoted as the "wo" group (without treatment). In the second group (n=5), the excised calvaria were divided into four segments and repositioned in the defect site to facilitate further recovery, referred to as the "w" group (with treatment). Blood samples were collected before and after surgery on days 1 and 3.

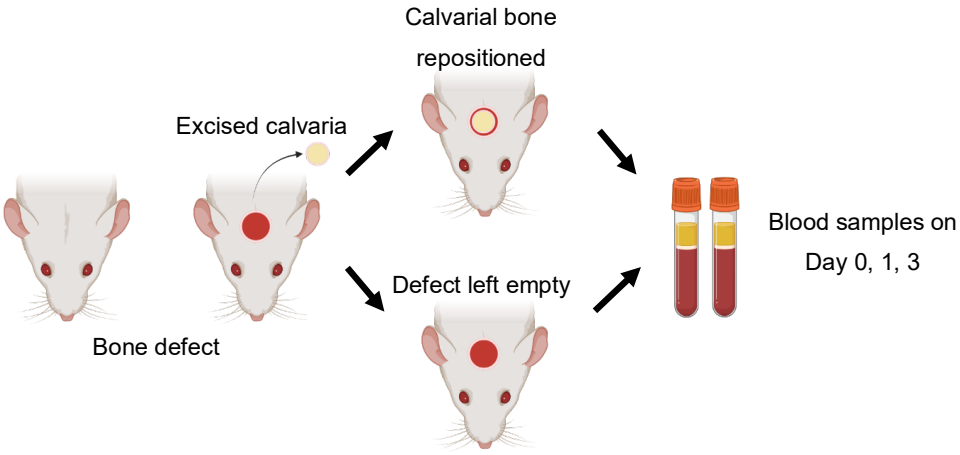

Figure 6 Illustration of the rat calvaria defect model and the blood sample collection.

2.1.3 Ethical aspects of sheep experiment

The ethics committee approved the experiment: Canton of Grisons, Switzerland. Ethics committee approval number: TVB2020/26.

2.1.4 Tibia critical size defect model on sheep

12 healthy female Swiss White Alpine Sheep within the age range of 2–5 years and bodyweight range of 60–79 kg were subjected to radiological and clinical assessments before enrollment. Acclimatization to post-surgical conditions was ensured for at least two weeks before the commencement of the experiment. The surgical procedure created critical bone defect (wedge of a length of 27 mm, width 13.7 mm and the length of the sides 19.2 mm), conducted with the surgeon blinded to the sheep's group, involved stepwise drilling (initially Ø3.5 mm, progressing to Ø4.9 mm) and insertion of four positive profile Steinmann pins (Ø5.0 mm) with a central thread into the medial aspect of the tibia. The T-bar was secured in the same plane between the two innermost Steinmann pins using two 2.7 mm conically-headed screws. Subsequently, a drilling guide affixed to the T-bar facilitated the creation of a Ø2.5 mm transcortical hole from the caudal aspect at the location of the bone wedge's apex. The defect created by the bone fragment is shown in Figure 7. The sheep serum was taken before surgery and on days 10, 22, and 29 after the surgery. Following a five-week observation period, the animals were euthanized with an overdose of pentobarbital.

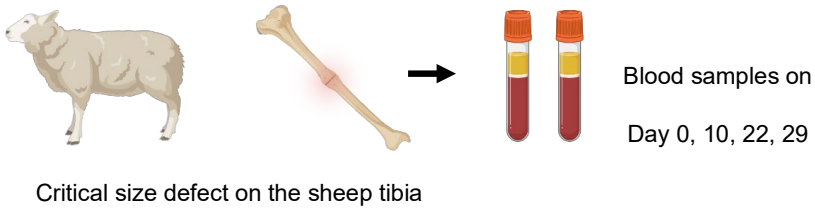

Figure 7 Illustration of sheep tibia defect model and the blood sample collection.

2.2 CaP biomaterials preparation

2.2.1 Synthesis of HAp and β-TCP

Calcium phosphate powders were synthesized *via* wet precipitation reaction following the equations below:

$$CaO + H_2O \rightarrow Ca(OH)_2$$

$$10Ca(OH)_2 + 6H_3PO_4 \rightarrow Ca_{10}(PO_4)_6(OH)_2 + 18H_2O$$

For the synthesis, the following reactants were used: calcium oxide (CaO, Fluka, from marble, ≥97 %, USA), orthophosphoric acid (H_3PO_4, Sigma, ≥85 %, USA), and deionized water. Calcium oxide was suspended in distilled water and milled at a rotation speed of 300 rpm with a Pulversette 5 planetary mill (Germany) to obtain a homogenous calcium hydroxide suspension. The acid solution was added to the calcium hydroxide suspension with a slow addition rate under stirring to avoid the formation of Ca-deficient apatite. The pH of the reaction media was adjusted in the range of 5.0-7.6, depending on the product phase composition. In short, the more acidic the pH, the more β-TCP phase, and the more alkaline the pH, the more HAp phase. The suspension was left to age for 20 hours at room temperature. Following aging, the suspension was filtered using a Buchner funnel, dried at 105 °C, and then ground in a mortar.

2.2.2 Synthesis of ACP

150 mM calcium chloride (≥98.0%, Supelco, USA) solution was prepared in deionized water to synthesize ACP. Subsequently, the pH of the calcium chloride solution was carefully adjusted to 11.5 using a 3M NaOH (≥99%, Emsure, Germany) solution. Following the pH

adjustment, an equal amount (150 ml) of 100 mM tri-sodium phosphate (85%, Sigma, USA) solution was added rapidly to the calcium chloride solution (total volume 300 ml). Throughout the process, continuous stirring was maintained. Immediately after precipitation, the suspension underwent centrifugation at 3000 rpm for 5 min, and the resulting precipitate was washed three times with deionized water. Later, the centrifuge tube containing the precipitate was immersed in liquid nitrogen for 15 minutes, followed by freeze-drying for 72 hours. The obtained power was stored in airtight containers until further processing (cold sintering).

2.2.3 Synthesis of ACP-Glu

To synthesize ACP with glutamate (ACP-Glu), a 150 mM calcium glutamate (99%, BenchChem, Germany) solution was prepared in Milli-Q® water. Subsequently, the pH of the calcium glutamate solution was carefully adjusted to 11.5 using a 3 M NaOH solution. Following the pH adjustment, an equal amount (150 ml) of 100 mM trisodium phosphate solution was added rapidly to the calcium glutamate solution (total volume 300 ml). Throughout the process, continuous stirring was maintained. Immediately after precipitation, the suspension underwent centrifugation at 3000rpm for 5 min, and the resulting precipitate was washed thrice with Milli-Q® water. Later, the centrifuge tube containing the precipitate was immersed in liquid nitrogen for 15 minutes, followed by freeze-drying for 72 hours. The obtained power was stored in airtight containers until further processing (cold sintering).

2.2.4 High-temperature sintering of CaP

2.2.4.1 Determination of CaP shrinkage

A pre-experiment was conducted before high-temperature sintering to determine the extent of calcium phosphate (CaP) shrinkage. Since different CaP phases exhibit varying shrinkage levels during the ceramic high-temperature sintering process, it is crucial to account for these differences when preparing the green ceramic bodies to ensure that the resulting samples are of nearly equal size. Maintaining uniform sample sizes is important because size disparities could influence cell adhesion to the CaP surface during cell experiments, potentially impacting the experimental outcomes.

CaP (pressed under the force of 30 kN) cylindrical tablets (height 2 mm, diameter 20 mm) prepared for high-temperature sintering were broken into small cubes (cross-sectional area 4 mm^2). The cubic sample was placed in the furnace of a heating microscope (EM301 Heating Microscope HT16 furnace, Hesse-instruments, Germany) to record and measure its shadow

change during the temperature increase effectively. Under light, the cross-section of the cubic sample produced a shadow, and the camera captured the shadow's area in real time. As the ceramic material shrinks during sintering, changes in the shadow's recorded area reflect the material's dimensional changes. The temperature was gradually increased to 1400 °C, with a heating rate of 80 °C/min from room temperature to 500 °C and 15 °C/min from 500 °C to 1400 °C. The recorded captured area changes during sintering were analyzed and presented as shrinkage curves.

2.2.4.2 Preparation of CaP tablets

The resulting powders from 2.2.1, 2.2.2, and 2.2.3 were compressed into cylindrical tablets (height 2 mm, diameter 20 mm) under a uniaxial force of 30 kN. The 0.71 g of the powder was weighed and transferred to an easy-retrieve cylindrical pressing die (Across International, Berkeley Heights, New Jersey, USA) with an inner diameter of 20 mm. The pressing die with the CaP powder inside was placed in a two-column lab press (PW 40; P/O/WEBER, Remshalden, Germany), and 30 kN was applied to the powder. The holding time of the applied force was 2 minutes. During pressing, the CaP powder was pressed into tablets with the same diameter as the die's inner diameter, as illustrated in Figure 8. The pressed tablets were then ready for further sintering procedures. As a result, pure HAp and β-TCP tablets were manufactured, and in the subsequent text, the HAp sample group is referred to as HAP and the β-TCP sample group is referred to as TCP. The biphasic calcium phosphates with a ratio of 95% HAp and 5% β-TCP were prepared and named as H95. The biphasic calcium phosphates with an 87% HAp and 13% β-TCP ratio were prepared and named H87. The biphasic calcium phosphates with a ratio of 58% HAp and 42% β-TCP were prepared and named as H58.

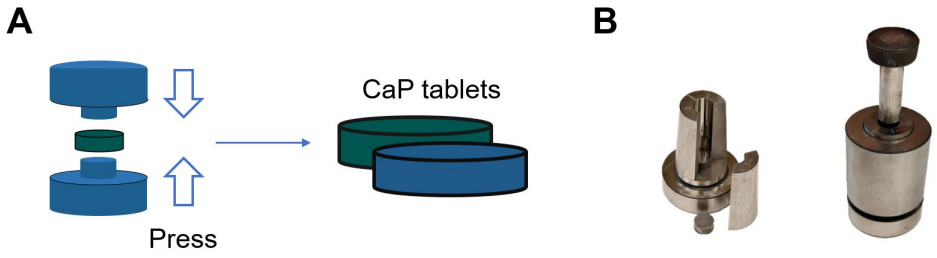

Figure 8 (A) Illustration of CaP tablets preparation. (B) Photo of the pressing die. (130)

2.2.4.3 Preparation of high-temperature sintered CaP samples.

The shrinkage curves derived from the CaP shrinkage study demonstrated the shrinkage behavior of pressed CaP tablets during sintering. However, these curves were not obtained for materials with fully formed structures and final dimensions. Consequently, based on the shrinkage curves, sintering trials of fully pressed tablets were individually evaluated to determine the most suitable size for each CaP type. The CaP cylindrical tablets (ø =20 mm), after compaction at 30 kN, were sintered using elevated temperatures. Because of the differences in CaP shrinkage ratios, the tablets were sintered at different temperatures to ensure the sizes were similar to the plate wells (ø =15 mm). The temperatures were adjusted according to the shrinkage curves and trials from 2.2.4.1. The temperatures for CaPs were: HAp: 990 °C; H95: 1030 °C; H58: 1135 °C; TCP: 1100 °C. The heating-up time was 3 hours, and the holding time was 1 hour.

2.2.5 Cold sintering of CaP samples

0.3 g of ACP, ACP-Glu, and HAp powders were used to prepare individual samples. After weighing, the powder was transferred to a 13 mm inner-diameter split-sleeve pressing die made of W18Cr4V hardened carbon tool steel (Across International, Berkeley Heights, New Jersey, USA). Transparent tape was used to cover core die surfaces, preventing sticking, scratching, and contamination. A PW 100 ES two-column electrohydraulic laboratory press (P/O/WEBER, Germany) was used for sample compression, applying a uniaxial pressure of 1.5 GPa. The pressure was incrementally raised at approximately 15 MPa/s and maintained for 5 minutes. Afterward, the pressure was gradually released, and the compacted sample was extracted from the die. The cold sintering process was carried out at 18 to 25 °C.

2.3 CAP characterization

2.3.1 X-Ray diffraction (XRD) analysis

To verify the phase compositions of CaPs, all sintered CaP discs were characterized by XRD (PANalytical Aeris, Netherlands). The characterization analysis was performed with X'Pert Data Collector, X'Pert Data Viewer, X'PertHighScore, and the International Centre for Diffraction Data PDF-2 (ICDD). XRD patterns were recorded using 40 kV and 15 mA, K-α1,2 wavelengths 1.541, step size 0.0435°, within range 2θ from 10°to 70°, time per step 147.39 ms, for crystalline phase identification, succeeding ICDD entries were used. The crystallographic patterns and corresponding peaks of HAp (ICDD 09-0432) and β-TCP (ICDD 09-0169) were

identified using X'PertHighScore software (Malvern Panalytical, Worcestershire, UK), based on data from the ICDD database.

2.3.2 Scanning electron microscope (SEM) imaging

CaP disks were mounted on sample holders with double-sided carbon tape, sputter-coated with carbon (LEICA EM ACE200, Flash, 20 pulses, Germany), and one connective line was drawn with silver paint. SEM images were acquired at 5 kV, 1 µs scanning speed, and a distance of 3.03 mm (Tescan Vega SEM, Czech) using frame averaging with 50 frames.

2.3.3 Determination of glutamate release from ACP-Glu

The cold-sintered ACP-Glu tablets were submerged in 1 ml of culture medium (DMEM, Thermo Fisher #11965, USA) in a 24-well plate (surface-treated, Costar, USA). 3 individual groups were used in parallel. The 50µL aliquots of dissolution media were collected into Eppendorf tubes at 3, 6, 9, 24, 48, and 72 hours after the initial sample immersion in DMEM. The release experiments were terminated after 72 hours of sample immersion, aligning with the 72-hour media exchange interval utilized in the MC3T3-E1 preosteoblast in vitro studies. Methanol (200 µL) was added to the collected media (50 µL), so the final methanol concentration was 80%. The collected samples were dried by vacuum centrifuge (Vacufuge plus - Centrifuge Concentrator, Eppendorf, Germany) and reconstituted with 10 µL of the isotopically labeled internal standard mix and 90 µL of methanol. Then, the samples were transferred into glass vials for further LC-MS analysis for detailed glutamate levels.

2.3.4 Determination of specific surface area

The specific surface area was measured with the N_2 adsorption system QuadraSorb SI (Quantachrome Instruments, USA). Prepared discs were broken into smaller pieces to fit the container. The samples underwent degassing in an AUTOSORB degasser (Quantachrome Instruments, USA) for 24 hours under vacuum at room temperature before generating the adsorption-desorption isotherms. The specific surface area of the compacted samples was determined using the Brunauer-Emmett-Teller model.

2.4 In vitro studies

2.4.1 Cell culture of NIH/3T3 cell line

NIH/3T3 fibroblast-like cells (ATCC CRL-1658, ECACC 93061524, UK) were cultured in Dulbecco's Modified Eagle's medium (DMEM, Gibco, USA) supplemented with 10% calf serum (Sigma, USA) and 1% Penicillin-Streptomycin (Gibco, USA). The cells were incubated at 37 °C in a 5% CO_2 environment for 3 days after thawing and before further experiments. The cells at passage 7 were seeded on material surfaces in a surface-treated 24-well culture plate (surface-treated, Costar, USA) with 4 replicates of each group. The seeding density was 6×10^4 cells/ml and 1 ml per well/tablet. The cells seeded in wells without materials were used as control groups. No negative control group was set; only a positive control was needed for metabolite extraction.

2.4.2 Cell culture of the MC3T3-E1 cell line

MC3T3-E1 preosteoblast-like cell lines (ATCC, USA) were cultured in Dulbecco's Modified Eagle's medium (DMEM, Gibco, USA) supplemented with 10% fetal bovine serum (heat-inactivated, Sigma, USA) and 1% Penicillin-Streptomycin (Gibco, USA). Cell culture media was modified with an extra 50µg/ml L-ascorbic acid (also known as vitamin C, 99%, Sigma, USA), according to the literature (131). The media recipe of DMEM lacks extra glutamate, which can perfectly mimic the bone injury situation shown in section 3.1 (Metabolic changes during bone healing in animal models). The specific cell culture duration is described later from 2.6.5 to 2.6.9. The cells at passage 5 were seeded on material surfaces in a surface-treated 24-well culture plate (surface-treated, Costar, USA) with 6 replicates for each group. The seeding density was 3.5×10^4 cells/ml and 1 ml per well/tablet. The cells seeded in wells without materials were used as control groups.

2.4.3 LDH cytotoxicity assay

In the LDH cytotoxicity assay (Thermo Fisher, USA), 50 µl of supernatant culture media (collected from the in vitro experiment described in section 2.6.2) was transferred into a 96-well plate (Tecan, Switzerland), followed by the addition of 50 µl of prepared LDH assay reagent. The plate was incubated at room temperature (20 °C) for 30 minutes, protected from light. 50 µl of stop solution was added to each well to stop the reaction. Absorbance was measured at 450 nm using a plate reader (Tecan, Infinite 300 PRO, Switzerland). Complete

cell-free culture media with the assay reagent served as the blank control. The LDH assay was performed for the ACP-Glu biomaterials experiment on days 1, 3, and 5. Statistical analysis was conducted using one-way ANOVA and a post hoc Tukey test to evaluate group differences.

2.4.4 Cell Counting Kit-8 viability assay.

Cell Counting Kit-8 (CCK-8, Sigma) was used to determine cell viability (132). The assay was applied for the NIH/3T3 cell line with heat-treated CaP tablets on days 1, 3, and 5. For the MC3T3-E1 cell line with cold sintered CaP tablets, the assay was applied on day 5. As the technical manual suggested, the assay was added directly to the cells in the culture wells, with 10% of the total volume. In detail, a 100 µl assay kit was added to 1 ml of culture media. The plate was incubated at 37 °C in a 5% CO_2 environment for 2 hours. The media was taken into a 96-well plate and read by a plate reader (Tecan, Infinite 300 PRO) under the absorbance of 450 nm. One-way ANOVA followed by a post hoc Tukey test was used to detect group differences.

2.4.5 Cell attachment on material surfaces

The cell attachment on high-temperature sintered samples (HAP, H95, H58, and TCP) was evaluated using SEM. After 24 h of incubation in culture media, high-temperature sintered sample discs were removed, and non-attached NIH-3T3 cells were rinsed with phosphate-buffered saline (PBS, Sigma, USA). Samples were washed twice with PBS (37 °C) and fixed in 4% paraformaldehyde solution for 40 minutes at room temperature. Then, samples were washed three times with room temperature PBS and dehydrated with gradual ethanol/water dehydration (ethanol concentration gradually increase as 25%, 50%, 75%, 90%, 100%; 5 minutes each) and dried for 20 minutes in fume hood under room temperature after adding one drop of hexamethyldisilane (Sigma, ⩾99%, USA) on top of the material. Dried samples were mounted on sample holders with double-sided carbon tape and sputter-coated with carbon (LEICA EM ACE200, Flash, 20 pulses, Germany), and one connective line was drawn with silver paint. SEM images were acquired at 5 kV, 1 uS scanning speed, and a distance of 3.03 mm (Tescan Vega SEM, Switzerland) using frame averaging with 50 frames.

2.4.6 Colorimetric alkaline phosphatase (ALP) assay

ALP assay was applied to evaluate the ALP level of the cells on different materials (from 2.4.2) to evaluate the initial stages of osteogenesis. 4 mg/ml p-nitrophenyl phosphate (pNPP, Sigma,

USA) solution was prepared from p-nitrophenyl phosphate tablets (Sigma, USA). ALP activity was assessed by measuring the formation of p-nitrophenol (p-NP) from pNPP, using a standard curve prepared from a p-nitrophenol stock solution (Sigma, USA). At each time point, 100 µL of culture media supernatant was collected in 1.5 mL Eppendorf vials. Subsequently, 100 µL of deionized water, 250 µL of alkaline buffer (Sigma, USA), and 50 µL of pNPP solution were added sequentially. The vials were gently shaken by hand for thorough mixing and incubated at 37 °C for 15 minutes. After incubation, 100 µL of the solution was transferred into a 96-well plate (Tecan, Switzerland) and measured at 405 nm using a plate reader. ALP levels were assessed on days 3, 7, and 14, with triplicates for each group. One-way ANOVA followed by a post hoc Tukey test was used to detect group differences.

2.4.7 Free calcium analysis

The calcium level in conditioned media from MC3T3-E1 cells cultured on ACP, ACP-Glu, HAP, and CNT was measured on day 10, with 7 replicates. Calcium concentration in media was determined using a calcium colorimetric assay kit (Sigma, USA). For each sample, 50 µL conditioned media was transferred to a 96-well plate (Tecan, Switzerland), followed by the addition of 90 µL chromogenic reagent and 60 µL calcium assay buffer provided with the assay kits was then added to each well. The plate was incubated at room temperature for 15 minutes, protected from light, and then immediately read by the plate reader (Tecan, Switzerland), with the absorbance at 575 nm. A standard curve was generated using the calcium standard provided with the kit, and calcium levels were calculated accordingly. Statistical analysis was performed using one-way ANOVA and a post hoc Tukey test to detect group differences.

2.4.8 Free phosphate analysis

Phosphate in conditioned media of MC3T3-E1 cells cultured on ACP, ACP-Glu, HAP, and CNT groups was measured on day 10, with 6 replicates. A phosphate assay kit (Sigma, USA) was applied to measure the free phosphate level in the media. 50 µL conditioned media was taken into the 96-well plate (Tecan, Switzerland), followed by 100 µL of the malachite green reagent to each well. The plate was incubated for 30 minutes at room temperature, avoiding light interference. The plate reader (Tecan, Switzerland) set to the absorbance at 620 nm was employed for measurements. A standard curve was generated using the phosphate standard provided with the kit, and phosphate levels were calculated accordingly. One-way ANOVA followed by a post hoc Tukey test was used to detect group differences.

2.4.9 OPN (Osteopontin) and OCN (Osteocalcin) activity

Mouse Osteocalcin ELISA Kit provided by Abcam (ab285236, UK) and Mouse Osteopontin ELISA Kit (RAB0437) provided by Sigma (USA) were applied to test the OPN and OCN levels in culture media after culturing MC3T3-E1 cells with ACP, ACP-Glu, HAP, and CNT groups for 7 days and 14 days. Media samples were collected in 1.5 mL Eppendorf tubes and stored at -80 °C for further analysis. 100 µl conditioned media was added to each well for the OCN ELISA kit, and 50 µl conditioned media was added to each well for the OPN ELISA kit. The assay was applied according to the manufacturer's guidance. According to the user manual, biotinylated detection antibody, HRP Conjugate working solution, substrate, and stop solution were sequentially added to the wells, with washing steps between each addition. Absorbance was measured at 450 nm using a microplate reader (Tecan, Switzerland).

2.4.10 Alizarin Red staining

In this study, Alizarin Red solution (MilliporeSigma, USA) was applied. To avoid staining the materials, MC3T3-E1 cells were not directly cultured on them. The materials were left on the transwell insert on top of the cultured cells (Figure 9). The investigation focused on the sample groups (ACP, ACP-Glu, HAP, and CNT) cultured for 21 days on a 6-well plate with 3 replicates. After removing the culture media, cells were gently rinsed with PBS. Subsequently, the cells were fixed with 4% paraformaldehyde at room temperature for 20 minutes. The volume of 4% paraformaldehyde was 1 ml per well. After fixation, paraformaldehyde was aspirated, and the cells were further rinsed with PBS. Alizarin Red solution, 1 ml per well, was added to the wells, and staining proceeded for 15 minutes at room temperature. Following staining, the Alizarin Red solution was removed, and the wells were washed with deionized water 2 times. Microscope images were captured by a microscope (Optika, Italy) to evaluate the degree of mineral deposits that were stained red. Through this, the cell mineralization ability can be evaluated.

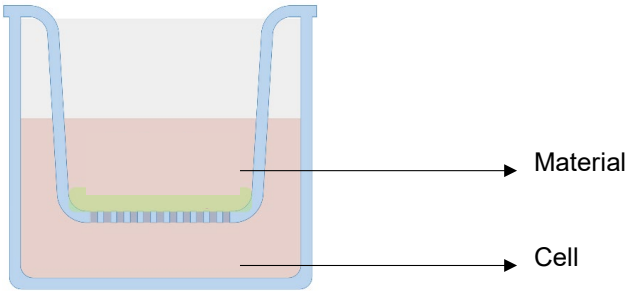

Figure 9 Illustration of Alizarin Red staining layout. Cells were cultured at the bottom (wells), and the biomaterials were placed in transwells. Staining was applied to the cells directly.

2.5 Metabolomics analysis

2.5.1 Liquid chromatography–mass spectrometry (LC-MS) based metabolomics

Targeted quantitative metabolite analysis was conducted using HILIC-based liquid chromatography and mass spectrometric detection employing an Orbitrap Exploris 120 system (Thermo-Fisher Scientific, USA). Metabolites were separated on an ACQUITY UPLC BEH Amide 1.7 µm 2.1 x 100 mm analytical column (Waters, USA). The gradient elution was carried out using 0.15% formic acid (≥98%, Sigma, USA) and 10 mM ammonium formate (≥99.0%, Sigma, USA) in water as mobile phase A and a solution of 0.15% formic acid and 10 mM ammonium formate in 85% acetonitrile as mobile phase B. The initial conditions were set to 100% mobile phase A. After 6 minutes, the mobile phase A level was reduced to 94.1%. From 6.1 to 10 min, mobile phase A was set to 82.4%, and from 10 to 12 min, mobile phase A was set to 70.6%. The column was then equilibrated for 6 min at initial conditions. The total analysis time was 18 minutes. The mobile phase flow rate was 0.4 mL/min; the injection volume was 2 µL, and the column temperature was 40 °C. For MS detection, an Orbitrap Exploris 120 mass spectrometer was used. The MS analysis was performed in ESI positive and ESI negative modes, Full Scan mode, with a mass range from 50 to 500 m/z. The ESI spray voltage was set to 3.5 kV in positive mode and 2.5 kV in negative mode, the gas heater temperature was set to 400 °C, the capillary temperature was set to 350 °C, the auxiliary gas flow rate was set to 12 arbitrary units, and the nebulizing gas flow rate was set to 50 arbitrary units. Seven-point calibration curves with internal standards (carnitine NSK-B-1 and amino acid MSK-A2-1.2, Cambridge Isotope Laboratories, USA) were used for quantitative analysis. Tracefinder 51.1 General Quan (Thermo-Fisher Scientific, USA) software was used for LC-MS data processing and quantification.

The metabolite profiles were analyzed using MetaboAnalyst 5.0 and GraphPad Prism 9. The data were expressed as mean ± SD. The metabolite concentration data were normalized by Log transformation and Pareto scaling (mean-centered and divided by the square root of the standard deviation of each variable) for statistical analysis. Pathway and enrichment analysis used the Small Molecule Pathway Database as the pathway library.

2.5.2 Metabolite analysis of animal serum

Metabolites were extracted through a methanol-based extraction protocol. 10 µL serum was taken into an empty Eppendorf tube and mixed with 80 µL methanol and 10 µL standard (the total methanol ratio is 80%). Each sample was vortexed for 15 seconds and then centrifuged at 6000 rpm (Microspin 12, BioSan, Latvia). The liquid was transferred into an HPLC glass vial. Targeted quantitative metabolite analysis was conducted using a HILIC-based separation technique and mass spectrometric detection utilizing the Thermo Orbitrap QExactive mass spectrometer (Thermo-Fisher Scientific, USA).

2.5.3 Intercellular metabolites collection

Cells were cultured in triplicate under the conditions described in 2.4. Before the extraction and cell culture media were removed, cells were washed with ammonium bicarbonate (≥99.5%, NH_4HCO_3, Sigma, USA) solution (75 mM, 37 °C) to eliminate the influence of metabolites in the culture medium. Cells were quenched with 1 mL of cold 80% v/v methanol (≥99.9%, CH_3OH, Sigma, USA) per well and harvested by scraping. The cold methanol effectively reduced enzymatic activity while lysing the cells. The collected samples were vortexed for 15 seconds to ensure complete dissolution of metabolites, followed by centrifugation at 6000 rpm (Microspin 12, BioSan, Latvia) at room temperature for 5 minutes. The supernatant, containing the metabolites, was collected to separate it from the solid phase, which consisted of organelle fragments and proteins. Despite the low temperature, these proteins may contain functional enzymes capable of reacting with metabolites. The collected supernatant was dried by a vacuum centrifuge. Afterward, 10 µL of the isotopically labeled internal standard mix (Chromsystems, Germany) was added to dried samples, followed by 90 µL of methanol. Reconstituted samples were transferred to glass vials and applied for LC-MS analysis.

2.5.4 Metabolite adsorption on CaP tablets

The experiments were divided into two sections to evaluate the metabolites adsorbed on CaP tablet surfaces.

In the first part, the high-temperature sintered HAp tablets were used to detect whether small molecule metabolites can adhere to the material surface. The same complete culture media used in cell culture (3.4.1), Dulbecco's Modified Eagle's medium (DMEM, Gibco, USA), supplemented with 10% calf serum (Sigma, USA) and 1% Penicillin-Streptomycin (Gibco, USA), was applied with the materials with 1 mL per well in a 24-well plate. Tablets were submerged in the culture media. The submersion continued for 1 day, and 3 replicates were set for each group. Wells containing only culture media without CaP tablets served as comparison control groups. Before sample collection, the media supernatant was carefully removed, and the wells were rinsed with ammonium bicarbonate solution, followed by quenching with cold 80% (v/v) methanol to match the protocol used for intracellular metabolite extraction. These steps are performed to remove possible metabolites collected in the culture medium, and the metabolites that are adsorbed on CaP or culture plate surfaces would be dissolved in 80% (v/v) methanol solution. The methanol-metabolite solution was collected by pipetting and scraping. Scraping the CaP and culture plate surfaces was used to simulate the operation process of cell experiments, so that the results could better reflect the effect of surface adsorption of metabolites in cell experiments. The extracts were dried by vacuum centrifuge, and 10 μL of the isotopically labeled internal standard mix (Metabolomics QReSS Standard Mix 1, Cambridge Isotope Laboratories, USA) was added to the dried samples, followed by 90 μL of methanol. Reconstituted samples were transferred to glass vials and used for LC-MS analysis. The wells without materials but submersed with media were used as the control. The metabolite profile results were analyzed as described in 2.5.5. Because of the expected variance of mass spectrometry measurements (typical CV of 5%), a fold change greater than 0.1 compared to the intracellular results is considered adsorbed.

The second part used cold-sintered HAp, ACP, and ACP-Glu tablets. The control group was the 24-well plate (surface-treated culture plate) without any material. For each group, 3 tablets (wells) were applied respectively. HAp, ACP, and ACP-Glu tablets were sterilized with 70 % ethanol for 1 hour and UV light for 30 minutes on each side before submersion in culture medium (DMEM, Thermo Fisher #11965, USA) 1mL for each well. The submersion continued for 3 days to ensure the complete adsorption of small molecules. On day 3, the medium was

taken out; the tablets were washed with ammonium bicarbonate (NH_4HCO_3, ≥99.5%, Sigma-Aldrich, USA) solution (75 mM) 2 times to ensure the remaining free small molecules were washed away. Then, the tablets were submerged in 1mL 80 % v/v methanol and shaken on an orbital shaker (OS-10, BioSan, Latvia) for 5 minutes at 60 RPM. The methanol was later collected in Eppendorf microtubes and vacuum centrifuged (Vacufuge plus - Centrifuge Concentrator, Eppendorf, Germany). Afterwards, 10 µL of the isotopically labeled internal standard mix was added to dried samples, followed by 90 µL of methanol. Reconstituted samples were transferred to glass vials and applied for liquid chromatography-mass spectrometry (LC-MS) analysis.

2.5.5 Statistical analysis

The metabolite profiles were analyzed by MetaboAnalyst 5.0 and GraphPad Prism 9 (133). The data were expressed as mean ± SD with at least 3 replicates. Metabolomics data were normalized by Log transformation and Pareto scaling (mean-centered and divided by the square root of the standard deviation of each variable) for statistical analysis. Volcano plots were made using the data from t-tests and fold change calculations. Analysis of variance (ANOVA), a collection of statistical models and their associated estimation procedures used to analyze the differences among means, was applied in multiple comparisons to select the most significant metabolite. PCA, a dimensionality reduction technique used to transform and summarize data into a smaller set of uncorrelated variables called principal components, capturing the most significant variance in the original dataset, was applied to distinguish the differences between the groups. An ensemble machine learning technique, Random Forest, was utilized to screen for specific metabolites. This machine-learning technique combines multiple decision trees to make more accurate predictions or classifications by aggregating the results of individual trees. It improves model robustness and generalization while reducing the risk of overfitting. In the classification processes with rats, both models ran 500 trees, and the sheep models ran 5000 trees. Pathway and enrichment analysis used the Small Molecule Pathway Database as the pathway library. Visualization of the enrichment network of metabolites correlation was performed by Metscape in Cytoscape 3.9.1.

3 Results and Discussion

3.1 Metabolic changes during bone healing in animal models

3.1.1 Critical-size calvaria defect model

As described in the method section, in the critical-size rat calvaria defect model, the experimental group where the calvaria had been removed and repositioned back is considered as animals with treatment, and the experimental group where the calvaria had been removed but kept empty, leaving the defect, is considered as animals without treatment.

3.1.1.1 Overview of metabolite profiles

The obtained serum metabolites are summarized in the heatmap below (see Figure 10). Due to the importance of amino acids in metabolic networks, major amino acids are the primary research targets of targeted metabolomics. There are apparent differences between the metabolite profiles obtained from the initial and the samples after the surgery. Compared with the beginning (day 0), the overall metabolite level in the heat map after 1 day and 3 days is lower. This overall profile (Figure 10) shows that the metabolite levels (24 out of 32) decreased mainly after the bone defect was created and during the healing process. The decrease in the metabolite levels happened in both experimental groups, indicating that even with the autograft, there is still a significant depletion of the metabolites in critical-size hard tissue defects.

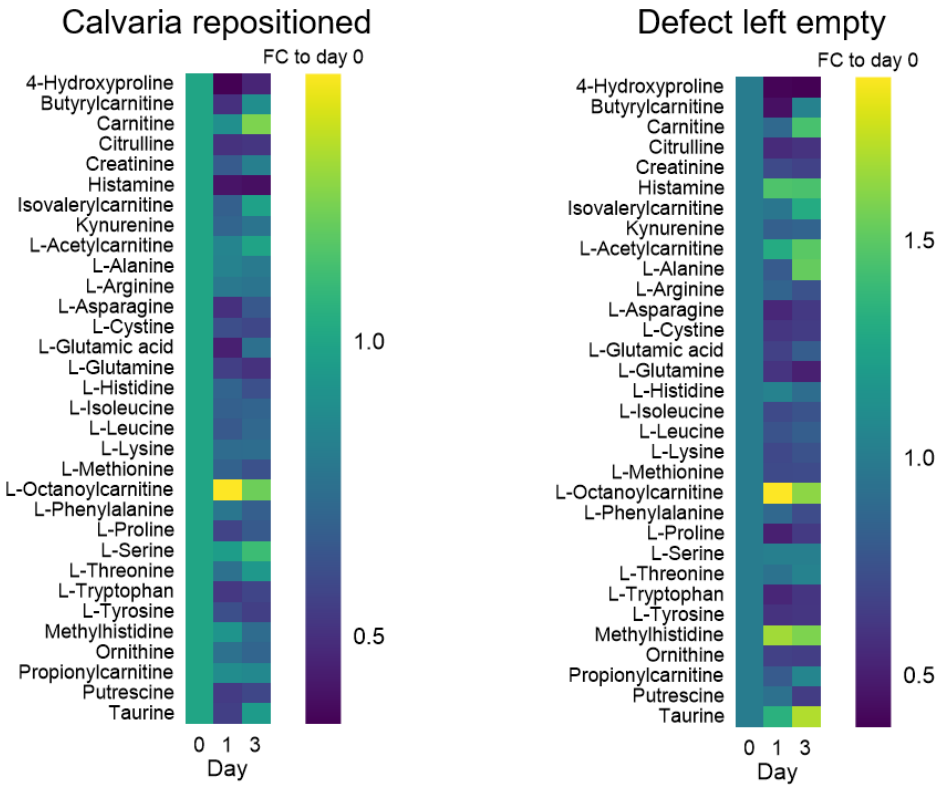

Figure 10 Fold changes (FC) compared to Day 0 of serum metabolites of rats with replaced calvaria (left) and serum metabolites of rats without the calvaria repositioned to the defect (right).

PCA plots (Figure 11) show that the metabolite profiles significantly changed after critical defect creation surgeries. This suggests that the surgical procedure had a substantial impact on the metabolic profiles of the animals. The two time points (day 1 and day 3) after the surgery, however, presented clustering. The PCA plots show that, at day 1 and day 3 post-surgery, the metabolite profiles in both groups cluster together. This suggests that, over time, there is a convergence or similarity in the metabolic changes in response to the surgery.

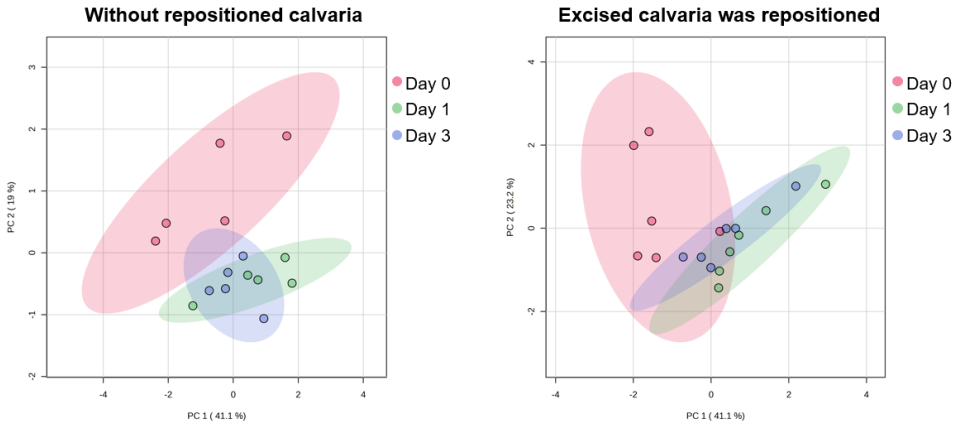

Figure 11 PCA plots of metabolite profiles.

3.1.1.2 Identification of metabolic changes during bone healing

In order to screen the metabolites with the most significant changes, correlation analysis and random forest were applied. Both methods can identify and rank the metabolites with the most statistically significant changes.

Correlation analysis can be performed either against a given feature or against a given pattern. The pattern is specified as a series of numbers separated by "-," representing the time in days 0, 1, and 3. Figure 12 shows the correlation patterns of the top 25 metabolites.

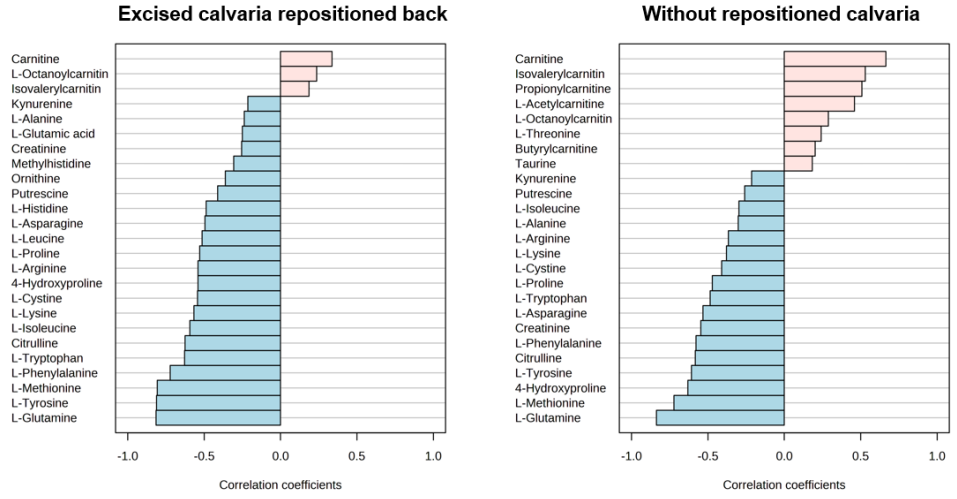

Figure 12 Correlation pattern of the top 25 metabolites correlated with day 0, 1, and 3. The value represents the positive and negative linear correlation.

Only carnitine and carnitine derivatives (isovalerylcarnitine, propionylcarnitine, acetylcarnitine, octanoylcarnitine) presented a positive correlation within both experimental groups over time. The correlation coefficient of carnitine is 0.33 in the repositioned calvaria group and 0.66 (significant) in the group where defects were left empty. This suggests that serum from animals with critical size defects exhibits higher carnitine levels than in pre-defect conditions. Carnitine and its derivatives are essential for transporting long-chain fatty acids into the mitochondria, which are the energy-producing organelles in cells (134). This process allows fatty acids to be oxidized to generate ATP, the primary source of cellular energy. During injury and recovery, the body may require more energy to support various processes such as tissue repair, inflammation, and immune responses. Hence, higher carnitine levels may facilitate the fulfillment of increased energy requirements. Carnitine has been shown to have anti-inflammatory properties, which can be beneficial in the context of injury. It may help to modulate the immune response, reduce inflammation, and promote healing (135).

Glutamine stands out as the metabolite with the strongest negative correlation to time, with a correlation coefficient of -0.82 in the group where the calvaria was repositioned and -0.84 in the group where the defect was left empty. Glutamine levels decreased significantly for both experimental groups: from 44.5 µM to 37.4 µM (Figure 13).

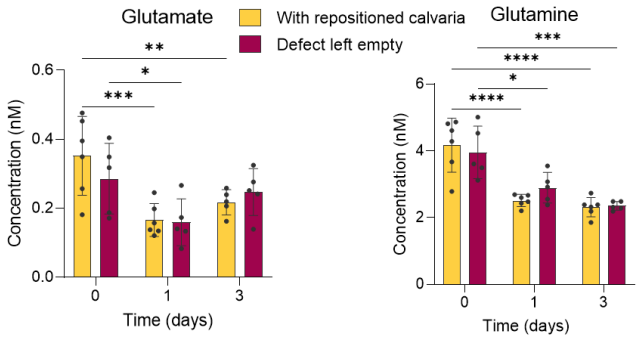

*Figure 13 Concentration of glutamate and glutamine in serum (*P < 0.05; **P < 0.01; ***P < 0.001; ****P < 0.0001)*

Random forest identified glutamine as a critical variable in explaining the time-dependent changes in the context of bone injury. In Figure 14, the color represents the trend of how this metabolite typically responds under different conditions, offering insights into its relative contribution to the model's predictions. The observation that both PCA plots and random forest analysis identify glutamine as a key metabolite that decreases over time strengthens the confidence in the reliability of this finding. Both methods demonstrated that glutamine levels

decrease after bone injury, serving as a marker of critical-size defects. Glutamine is mainly metabolized into glutamate. Lower glutamine levels have clinical implications in wound healing, limiting patient recovery and outcomes. It could indicate a higher demand for glutamine in the body during the initial stages of injury and healing. In addition, dietary supplementation of glutamine can increase α-ketoglutaric acid levels and, therefore, enhance the tricarboxylic acid cycle (TCA cycle). The results suggest that clinicians should consider monitoring glutamine levels in patients recovering from bone injuries and supplementing if levels are insufficient.

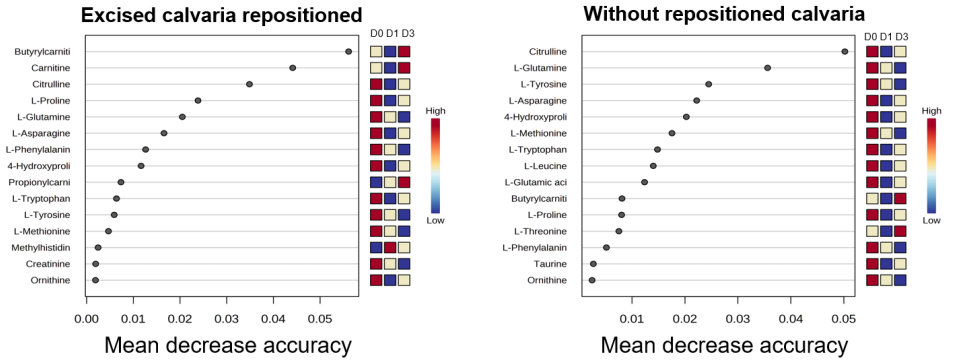

Figure 14 Random Forest identification of most influential variables. The number of trees was controlled at 500, with 7 predictors.

Glutamine is a versatile amino acid with critical roles in cellular metabolism and signaling pathways. Significantly, a substantial portion (around 97%) of glutamine undergoes degradation to form glutamate, subsequently serving as a substrate for synthesizing urea and glucose or as an energy source for ATP generation (see Figure 15). It is important to mention that while glutamine plays a pivotal role as a precursor for numerous critical compounds (e.g., purines, glucosamine, etc.), these account for a relatively small portion (<3%) of the overall glutamine metabolic processes (Figure 15). Additionally, glutamine functions as an anabolic signaling molecule, often activating the mammalian target of rapamycin (138). During injury and recovery, there is an increased metabolic demand, particularly for energy, as the body undergoes various repair processes (136). Glutamine is often used as an energy source in these situations, which can reduce its levels. As the significant downstream of glutamine, glutamate can serve as a precursor for synthesizing glutamine in the body. When glutamine is depleted, supplying glutamate via biomaterials could aid in restoring glutamine levels (139). Cells can

absorb glutamate and enzymatically convert it into glutamine. This process is crucial for tissues with elevated metabolic demands, such as bone and muscle, during healing.

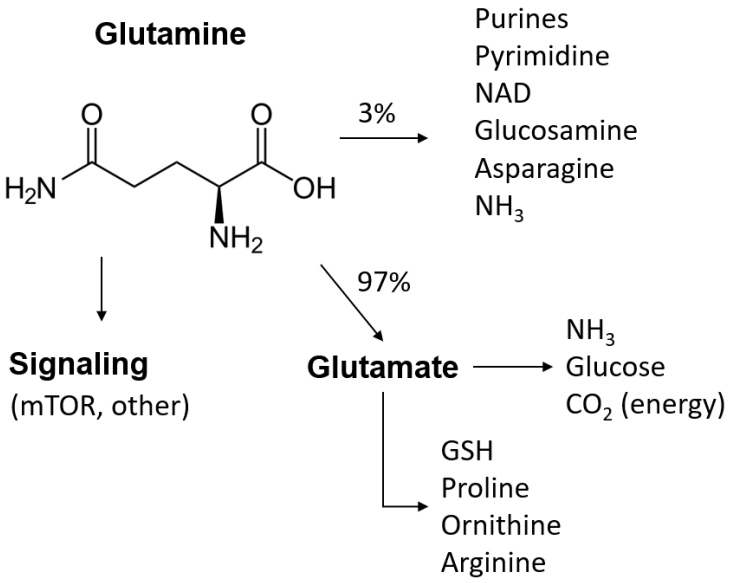

Figure 15 The metabolism of glutamine (138,139)

Given the significance of glutamate and glutamine, their concentration changes were further analyzed across both experimental sample groups at day 0, day 1, and day 3 (Figure 16). The results revealed a similar trend from the experimental groups with and without the repositioned calvaria bone fragments. Nevertheless, a decrease in glutamate concentration was observed in both experimental groups. In the group with repositioned calvaria, levels declined from 0.35nM to 0.17 nM on day 1 and to 0.22 nM on day 3. Similarly, in the group with empty defects, concentrations dropped from 0.29 nM to 0.16 nM on day 1 and to 0.26 nM on day 3. (Figure 13). It might indicate that glutamate shortage has been alleviated to some extent. At the same time, glutamine concentration in the experimental samples decreased.

3.1.2 Sheep tibia critical size defect model

3.1.2.1 Identification of metabolic changes during bone healing

Serum of the sheep with critical size defect (wedge of a length of 27 mm, width 13.7 mm and the length of the sides 19.2 mm) at tibia were collected and analyzed as described in 2.1.4 The

sheep serum was taken before surgery and on days 10, 22, and 29 after the critical size defect at tibia was created. In total, 46 metabolites were targeted for detection and quantification. The overall serum metabolites profile is shown in Figure 16.

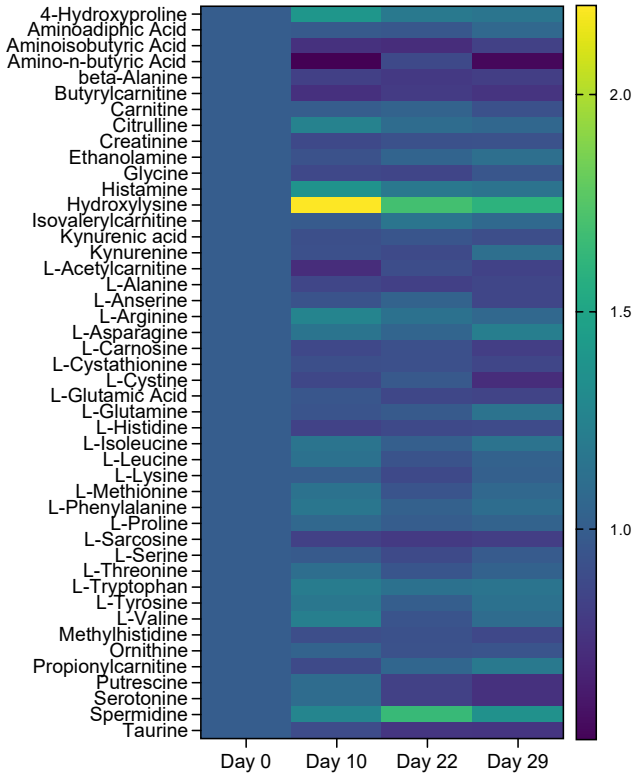

Figure 16 The serum metabolite profile from sheep with critical-size tibial defects is presented as fold changes in a heatmap, with metabolite concentrations normalized to the values obtained on Day 0.

A chronological correlation pattern search was systematically conducted from Day 0 and progressed through Day 10, Day 22, and Day 29 (as illustrated in Figure 17). The findings indicated that myristoyl carnitine exhibited the most substantial downregulation over time, followed by glutamate, taurine, and carnosine. The results showed that myristoylcarnitine is very sensitive to bone injury (Figure 17), the subsequent treatment (mechanical stress), or the overall physiological changes during the healing and recovery process. Myristoylcarnitine is a fatty acid myristic acid derivative and plays a role in fatty acid metabolism (134). The downregulation of myristoylcarnitine may reflect a shift in metabolic priorities. During injury and healing, the body's metabolic focus may shift toward energy production, tissue repair, and

other processes. The inflammation and oxidative stress during bone healing can influence fatty acid metabolism, potentially leading to changes in metabolites like myristoylcarnitine (141). During the long-term bone repair process, the intensity of inflammation seriously affects the healing effect.

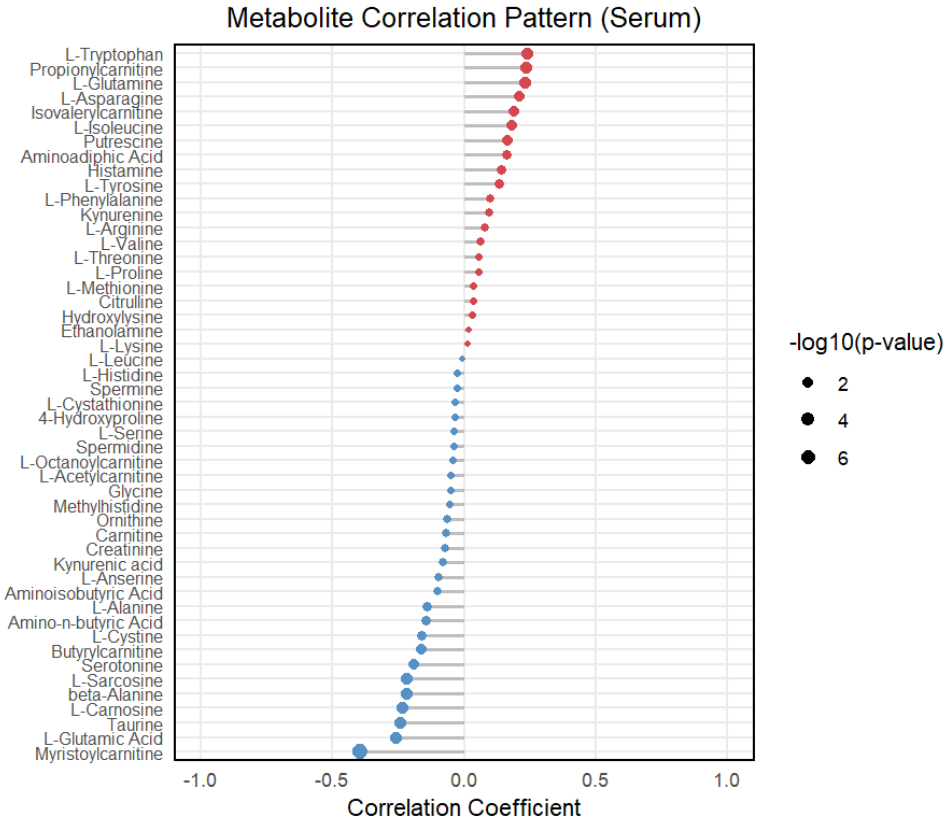

Figure 17 Correlation pattern of the top 25 metabolites correlated with day 0, 10, 22, and 29. The correlation coefficient of L-Glutamic acid is -0.26053 (p=0.000226), ranked as the second-most-impacted metabolite.

Similar to the serum data analysis from the rat model, a rigorous analysis using random forest was applied to investigate the factors influencing the time-dependent changes in the context of bone injury and subsequent healing in the sheep model. The study pinpointed glutamate as a critical variable that substantially impacted the observed changes over time (see Figure 18). The noteworthy finding is the consistent downward trend in glutamate levels across all time points examined, namely, from the baseline measurement at day 0 through the subsequent evaluations at day 10, day 22, and concluding at day 29, according to the color changes in the

line of L-glutamic acid (glutamate). Among many metabolites, glutamate tends to decrease gradually with time. This progressive reduction in glutamate levels throughout the healing process underscores the significance of glutamate as an informative marker representing the temporal dynamics of the healing process in response to bone injury.

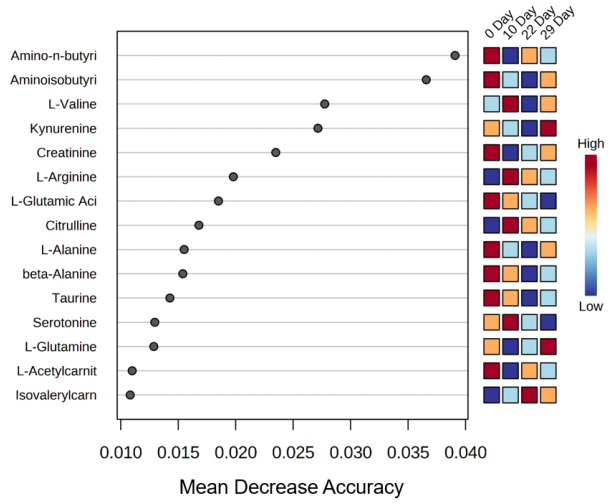

Figure 18 Random Forest identification of most influential variables. The number of trees was controlled at 5000, with 7 predictors.

Taking the glutamate data by itself, there is a significant decrease. The significance, represented by the P-value (Figure 19), also showed a more substantial value when the time gap changed from 0.445 nM (D0) to 0.374 nM (D29). In other words, the longer the interval, the smaller the P-value and the more significant the difference. This indicates that the decrease becomes more pronounced as the observation period extends. Interestingly, there is no significant difference between day 22 and day 29, indicating that the downward trend of glutamate had already gradually stopped and leveled off. The decrease in glutamate levels throughout the healing process suggests potential metabolic alterations, cellular activity shifts, or biochemical pathway variations. Further investigation is warranted to elucidate the specific mechanisms and functional implications of this observed glutamate decrease in the context of bone injury and healing, as it holds valuable insights into the underlying processes and potential therapeutic targets in bone regeneration and repair.

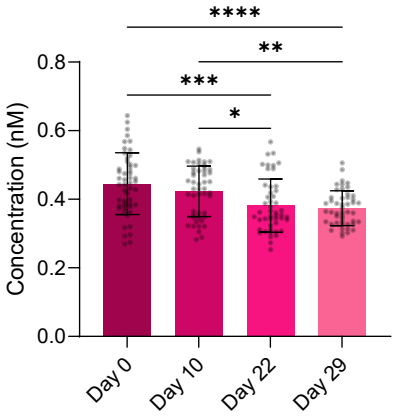

*Figure 19 Glutamate level of serum during bone healing. (*P < 0.05; **P < 0.01; ***P < 0.001; ****P < 0.0001).*

Glutamate, a crucial carbon source in the TCA cycle, plays a central role in metabolic processes that impact energy production and cellular functions (142). Glutamate is pivotal in transamination, facilitating the removal of α-amino nitrogen from amino acids. This process is essential for preserving nitrogen balance and enabling the synthesis of various nitrogen-containing compounds vital for cellular activities. Amino acids belonging to the "glutamate family," including arginine, ornithine, proline, histidine, and glutamine, rely on converting to glutamate for their metabolic clearance (143). Glutamate has been applied in tissue engineering as a poly(glutamic acid) biomaterial (144). Poly(glutamic acid) can also be combined with CaPs for bone tissue engineering (145). It has been proven that such poly(glutamic acid)-based biomaterials can promote tissue regeneration and regulate a macrophage-regulating microenvironment. The findings of the glutamate level are consistent with rat model experiments. Identifying glutamate as a downregulated metabolite opens the possibility of developing targeted therapeutic interventions.

The consistent findings across two mammalian species powerfully demonstrate the crucial role of glutamate and its metabolism in hard tissue repair, enhancing the reliability of our conclusions. These results provide a solid foundation for developing innovative biomaterials targeting glutamate-related pathways.

3.2 Development of CaPs scaffolds

The study of CaP biomaterials consists of two main parts. The first focuses on investigating the effects of CaP materials on cell metabolism to deepen the understanding of cell-material interactions at the molecular level. Given the limited knowledge on integrating metabolomics with ceramic materials, it is essential to study common calcium phosphate materials to establish a metabolic perspective on these interactions, which will contribute to advancements in biomaterials research. The second part aims to develop novel CaP-based biomaterials inspired by findings from previous animal serum metabolomics studies. These newly developed materials were further characterized and evaluated for their potential applications.

3.2.1 The preparation of CaPs scaffolds

3.2.1.1 Shrinkage measurement from hot sintering

This preliminary experiment was conducted to ensure that the CaP biomaterials prepared for subsequent cell experiments have comparable surface areas for cell culture. The results are shown in Figure 20, where HAp and BCP start shrinking at lower temperatures, starting at 700 °C. HAp's shrinkage stops at 1150 °C. The temperature represents the point where grain rearrangements and densification stabilize. β-TCP starts shrinking at around 1000 °C. HAP has a hexagonal crystal structure and a lower activation energy for sintering (Table 2). In contrast, β-TCP has a rhombohedral structure and requires higher temperatures to activate significant atomic diffusion and densification (Table 2). The shrinkage test here is a preliminary experiment for the cell experiment of CaP material to have a basic view of how those pressed CaP tablets behave during high-temperature sintering.

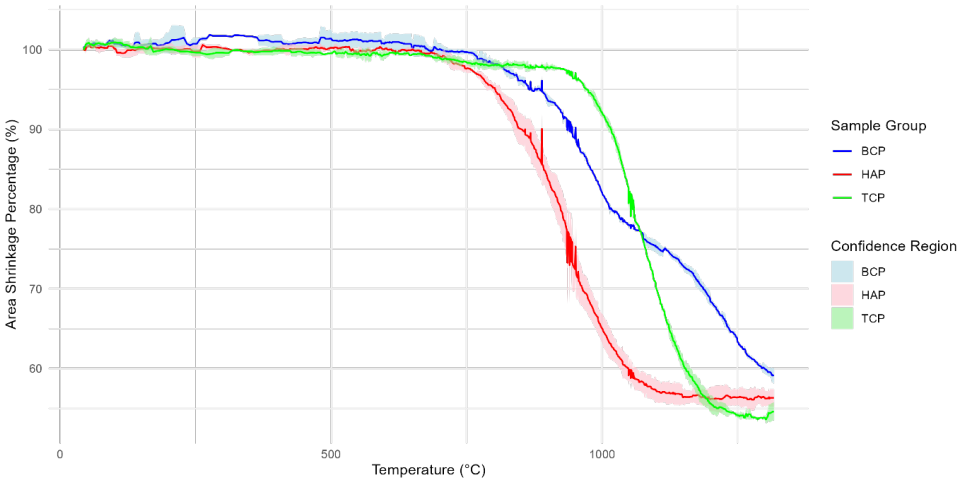

Figure 20: The changes in surface area (fold changes) during high-temperature sintering with different materials

3.2.1.2 High-temperature sintered CaPs

As a preliminary experiment for cell experiments, some attempts were made to test the sizes of different CaPs after sintering. Similar cell culture areas can narrow the gap between groups, making the variables appear in the material rather than the area. Different trials were made to prepare the CaP tablets with suitable sizes that fit the 24-well cell culture plate, as shown in Table 3 below. The tests resulted in the temperature selection used for sample preparation for *in vitro* studies (HAp: 990 °C; H95: 1030 °C; H58: 1135 °C; TCP: 1100 °C).

Table 3 CaP tablets sintered under different temperatures

Material	Temperature℃	Diameter(mm)	Height(mm)
β-TCP	1100	14.94±0.08	1.36±0.01
β-TCP	1060	16.01±0.10	1.49±0.01
58/42	1270	14.57 ±0.07	1.47±0.01
58/42	1250	14.28±0.08	1.50±0.01
58/42	1185	14.18±0.08	1.35±0.01
58/42	1135	14.44±0.05	1.35±0.01
87/13	1205	15.30±0.12	1.49±0.01
87/13	1175	15.70±0.10	1.54±0.01
87/13	1100	16.67±0.09	1.60±0.01
87/13	1000	17.48±0.08	1.62±0.01
95/5	1000	15.09±0.05	1.36±0.01
95/5	1030	14.83±0.05	1.35±0.01
HAp	1000	14.93±0.05	1.24±0.01
HAp	990	14.88±0.06	1.35±0.01
HAp	950	15.43±0.06	1.42±0.01

3.2.1.3 Cold-sintered CaPs

Because glutamic acid, as an organic small molecule, will be inactivated and degraded at high temperatures, the subsequent processing of the material must be carried out at room temperature or low temperature. As mentioned in the introduction, cold sintering is a suitable and promising ceramic material processing technology that prepares the bioceramic material within an acceptable temperature range.

Figure 21 displays a photograph of the cold-sintered CaPs. Tablets were fabricated under a pressure of 1.5 GPa (detailed in Section 2.2.5), with 6 mm and 13 mm diameters selected for subsequent experiments.

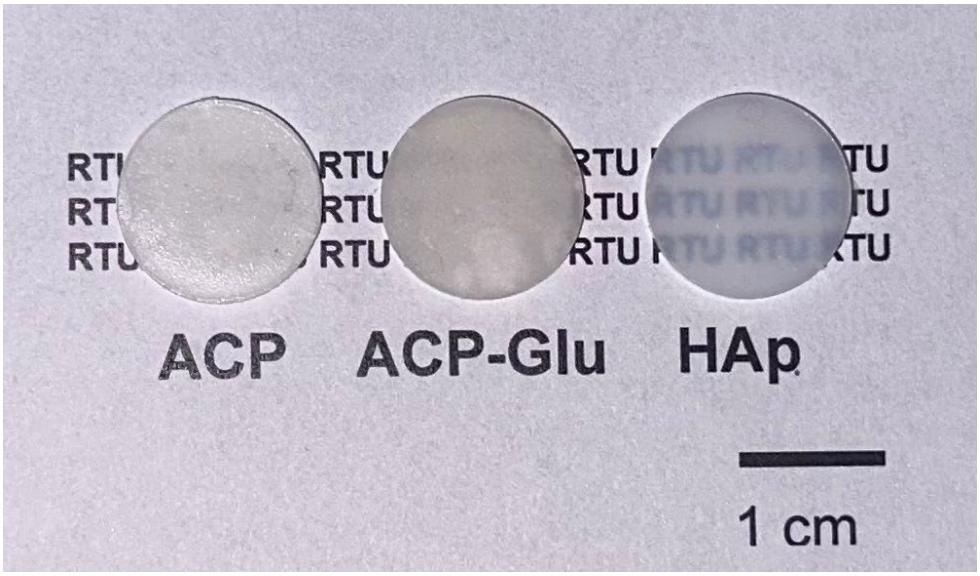

Figure 21 The photograph of cold-sintered ACP, ACP-Glu, and HAp

3.2.2 Characterization of CaPs

3.2.2.1 XRD of CaPs

The crystalline phase of all heat-treated CaP tablets was determined by XRD, as described in section 2.3.1, to verify the composition of CaPs. The following International Center for Diffraction Data (ICDD) entries were used for crystalline phase identification: ICDD 09-0432 for hydroxyapatite and ICDD 09-0169 for β-tricalcium phosphate. The obtained pure samples of HAp and β-TCP were consistent with the ICDD patterns (Figure 22). HAp characteristic maxima, with the highest intensities, were easily discernible at 25.9° 2θ, as well as the double maxima between 31.7° and 32.2° 2θ, and a single peak at 34° 2θ. β-TCP maxima were also clearly identified at 20°, 30°, 31°, and 41° 2θ. The percentages of β-TCP and HAp present in the biphasic calcium phosphate samples, H58 and H95, were calculated using the Rietveld refinement method. The XRD technique was insufficient to detect β-TCP in the H95 XRD pattern; however, its presence in H58 was evident, with maxima observed at 20°and 41° 2θ (Figure 23). Additionally, the intensity of the HAp characteristic maxima was slightly diminished in the H58 sample. The high-temperature-treated ceramics were well-suited for subsequent biological testing.

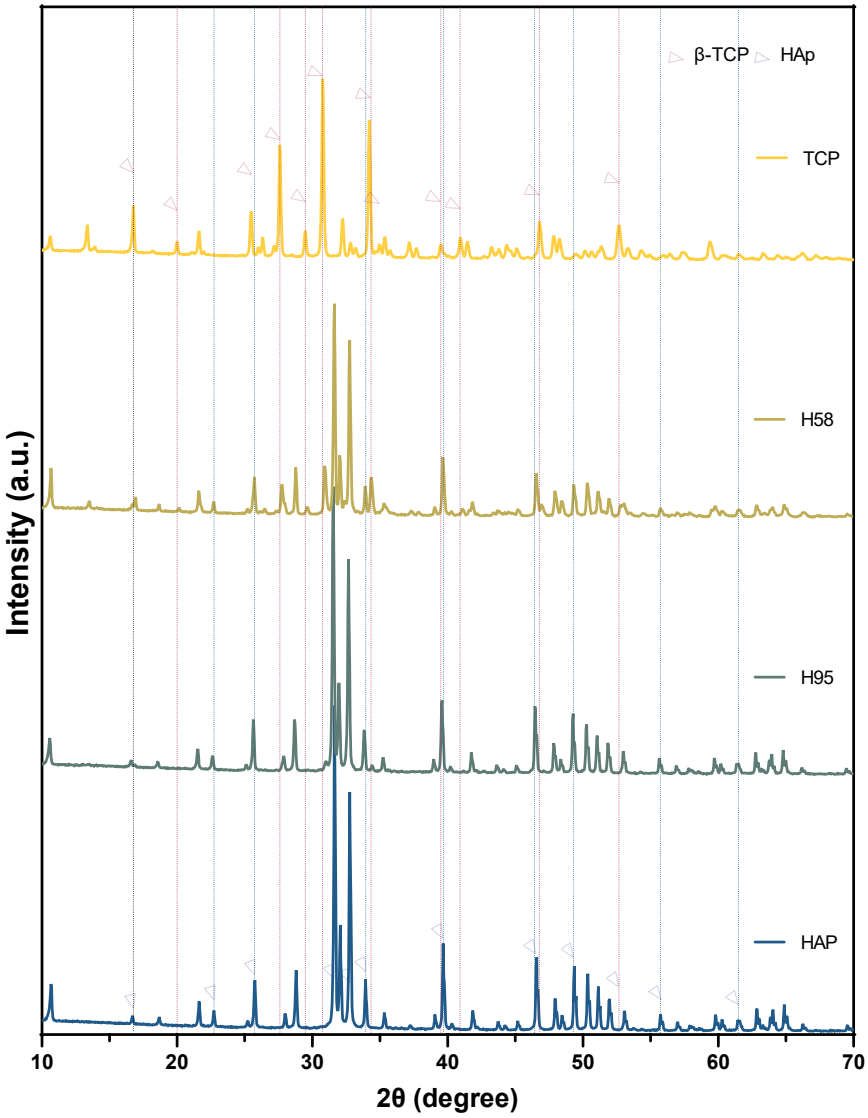

Figure 22 XRD pattern of TCP, H58, H95, and HAP

For the cold-sintered samples, the XRD patterns are shown in Figure 23. The lack of crystalline order confirms the formation of synthesized ACP and ACP-Glu.

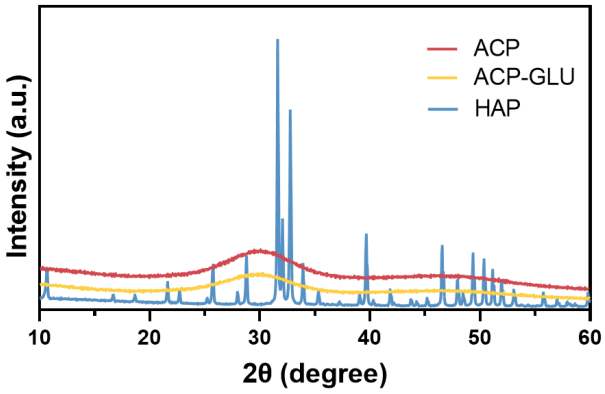

Figure 23 XRD pattern of HAP, ACP-Glu, and ACP

3.2.2.2 Evaluation of CaP Morphology

The morphology of the high-temperature sintered material tablets was evaluated using scanning electron microscopy (SEM) and is shown in Figure 24. SEM images did not reveal pore structures at higher resolutions (20000×). These surfaces exhibit uniformity at the macro-level, making them advantageous for studying cell-material interactions. However, at the micrometer scale, the material surface contains irregular bumps and depressions. The grain sizes of TCP (β-TCP) and H58 (a calcium phosphate composition with 58% HAp and 42% β-TCP) are relatively larger (~1 µm) than the CaP with higher HAP content (~0.4µm for H95 and ~0.3µm for HAP), likely due to their higher sintering temperatures (H58: 1135 °C; TCP: 1100 °C). Additionally, a few sporadic holes can occasionally be observed along the grain boundaries, resulting from incomplete sintering of particles.

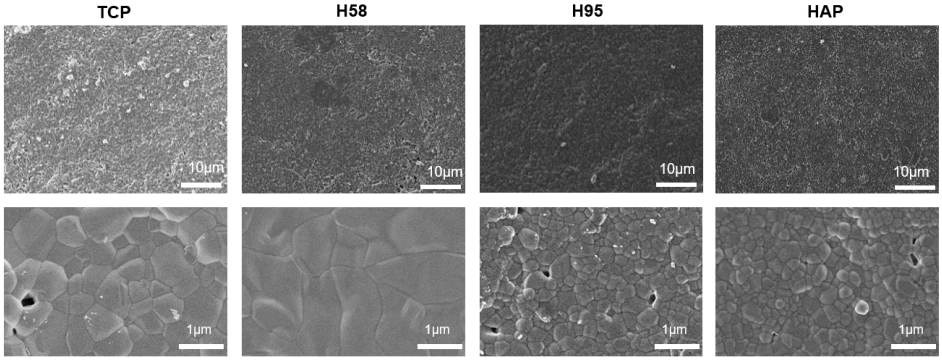

Figure 24 SEM images of high-temperature sintered CaPs at two magnifications: 2,000× (top) and 20,000× (bottom).

The morphology of the cold-sintered calcium phosphate tablets is shown in Figure 25. Given that MC3T3-E1 cells are approximately 20–40 μm in diameter, the cold-sintered tablets appear macroscopically flat to the cells (146). The compacted samples display a grain-like structure with spherical particles, each about 30 nm in size (Figure 25 B and D). Both ACP and ACP-Glu materials exhibit similar surface features and microstructures.

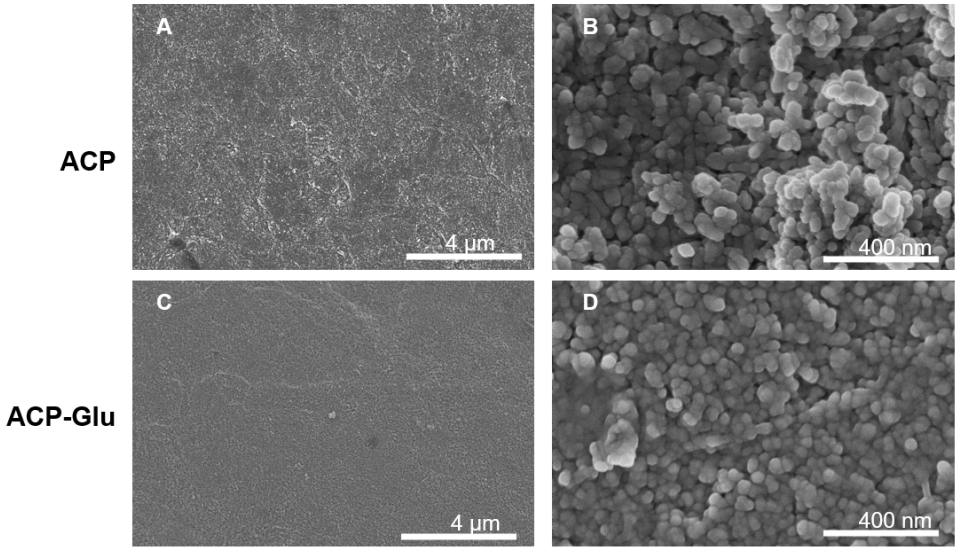

Figure 25 SEM images of cold-sintered CaPs.

3.2.2.3 Specific surface area

Specific surface area (SSA) assessments based on the BET theory revealed distinct differences among the calcium phosphate (CaP) materials based on their sintering methods. Both pure HAp and β-TCP exhibited higher specific surface areas (31.8 and 20.1 m^2/g, respectively) compared to their corresponding composites—15.8 m^2/g for H95 and 10.0 m^2/g for H58. Phase interactions in BCPs (H58 and H95) promote densification and grain growth, reducing porosity and surface area. In contrast, pure HAp and β-TCP maintain their inherent porous structures, leading to relatively higher surface areas after sintering. In the cold sintering group, HAp tablets demonstrated greater surface areas (53.2 m^2/g) than ACP (15.0 m^2/g) and ACP-Glu (10.8 m^2/g) synthesized in the presence of glutamate (Figure 26), while the SSA of ACP-Glu is slightly lower than ACP. HAp has a more stable and structured crystalline network, which resists excessive particle fusion during cold sintering, retaining a higher surface area. ACP is inherently more prone to densification due to its disordered nature, but ACP-Glu experiences

even greater densification. The presence of glutamate may promote particle rearrangement, further reducing porosity and surface area compared to pure ACP.

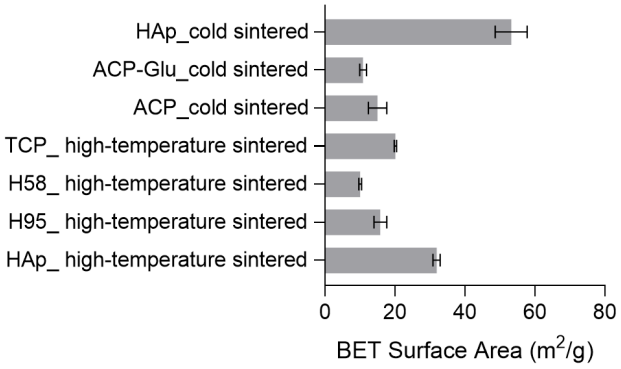

Figure 26 Specific surface area (SSA) assessments based on the BET

3.2.2.4 The influence of CaPs on culture media

High-temperature sintered CaPs did not affect the pH of the culture medium (Figure 27A). In the absence of cells, immersion for 24 h reduced the calcium concentration of the culture medium by 50% of the original calcium concentration (Figure 27C). On the contrary, the concentration of phosphate ions increased 2 times by all 4 bioceramic materials (Figure 27B). The addition of CaPs could cause precipitation of calcium phosphate compounds. This led to decreased free calcium ion concentration in the media as calcium ions bind to phosphate ions and precipitate out of solution.

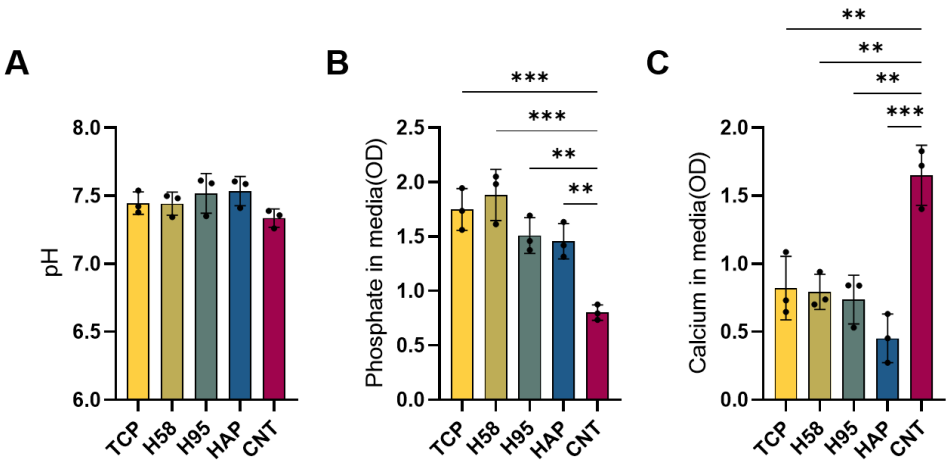

*Figure 27 The influence of CaPs to culture media. A. pH. B. Free phosphate groups in media. C. Free calcium ions in media. (*P < 0.05; **P < 0.01; ***P < 0.001; ****P < 0.0001)*

3.2.2.5 In vitro evaluation of high-temperature sintered CaPs

Cell viability responding to a biomaterial is a critical parameter commonly assessed during biomaterial evaluation. Furthermore, for quantitative metabolite analysis, different cell numbers can influence quantitative results; hence, it is crucial to normalize the obtained data to the cell numbers. The CCK-8 measures the metabolic activity of cells by reacting with NAD(H) and NADP(H), therefore reflecting the total number of viable cells. The cell viability for material groups was similar to the surface-treated culture plate (cell viability between 70% to 130% is considered as nontoxic and similar). From the qualitative analysis of SEM images, it can be seen that the cell morphology and adhesion did not change significantly in the short-term (Day 1) culture due to the different composition of calcium phosphate ceramic materials (Figure 28B).

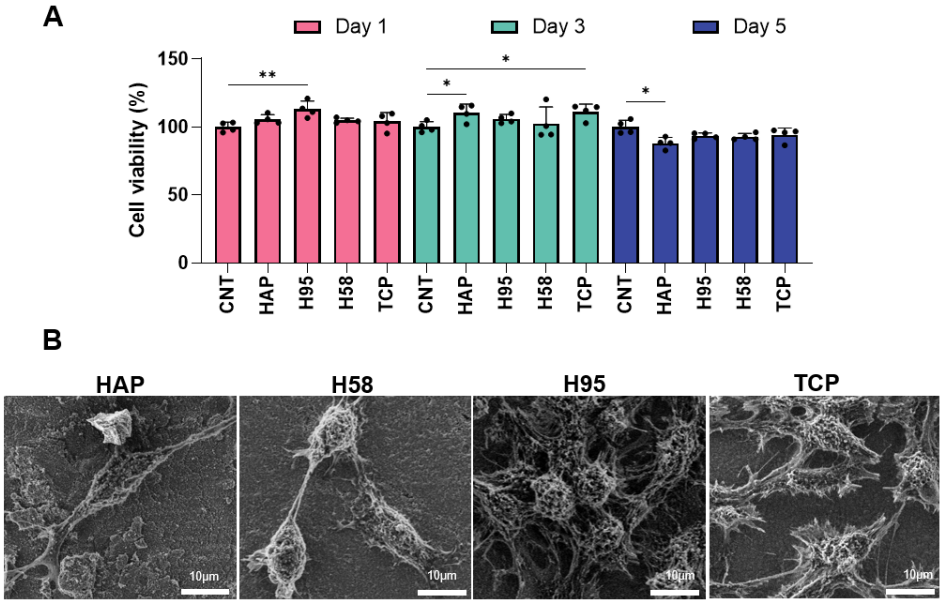

Figure 28 A. Cell viability on day 1, day 3, and day 5 (cells cultured on CaPs). B. SEM images of fibroblasts attached on high temperature sintered CaPs.

3.2.2.6 Glu release by ACP-Glu

Various compound release models were tested to simulate the release rate, including the Zero-Order and First-Order Release Models. Both zero-order and first-order models described the cumulative glutamate release well ($R^2 = 0.995$ for both models). The fitted curves were visually overlapping over 0–72 h, and the two models are statistically hard to distinguish at our sample size. The glutamate release rate was calculated to be approximately 0.01454 nmol (2.14 ng) per hour. This steady, controlled release allows for precise dosage control in bone tissue, helping to achieve the desired therapeutic effect while minimizing potential side effects caused by excessive release, thereby enhancing the desired therapeutic effect while minimizing potential side effects from rapid release. Because the improvement in fit was small relative to experimental uncertainty, the goodness-of-fit was assessed by both pseudo-R^2 from nonlinear regression and by visual inspection of residuals was applied. It is important to note that the experimental setup utilized a stationary environment to mimic in vitro conditions. In real biological scenarios, where various factors such as cell types (e.g., osteoclasts) and dynamic elements like blood flow are present, glutamate's release or uptake rate may differ.

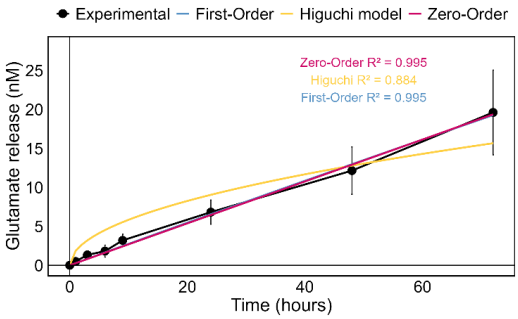

Figure 29 The cumulative release of glutamate from ACP-Glu. Fitting curves and R^2 values of 3 drug release models.

3.3 Metabolite analysis

3.3.1 Metabolomics of NIH/3T3 with CAPs

3.3.1.1 Metabolite adsorption of HAp compared with intercellular metabolites

Evaluating whether the experimental condition could introduce bias in metabolite measurements is essential to ensure accurate data interpretation. The experimental procedure included immersion of the CaP disk in cell culture media, seeding the cells (NIH/3T3) directly on the material, and extracting the intercellular metabolites. Typical cell culture media contains a plethora of metabolites to ensure proper cellular functions. These small molecules can adhere to biomaterial surfaces and could be co-extracted with intercellular metabolites, resulting in inaccurate metabolite data. Employing the methodology outlined in section 2.5.4, the analysis revealed the adsorption of 29 distinct metabolites from NIH/3T3 cell lines onto the CaP surface, persisting even after rigorous washing with PBS. Compared to the control (cell culture plate), more metabolites (3 metabolites with over 0.5-fold changes) are adsorbed onto CaP surfaces (HAp in this case). In general, CaPs showed a higher affinity with the positively charged amino acids (basic side chains). Lactic acid is adsorbed on both the CaP and control groups, while the lactic acid level on the CaP surface is almost 2.75 times higher than that of the control. Compared with the control, sulfur-containing amino acids (methionine, taurine, and cystine) are found at very high levels on CaP surfaces. The level of metabolites adsorbed onto calcium phosphate surfaces and culture plate surfaces was compared to intracellular metabolite levels and expressed as fold change (Figure 30).

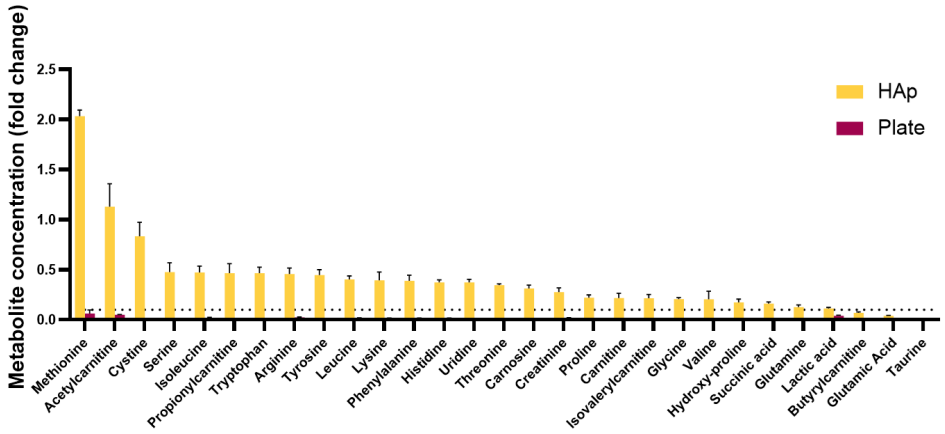

Figure 30 The level of metabolites adsorbed onto calcium phosphate surfaces and culture plate surfaces. The levels were compared to intracellular metabolite levels and expressed as fold change. The group to compare was a 24-well culture plate (Purple color, material PS, surface treated), and for intracellular metabolite levels, average values for the materials group collected on day 1 were used. Metabolites with a high adsorption rate (a fold change greater than 0.1 compared to the intracellular results) were excluded from further analysis. Dashed line: fold change = 0.1. n=3.

3.3.1.2 Metabolite adsorption on cold sintered ACP, ACP-G, and HAp

In total, 30 metabolites were targeted tested, and 28 are presented because of the undetected data. The overview profile is shown by a heatmap in Figure 31. The material groups, including ACP, ACP-Glu and HAp, all presented a higher adsorption of amino acids compared to the control groups (culture plate cultured cells). All calcium phosphate tablets have a similar affinity for octanoylcarnitine compared with the control. The extremely high glutamate level in the ACP-Glu group was due to the original glutamate from the material, but not entirely because of the free glutamate adhesion from the media.

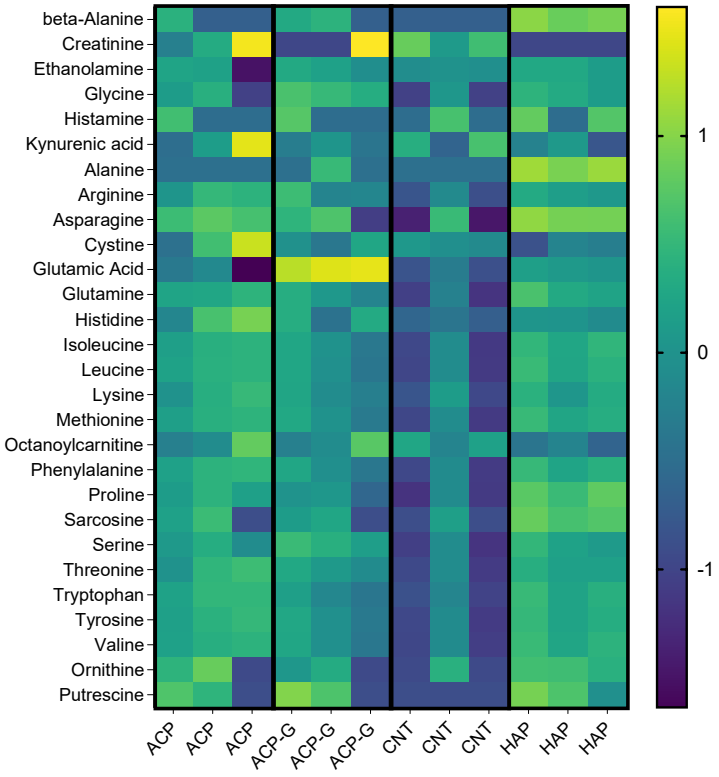

Figure 31 Heatmap with fold changes (FC) of metabolites adsorption on ACP, ACP-Glu, and HAp compared to CNT.

Principal component analysis (PCA) revealed distinct clustering patterns between the material groups and the control (Figure 32). The control group exhibited greater variation compared to the calcium phosphate groups. Overall, the differences between groups were relatively small, indicating that the materials have comparable adsorption capacities for small molecules.

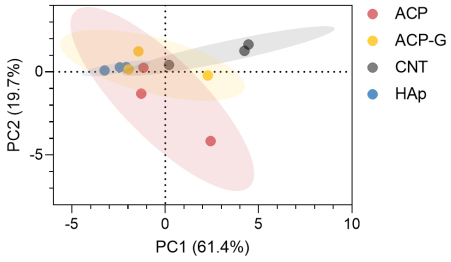

Figure 32 PCA plots of metabolite adhesion on ACP, ACP-Glu, HAp, and CNT (culture plate)

The data obtained revealed that putrescine is the most significant metabolite that adhered to the calcium phosphate surface, not the culture plate. It is a polyamine that plays a vital role in cell growth (147). It supports this process by modulating gene expression, promoting protein synthesis, and facilitating DNA replication. Putrescine acts as a precursor for synthesizing other polyamines like spermidine and spermine, which also play essential roles in cell growth. Putrescine may play a role in wound healing by promoting cell migration, tissue remodeling, and angiogenesis (forming new blood vessels), which are all necessary for bone regeneration (148). The different ability to capture putrescine may be one of the merits why calcium phosphates are recognized as the ideal biomaterials for bone regeneration.

Among all the amino acids, cystine showed a similar level between all CaP groups and the control (Figure 33). Other amino acid levels were found to be higher in cold-sintered samples than in those in the control group. As mentioned before, calcium phosphates are known for their bioactivity and biocompatibility. The increased affinity for amino acids suggests they can readily interact with organic molecules, such as proteins and peptides. This is advantageous for promoting interactions with cells and biological molecules at the bone-implant interface. The higher affinity of CaPs for amino acids may lead to increased protein adsorption on their surfaces, which has been studied very often in the biomaterials field (33,149). The enhanced interaction with biological molecules makes them suitable for orthopedics and tissue engineering applications. Of note, both ACP and ACP-Glu showed less affinity to alanine.

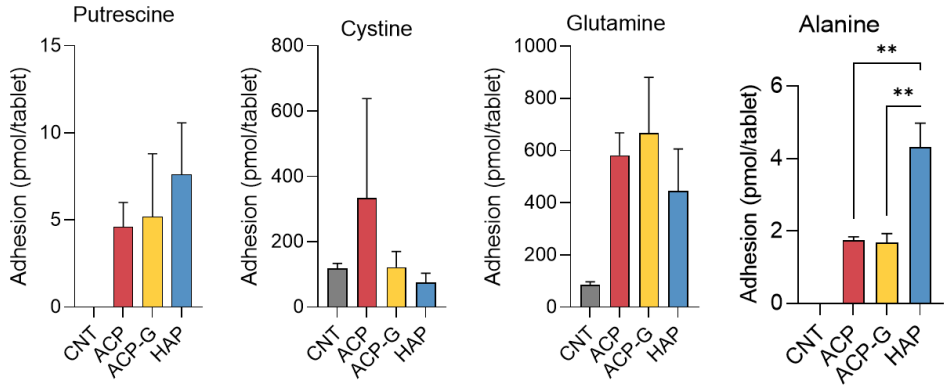

*Figure 33 Examples of adhered metabolites. (*P < 0.05; **P < 0.01; ***P < 0.001; ****P < 0.0001)*

3.3.1.3 Metabolite profiling of HAp, H95, H58, TCP, and cold sintered ACP

The metabolite profile of 3T3 fibroblast cultured on CaP tablets is presented in Figure 34. ACP showed a lower overall level of most of the metabolites presented here.

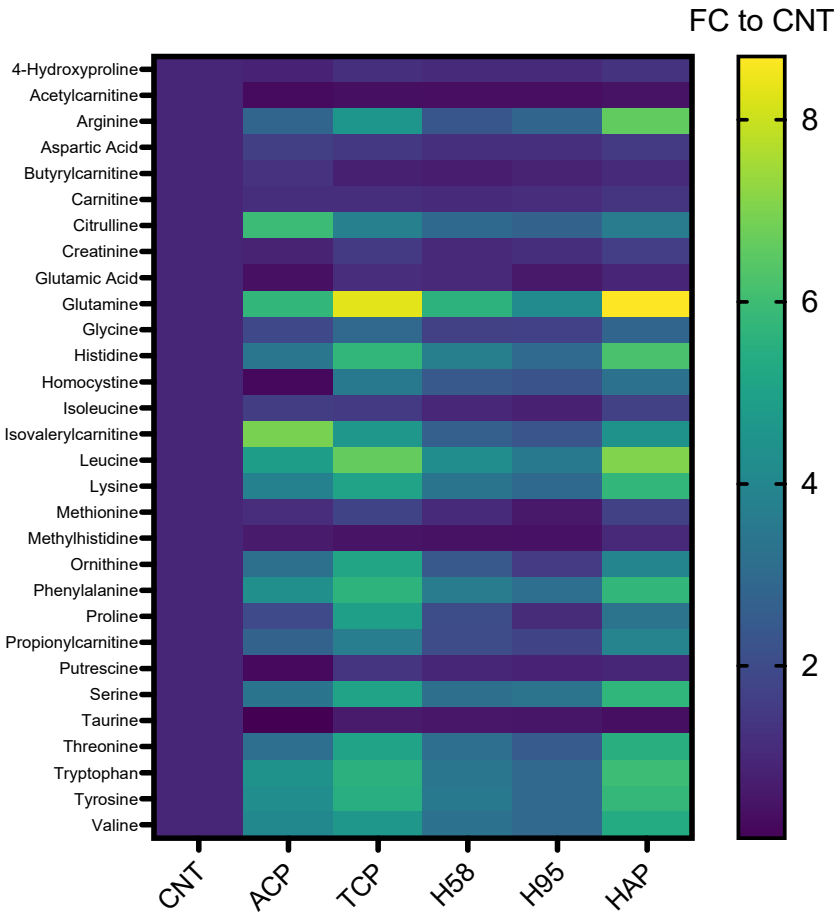

Figure 34 Heatmap of intracellular metabolites of NIH/3T3 on CNT, ACP, TCP, H58, H95, and HAp, presented by fold changes (FC) compared to control (CNT).

The PCA plot shows that the CNT group has a cluster dependent on the CaP groups (Figure 35). ACP shows a different distribution from the other crystalized CaPs, especially in PC1, which has the most considerable weight (61.6%). Cell metabolism behaves differently in amorphous materials than in crystalline ceramic materials.

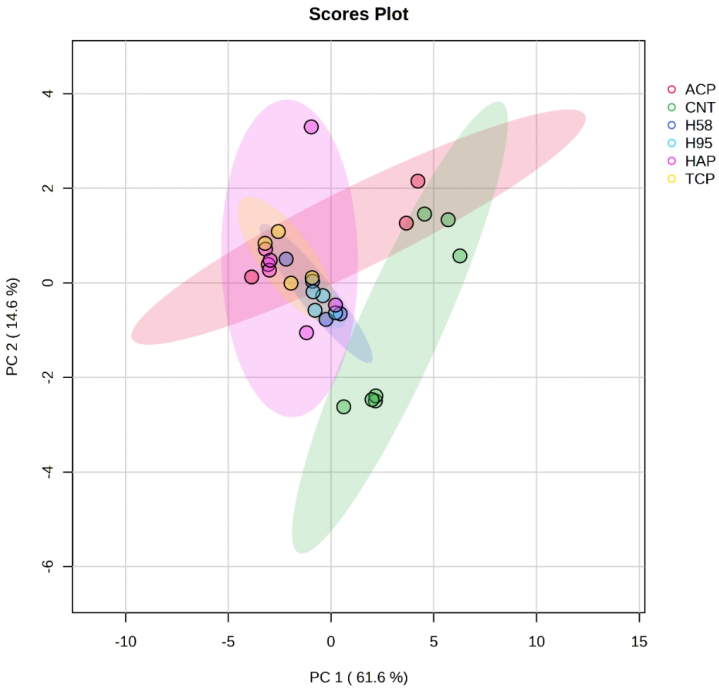

Figure 35 PCA plots of fibroblast cell metabolites with different materials

3.3.1.4 The influence of time and composition on metabolism

Due to the unique results observed in the ACP group, the other CaP groups were analyzed separately to investigate metabolic differences between calcium phosphate-based materials and the control. However, in this study, PCA did not distinguish CaP samples with different phase compositions into clearly defined clusters (Figure 36). Although a few metabolites increase or decrease with the changes in HAp content, the correlation coefficients are too low to conclude.

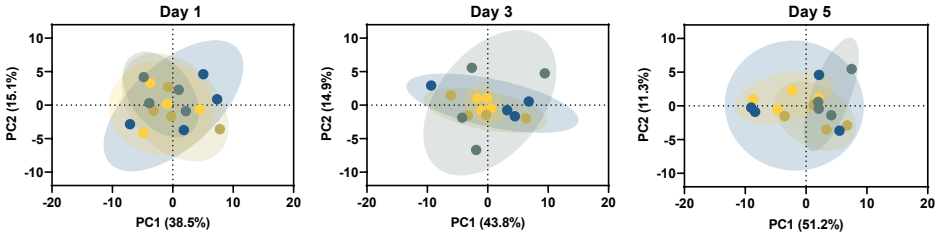

Figure 36 PCA plots of all 4 types of crystalline CaPs on Day 1, Day 3, and Day 5.

Statistical data analysis, including PCA and t-test, is performed to identify metabolites with significant changes induced by CaPs. PCA score plots revealed a close clustering of the CaP materials group and a substantial separation between the materials and control groups (Figure 37). The metabolite changes at the earlier time point presented a more significant variation than the later time points, suggesting a more substantial distinction between CaPs and control groups at the initial phase.

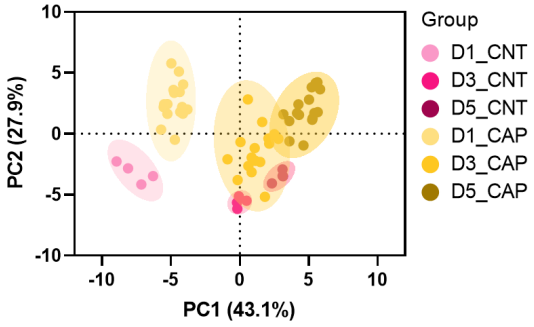

Figure 37 Cluster analysis by PCA with all CaP and control groups from days 1, 3, and 5 (n=4).

Proline is up to 5 times upregulated in CaP groups over all 3 time points. Notably, the reduction of any amino acid is not observed with CaP groups. On the other hand, compounds of energy metabolism are significantly impacted by CaPs. For example, ATP concentrations in material groups (1.43nM) are 4 times lower than in the control groups (6.90nM). At the same time, levels of fructose 1,6-bisphosphate (FBP), a critical molecule in the glycolysis metabolic pathway, are 10 times reduced in cells exposed to CaPs: from 42.30nM of CNT to 5.07nM of CAP (Figure 38). As a result, CaP biomaterials can interfere with glucose metabolism, reducing glycolytic flux and ATP production. CaPs could impact oxidative phosphorylation, leading to lower ATP levels.

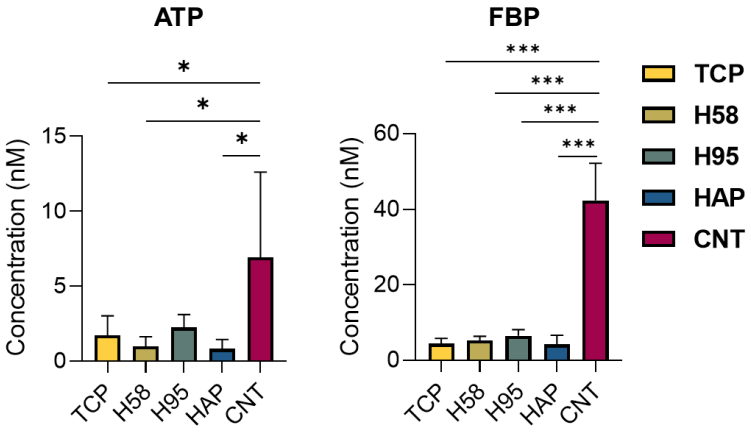

*Figure 38 Intracellular level of ATP and FBP. *P<0.05, ***P<0.001 (n=4). (*P < 0.05; **P < 0.01; ***P < 0.001; ****P < 0.0001)*

The heatmap of nucleotides and pentose phosphate pathway/glycolysis metabolites on day 1 is presented in the Figure 39. There is a noticeable decrease in nucleoside and FBP among the CAP groups and an increase in F6P and G6P in the CAP groups. This indicated that the calcium phosphate materials hugely impacted energy production.

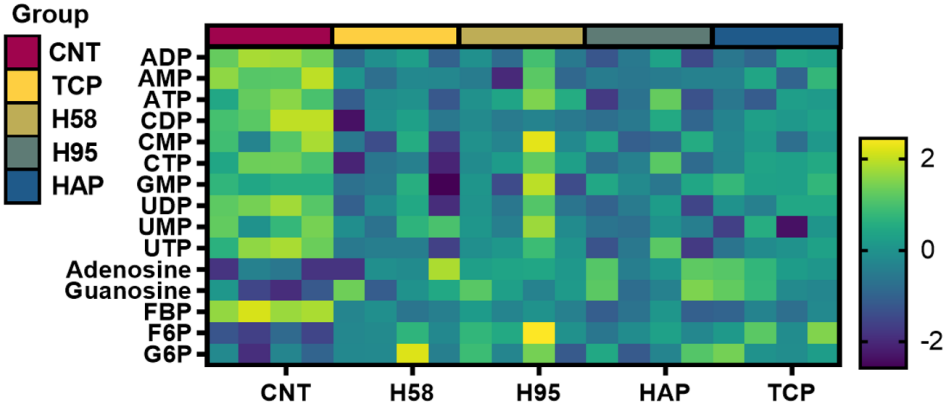

Figure 39 Heatmap of energy metabolites change profile of the CaP groups and CNT on Day 1. Presented by the magnitude of individual values within a dataset as a color.

3.3.1.5 Pathway analysis of high-temperature sintered CaPs compared with CNT.

The fold changes of metabolites in carbohydrate metabolism are shown in the Figure 40. A substantial disturbance of energy metabolism and higher energy consumption of the cells caused by CaPs is presumed. The levels of G6P and F6P, two intermediates in the glycolysis

pathway formed in the first and second steps, respectively, are higher than compared to the control. In contrast, the FBP, developed at the sixth step of glycolysis, is significantly decreased by CaPs. The enzyme that catalyses the irreversible conversion of F6P, phosphofructokinase-1 (PFK-1), is the rate-limiting enzyme of glycolysis (150).

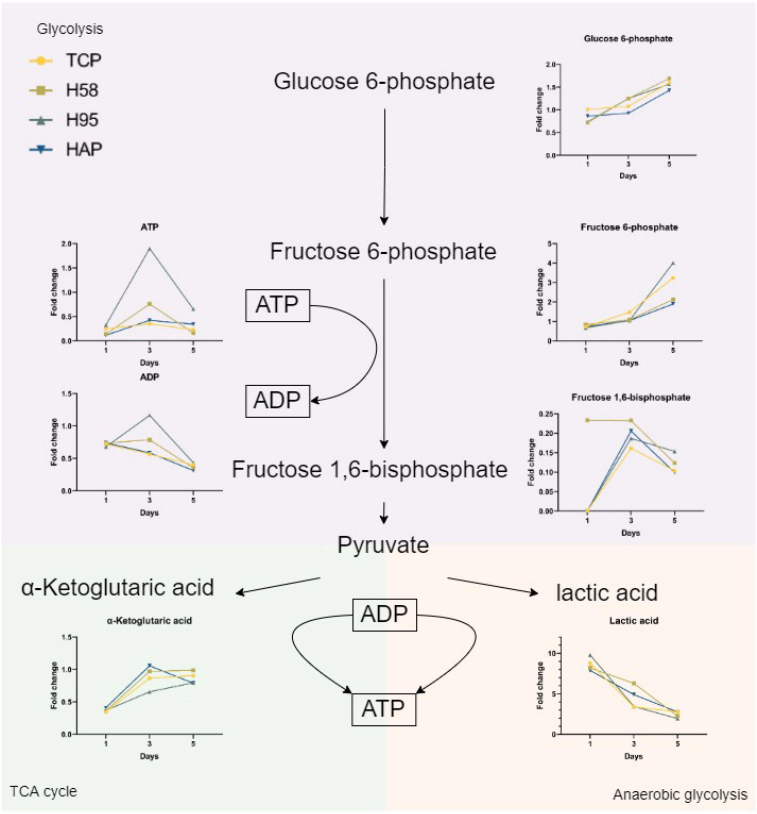

Figure 40 The changes of metabolites involved in glycolysis (carbohydrate metabolism) happened on CaPs. Presented by fold changes compared to CNT at each time point.

Lactic acid level, the end product of anaerobic glycolysis, can indicate cellular glycolysis metabolism. An initial period of high anaerobic glycolysis is anticipated, followed by a decline in anaerobic glycolysis. At the same time, α-ketoglutaric acid, a key metabolite in the TCA cycle, is 2 times lower than the control and increased to almost the same level on day 5. The production of α-ketoglutarate by isocitrate dehydrogenase and reduction by α-ketoglutarate decarboxylase are irreversible, making it a valuable metabolite when analyzing the TCA cycle (151–153). α-ketoglutarate decarboxylase is also considered a rate-limiting step of the TCA cycle (154). The depletion of α-ketoglutarate on the first day indicated a high energy consumption requirement from the TCA cycle. Because anaerobic glycolysis is usually

enhanced when the TCA cycle cannot provide enough energy or when there is a limited oxygen supply, the α-ketoglutarate and lactic acid levels indicate a higher energy consumption of the cells when they attach the CaPs. Also, this additional enhanced consumption decayed over time. The overall effect of calcium phosphate on cell metabolism is shown in Figure 41. The significant upregulation of amino acids and downregulation of nucleotides are noticed in this map. The initial exposure to CaPs resulted in a shock pressure on the energy metabolism response to biomaterials, presented by more extensive variability in metabolite profiles.

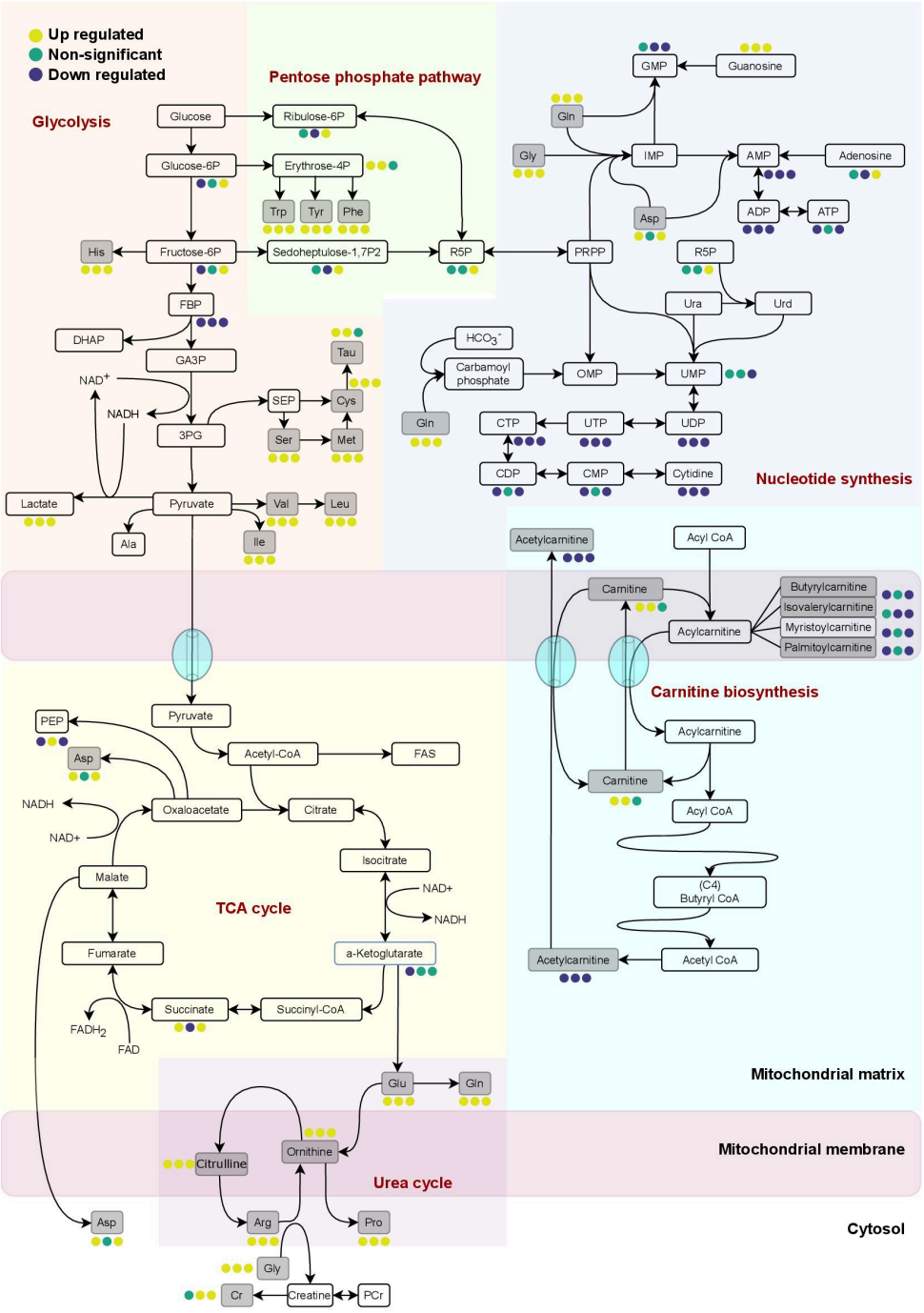

Figure 41 The metabolic pathway map of detected metabolites. Metabolites were marked as up/down regulated or non-significant changes by color code. The covered pathways include glycolysis, the pentose phosphate pathway, nucleotide synthesis, the TCA cycle, carnitine biosynthesis, and the urea cycle.

3.3.2 Metabolomics of MC3T3-E1 with ACP, ACP-Glu, and HAp

3.3.2.1 Metabolite profiling

To assess the impact of ACP-Glu biomaterials on cell metabolism, a targeted metabolomic analysis was conducted on cells cultured on cold-sintered ACP, ACP-Glu, and HAp, with a blank culture plate (CNT) serving as the control. ACP, as a calcium phosphate carrier without glutamate, was selected as the primary control for ACP-Glu, while HAp and CNT served as supplementary reference groups. The metabolite profiles of osteoblasts cultured on ACP, ACP-Glu, and HAp tablets are presented in Figure 42, revealing significant metabolic differences between CNT and all CaP groups. Notably, ACP and ACP-Glu exhibit distinct metabolite levels—particularly in amino acids—compared to HAp. Among these differences, glycine levels show an opposite trend between amorphous calcium phosphates (ACP and ACP-Glu) and crystalline HAp.

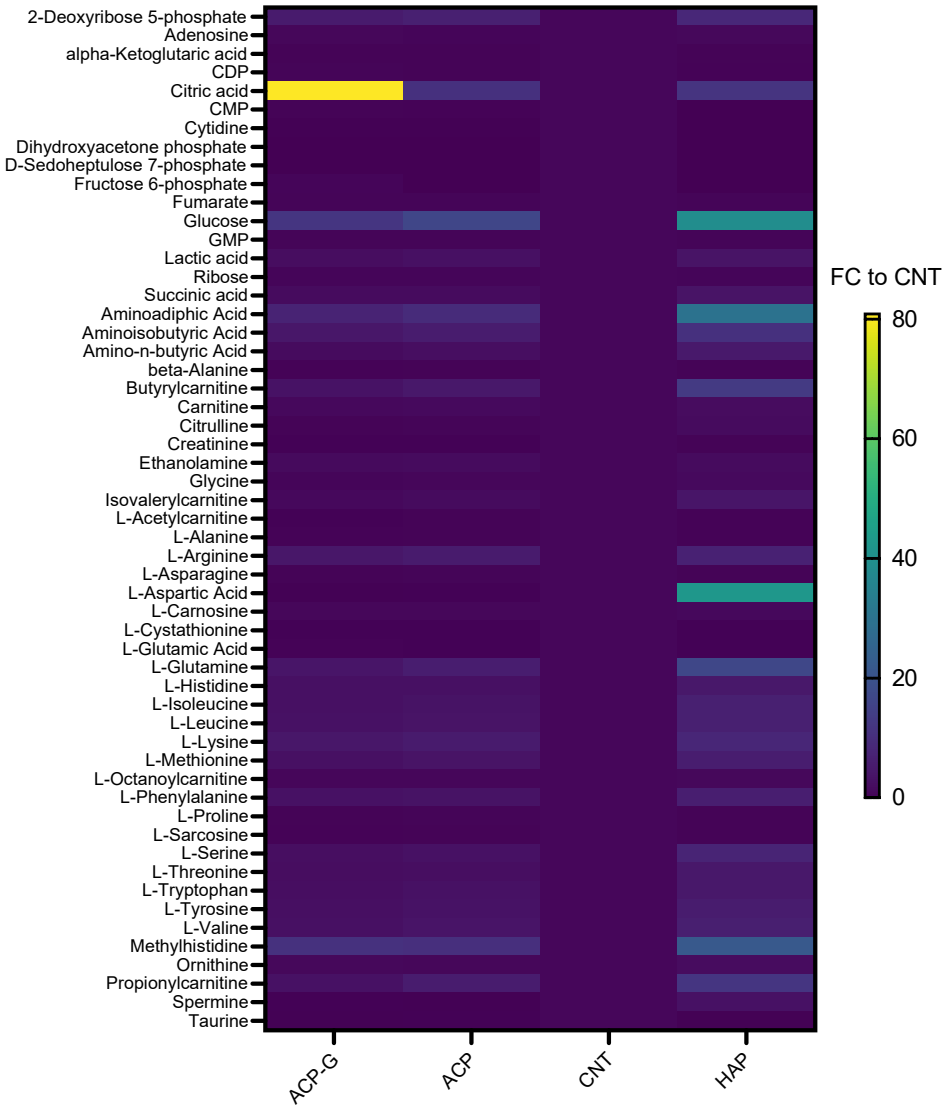

Figure 42 Heatmap profile of intracellular metabolites of MC3T3-E1 on ACP, ACP-Glu, and HAp. Presented by fold changes (FC) compared to CNT.

The PCA plots in Figure 43 show that the CNT group has a cluster dependent on the CaP groups. There are significant differences between HAP and the other two materials. The ACP-Glu also separates from the ACP, especially in PC 2 (12.6%). This may be because ACP and ACP-Glu shows different overall levels of most metabolites, especially amino acids.

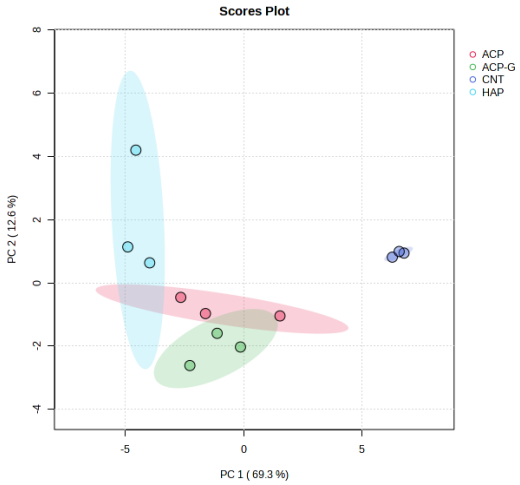

Figure 43 PCA plots of osteoblast cellar metabolites with different materials

3.3.2.2 ACP-Glu compared against CNT.

The comparison between manufactured ACP-Glu and blank control was firstly analyzed using volcano plot and shown in Figure 44. Two metabolites, glucose 6-phosphate and citric acid, stand out due to their significant alterations. Glucose 6-phosphate is notably reduced compared with CNT, while citric acid is notably upregulated. The concentration of citric acid is around 8 times higher than the other two CaPs, and about 80 times higher than the CNT (Figure 45). Glucose 6-phosphate is a critical molecule in glucose metabolism; being down-regulated suggests alterations in energy metabolism or cellular signaling pathways. As the second metabolite in glycolysis, the initial reaction of glucose metabolism is inhibited. The inhabitation is caused by extra gluconeogenesis function provided by glutamate. Citric acid is an intermediate in the TCA cycle; being upregulated could indicate changes in energy production or the utilization of cellular resources. The significant changes involve energy metabolism, nucleotide synthesis, neurotransmitter regulation, and cellular signaling.

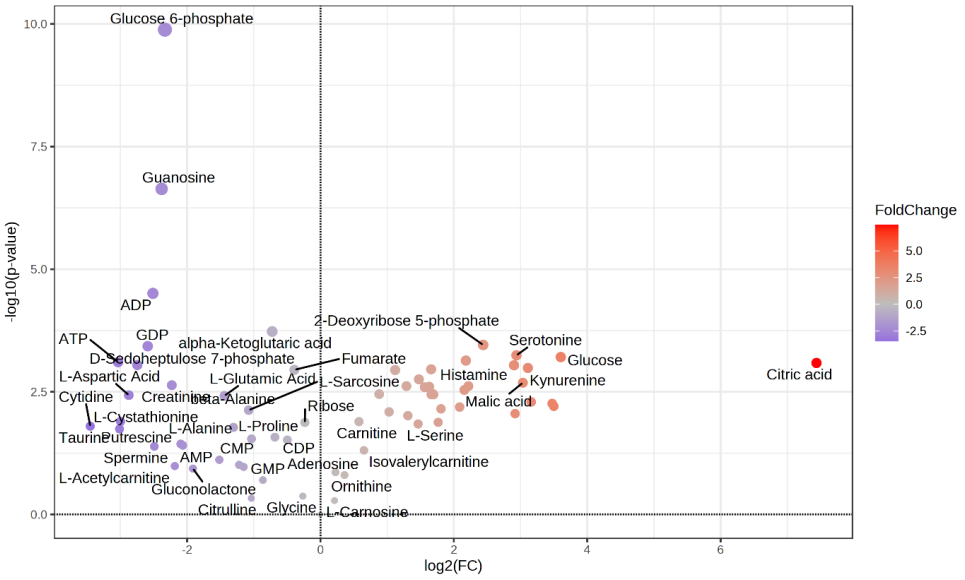

Figure 44 Volcano plot of significant metabolites compared between ACP-Glu and CNT, presented by fold changes and p-values.

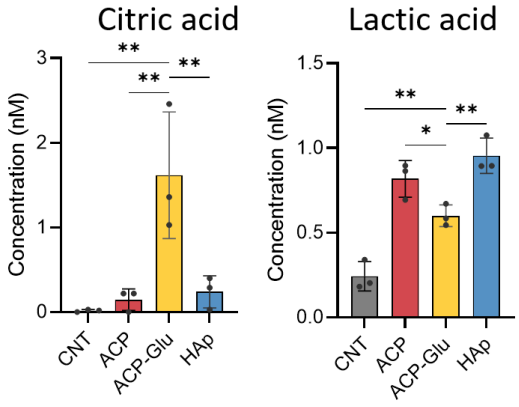

*Figure 45 Detected intracellular citric acid and lactic acid concentration. (*P < 0.05; **P < 0.01; ***P < 0.001; ****P < 0.0001)*

The metabolism pathway enrichment analysis showed the pathways that are altered by ACP-Glu ceramic tablets (Figure 46). Of which, the Warburg effect is the most significant one. This metabolic phenomenon involves a shift in energy production from oxidative phosphorylation to glycolysis, even in the presence of oxygen. Glutamate can influence this pathway by altering cellular energy metabolism. Glutamate, as a critical metabolite, can affect the glycolysis or mitochondrial function rate, potentially influencing ATP production and the cellular redox state

(155). This shift can impact bone cells' energy requirements for growth, repair, and mineralization processes.

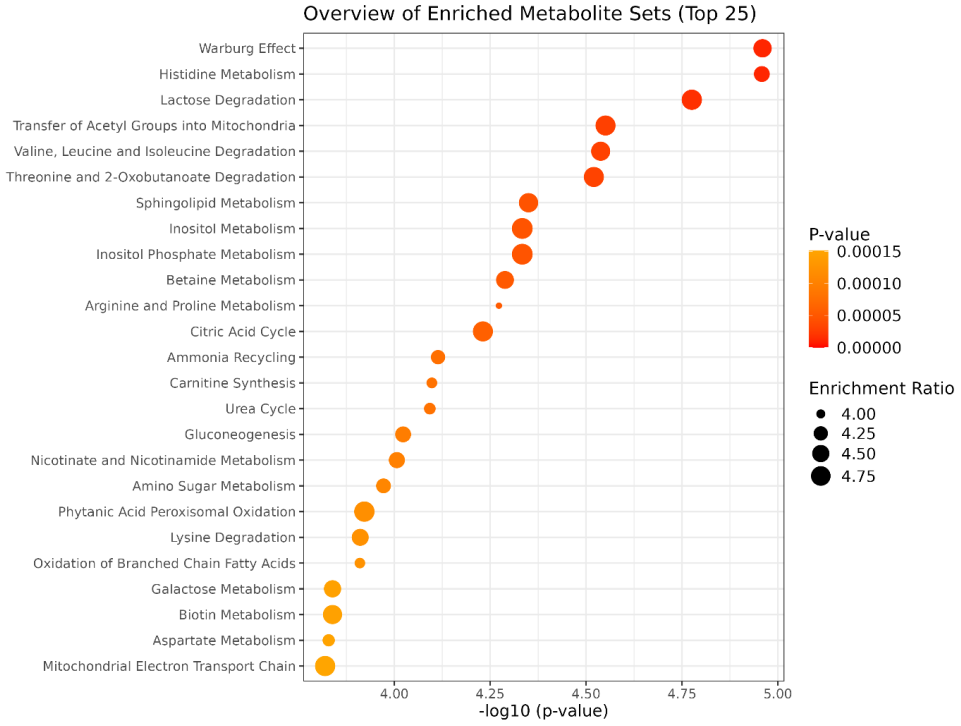

Figure 46 Pathway enrichment analysis of ACP-Glu compared with CNT.

Not only compared with CNT, the pre-osteoblasts cultured with ACP-Glu presents a significantly high level of citric acid. The concentration is around 8 times higher than the other two CaPs, and 80 about times higher than the CNT, shown in Figure 45. The function of TCA cycle interaction will be discussed in 3.3.2.4.

3.3.2.3 ACP-Glu compared against HAp.

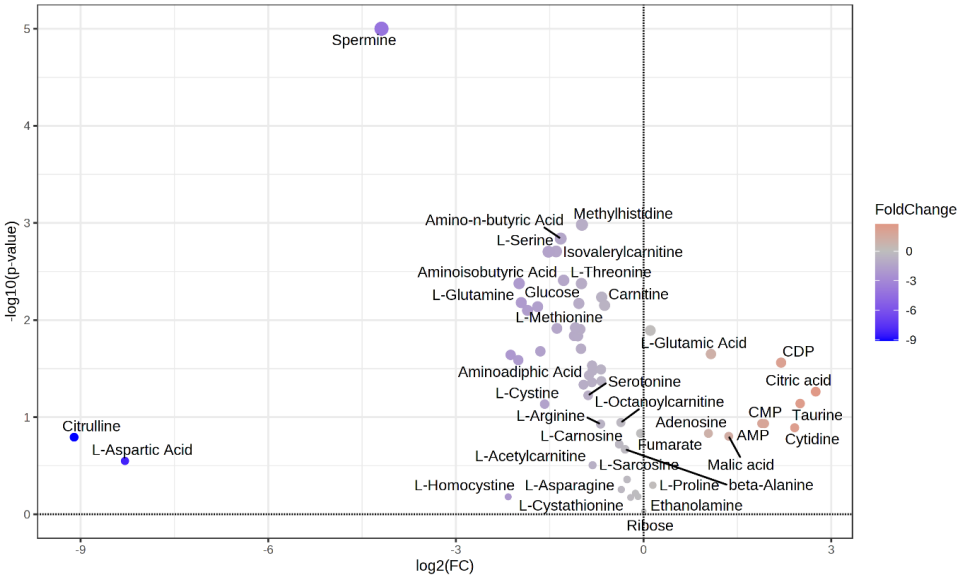

Figure 47 Volcano plot of significant metabolites compared between ACP-Glu and HAp, presented by fold changes and p-values.

The difference between ACP-Glu and HAp is presented by volcano plot in Figure 47. The comparison between ACP-Glu and HAp highlights the differences in metabolite levels, particularly the higher levels of CDP (2 times) and citric acid (8 times), as well as the lower levels of spermine (0.05 times) in ACP-Glu. Spermine is a polyamine involved in various cellular processes, including cell growth, differentiation, and gene expression regulation.

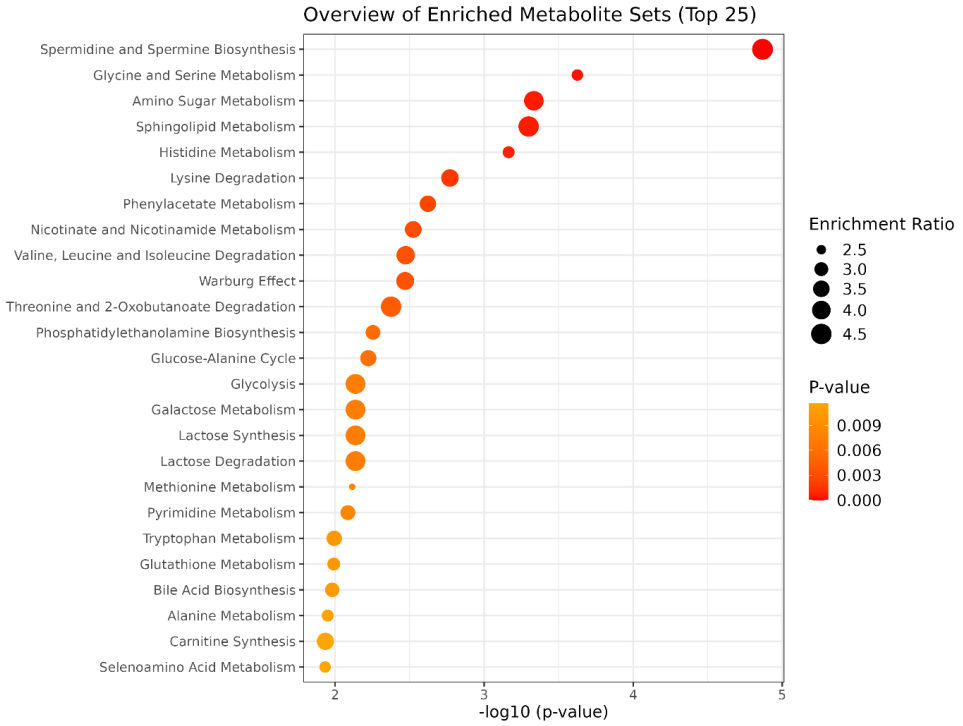

Figure 48 Pathway enrichment analysis of ACP-Glu compared with HAp.

The spermidine and spermine biosynthesis, parallel with the volcano plots, showed an intense alteration with spermine biosynthesis, compared between ACP-Glu and HAp (p=0.000013) (Figure 48). Glutamate contributes to polyamine synthesis, including spermidine and spermine (156). It serves as a precursor in this pathway, converted to putrescine, further leading to the synthesis of spermidine and spermine. The presence of glutamate in ACP-Glu might modulate the availability or utilization of these polyamines, thus impacting cellular processes like proliferation, gene expression, and potentially bone cell behavior.

3.3.2.4 ACP-Glu compared against ACP.

4 Figure 49 presents the metabolites difference between cells from ACP-Glu and ACP. When comparing ACP and ACP-Glu, notable elevations in citric acid (8 times) and malic acid (3 times) levels are observed within the ACP-Glu groups (Figure 49). Consistent with previous assessments, these metabolites are closely associated with energy metabolism, particularly within the TCA cycle. Elevated adenosine levels indicate increased turnover or synthesis of ATP. This could suggest higher energy demands or alterations in ATP utilization or recycling within the cells treated with ACP-Glu. From this result, we can

conclude that ACP-Glu has a distinct impact on cellular metabolism, particularly in pathways associated with energy production. The higher levels of TCA cycle intermediates and adenosine in the ACP-Glu group than ACP imply potential enhancements or modifications in cellular energy metabolism, possibly leading to increased ATP production or turnover.

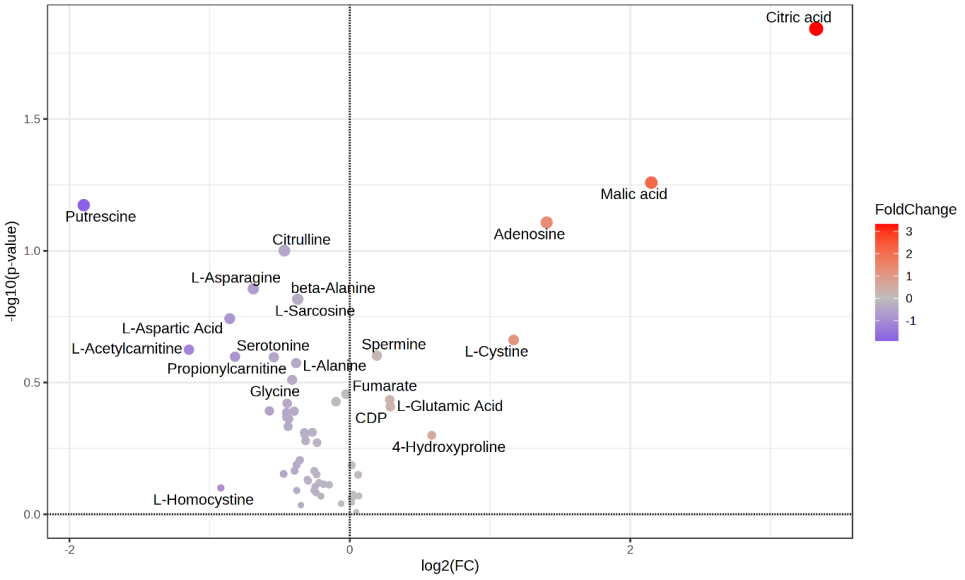

Figure 49 Pathway enrichment analysis of ACP-Glu compared with ACP.

Compared between ACP-Glu and ACP, the glutamate can again significantly influence the energy metabolism as it did with the control group (shown in Figure 50 by the form of enrichment pathway analysis). Moreover, ACP-Glu can also affect the efficiency of acetyl group transport and subsequent energy production in the mitochondria. Glutamate is a precursor to alpha-ketoglutarate, a key intermediate in the TCA cycle. Through transamination, glutamate can donate its amino group to form alpha-ketoglutarate, which enters the TCA cycle (157). The modification amplified energy production in osteoblasts. In contrast to the CNTs comparison, the impact on histidine and lactose metabolism pathways is relatively insignificant. When juxtaposed with metabolomic studies involving fibroblast cells and CaPs, CaPs could notably influence amino acid metabolism (3.3.1.3). The absence of discernible differences in histidine and lactose metabolism pathways among calcium phosphates can be considered more due to the appearance of CaPs.

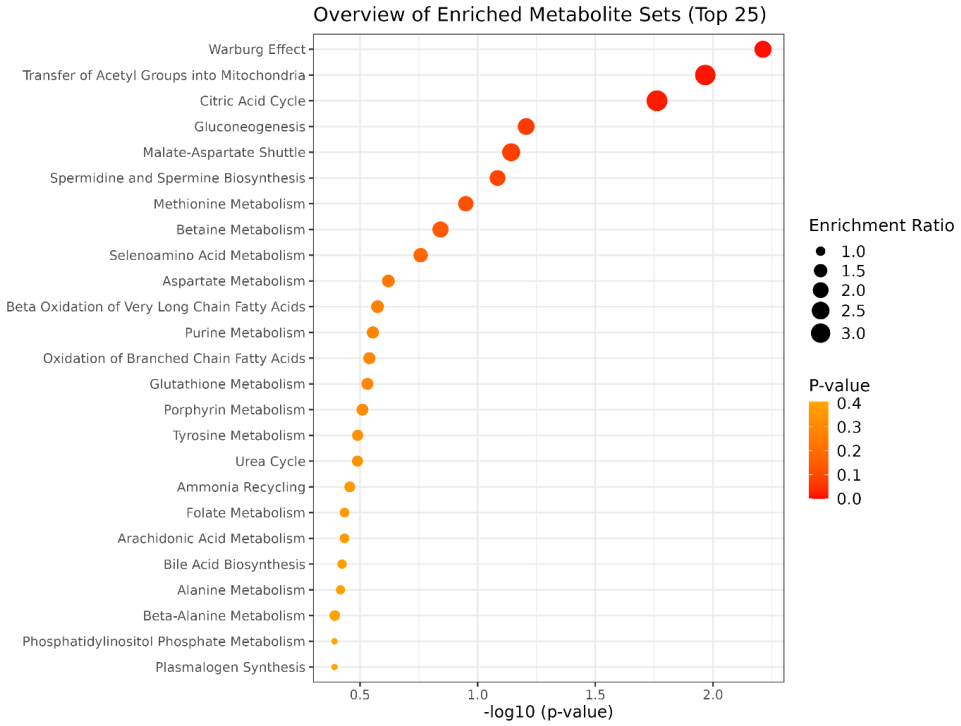

Figure 50 Pathway enrichment analysis of ACP-Glu compared with ACP.

The pathway illustration (Figure 51) shows the downregulation of metabolites in glycolysis, encompassing the primary sugar substrate, glucose. The introduction of a glutamate supplement appears to attenuate the activity of anaerobic glycolysis. Furthermore, the heightened anaerobic glycolysis induced by CaPs appears to be mitigated by the presence of glutamate. Notably, metabolites within the TCA cycle either remained unchanged or exhibited an upregulation, suggesting a potential augmentation in TCA cycle activity.

The map also depicts an alternative metabolic route leading to the synthesis of other amino acids. While glutamine experiences a reduction, the levels of two other amino acids, ornithine and proline, remain unaltered. Considering the variations in these metabolic pathways, it becomes evident that the additional glutamate from the substrate actively participates in the TCA cycle.

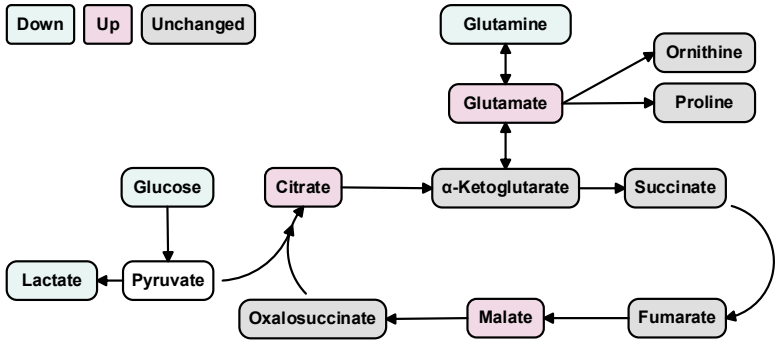

Figure 51 Glutamine and glucose metabolism pathway maps compared between ACP-Glu and ACP. "Up" means the metabolite concentrations higher in ACP-Glu while "Down" means the metabolites concentration is lower in ACP-Glu.

4.1.1.1 Summary of the ACP-Glu metabolomics comparison

ACP-Glu shows a unique metabolic profile. The results showed an alteration in key energy-related pathways, including the TCA cycle and glycolysis. As mentioned in 3.3.2.4, elevated citric acid and malic acid levels suggest increased activity within the TCA cycle and potentially enhanced ATP production or turnover. ACP-Glu influences polyamine biosynthesis pathways, affecting spermidine and spermine levels. As the one amino acid, glutamate in ACP-Glu affects pathways related to amino acid interconversion, such as glycine and serine metabolism. This can impact one-carbon metabolism and various cellular processes. Lower levels of these polyamines compared to HAp might indicate altered cellular proliferation or gene expression regulation, which needs further research. These metabolic alterations signify the potential of ACP-Glu to influence bone cell behavior, potentially impacting processes crucial for bone health, regeneration, and remodelling

4.2 In vitro evaluation of osteogenesis by ACP-Glu

To assess the potential of ACP-Glu as a biomaterial for bone tissue engineering, a series of in vitro experiments was conducted, comparing ACP-Glu with ACP, cold-sintered HAp, and a blank cell culture plate as controls.

4.2.1 Biocompatibility test

The general biocompatibility of the materials is tested by direct cell viability and indirect released LDH activity.

4.2.1.1 Cell viability by Cell Counting Kit-8 assay

The cell proliferation is presented by metabolic activity, tested by the Cell Counting Kit-8 assay in Figure 52. The cell viability assessment using CCK-8 indicated that ACP-Glu exhibited significantly higher cell viability (135%) compared to both the control (P = 0.0102) and HAp (P = 0.017), with no significant difference observed between ACP and ACP-Glu (P = 0.51). The lower cell viability in the absence of glutamate supply suggests that glutamate is involved in various cellular processes, including energy metabolism, protein synthesis, and neurotransmission. The lack of glutamate can compromise these processes and reduce cell viability. As discussed in 3.4.2.1 (Free calcium and phosphate in the media), the increased release of calcium ions from ACP-Glu may benefit cell viability. Calcium ions play a crucial role in cell signaling, and their presence in the culture medium can enhance various cellular functions, including proliferation and survival (158). A low glutamate environment negatively influences the proliferation here. This can further impact the function, such as mineralization. Together with the metabolomics analysis from 3.3.2, the enhanced energy metabolism stimulated by glutamate could be why cells had higher activity.

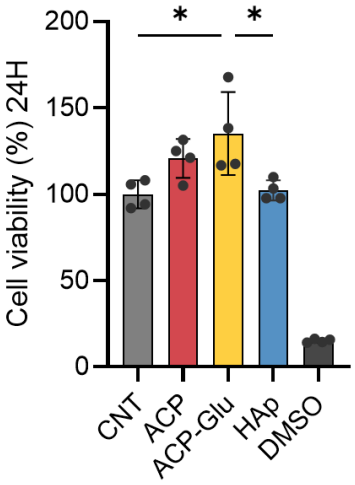

*Figure 52 Cell proliferation of MC3T3-E1 cultured after 24 hours. (*P < 0.05; **P < 0.01; ***P < 0.001; ****P < 0.0001)*

4.2.1.2 Assessment of cytotoxicity by LDH cell viability assay

Testing the cytotoxicity of materials is the basis for evaluating materials in vitro cell experiments. The LDH assay measures the release of LDH, an enzyme released when cell membranes are damaged. The MC3T3-E1 cell line cultured on all groups was tested at 3

different time points; no significant difference was noticed between the groups in the released LDH level (cytotoxicity test shown in Figure 53). The lack of differences in LDH release over time indicated that the cell membranes remained relatively intact and that cells maintained their structural integrity and health during the experiment. Although a cell viability difference is noticed on the proliferation side, all the groups showed no cytotoxicity. Focusing on ACP-Glu biomaterial, this result also verified that the release of glutamate did not cause damage to cell structure and lead to cell death. This requires no verification, but there have been many in-depth reports on the cytotoxicity induced by excessive supply of amino acids (159).

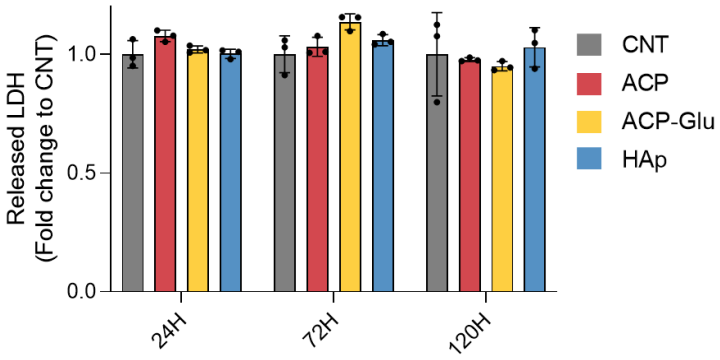

Figure 53 Released LDH level of all groups after culturing for 24, 72, and 120 hours. As a representative of the value that will increase with cytotoxicity, no significant difference among the groups was found in the LDH release amount.

4.2.2 Intracellular and extracellular calcium and phosphate level evaluation

Intracellular and extracellular calcium and phosphate levels were detected with the conditioned media and within cells after 10 days of incubation. The mineralization process of osteoblasts under the influence of biomaterials is relatively complex, and a long period after the differentiation can provide more valuable comparative information. The calcium and phosphate released from the materials and the intake into the cells could be compared to evaluate the calcium deposition and matrix mineralization ability.

4.2.2.1 Free calcium and phosphate in the media

Both ACP and ACP-Glu showed enhanced calcium ion release properties even in the presence of interference from pre-existing calcium ions in the culture medium. This suggests that the amorphous crystals dissolve faster compared to cold-sintered hydroxyapatite. Osteoblasts near the material can uptake these calcium ions from the media, which can then be used for bone mineralization and other cellular processes (160). In tissue engineering and regenerative

medicine, the goal is often to create biomaterials that mimic the natural bone microenvironment as closely as possible. Therefore, calcium phosphate materials are designed to facilitate the interaction of osteoblasts with both the material surface and the released calcium ions, providing a suitable environment for bone tissue formation and mineralization. The ability of osteoblasts to access calcium from these sources is crucial for the success of such materials in promoting bone regeneration. Amorphous calcium phosphate has higher solubility compared to HAp (44). This means ACP dissolves in aqueous solutions, including culture media, releasing calcium and phosphate ions into the surrounding liquid. The lack of a defined crystal structure in ACP results in faster dissolution kinetics. This makes the difference in the solubility of ACP under different environments (temperature, pH) more prominent.

To evaluate the potential of ACP-Glu as a biomaterial for bone tissue engineering, a series of in vitro experiments was conducted on ACP-Glu, ACP, and cold-sintered HAp, with a blank cell culture plate serving as a baseline reference rather than a direct comparison group. Given that the control group lacks calcium phosphate materials, its role is limited to observing baseline cellular metabolism without significant calcium or phosphate exchange, as cellular responses in the absence of calcium phosphate differ fundamentally from those in its presence.

Notably, the calcium released from ACP-Glu is also higher than from ACP, 1.6 times on day 10 and 2 times on day 14. Glutamate, an amino acid, can have a complex effect on calcium ions. Studies have shown that amino acids have higher solubility in the presence of calcium ions (161,162). Being part of a solute, their interactions are predictable, which may increase the solubility of the ACP (163). Glutamate can form soluble complexes with calcium, making it easier for the ACP-Glu to release calcium ions into the surrounding media. On the other hand, consider the other part of the material, phosphate; glutamate can also be complexed with phosphate ions, potentially reducing their availability to interact with calcium ions within the ACP-Glu structure (164). This could further promote the release of calcium from ACP-Glu.

As mentioned earlier, glutamate can form a complex with calcium ions, potentially increasing their release (Figure 54). However, this complexation effect cannot extend to phosphate ions to the same extent. The chemical interactions between glutamate and these ions can differ, resulting in a more pronounced effect on calcium release than phosphate. At the same time, it is essential to note that the released calcium and phosphate are tested from the media cultured with cells. Moreover, this incubation has continued for 10 days, and the osteoblast-like cell lines could have various behaviors towards the free ions in the media and the material matrix

itself, such as dynamically simultaneous uptake and release of calcium ions. This biological process can affect the interaction of the material with the surrounding media, increasing the volume of the mineralized layer or increasing or decreasing the calcium ion level in the microenvironment (culture medium). These surface modifications or mineralization caused by cells would have different effects on calcium and phosphate levels in the collected media.

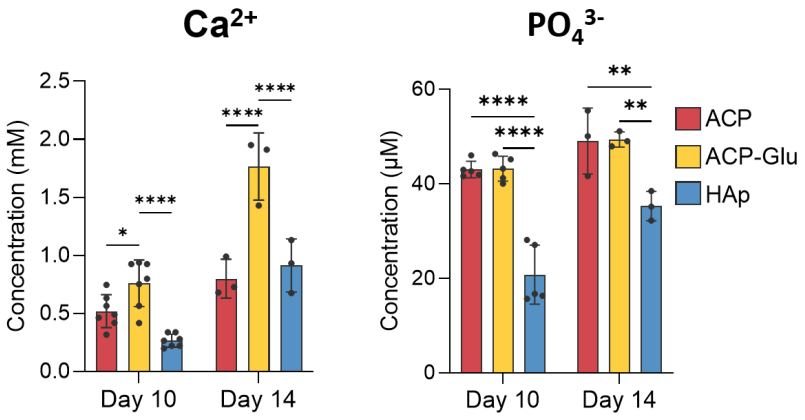

*Figure 54 Calcium and phosphate in the media on day 10 and day 14. (*P < 0.05; **P < 0.01; ***P < 0.001; ****P < 0.0001)*

4.2.2.2 Intracellular calcium and phosphate levels

Intracellular calcium and phosphate levels were measured after 14 days of cell culture (shown in Figure 55 by the form of OD level from absorbance plate reading). ACP-Glu, as the source of calcium, provided 1.4 times higher cell calcium levels than ACP. Unlike calcium, the phosphate in cells showed no significant differences between all three groups. With the free ion in the culture media, ACP-Glu can provide a high calcium environment and facilitate calcium intake. Glutamate, present in ACP-Glu, could play a role in influencing calcium metabolism. It can affect calcium signaling and cellular responses, potentially enhancing cell calcium uptake (165). In non-neuronal cells, including bone cells, glutamate can influence intracellular calcium signaling pathways. Activation of glutamate receptors can lead to calcium release from intracellular stores, such as the endoplasmic reticulum, and initiate a range of cellular responses (166). Notably, the data is from only one time point, which is already after 14 days of culture. There may be unknown influences from many other factors during this period, such as calcium and phosphorus deposits caused by parts mineralized on the CaP tablets.

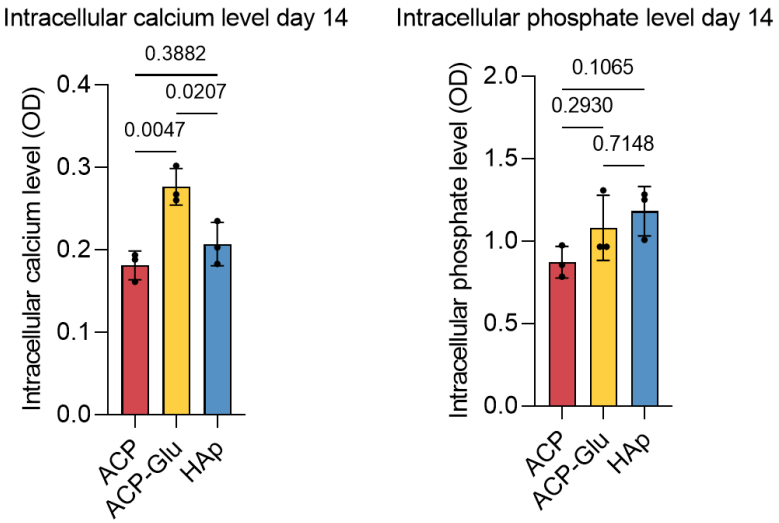

*Figure 55 Intracellular calcium and phosphate levels of MC3T3-E1 cells cultured on ACP, ACP-Glu, and HAp. Cells were collected on day 14. (*P < 0.05; **P < 0.01; ***P < 0.001; ****P < 0.0001)*

4.2.3 Osteogenesis evaluation

4.2.3.1 ALP activity

ALP level is tested from the conditioned media. ALP is essential for the mineralization of the extracellular matrix in bone tissue. As pre-osteoblast cells mature into osteoblasts, they become responsible for synthesizing the bone matrix, which includes collagen and other proteins. ALP helps initiate and promote the mineralization of this matrix by dephosphorylating compounds like inorganic pyrophosphate, which inhibits mineralization. The ALP level, sown in Figure 56 by ford changes, at the initial point is similar, with no p-value lower than 0.05 (Two-way ANOVA). The ALP level of ACP-Glu showed a significantly higher level at later points. As an osteogenic marker, ALP indicates the initial osteoblast differentiation, and the osteogenesis activity progresses. However, the ALP level tested in this study is from the culture media, which is not directly from the ALP in cells. Compared with the detection of intracellular content, there is an inevitable delay in this marker. The results supported that the ACP-Glu ceramic tablet triggered better osteogenic differentiation than the control, ACP, and HAp.

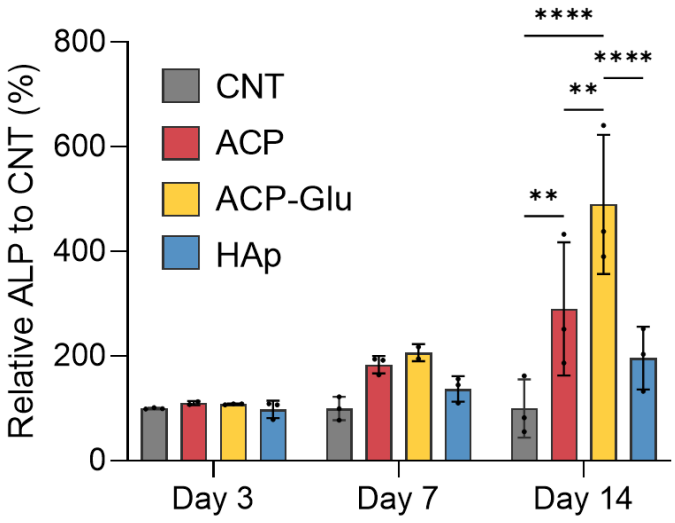

*Figure 56 Extracellular ALP activity of MC3T3-E1 cultured on cold sintered CaPs on days 3, 7, and 14. (*P < 0.05; **P < 0.01; ***P < 0.001; ****P < 0.0001)*

ALP plays a role in regulating phosphate levels in the body, particularly during bone mineralization. Dephosphorylating phosphate-containing compounds help control the balance of minerals necessary for bone formation.

4.2.3.2 Evaluation of the released OPN and OCN levels

Detecting OPN (osteopontin) and OCN (osteocalcin) levels in cell experiments helps evaluate osteogenic differentiation and bone matrix formation, which are crucial for assessing biomaterial performance in bone tissue engineering. To get better contrast change, the assessment of OPN and OCN involved measuring their released levels in the culture media on both day 7 and day 14 to ensure the pre-osteoblast differentiation, as they are later markers in the pre-osteoblast cell line in vitro model. The ACP-Glu group exhibited a significantly higher level of OPN at both time points. OPN is an intrinsically disordered protein featuring a notable negative charge, with approximately 25% of the protein's composition comprising aspartate or glutamate residues (167). As the supplier of one of the significant compositions of this protein, ACP-Glu may contribute to the manufacturing of OPN as well.

The OCN level on day 7 showed a similar result. OCN is a marker of mature osteoblasts involved in bone matrix production (Figure 57). The similar OCN levels on day 7 may indicate that the cells in all groups are at a relatively early stage of osteoblast differentiation. The influence of the presence/lack of glutamate showed up on day 14. This indicated that the cells

in the ACP-Glu group had progressed further in their differentiation and maturity. Glutamate in the ACP-Glu group may have influenced osteoblast activity and differentiation.

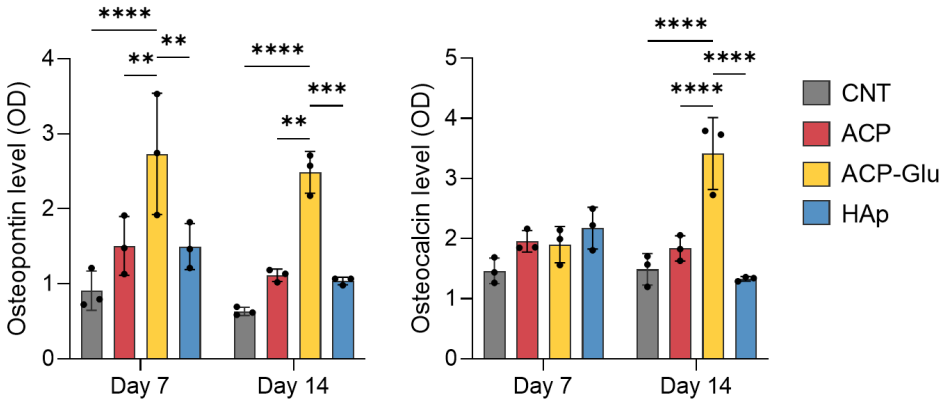

*Figure 57 Released (extracellular) OPN and OCN levels in culture media. (*P < 0.05; **P < 0.01; ***P < 0.001; ****P < 0.0001)*

4.2.4 Mineralization evaluation of ACP and ACP-Glu

In order to compare the mineralization capacity of ACP-Glu and ACP, Alizarin Red staining was applied to cultured MC3T3-E1 cells. The findings revealed distinct patterns among the experimental groups in the context of Alizarin Red staining to assess mineralization. As shown in Figure 58, after 21 days of culture, ACP-Glu groups presented a better mineralization result. From the macroscale image, the upper groups (ACP-Glu) presented more intense red on the well-plate surfaces. An optical microscope was used to observe the magnified stained parts; larger mineralized deposits were detected in the ACP-Glu groups (red-stained parts). Although the material that penetrated the filter itself may have a certain impact on the accuracy of the experiment, the results were still significant. Not only calcium but also glutamate released from the materials benefit the osteogenesis process of osteoblasts. The lack of glutamate can limit the mineralization progress of osteoblasts, and the presence of glutamate-containing material could enhance the primary responsibilities of osteoblasts: forming a new ossification structure. This result further demonstrated the superiority of ACP-Glu in terms of osteogenic induction.

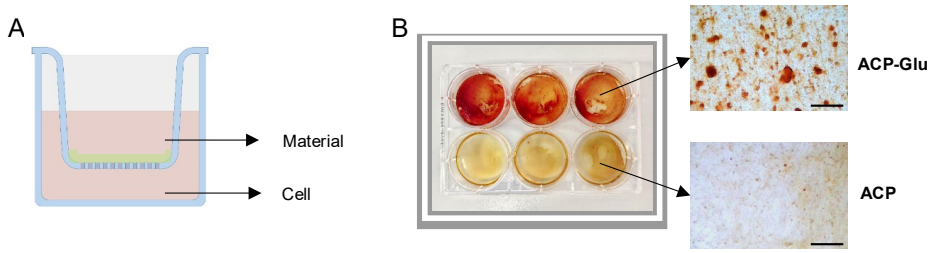

Figure 58 Alizarin Red staining (A) Illustration of indirect cell culture with materials. (B) The overall view of Alizarin Red staining captured by a camera and the microscope. ACP-Glu is up and ACP is down in the figure. Scale bar = 30μm.

5 Conclusions

1. Critical-size bone defects lead to significant metabolic fluctuations, notably depleting nutritional metabolites and reducing glutamine and glutamate.
2. Calcium phosphates (CaPs) adsorb low molecular metabolites, particularly amino acids, and influence cellular amino acid and energy metabolism pathways.
3. Anaerobic metabolism increases when cells come into contact with CAPs, especially on day 1.
4. Amorphous calcium phosphate (ACP) with glutamate (ACP-Glu) demonstrates controlled and gradual release of glutamate in 3 days, which is critical for supporting cellular functions during tissue repair.
5. Cold-sintered ACP-Glu outperforms hydroxyapatite and ACP in promoting cellular mineralization processes, with 2 times higher OCN and OPN levels and more prominent Alizarin Red staining results.
6. ACP-Glu changes energy metabolism, particularly enhancing the tricarboxylic acid cycle post-gluconeogenesis. Exposure to ACP-Glu resulted in 8 times higher intracellular citric acid level than other investigated CAPs.

6 References

1. LANGER R, P. VACANTI J. Tissue Engineering. Science (80-). 1993;260(5110):920–6.
2. Kwon SG, Kwon YW, Lee TW, Park GT, Kim JH. Recent advances in stem cell therapeutics

and tissue engineering strategies. Biomater Res. 2018;22(1):1–8.

3. Koons GL, Diba M, Mikos AG. Materials design for bone-tissue engineering. Nat Rev Mater [Internet]. 2020;5(8):584–603. Available from: http://dx.doi.org/10.1038/s41578-020-0204-2

4. Curvello R, Kast V, Ordóñez-Morán P, Mata A, Loessner D. Biomaterial-based platforms for tumour tissue engineering. Nat Rev Mater. 2023;(April).

5. Fan J, Abedi-Dorcheh K, Vaziri AS, Kazemi-Aghdam F, Rafieyan S, Sohrabinejad M, et al. A Review of Recent Advances in Natural Polymer-Based Scaffolds for Musculoskeletal Tissue Engineering. Polymers (Basel). 2022;14(10).

6. Da Silva AC. Structure and percolation of bioglasses. Vol. 53, Advanced Structured Materials. 2016. 49–84 p.

7. Sarkar A. Biosensing, Characterization of Biosensors, and Improved Drug Delivery Approaches Using Atomic Force Microscopy: A Review. Front Nanotechnol. 2022;3(January):1–19.

8. Wei F, Liu S, Chen M, Tian G, Zha K, Yang Z, et al. Host Response to Biomaterials for Cartilage Tissue Engineering: Key to Remodeling. Front Bioeng Biotechnol. 2021;9(May):1–19.

9. Zheng X, Zhang P, Fu Z, Meng S, Dai L, Yang H. Applications of nanomaterials in tissue engineering. RSC Adv. 2021;11(31):19041–58.

10. Armiento AR, Hatt LP, Sanchez Rosenberg G, Thompson K, Stoddart MJ. Functional Biomaterials for Bone Regeneration: A Lesson in Complex Biology. Adv Funct Mater. 2020;30(44):1–41.

11. Dorozhkin S V. A detailed history of calcium orthophosphates from 1770s till 1950. Mater Sci Eng C [Internet]. 2013;33(6):3085–110. Available from: http://dx.doi.org/10.1016/j.msec.2013.04.002

12. Misch CM. Autogenous bone: Is it still the gold standard? Implant Dent. 2010;19(5):361.

13. Giannoudis P V., Dinopoulos H, Tsiridis E. Bone substitutes: an update. Injury. 2005;36 Suppl 3:20–7.

14. Fernandez de Grado G, Keller L, Idoux-Gillet Y, Wagner Q, Musset AM, Benkirane-Jessel N, et al. Bone substitutes: a review of their characteristics, clinical use, and perspectives for large bone defects management. J Tissue Eng. 2018;9.

15. Wang W, Yeung KWK. Bone grafts and biomaterials substitutes for bone defect repair: A review. Bioact Mater [Internet]. 2017;2(4):224–47. Available from: https://doi.org/10.1016/j.bioactmat.2017.05.007

16. Wang S, Liu L, Li K, Zhu L, Chen J, Hao Y. Pore functionally graded Ti6Al4V scaffolds for bone tissue engineering application. Mater Des [Internet]. 2019;168:107643. Available from: https://doi.org/10.1016/j.matdes.2019.107643

17. Jodati H, Yılmaz B, Evis Z. A review of bioceramic porous scaffolds for hard tissue applications: Effects of structural features. Ceram Int. 2020;46(10):15725–39.

18. Garcia-Gonzalez D, Rusinek A, Bendarma A, Bernier R, Klosak M, Bahi S. Material and structural behaviour of PMMA from low temperatures to over the glass transition: Quasi-static and dynamic loading. Polym Test [Internet]. 2020;81(October 2019):106263. Available from: https://doi.org/10.1016/j.polymertesting.2019.106263

19. Yousefi AM. A review of calcium phosphate cements and acrylic bone cements as injectable materials for bone repair and implant fixation. J Appl Biomater Funct Mater. 2019;17(4).

20. Fan W, Fu D, Zhang L, Xiao Z, Shen X, Chen J, et al. Enoxaparin sodium bone cement plays

an anti-inflammatory immunomodulatory role by inducing the polarization of M2 macrophages. J Orthop Surg Res [Internet]. 2023;18(1):1–15. Available from: https://doi.org/10.1186/s13018-023-03865-8

21. Hanstein T. A Literature Review of the Clinical Evidence Situation of Bone Cements. 2018;7(March):31–6.

22. Zhao C, Liu W, Zhu M, Wu C, Zhu Y. Bioceramic-based scaffolds with antibacterial function for bone tissue engineering: A review. Bioact Mater [Internet]. 2022;18(December 2021):383–98. Available from: https://doi.org/10.1016/j.bioactmat.2022.02.010

23. Kumar R, Mohanty S. Hydroxyapatite: A Versatile Bioceramic for Tissue Engineering Application. J Inorg Organomet Polym Mater. 2022;32(12):4461–77.

24. Heise U, Osborn JF, Duwe F. Hydroxyapatite ceramic as a bone substitute. Int Orthop. 1990;14(3):329–38.

25. Sun W, Fan J, Wang S, Kang Y, Du J, Peng X. Biodegradable Drug-Loaded Hydroxyapatite Nanotherapeutic Agent for Targeted Drug Release in Tumors. ACS Appl Mater Interfaces. 2018;10(9):7832–40.

26. Mo X, Zhang D, Liu K, Zhao X, Li X, Wang W. Nano-Hydroxyapatite Composite Scaffolds Loaded with Bioactive Factors and Drugs for Bone Tissue Engineering. Int J Mol Sci. 2023;24(2).

27. Qian G, Xiong L, Ye Q. Hydroxyapatite-based carriers for tumor targeting therapy. RSC Adv. 2023;13(24):16512–28.

28. Harun WSW, Asri RIM, Alias J, Zulkifli FH, Kadirgama K, Ghani SAC, et al. A comprehensive review of hydroxyapatite-based coatings adhesion on metallic biomaterials. Ceram Int. 2018;44(2):1250–68.

29. Jaafar A, Hecker C, Árki P, Joseph Y. Sol-gel derived hydroxyapatite coatings for titanium implants: A review. Bioengineering. 2020;7(4):1–23.

30. Jiang J, Han G, Zheng X, Chen G, Zhu P. Characterization and biocompatibility study of hydroxyapatite coating on the surface of titanium alloy. Surf Coatings Technol [Internet]. 2019;375(July):645–51. Available from: https://doi.org/10.1016/j.surfcoat.2019.07.067

31. Šupová M. Substituted hydroxyapatites for biomedical applications: A review. Ceram Int. 2015;41(8):9203–31.

32. Collins MN, Ren G, Young K, Pina S, Reis RL, Oliveira JM. Scaffold Fabrication Technologies and Structure/Function Properties in Bone Tissue Engineering. Adv Funct Mater. 2021;31(21).

33. Jeong J, Kim JH, Shim JH, Hwang NS, Heo CY. Bioactive calcium phosphate materials and applications in bone regeneration. Biomater Res. 2019;23(1):1–11.

34. Ali A, Bano S, Poojary S, Chaudhary A, Kumar D, Negi YS. Effect of cellulose nanocrystals on chitosan/PVA/nano β-TCP composite scaffold for bone tissue engineering application. J Biomater Sci Polym Ed [Internet]. 2022;33(1):1–19. Available from: https://doi.org/10.1080/09205063.2021.1973709

35. Shirakata Y, Setoguchi F, Sena K, Nakamura T, Imafuji T, Shinohara Y, et al. Comparison of periodontal wound healing/regeneration by recombinant human fibroblast growth factor-2 combined with β-tricalcium phosphate, carbonate apatite, or deproteinized bovine bone mineral in a canine one-wall intra-bony defect model. J Clin Periodontol. 2022;49(6):599–608.

36. Mohammed AHM, Shariff KA, Abu Bakar MH, Mohamad H. Recent methods in fabricating porous β-tricalcium phosphate scaffolds: A mini review. Mater Today Proc [Internet]. 2022;66:2702–4. Available from: https://doi.org/10.1016/j.matpr.2022.06.498

37. Vecstaudza J, Gasik M, Locs J. Amorphous calcium phosphate materials: Formation, structure and thermal behaviour. J Eur Ceram Soc [Internet]. 2019;39(4):1642–9. Available from: https://doi.org/10.1016/j.jeurceramsoc.2018.11.003

38. Lotsari A, Rajasekharan AK, Halvarsson M, Andersson M. Transformation of amorphous calcium phosphate to bone-like apatite. Nat Commun [Internet]. 2018;9(1). Available from: http://dx.doi.org/10.1038/s41467-018-06570-x

39. Ito T, Otsuka M. Application of calcium phosphate as a controlled-release device. Biol Pharm Bull. 2013;36(11):1676–82.

40. Dorozhkin S V. Amorphous calcium (ortho)phosphates. Acta Biomater [Internet]. 2010;6(12):4457–75. Available from: http://dx.doi.org/10.1016/j.actbio.2010.06.031

41. KOJIMA Y, SAKAMA K, TOYAMA T, YASUE T, ARAI Y. Dehydration of Water Molecule in Amorphous Calcium Phosphate. Phosphorus Res Bull. 1994;4(0):47–52.

42. Edén M. Structure and formation of amorphous calcium phosphate and its role as surface layer of nanocrystalline apatite: Implications for bone mineralization. Materialia [Internet]. 2021;17(April):101107. Available from: https://doi.org/10.1016/j.mtla.2021.101107

43. Shahrezaee M, Raz M, Shishehbor S, Moztarzadeh F, Baghbani F, Sadeghi A, et al. Synthesis of Magnesium Doped Amorphous Calcium Phosphate as a Bioceramic for Biomedical Application: In Vitro Study. Silicon. 2018;10(3):1171–9.

44. Luginina M, Orru R, Cao G, Luginina M, Grossin D, Brouillet F, et al. First successful stabilization of consolidated amorphous calcium phosphate (ACP) by cold sintering: Toward highly-resorbable reactive bioceramics. J Mater Chem B. 2020;8(4):629–35.

45. Chen Y, Gu W, Pan H, Jiang S, Tang R. Stabilizing amorphous calcium phosphate phase by citrate adsorption. CrystEngComm. 2014;16(10):1864–7.

46. Zhao J, Liu Y, Sun W Bin, Yang X. First detection, characterization, and application of amorphous calcium phosphate in dentistry. J Dent Sci [Internet]. 2012;7(4):316–23. Available from: http://dx.doi.org/10.1016/j.jds.2012.09.001

47. Furkó M, Balázsi K, Balázsi C. Comparative study on preparation and characterization of bioactive coatings for biomedical applications - A review on recent patents and literature. Rev Adv Mater Sci. 2017;48(1):25–51.

48. Combes C, Rey C. Amorphous calcium phosphates: Synthesis, properties and uses in biomaterials. Acta Biomater [Internet]. 2010;6(9):3362–78. Available from: http://dx.doi.org/10.1016/j.actbio.2010.02.017

49. Ma Z, Chen F, Zhu YJ, Cui T, Liu XY. Amorphous calcium phosphate/poly(D,L-lactic acid) composite nanofibers: Electrospinning preparation and biomineralization. J Colloid Interface Sci [Internet]. 2011;359(2):371–9. Available from: http://dx.doi.org/10.1016/j.jcis.2011.04.023

50. Chahal AS, Schweikle M, Lian AM, Reseland JE, Haugen HJ, Tiainen H. Osteogenic potential of poly(ethylene glycol)-amorphous calcium phosphate composites on human mesenchymal stem cells. J Tissue Eng. 2020;11.

51. Liao H, Yu HP, Song W, Zhang G, Lu B, Zhu YJ, et al. Amorphous calcium phosphate nanoparticles using adenosine triphosphate as an organic phosphorus source for promoting tendon–bone healing. J Nanobiotechnology [Internet]. 2021;19(1):1–17. Available from: https://doi.org/10.1186/s12951-021-01007-y

52. Vakifahmetoglu C, Karacasulu L. Cold sintering of ceramics and glasses: A review. Curr Opin Solid State Mater Sci. 2020;24(1).

53. Galotta A, Sglavo VM. The cold sintering process: A review on processing features,

densification mechanisms and perspectives. J Eur Ceram Soc [Internet]. 2021;41(16):1–17. Available from: https://doi.org/10.1016/j.jeurceramsoc.2021.09.024

54. Hong W Bin, Li L, Cao M, Chen XM. Plastic deformation and effects of water in room-temperature cold sintering of NaCl microwave dielectric ceramics. J Am Ceram Soc. 2018;101(9):4038–43.

55. Guo N, Shen HZ, Shen P. One-step synthesis and densification of BaTiO3 by reactive cold sintering. Scr Mater [Internet]. 2022;213(January):114628. Available from: https://doi.org/10.1016/j.scriptamat.2022.114628

56. Rubenis K, Zemjane S, Vecstaudza J, Bitenieks J, Locs J. Densification of amorphous calcium phosphate using principles of the cold sintering process. J Eur Ceram Soc [Internet]. 2021;41(1):912–9. Available from: https://doi.org/10.1016/j.jeurceramsoc.2020.08.074

57. Rubenis K, Zemjane S, Vecstaudza J, Lazdovica K, Bitenieks J, Wiecinski P, et al. Sintering of amorphous calcium phosphate to near-full density by uniaxial compaction at room temperature. J Eur Ceram Soc [Internet]. 2022;42(13):6199–205. Available from: https://doi.org/10.1016/j.jeurceramsoc.2022.06.041

58. Thomas M V., Puleo DA. Calcium sulfate: Properties and clinical applications. J Biomed Mater Res - Part B Appl Biomater. 2009;88(2):597–610.

59. Aguiar H, Chiussi S, López-Álvarez M, González P, Serra J. Structural characterization of bioceramics and mineralized tissues based on Raman and XRD techniques. Ceram Int [Internet]. 2018;44(1):495–504. Available from: https://doi.org/10.1016/j.ceramint.2017.09.203

60. Suga M, Asahina S, Sakuda Y, Kazumori H, Nishiyama H, Nokuo T, et al. Recent progress in scanning electron microscopy for the characterization of fine structural details of nano materials. Prog Solid State Chem [Internet]. 2014;42(1–2):1–21. Available from: http://dx.doi.org/10.1016/j.progsolidstchem.2014.02.001

61. Zou G, She J, Peng S, Yin Q, Liu H, Che Y. Two-dimensional SEM image-based analysis of coal porosity and its pore structure. Int J Coal Sci Technol [Internet]. 2020;7(2):350–61. Available from: https://doi.org/10.1007/s40789-020-00301-8

62. Kalaskar DM, Demoustier-Champagne S, Dupont-Gillain CC. Interaction of preosteoblasts with surface-immobilized collagen-based nanotubes. Colloids Surfaces B Biointerfaces [Internet]. 2013;111:134–41. Available from: http://dx.doi.org/10.1016/j.colsurfb.2013.05.035

63. Thiberge S, Nechushtan A, Sprinzak D, Gileadi O, Behar V, Zik O, et al. Scanning electron microscopy of cells and tissues under fully hydrated conditions. Proc Natl Acad Sci U S A. 2004;101(10):3346–51.

64. Sayed E, Haj-Ahmad R, Ruparelia K, Arshad MS, Chang MW, Ahmad Z. Porous Inorganic Drug Delivery Systems—a Review. AAPS PharmSciTech. 2017;18(5):1507–25.

65. Hernandez JL, Woodrow KA. Medical Applications of Porous Biomaterials: Features of Porosity and Tissue-Specific Implications for Biocompatibility. Adv Healthc Mater. 2022;11(9):1–25.

66. Karageorgiou V, Kaplan D. Porosity of 3D biomaterial scaffolds and osteogenesis. Biomaterials. 2005;26(27):5474–91.

67. Yao X, Peng R, Ding J. Cell-material interactions revealed via material techniques of surface patterning. Adv Mater. 2013;25(37):5257–86.

68. Bodhak S, Bose S, Bandyopadhyay A. Electrically polarized HAp-coated Ti: In vitro bone cell-material interactions. Acta Biomater [Internet]. 2010;6(2):641–51. Available from: http://dx.doi.org/10.1016/j.actbio.2009.08.008

69. Abaricia JO, Farzad N, Heath TJ, Simmons J, Morandini L, Olivares-Navarrete R. Control of innate immune response by biomaterial surface topography, energy, and stiffness. Acta Biomater. 2021;133:58–73.

70. Zhou K, Li Y, Zhang L, Jin L, Yuan F, Tan J, et al. Nano-micrometer surface roughness gradients reveal topographical influences on differentiating responses of vascular cells on biodegradable magnesium. Bioact Mater [Internet]. 2021;6(1):262–72. Available from: https://doi.org/10.1016/j.bioactmat.2020.08.004

71. Batool F, Özçelik H, Stutz C, Gegout PY, Benkirane-Jessel N, Petit C, et al. Modulation of immune-inflammatory responses through surface modifications of biomaterials to promote bone healing and regeneration. J Tissue Eng. 2021;12.

72. Abaricia JO, Shah AH, Chaubal M, Hotchkiss KM, Olivares-Navarrete R. Wnt signaling modulates macrophage polarization and is regulated by biomaterial surface properties. Biomaterials. 2020;243.

73. Martin KE, García AJ. Macrophage phenotypes in tissue repair and the foreign body response: Implications for biomaterial-based regenerative medicine strategies. Acta Biomater [Internet]. 2021;133(xxxx):4–16. Available from: https://doi.org/10.1016/j.actbio.2021.03.038

74. González-García C, Cantini M, Ballester-Beltrán J, Altankov G, Salmerón-Sánchez M. The strength of the protein-material interaction determines cell fate. Acta Biomater. 2018;77:74–84.

75. Othman Z, Cillero Pastor B, van Rijt S, Habibovic P. Understanding interactions between biomaterials and biological systems using proteomics. Biomaterials [Internet]. 2018;167:191–204. Available from: https://doi.org/10.1016/j.biomaterials.2018.03.020

76. Nonoyama T, Kinoshita T, Higuchi M, Nagata K, Tanaka M, Kamada M, et al. Arrangement techniques of proteins and cells using amorphous calcium phosphate nanofiber scaffolds. Appl Surf Sci [Internet]. 2012;262:8–12. Available from: http://dx.doi.org/10.1016/j.apsusc.2011.12.009

77. Rahmany MB, Van Dyke M. Biomimetic approaches to modulate cellular adhesion in biomaterials: A review. Acta Biomater [Internet]. 2013;9(3):5431–7. Available from: http://dx.doi.org/10.1016/j.actbio.2012.11.019

78. Li H, Liu M, Wang X, Wang H, Mo X, Wu J. Nanofiber Configuration of Electrospun Scaffolds Dictating Cell Behaviors and Cell-scaffold Interactions. Chem Res Chinese Univ. 2021;37(3):456–63.

79. Mao Z, Yu S, Ren T, Gao C. Gradient biomaterials and their impact on cell migration. Polym Biomater Tissue Regen From Surface/Interface Des to 3D Constr. 2016;(March):151–85.

80. Battiston KG, Cheung JWC, Jain D, Santerre JP. Biomaterials in co-culture systems: Towards optimizing tissue integration and cell signaling within scaffolds. Biomaterials [Internet]. 2014;35(15):4465–76. Available from: http://dx.doi.org/10.1016/j.biomaterials.2014.02.023

81. Albrektsson T, Johansson C. Osteoinduction, osteoconduction and osseointegration. Eur Spine J. 2001;10:S96–101.

82. Fan J, Jahed V, Klavins K. Metabolomics in bone research. Metabolites. 2021;11(7).

83. Grankvist N, Watrous JD, Lagerborg KA, Lyutvinskiy Y, Jain M, Nilsson R. Profiling the Metabolism of Human Cells by Deep 13C Labeling. Cell Chem Biol. 2018;25(11):1419-1427.e4.

84. Duda GN, Geissler S, Checa S, Tsitsilonis S, Petersen A, Schmidt-Bleek K. The decisive early phase of bone regeneration. Nat Rev Rheumatol. 2023;19(2):78–95.

85. Einhorn TA, Gerstenfeld LC. Fracture healing: Mechanisms and interventions. Nat Rev Rheumatol [Internet]. 2015;11(1):45–54. Available from:

http://dx.doi.org/10.1038/nrrheum.2014.164

86. Ponzetti M, Rucci N. Osteoblast differentiation and signaling: Established concepts and emerging topics. Int J Mol Sci. 2021;22(13).

87. Casado-Díaz A, Ferreiro-Vera C, Priego-Capote F, Dorado G, Luque-De-Castro MD, Quesada-Gómez JM. Effects of arachidonic acid on the concentration of hydroxyeicosatetraenoic acids in culture media of mesenchymal stromal cells differentiating into adipocytes or osteoblasts. Genes Nutr. 2014;9(1).

88. Chen G, Deng C, Li YP. TGF-β and BMP signaling in osteoblast differentiation and bone formation. Int J Biol Sci. 2012;8(2):272–88.

89. Zheng C, Wang J, Liu Y, Yu Q, Liu Y, Deng N, et al. Functional selenium nanoparticles enhanced stem cell osteoblastic differentiation through BMP signaling pathways. Adv Funct Mater. 2014;24(43):6872–83.

90. Altmann B, Steinberg T, Giselbrecht S, Gottwald E, Tomakidi P, Bächle-Haas M, et al. Promotion of osteoblast differentiation in 3D biomaterial micro-chip arrays comprising fibronectin-coated poly(methyl methacrylate) polycarbonate. Biomaterials [Internet]. 2011;32(34):8947–56. Available from: http://dx.doi.org/10.1016/j.biomaterials.2011.08.023

91. Chen K, Jiao Y, Liu L, Huang M, He C, He W, et al. Communications Between Bone Marrow Macrophages and Bone Cells in Bone Remodeling. Front Cell Dev Biol. 2020;8(December):1–15.

92. Robling AG, Bonewald LF. The Osteocyte: New Insights. Annu Rev Physiol. 2020;82(5):485–506.

93. Matsuzaka T, Matsugaki A, Nakano T. Control of osteoblast arrangement by osteocyte mechanoresponse through prostaglandin E2 signaling under oscillatory fluid flow stimuli. Biomaterials [Internet]. 2021;279(October):121203. Available from: https://doi.org/10.1016/j.biomaterials.2021.121203

94. Bernhardt A, Skottke J, von Witzleben M, Gelinsky M. Triple culture of primary human osteoblasts, osteoclasts and osteocytes as an in vitro bone model. Int J Mol Sci. 2021;22(14).

95. Shah FA, Thomsen P, Palmquist A. A Review of the Impact of Implant Biomaterials on Osteocytes. J Dent Res. 2018;97(9):977–86.

96. Qin L, Liu W, Cao H, Xiao G. Molecular mechanosensors in osteocytes. Bone Res [Internet]. 2020;8(1):1–24. Available from: http://dx.doi.org/10.1038/s41413-020-0099-y

97. Tatsumi S, Ishii K, Amizuka N, Li M, Kobayashi T, Kohno K, et al. Targeted Ablation of Osteocytes Induces Osteoporosis with Defective Mechanotransduction. Cell Metab. 2007;5(6):464–75.

98. Thompson WR, Rubin CT, Rubin J. Mechanical regulation of signaling pathways in bone. Gene [Internet]. 2012;503(2):179–93. Available from: http://dx.doi.org/10.1016/j.gene.2012.04.076

99. Verbruggen SW, Vaughan TJ, McNamara LM. Mechanisms of osteocyte stimulation in osteoporosis. J Mech Behav Biomed Mater [Internet]. 2016;62:158–68. Available from: http://dx.doi.org/10.1016/j.jmbbm.2016.05.004

100. Aw Yong KM, Horst E, Neale D, Royzenblat S, Lahann J, Greineder C, et al. A Bioreactor for 3D In Vitro Modeling of the Mechanical Stimulation of Osteocytes. Front Bioeng Biotechnol. 2022;10(March):1–11.

101. Bolamperti S, Villa I, Rubinacci A. Bone remodeling: an operational process ensuring survival and bone mechanical competence. Bone Res. 2022;10(1).

102. Soysa NS, Alles N. Osteoclast function and bone-resorbing activity: An overview. Biochem Biophys Res Commun [Internet]. 2016;476(3):115–20. Available from: http://dx.doi.org/10.1016/j.bbrc.2016.05.019

103. Duque G, Troen BR. Understanding the mechanisms of senile osteoporosis: New facts for a major geriatric syndrome. J Am Geriatr Soc. 2008;56(5):935–41.

104. McDonald MM, Khoo WH, Ng PY, Xiao Y, Zamerli J, Thatcher P, et al. Osteoclasts recycle via osteomorphs during RANKL-stimulated bone resorption. Cell. 2021;184(5):1330-1347.e13.

105. Fomby P, Cherlin AJ, Hadjizadeh A, Doillon CJ, Sueblinvong V, Weiss DJ, et al. Stem cells and cell therapies in lung biology and diseases: Conference report. Ann Am Thorac Soc [Internet]. 2010;12(3):181–204. Available from: http://dx.doi.org/10.1016/j.trsl.2010.06.007

106. Sachit T S NM. New bioactive glass scaffolds with exceptional qualities for bone tissue regeneration: response of osteoblasts and osteoclasts. Mater Res Express. 2019;0–18.

107. Xiao L, Ma Y, Crawford R, Mendhi J, Zhang Y, Lu H, et al. The interplay between hemostasis and immune response in biomaterial development for osteogenesis. Mater Today [Internet]. 2022;54(April):202–24. Available from: https://doi.org/10.1016/j.mattod.2022.02.010

108. Lu LY, Loi F, Nathan K, Lin TH, Pajarinen J, Gibon E, et al. Pro-inflammatory M1 macrophages promote Osteogenesis by mesenchymal stem cells via the COX-2-prostaglandin E2 pathway. J Orthop Res. 2017;35(11):2378–85.

109. Maruyama M, Rhee C, Utsunomiya T, Zhang N, Ueno M, Yao Z, et al. Modulation of the Inflammatory Response and Bone Healing. Front Endocrinol (Lausanne). 2020;11(June):1–14.

110. O'Driscoll SWM, Saris DBF, Ito Y, Fitzimmons JS. The chondrogenic potential of periosteum decreases with age. J Orthop Res. 2001;19(1):95–103.

111. Chen Y, Li EM, Xu LY. Guide to Metabolomics Analysis: A Bioinformatics Workflow. Metabolites. 2022;12(4).

112. Theodoridis G, Gika HG, Wilson ID. Mass spectrometry-based holistic analytical approaches for metabolite profiling in systems biology studies. Vol. 30, Mass Spectrometry Reviews. 2011. p. 884–906.

113. Chen N, Wang HB, Wu BQ, Jiang JH, Yang JT, Tang LJ, et al. Using random forest to detect multiple inherited metabolic diseases simultaneously based on GC-MS urinary metabolomics. Talanta [Internet]. 2021;235(July):122720. Available from: https://doi.org/10.1016/j.talanta.2021.122720

114. Kokla M, Virtanen J, Kolehmainen M, Paananen J, Hanhineva K. Random forest-based imputation outperforms other methods for imputing LC-MS metabolomics data: A comparative study. BMC Bioinformatics. 2019;20(1):1–11.

115. Armiñán A, Palomino-Schätzlein M, Deladriere C, Arroyo-Crespo JJ, Vicente-Ruiz S, Vicent MJ, et al. Metabolomics facilitates the discrimination of the specific anti-cancer effects of free- and polymer-conjugated doxorubicin in breast cancer models. Biomaterials. 2018;162:144–53.

116. McNamara LE, Sjöström T, Burgess KEV, Kim JJW, Liu E, Gordonov S, et al. Skeletal stem cell physiology on functionally distinct titania nanotopographies. Biomaterials. 2011;32(30):7403–10.

117. Mei J, Xu D, Wang L, Kong L, Liu Q, Li Q, et al. Biofilm Microenvironment-Responsive Self-Assembly Nanoreactors for All-Stage Biofilm Associated Infection through Bacterial Cuproptosis-like Death and Macrophage Re-Rousing. Adv Mater. 2023;35(36).

118. Zhang A, Sun H, Wang P, Han Y, Wang X. Recent and potential developments of biofluid analyses in metabolomics. J Proteomics [Internet]. 2012;75(4):1079–88. Available from:

http://dx.doi.org/10.1016/j.jprot.2011.10.027

119. Bellissimo MP, Roberts JL, Jones DP, Liu KH, Taibl KR, Uppal K, et al. Metabolomic associations with serum bone turnover markers. Nutrients. 2020;12(10):1–14.

120. Jagtap VR, Ganu J V. Effect of antiresorptive therapy on urinary hydroxyproline in postmenopausal osteoporosis. Indian J Clin Biochem. 2012;27(1):90–3.

121. Xiao HH, Sham TT, Chan CO, Li MH, Chen X, Wu QC, et al. A metabolomics study on the bone protective effects of a lignan-rich fraction from Sambucus Williamsii Ramulus in aged rats. Front Pharmacol. 2018;9(AUG).

122. Ibrahim H, Alnachoukati O, Baxter BA, Chapin T, Schroeppel T, Dunn J, et al. Non-Targeted Metabolomics Signature in the Plasma and Bone Marrow of Patients with Long Bone Injuries. Curr Metabolomics Syst Biol. 2019;7(1):51–66.

123. Almadi T, Cathers I, Chow CM. Associations among work-related stress, cortisol, inflammation, and metabolic syndrome. Psychophysiology. 2013;50(9):821–30.

124. Jasperson LK, Bucher C, Panoskaltsis-Mortari A, Taylor PA, Mellor AL, Munn DH, et al. Indoleamine 2,3-dioxygenase is a critical regulator of acute graft-versus-host disease lethality. Blood. 2008;111(6):3257–65.

125. Roberts JN, Sahoo JK, McNamara LE, Burgess K V., Yang J, Alakpa E V., et al. Dynamic Surfaces for the Study of Mesenchymal Stem Cell Growth through Adhesion Regulation. ACS Nano. 2016;10(7):6667–79.

126. Zhu T, Jiang M, Zhang M, Cui L, Yang X, Wang X, et al. Biofunctionalized composite scaffold to potentiate osteoconduction, angiogenesis, and favorable metabolic microenvironment for osteonecrosis therapy. Bioact Mater [Internet]. 2022;9(March 2021):446–60. Available from: https://doi.org/10.1016/j.bioactmat.2021.08.005

127. Chen J, Ma S, Yang H, Liang X, Yao H, Guo B, et al. Generation and metabolomic characterization of functional ductal organoids with biliary tree networks in decellularized liver scaffolds. Bioact Mater [Internet]. 2023;26(March):452–64. Available from: https://doi.org/10.1016/j.bioactmat.2023.03.012

128. Li D, Hu X, Zhang S. Biodegradation of graphene-based nanomaterials in blood plasma affects their biocompatibility, drug delivery, targeted organs and antitumor ability. Biomaterials [Internet]. 2019;202(January):12–25. Available from: https://doi.org/10.1016/j.biomaterials.2019.02.020

129. Barcik J, Ernst M, Buchholz T, Constant C, Mys K, Epari DR, et al. The absence of immediate stimulation delays bone healing. Bone [Internet]. 2023;175(April):116834. Available from: https://doi.org/10.1016/j.bone.2023.116834

130. Salma K, Berzina-Cimdina L, Borodajenko N. Calcium phosphate bioceramics prepared from wet chemically precipitated powders. Process Appl Ceram. 2010;4(1):45–51.

131. Izumiya M, Haniu M, Ueda K, Ishida H, Ma C, Ideta H, et al. Evaluation of mc3t3-e1 cell osteogenesis in different cell culture media. Int J Mol Sci. 2021;22(14):1–12.

132. Fan J, Schiemer T, Vaska A, Jahed V, Klavins K. Cell via Cell Viability Assay Changes Cellular Metabolic Characteristics by Intervening with Glycolysis and Pentose Phosphate Pathway. Chem Res Toxicol [Internet]. 2023 Jan 8;0(0). Available from: https://pubs.acs.org/doi/10.1021/acs.chemrestox.3c00339

133. Pang Z, Zhou G, Ewald J, Chang L, Hacariz O, Basu N, et al. Using MetaboAnalyst 5.0 for LC–HRMS spectra processing, multi-omics integration and covariate adjustment of global metabolomics data. Nat Protoc. 2022;17(8):1735–61.

134. Longo N, Frigeni M, Pasquali M. Carnitine transport and fatty acid oxidation. Biochim Biophys Acta - Mol Cell Res [Internet]. 2016;1863(10):2422–35. Available from: http://dx.doi.org/10.1016/j.bbamcr.2016.01.023

135. Keshani M, Alikiaii B, Askari G, Yahyapoor F, Ferns GA, Bagherniya M. The effects of l-carnitine supplementation on inflammatory factors, oxidative stress, and clinical outcomes in patients with sepsis admitted to the intensive care unit (ICU): study protocol for a double blind, randomized, placebo-controlled clinical trial. Trials. 2022;23(1):1–10.

136. Yoo HC, Yu YC, Sung Y, Han JM. Glutamine reliance in cell metabolism. Exp Mol Med [Internet]. 2020;52(9):1496–516. Available from: http://dx.doi.org/10.1038/s12276-020-00504-8

137. Ishak Gabra MB, Yang Y, Li H, Senapati P, Hanse EA, Lowman XH, et al. Dietary glutamine supplementation suppresses epigenetically-activated oncogenic pathways to inhibit melanoma tumour growth. Nat Commun [Internet]. 2020;11(1). Available from: http://dx.doi.org/10.1038/s41467-020-17181-w

138. Watford M. Glutamine and glutamate: Nonessential or essential amino acids? Anim Nutr [Internet]. 2015;1(3):119–22. Available from: http://dx.doi.org/10.1016/j.aninu.2015.08.008

139. Yan J, Horng T, Csóka B, Selmeczy Z, Koscsó B, Németh ZH, et al. Mitohormesis reprogrammes macrophage metabolism to enforce tolerance. Front Immunol [Internet]. 2020;5(1):318–32. Available from: http://dx.doi.org/10.1016/j.jallcom.2017.01.038

140. Pollot BE, Rathbone CR, Wenke JC, Guda T. Natural polymeric hydrogel evaluation for skeletal muscle tissue engineering. J Biomed Mater Res - Part B Appl Biomater. 2018;106(2):672–9.

141. Namgaladze D, Brüne B. Macrophage fatty acid oxidation and its roles in macrophage polarization and fatty acid-induced inflammation. Biochim Biophys Acta - Mol Cell Biol Lipids [Internet]. 2016;1861(11):1796–807. Available from: http://dx.doi.org/10.1016/j.bbalip.2016.09.002

142. Koda S, Hu J, Ju X, Sun G, Shao S, Tang RX, et al. The role of glutamate receptors in the regulation of the tumor microenvironment. Front Immunol. 2023;14(February):1–21.

143. Brosnan JT. Glutamate, at the interface between amino acid and carbohydrate metabolism. J Nutr [Internet]. 2000;130(4 SUPPL.):988S-990S. Available from: https://doi.org/10.1093/jn/130.4.988S

144. Nguyen TT, Hu CC, Sakthivel R, Nabilla SC, Huang YW, Yu J, et al. Preparation of gamma poly-glutamic acid/hydroxyapatite/collagen composite as the 3D-printing scaffold for bone tissue engineering. Biomater Res [Internet]. 2022;26(1):1–15. Available from: https://doi.org/10.1186/s40824-022-00265-7

145. Park S Bin, Sung MH, Uyama H, Han DK. Poly(glutamic acid): Production, composites, and medical applications of the next-generation biopolymer. Prog Polym Sci [Internet]. 2021;113:101341. Available from: https://doi.org/10.1016/j.progpolymsci.2020.101341

146. Gibon E, Batke B, Jawad MU, Fritton K, Rao A, Yao Z, et al. MC3T3-E1 osteoprogenitor cells systemically migrate to a bone defect and enhance bone healing. Tissue Eng - Part A. 2012;18(9–10):968–73.

147. Farriol M, Segovia-Silvestre T, Castellanos JM, Venereo Y, Orta X. Role of putrescine in cell proliferation in a colon carcinoma cell line. Nutrition. 2001;17(11–12):934–8.

148. Lim HK, Rahim AB, Leo VI, Das S, Lim TC, Uemura T, et al. Polyamine Regulator AMD1 Promotes Cell Migration in Epidermal Wound Healing. J Invest Dermatol [Internet]. 2018;138(12):2653–65. Available from: https://doi.org/10.1016/j.jid.2018.05.029

149. Paital SR, Dahotre NB. Calcium phosphate coatings for bio-implant applications: Materials, performance factors, and methodologies. Mater Sci Eng R Reports. 2009;66(1–3):1–70.

150. Zuo J, Tang J, Lu M, Zhou Z, Li Y, Tian H, et al. Glycolysis Rate-Limiting Enzymes: Novel Potential Regulators of Rheumatoid Arthritis Pathogenesis. Front Immunol. 2021;12(November):1–17.

151. Stubbs RT, Yadav M, Krishnamurthy R, Springsteen G. A plausible metal-free ancestral analogue of the Krebs cycle composed entirely of α-ketoacids. Nat Chem. 2020;12(11):1016–22.

152. Zdzisińska B, Żurek A, Kandefer-Szerszeń M. Alpha-Ketoglutarate as a Molecule with Pleiotropic Activity: Well-Known and Novel Possibilities of Therapeutic Use. Arch Immunol Ther Exp (Warsz). 2017;65(1):21–36.

153. Martínez-Reyes I, Chandel NS. Mitochondrial TCA cycle metabolites control physiology and disease. Nat Commun [Internet]. 2020;11(1):1–11. Available from: http://dx.doi.org/10.1038/s41467-019-13668-3

154. Hansen GE, Gibson GE. The α-Ketoglutarate Dehydrogenase Complex as a Hub of Plasticity in Neurodegeneration and Regeneration. Vol. 23, International journal of molecular sciences. 2022.

155. Hillen AEJ, Heine VM. Glutamate Carrier Involvement in Mitochondrial Dysfunctioning in the Brain White Matter. Front Mol Biosci. 2020;7(July):1–8.

156. Majumdar R, Barchi B, Turlapati SA, Gagne M. Glutamate , Ornithine , Arginine , Proline , and Polyamine Metabolic Interactions : The Pathway Is Regulated at the Post-Transcriptional Level. 2016;7(February):1–17.

157. Maus A, Peters GJ. Glutamate and α-ketoglutarate: key players in glioma metabolism. Amino Acids. 2017;49(1):21–32.

158. Qu Y, Sun Y, Yang Z, Ding C. Calcium Ions Signaling: Targets for Attack and Utilization by Viruses. Front Microbiol. 2022;13(July).

159. Lee S, Choi MC, Al Adem K, Lukman S, Kim TY. Aggregation and Cellular Toxicity of Pathogenic or Non-pathogenic Proteins. Sci Rep. 2020;10(1):1–14.

160. Salhotra A, Shah HN, Levi B, Longaker MT. Mechanisms of bone development and repair. Nat Rev Mol Cell Biol [Internet]. 2020;21(11):696–711. Available from: http://dx.doi.org/10.1038/s41580-020-00279-w

161. Tang N, Skibsted LH. Calcium binding to amino acids and small glycine peptides in aqueous solution: Toward peptide design for better calcium bioavailability. J Agric Food Chem. 2016;64(21):4376–89.

162. Aliyeva M, Brandão P, Gomes JRB, Coutinho JAP, Ferreira O, Pinho SP. Solubilities of Amino Acids in Aqueous Solutions of Chloride or Nitrate Salts of Divalent (Mg2+or Ca2+) Cations. J Chem Eng Data. 2022;67(6):1565–72.

163. Mackay MW, Fitzgerald KA, Jackson D. The solubility of calcium and phosphate in two specialty amino acid solutions. J Parenter Enter Nutr. 1996;20(1):63–6.

164. Pal MM. Glutamate: The Master Neurotransmitter and Its Implications in Chronic Stress and Mood Disorders. Front Hum Neurosci. 2021;15(October):1–4.

165. Pei Z, Lee KC, Khan A, Erisnor G, Wang HY. Pathway analysis of glutamate-mediated, calcium-related signaling in glioma progression. Biochem Pharmacol. 2020;176.

166. Hogan-Cann AD, Anderson CM. Physiological Roles of Non-Neuronal NMDA Receptors. Trends Pharmacol Sci [Internet]. 2016;37(9):750–67. Available from:

http://dx.doi.org/10.1016/j.tips.2016.05.012

167. Kariya Y, Kariya Y. Osteopontin in Cancer: Mechanisms and Therapeutic Targets. Int J Transl Med. 2022;2(3):419–47.

Appendix 1: Published manuscripts

metabolites

MDPI

Review

Metabolomics in Bone Research

Jingzhi Fan [1,2], Vahid Jahed [1,2] and Kristaps Klavins [1,2,*]

[1] Rudolfs Cimdins Riga Biomaterials Innovations and Development Centre of RTU, Institute of General Chemical Engineering, Faculty of Materials Science and Applied Chemistry, Riga Technical University, Pulka St 3, LV-1007 Riga, Latvia; jingzhi.fan@rtu.lv (J.F.); vahid.jahedzomorrodi@rtu.lv (V.J.)

[2] Baltic Biomaterials Centre of Excellence, Headquarters at Riga Technical University, Pulka St 3, LV-1007 Riga, Latvia

* Correspondence: kristaps.klavins_3@rtu.lv

Abstract: Identifying the changes in endogenous metabolites in response to intrinsic and extrinsic factors has excellent potential to obtain an understanding of cells, biofluids, tissues, or organisms' functions and interactions with the environment. The advantages provided by the metabolomics strategy have promoted studies in bone research fields, including an understanding of bone cell behaviors, diagnosis and prognosis of diseases, and the development of treatment methods such as implanted biomaterials. This review article summarizes the metabolism changes during osteogenesis, osteoclastogenesis, and immunoregulation in hard tissue. The second section of this review is dedicated to describing and discussing metabolite changes in the most relevant bone diseases: osteoporosis, bone injuries, rheumatoid arthritis, and osteosarcoma. We consolidated the most recent finding of the metabolites and metabolite pathways affected by various bone disorders. This collection can serve as a basis for future metabolomics-driven bone research studies to select the most relevant metabolites and metabolic pathways. Additionally, we summarize recent metabolic studies on metabolomics for the development of bone disease treatment including biomaterials for bone engineering. With this article, we aim to provide a comprehensive summary of metabolomics in bone research, which can be helpful for interdisciplinary researchers, including material engineers, biologists, and clinicians.

Keywords: metabolomics; bone homeostasis; osteoporosis; bone regeneration; osteosarcoma; biomaterials

Citation: Fan, J.; Jahed, V.; Klavins, K. Metabolomics in Bone Research. *Metabolites* **2021**, *11*, 434. https://doi.org/10.3390/metabo11070434

Academic Editors: Leonardo Tenori and Helen G. Gika

Received: 30 April 2021
Accepted: 28 June 2021
Published: 1 July 2021

1. Introduction

Bone is the primary tissue in the skeleton system. At first glance, bone tissue might appear to be a static and rugged part of the body with almost no dynamics. However, the first impression is deceiving. Bone homeostasis is a very dynamic and complex process closely linked to other organism functions, including immunity. Moreover, the disturbances in these processes are associated with numerous diseases, chronic or acute, that severely affect life quality and are even life-threatening.

Among them, osteoporosis, the most well-known bone disorder, has a high prevalence rate, and the rate for osteopenia is even higher [1]. This chronic bone disease has a preference among postmenopausal women (over 10%) and the aged population [2,3], and it highly increases the risk of osteoporotic fracture. Pathologic fracture can also arise from weakened bone caused by tumors. Bone fracture, including traumatic and pathological caused, is a malignant medical condition that frequently happens for various reasons. The loss of productivity and individual disability after fracture dictates a high demand for hard tissue healing studies. It has become evident that a much deeper understanding of hard tissue and related diseases is needed to develop a novel diagnosis, prognosis, and treatment approaches. The need for this will only increase due to the ageing population.

In this regard, metabolomics—a large-scale study of metabolites that are directly involved in biochemical activity holds great promise to advance our knowledge on bone

tissue (patho)physiology. Describing the metabolite pathways involved in a disease can greatly promote understanding disease development, diagnosis, and prognosis [4]. Moreover, the prominent biomarker identification can be incorporated with the traditional diagnostic methods to improve diagnostic accuracy. Additionally, metabolite ability to modulate phenotype directly through biochemical reaction can pave the road for developing new treatment approaches, especially blockers, competitive inhibitors, and accelerants.

In recent years, there has been a growing interest in metabolomics for bone tissue-related research, which has resulted in an improved understanding of underlying cellular processes during bone homeostasis and disease. However, the available information about bone–immune system and cell–cell interactions is still sparse and systematic studies are needed to deepen our understanding about these interactions. This review provides an overview of the metabolic processes relevant to bone homeostasis and the most prevalent bone diseases. It summarizes recent studies that employ metabolomics to better understand bone metabolism (Figure 1B). With this review, we want to showcase the role and value of metabolomics in bone research and encourage incorporating metabolomics in more bone-related studies, as it is providing unique insights.

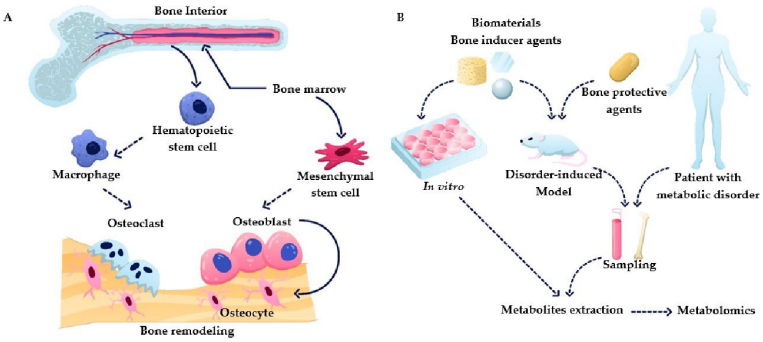

Figure 1. (**A**) Overview of bone remodeling processes, including osteogenesis and osteoclastogenesis. (**B**) Summary of metabolomics applications in bone research.

2. Metabolism of Bone Cells

2.1. Bone Homeostasis

Bone is the primary tissue in the skeleton system, providing the function of structure support, hematopoiesis location, and mineral storage. To perform these functions, bone has a complex structure that contains compact bone and cancellous bone, with the composition of organic and inorganic composites containing living cells [5]. The bone remodeling process is a cascade of regular activities in which three cell types, including osteoblasts, osteoclasts, and osteocytes, play crucial roles (shown in Figure 1). Bone undergoes continuous resorption carried out by osteoclasts and formation by osteoblasts, which are linked cell activities that form a dynamic equilibrium in bone tissue [6]. To briefly summarize this complex process, osteoclast precursors are activated to start resorption stages by cytokines such as receptor activator of nuclear factor-kB (RANK) and macrophage colony-stimulating factor (M-CSF) released by bone lining cells upon receiving a biochemical signal such as hormones (e.g., parathyroid) or mechanical signal (due to bone damage). Osteoclasts, specialized cells developed from the monocyte/macrophage lineage, can contact the bone matrix to form a sealed bone resorption area, playing a role in degrading bone tissue [7]. The activity of the osteoclast is terminated by the formation of resorption pits on the bone

surface. During the formation process, osteoblasts deposit the osteoid into the resorbed site to form a mineralized matrix. Osteoblasts are then either apoptotic or buried as osteocytes in new bone layers. It is crucial to maintain a balance between osteoclasts and osteoblasts. Bone remodeling is a dynamic and lifelong process. An imbalance in this process leads to bone disorders. It can cause several diseases, such as overactive osteoclasts and bone turnover, which would lead to osteopenia and osteoporosis, while abnormal osteoblasts elevate the risks for hyperosteogeny and tumor [3,8].

Cell differentiation is an integral part of bone homeostasis, as the osteoclast is derived from hematopoietic cells, while osteoblasts are produced from the differentiation of bone marrow stem cells (MSCs). The differentiation from MSC to osteoblast and from monocyte-macrophage lineage to osteoclast involves metabolic changes and adaptions. Metabolomics is one of the key methodologies to study these processes and deepen the understanding of osteogenesis and osteoclastogenesis and their relationship with bone diseases. MSCs, the precursor of osteoblasts, predominantly utilize glycolysis as the energy source within the bone marrow; however, the energy metabolism shifts to oxidative phosphorylation during the differentiation [9,10]. Hypoxia-inducible factor 1 α (HIF-1α) works as a regulator of MSC energy metabolism during osteogenic and chondrogenic differentiation [11]. HIF-1α can promote glycolysis and inhibit oxidative phosphorylation (OxPhos) and is most active in undifferentiated MSCs [12]. MSCs have been shown to grow and proliferate in the glycolysis pathway in hypoxic condition. At the same time, they undergo a metabolic shift to the tricarboxylic acid (TCA) pathway to supply the required energy to differentiate into the bone cells [9]. As a result, a higher OxPhos activity with an unaltered or decrease in glycolysis happens in MSCs differentiation [9,12,13]. In mature osteoblasts, glycolysis produces most of the needed energy for osteoblasts to maintain the functionality [14]. The well-known osteogenic factor, bone morphogenetic protein, can boost glucose metabolism and therefore enhance the development of bone and cartilage [15].

During osteoclastogenesis, both glycolysis and OxPhos were found increased, as indicated with a higher glucose consumption and lactate production [16]. This means that glycolysis and mitochondrial processing both play a role in the differentiation and absorption. Increased expression of glycolytic genes, including hexokinase, phosphofructokinase, and pyruvate kinase, was found during osteoclastogenesis [17]. The final osteoclasts may become apoptosed, which makes them difficult to study [18]. However, there is some evidence which indicates an alternative fate for RANKL-stimulated osteoclasts-osteomorphs production, [19]. The lifespan of osteoclasts is generally considered to be as long as 2 weeks [20]. Nevertheless, Jacome-Galarza et al. described a mechanism upon which osteoclasts could be maintained in bone, leading to compensate for osteoclast deficiency in vivo [21].

Lipid metabolism can also alter the differentiation and function of bone cells. Long-chain polyunsaturated fatty acids, such as docosahexaenoic acid and arachidonic acid, can directly suppress the differentiation and activity of osteoclasts [22]. As part of lipid rafts to control the signal transduction during osteoclastogenesis, cholesterol can alter the RANK-RANKL signal transduction, resulting in increased bone resorption under a high content of cholesterol [23]. Similarly, phosphoinositide, a membrane lipid, regulates calcium signaling and influences osteoclast differentiation [23]. The changes of 18 metabolites, most of which were lysophosphatidylcholines, were detected in the study of differentiation inhibition with estradiol [24]. The enzymatic expression changes explained this inhibition during osteoclast differentiation and oxidative/anti-oxidative imbalance during osteoclast proliferation. It also should be pointed out that lipids are used as an energy source which in turn can influence cell functions. Low lipid levels in the skeletal stem cells environment leads to chondrogenesis rather than osteogenesis due to the osteoblasts dependency on the fatty acid oxidation (FAO) [25].

The metabolism studies on osteogenesis and osteoclastogenesis provide a guide to regulate the differentiation of precursor cells by altering the metabolic pathways. Monitoring the cell function upon exposure to a change in its surrounding environment allows

for controlling cells' behavior. Osteogenesis differentiation from MSCs can be guided by parathyroid hormone by enhancing glycolysis to increase bone formation [24]. Lee et al. attempted to regulate adipocyte and osteoblast differentiation from MSCs using several metabolites. Among them, ergosterol peroxide and 9,11-dehydroergosterol peroxide were found to inhibit the differentiation toward adipocytes. Diterpenes dehydroabietic acid, 7-oxocallitrisic acid, and pimaric acid, on the other hand, induced osteoblasts differentiation [24]. The effect of high and low amounts of energy source, oxygen, and ROS as environmental factors on a deviation of cellular behavior has been well reviewed recently [6].

2.2. Osteoimmunology

The close connection between the immune system and bone tissue generated the conception of osteoimmunology [26]. Immune cells have a remarkable effect on bone physiology by acting on osteogenesis and osteoclastogenesis. The activity of bone resorption is also regulated by interleukins, cytokines secreted by immune cells. Among all immune cells, macrophages play an essential regulatory role in bone regeneration. Macrophages are divided into two polarized extremes, pro-inflammatory M1 and anti-inflammatory M2 [27]. Extracellular amino acid levels can alter the immune system functions through altering macrophage phenotypes. Arginine (Arg), ornithine, tryptophan, and glutamine can be considered amino acid-based immunomodulators [28]. Arginine metabolism plays a critical role in macrophage polarization and characterization. The prominent metabolic feature of M1 macrophages is Arg catabolism to nitric oxide (NO) and citrulline using nitric oxide synthase (NOS). While for M2 macrophages, Arg is catabolized to ornithine and urea through arginase [27]. Therefore, the catabolic and anabolic activity of NOS and arginase processes can regulate the polarization of macrophage and thus influence the inflammation and regeneration in hard tissue [29]. Indeed, the chronic inflammation of the target tissue can be pharmacologically controlled by regulating NO and Arg production [30].

In bone regeneration processes, activation of M1 macrophages in the early inflammatory phase leads to the secretion of inflammatory cytokines such as tumor necrosis factor α (TNF-α), Interleukin 6 (IL-6), and IL-1b, which results in activation of the osteoclastogenesis cascade with consequential bone resorption [31]. The M1 macrophage effect on mesenchymal stem cell (MSC) osteogenesis through the COX-2-prostaglandin E2 pathway has also been reported [32]. M2 macrophages are involved in the secondary stages of bone repair, which can lead to fibrous capsule or bone formation. Fibrous capsule formation prevents bone marrow stem cells being connected to the surface of a biomaterial for further progress in osteogenesis. Therefore, the domination of the inflammatory phase of macrophages guarantees the long-term failure or success of bone regeneration in the subsequent stages. The protracted stage of the M1 phenotype results in more fibrous inducible cytokines are amplified and fibrous capsules are formed, helping M2 phenotypes [31]. The immune response elicited by primary M1 macrophages in the early stages determines the decision of secondary M2 macrophages to secrete specific cytokines. In summary, macrophages positively contribute to bone healing by secretion of osteogenesis-related growth factors or negatively interfering through fibrous-induced inflammatory cytokines.

From an energy metabolism point of view, macrophages are constantly switching from glycolysis to oxidative phosphorylation (OxPhos). It was proved that M1 phenotypes use glycolysis and pentose phosphate pathways to uptake required ATP. M1 phenotypes lead to metabolic perturbations in several metabolites of the TCA cycle, including citrate, succinate, and itaconate. Prolonged M1 polarization can be selected as a metabolic marker for the diagnosis of inflammatory diseases such as rheumatoid arthritis and metabolic disorders such as diabetes and osteoporosis [28]. On the contrary, glycolysis has been shown to not be relevant for M2 polarization, while the consumption of glutamine Gln can be upregulated to fuel the TCA cycle [33]. Elevated FAO and OxPhos pathways indicate M2 macrophage activity and sustain the inflammatory response [27]. Gln metabolism has been reported as the synergistic support for macrophage activation through M2 phenotype

differentiation [34]. Macrophages have the potential to uptake different types of lipids, including very low-density lipoprotein (VLD), low-density lipoprotein (LDL), and oxidized lipoproteins. Lysosomes convert the consumed lipids to free fatty acids and cholesterol, which eventually are involved in OxPhos and ETC pathways. As lipid-based macrophage modulators, fatty acid synthesis (FAS) and FAO guide M1 and M2 macrophage polarization, respectively [28]. This suggests that the tracking of metabolites involved in macrophage energy homeostasis can serve as a marker to evaluate a transition from the M1 phenotype towards M2. In fact, it has been demonstrated that metabolomics, through an elucidation of changes in macrophage polarization, provides accurate information about an inflammatory disease [28,35].

3. Metabolomics in Research of Bone Diseases

As demonstrated in the previous section, metabolism plays a crucial role in bone homeostasis, and disturbances can cause or are caused by several diseases. Therefore, it is evident that metabolite measurements could provide a valuable readout for bone disease research. Indeed, metabolomics has been used for the identification of possible biomarkers for the diagnosis and prediction of various bone-related diseases. Besides diagnosis, metabolomics has also been applied to monitor the treatment. Perturbations in several major metabolic pathways due to bone diseases have been reported. Specifically, arginine and its related metabolism pathways are critical in osteoimmunology. Energy metabolisms, including glycolysis and TCA cycle, are pivotal for bone cell differentiation and function. polyunsaturated fatty acids (PUFAs) are valuable for dietetic, clinical, and biological research of osteoporosis and arthritis. Furthermore, fatty acids, such as arachidonic acid, are exploitable to develop advanced treatments. The metabolites related to acute and chronic inflammation are also closely involved in bone defects. Additionally, energy-related metabolites such as lactate and glutamine are altered in bone cancer. These metabolites and pathways can be utilized to develop diagnosis, prognosis, and treatment procedures of bone diseases.

3.1. Osteoporosis

Osteoporosis (OP) is the most known and common bone disease. OP occurs worldwide in all populations, with a higher prevalence among postmenopausal women and aged people. A low bone mineral density, which increases fracture risk, is the hallmark of OP. OP is usually characterized by metabolic disorders of bone tissue, and usage of metabolomics to study pathophysiology has gained popularity [36]. Animal models are commonly used to study the molecular mechanisms of OP in vivo. Ovariectomized (OVX) mice is an animal model of OP that mimics postmenopausal women with low BMD. Using this model, ovarian extraction results in a decrease in estrogen and progesterone, with consequences elevating the rate of bone loss [36]. Lipid metabolisms, especially arachidonic acid metabolism, linoleic acid metabolism, and glycerophospholipid metabolism, are impacted by the decrease in estrogen [37,38]. Polyunsaturated fatty acids (PUFAs) are well known for their influence on BMD [39]. Two different families of PUFAs, n-3 PUFA, derived from α- linolenic acid, and n-6 PUFA, derived from linoleic acid, are frequently occurring in metabolomics studies with their opponent functions [22]. In fact, elevated levels of arachidonic acid (AA), an n-6 PUFA, have been observed in oophorectomized rats and postmenopausal women with OP [37,38,40]. Arachidonic acid can stimulate the expression of receptor activator of NF-kB ligand (RANKL), leading to a high plasma RANKL level [22]. As the cytokine essential for osteoclast differentiation, a high concentration of RANKL can remarkably promote osteoclastogenesis, resulting in the loss of bone tissue [41]. On the contrary, docosahexaenoic acid (DHA), an n-3 PUFA, suppresses osteoclast formation from human CD14-positive monocytes by the reduction of key signaling transduction pathways of kinases (JNK, ERK, and p38 MAPKs) [22,42]. Thus, DHA inhibits osteoclastogenesis by blocking RANKL-induced activation from primary macrophages. At the same time, prostaglandin and leukotrienes, the downstream metabolic products of arachidonic acid,

were also proved to impact Wnt signaling (osteoblastogenesis) and osteoclastic resorption, respectively [43,44]. A high-level accumulation of other lipid metabolites has been found in postmenopausal women and oophorectomized rats as well [45–47]. Lipid metabolisms not only impact osteoclastogenesis but also influence osteoblastogenesis. The increased lipid oxidation, followed by high oxidative stress, can activate peroxisome proliferator-activated receptor γ, consequently inhibiting osteoblastogenesis and promoting adipogenesis [48]. PUFAs also play various roles in osteoblastogenesis. Fatty acids can activate peroxisome proliferator-activated receptor γ (PPARγ) [49]. PPARγ plays a pivotal part in cell-fate determination, guiding the MSCs to differentiate into adipocytes [50]. This could explain the bone loss of the patients with a high-fat diet. AA decreases the expression of osteogenic markers and the osteoprotegerin/RANKL ratio, causing the appearance of adipocytes in MSC differentiating during osteoblastogenesis [51]. However, n-3 PUFA such as DHA and eicosapentaenoic acid do not have such an impact on MSCs [51,52]. In an attempt to characterize the pathological mechanism of the postmenopausal OP, metabolomics was employed to analyze the OVX mice-related femur tissue. The obtained data indicated altered levels of 93 lipid metabolites such as fatty acyls, glycerolipids, glycerophospholipids, sphingolipids, and sterols, among which levels of many fatty acids were increased in the OVX model [53]. To sum up, PUFAs play a critical role in osteoporosis by (1) promoting osteoclastogenesis through the expression of RANKL and (2) altering the differentiation of MSCs by inducing adipogenesis.

Ageing is another leading cause of low BMD. The fractures due to senile OP are highly life-threatening for the aged population, especially those over the age of 70 [1]. It is known that the functionality of osteoblasts, adipocytes, and osteoclasts changes with ageing. A higher adipogenesis level was estimated with the accumulation of bone marrow fat, not found in postmenopausal OP, which may be a critical cause for lower osteoclastogenic activity [54,55]. An in vitro study verified that adipocytes, with their metabolites, inhibit osteoblast differentiation by downregulating histone acetylation [56]. Again, lipid metabolism appears to have an essential role in the age-associated reduction of BMD, as demonstrated by a metabolomics study on senescent osteoblasts [57]. The authors identified the downregulation of n-3 PUFAs in the fatty acid metabolism due to the severe oxidative stress damage. The decrease in n-3 PUFAs, as explained before, could result in an elevation of bone loss through osteoclasts.

At the clinical level, a plasma metabolites profiling conducted on 1552 individuals to identify BMD-associated metabolomic markers detected a higher level of creatine, dimethylglycine, and glycine [58]. The authors suggested that these metabolites were causally negatively associated with BMD by altering bioenergetic processes as well as glycine and threonine metabolism pathways. As a major component of the protein collagen, hydroxyproline is also considered an OP-specific marker [59]. Serum metabolite components of postmenopausal women with low BMD were investigated using CE-MS and showed that the level of hydroxyproline could be a marker of OP [60]. Increased concentration of hydroxyproline indicates the degradation of collagen type I from the bone matrix and it was reduced after treatments [61]. Similarly, other catabolites developed in bone from collagen, such as deoxypyridinoline (collagen stabilizer) and pyridinoline (cross-linking compound of collagen fibers), can also serve as the markers of OP [59]. However, changes in their levels are the results rather than the causes of OP; therefore, they are more suitable for the development of diagnosis but not treatment.

3.2. Bone Injuries

Bone fractures have always been a relevant threat to public health worldwide. Several studies have recently been published investigating the metabolic processes during both inflammatory response and tissue regeneration after bone fractures.

Ibrahim et al. identified the changes in the plasma metabolite levels in patients who went through intramedullary reaming [62]. The precursors to extracellular matrix proteins, lipids, and cysteine displayed remarkable elevation after the surgery. At the same time, the

abundance of tryptophan decreased. Galactosamine and glucuronic acid, as the precursors of chondroitin sulphate, were elevated in the after-reaming plasma. The precursors of hyaluronic acid, such as acetylglucosamine, were also increased. The increase in these ECM building blocks indicates that the matrix remodeling is accelerated after the surgery. The increased lipids, including ceramides, myristoleate, and phosphoethanolamine, play well-recognized roles in inflammation. They modify inflammatory processes by impacting inflammatory cell signaling and gene expression patterns [63]. Additionally, glutathione and taurine, the downstream products of cysteine, are both antioxidants, protecting the cells from reactive oxygen species [64,65]. At the same time, 4-hydroxynonenal, which contributes to oxidative stress, was reduced after the reaming [66]. Linolenate, a precursor of arachidonate (an inflammatory mediator), was found to be increased, much like corticosterone and cortisol, which are inhibitors in the proinflammatory pathway [67]. Kynurenine, a metabolite of tryptophan, was elevated in the post-reaming plasma, while tryptophan itself declined, pointing towards an upregulated activity of the kynurenine pathway [68,69]. It should be pointed out that the increase in the kynurenine/tryptophan ratio has been considered a marker for indoleamine 2,3-dioxygenase (IDO) activity [69]. Thus, based on the anti-inflammatory mechanism of IDO, the increase in kynurenine benefits anti-inflammatory processes as well [70]. Due to the anti-inflammatory function, IDO is considered a critical regulator in graft-versus-host disease, and as such the mediation of IDO is important for implantable biomaterials [71]. Additionally, kynurenic acid, a metabolite of kynurenine through transferase, decreased the release of TNF-α, further reducing inflammation response [69,72]. Taking it all together, the metabolites profiling after surgery indicated that the body tends to reduce the inflammation response after wound healing.

Bone turnover markers, including the biomarkers of bone resorption, bone formation, and osteoclast regulatory proteins, have been utilized to evaluate bone homeostasis. As a result, the measurement of these markers can be employed to monitor the healing of fractured bones [73]. Veitch et al. detected the alterations of these markers following tibial shaft fracture in 24 weeks [74]. Both bone resorption and formation markers were elevated, which was in line with the observation from the animal model study using sheep conducted by Sousa et al. [75]. In the first two weeks, the catabolites of type-I collagen-like C-terminal telopeptide (bone resorption marker) had a higher increase compared to the bone formation markers, such as bone alkaline phosphatase and osteocalcin [74]. This highlighted that the activity of necrotic tissue resorption is high at the beginning stage of wound healing, following the reconstruction of bone tissue.

The metabolic signatures provide valuable clues to establish "the big picture" on bone regeneration from critical injury. There are seemingly microscopic but significant differences in defect and injury types; however, only a few studies are available. Therefore, further metabolite profiling studies considering all aspects of bone injuries are needed to understand the molecular mechanisms affected by injury and healing.

3.3. *Rheumatoid Arthritis*

Rheumatoid arthritis (RA) is commonly considered arthritis driven by autoimmune pathogenesis. The analysis of joint tissue metabolism, especially with immune cells, can ameliorate the understanding of pathogenesis and prognosis. The bone destruction of rheumatoid arthritis happens mainly due to the abnormal activation of osteoclasts [76]. Therefore, the overactivity of osteoclasts stimulated by various factors may cause and/or aggravate arthritis. Similar to the PUFAs in osteoporosis, n-6 PUFAs, as the precursor of inflammatory eicosanoids, are responsible for the cartilage loss and inflammation in RA [77]. The influence of n-3/n-6 PUFA intake on RA has already been extensively studied among dietary studies and clinical medicine, which suggest increasing the intake of n-3 PUFAs such as DHA and to avoid the intake of n-6 PUFAs such as AA [63,78,79]. Another fatty acid family, short-chain fatty acid (SCFA), is also relevant for arthritis. Lower butyrate (SCFA) levels in the blood of RA patients and arthritic mice have been reported [80].

The amelioration of the severity of systemic autoimmune inflammatory conditions was achieved by oral administration of SCFAs [81]. Furthermore, the butyrate ability to suppress the expression of inflammatory cytokines from T cells by promoting the expression of IL-10 has been demonstrated [82].

Energy metabolism is also abnormal in RA. Narasimhan et al. performed NMR-based metabolite profiling of the serum from patients with rheumatoid arthritis to identify the synovial joint biomarkers [83]. The metabolites with abnormal levels found in RA serum were associated with the TCA cycles, fatty acid, and amino acid metabolism. Among them, lactate and pyruvate were significantly upregulated. This can be explained by the higher bioenergetic and biosynthetic demands in the inflamed tissue [83]. The RA metabolic process of T cells that drives tissue inflammation could be attributed to the mitochondrial defect [84]. The mitochondrial DNA containments trigger T cell tissue invasion in the organelle assembled inflammasome and caspase-1. Another study demonstrated that the sugar metabolism of fibroblast-like synoviocytes was significantly disturbed by RA [85]. Kim et al. also pointed out that the sugar metabolism level in RA is higher than healthy people and higher than osteoarthritis, which makes it a distinct feature for RA [85]. As presented in the previous chapter, a high glycolysis level is a characteristic of osteoclastogenesis from monocytic progenitors with an increased glycolytic genes expression [17]. This switch of energy consumption can explain the tendency towards glycolysis and mitochondrial defect in RA. The symptoms of arthritis are caused by the destroyed cartilage; consequently, the abnormal enhancement of osteoclast and/or immune cell activity by fatty acids or glycolysis level is closely related with the disease conditions.

3.4. Osteosarcoma

As the most common histological form of the bone cancerous tumor, osteosarcoma causes severe symptoms by malignant neoplasia, threatening people of all ages [86,87]. A clear presentation of metabolic heterogeneity in oncogenesis and metastasis benefits early diagnosis and enhances the understanding of the clinical behavior of tumor tissue. Among all the pathologies, osteoblastic tumor holds the highest proportion, followed by chondroblastic and fibroblastic [86,88]. Several studies have been performed on osteosarcoma with a focus on abnormal metabolisms. An NMR profiling on blood serum samples revealed that energy metabolism was enormously altered throughout tumorigenesis [86]. The abnormal levels of amino acids, fatty acids, and glucose were found, suggesting an alternative energy source for cancer cells. In most cancer cases, glycolysis is considered to be the primary energy source for tumor tissue, while oxidative phosphorylation level is decreased [89]. A similar decrease in TCA cycle metabolite levels was detected in an in vitro experiment using osteosarcoma stem cells [90]. This preference for energic metabolism was verified by metabolite enrichment analysis, of which metabolite biomarkers involved in the glycolysis pathway were highly evaluated [90,91]. The lower TCA cycle level in osteosarcoma tumor tissue was explained by the down-regulation of mitochondrial function, accompanied by a reduction of glutamate, aspartate, and glutathione with an elevation of Gln [90,92]. The mitochondrial dysfunction caused by the expression of metastasis genes in osteosarcoma cells resulted in metabolic disorder and presented an aggressive phenotype [93].

The metabolite-based osteosarcoma biomarkers can be potentially employed not only for diagnosis but also to monitor disease progression. These metabolites can be attributed to the development of regulators for energy metabolism and cellular stress in osteosarcoma tumor tissue. Besides, targeting metabolic pathways provides new therapeutic strategies. For example, new osteosarcoma therapy targeting the amino acid metabolism of cancer stem cells has been suggested [90].

3.5. Summary of Metabolic Pathways Relevant in Bone Diseases

To comprehensively identify metabolic pathways that are affected during bones diseases, we conducted an integrating enrichment and pathway topology analysis from the

data of Table 1 by using Metabo Analyst 5.0 [94]. For this, we used the metabolites that are reported as significantly altered in osteoporosis, arthritis, and osteosarcoma.

The metabolic pathways prominently altered in both osteoporosis and arthritis are (1) aminoacyl-tRNA biosynthesis, (2) arginine and proline metabolism, (3) arginine biosynthesis, and (4) valine, leucine and isoleucine biosynthesis. At the same time, the most altered pathways from osteosarcoma are (1) alanine, aspartate and glutamate metabolism, (2) TCA cycle, and (3) arginine biosynthesis. Interestingly, a high degree of similarity of the most altered metabolic pathways has been found between osteoporosis and arthritis. This phenomenon may be caused by the pathophysiological similarity of these two diseases: abnormal resorption of the target tissue by osteoclasts, macrophages and/or some other immune cells. However, due to the limitation of the data sources and the diversity of various original studies, this conclusion needs further research and discussion. Most notably, arginine synthesis and metabolism are remarkably altered in all mentioned diseases. The metabolism of glutamate, a precursor of arginine, is also involved in OS. The immune system, therefore, plays a critical role in bone diseases as a regulator of immune responses and arginine, and its related metabolic pathways have great value for the future bone research [95]. It should be pointed out that metabolic pathways altered in bone diseases have been previously reported to be relevant in other diseases. The control of physiopathological processes such as angiogenesis, inflammation, and tumorigenesis is related to aminoacyl-tRNA synthesis [96]. Arginine and proline have important roles in wound healing, antioxidative reactions, and immune responses, as a result, the metabolites' variation after tissue injury is rational [97]. Obesity and cancer risk are also linked with proline metabolism, leading to various of complications [98]. The alteration of glycolysis, TCA cycle and glutaminolysis are typical signals in cancers, [99,100]. To conclude, some of the changes in metabolism observed in bone diseases reflect more general pathophysiological processes such as inflammation. Further studies are needed to elucidate how bone diseases may influence or be influenced by other diseases under a certain physical condition of the patients.

Table 1. Overview of reported metabolite changes in the different diseases, used analytical methods and corresponding references.

Ref.	Disease	Technique	Sample Type	Metabolite Changes
[46]	POP	GC/TOF-MS	Rat plasma	↑ Arachidonic acid, octadecadienoic acid, valine, leucine, isoleucine, homocysteine, hydroxyproline, ketone bodies ↓ Docosahexaenoic acid, dodecanoic acid, lysine
[53]	POP	UPLC/Q-TOF-MS	Rat bone tissue	↑ Lysophosphatidylcholine, phosphatidylcholine, ceramide, phosphoserine ↓ Uridine, hypoxanthine, xanthine, inosine, cytidine, phenylalanine, leucine, carnitine, proline, arginine
[101]	POP	1H NMR	Rat urine	↑ Trigonelline, phosphocreatine, pyruvate, methylamine, trimethylamine oxide ↓ Benzoic acid, dimethylamine, trimethylamine, threonic acid, alanine, leucine, 2-ketoglutarate, allantoin, acetate, formate
[47]	POP	GC/TOF-MS	Rat plasma	↑ Arachidonic acid, homocysteine, homocysteine, ethanedioic acid↓ Alanine, malic acid, citric acid, fructose involved
[45]	POP	GC-MS	Women serum	↑ Arachidonic acid, lysine, eicosadienoic acid, oleic acid, linoleic acid, allose, tryptophan ↓ Homoserine, 3-hydroxy-l-proline, pyruvic acid
[102]	POP	UPLC-Q-TOF/MS	Rat serum	↑ Lysine, linoleic acid, hippuric acid, octadecadienoic acid, carnitine, glucose, arginine, S-adenosylhomocysteine, ornithine, tryptophan, arachidonic acid, methionyl-hydroxyproline ↓ Homoserine, 3-hydroxy-l-proline, pyruvic acid, citric acid, estriol, 8-HETE, uric acid, glutamine, glyceraldehyde, palmitic acid, 4-oxoretinol, taurocholic acid
[103]	DOP	NMR	Human plasma	↑ Leucine, isoleucine valine, alanine, N-acetylglycoprotein, inositol, proline, glucose, glutamine, 1-methyl-histidine, tyrosine ↓ O-acetylglycoprotein, α-ketoglutaric acid, citrate, creatine

Table 1. *Cont.*

Ref.	Disease	Technique	Sample Type	Metabolite Changes
[83]	RA	NMR	Human synovial	↑ Threonine, xanthine, methylsuccinate, glutamate, methylmalonate, taurine, lactate, pyruvate, propylene glycol, leucine, tyrosine, 3-hydroxybutyrate ↓ Creatinine, creatine, o-acetyl carnitine, L-carnitine, betaine, choline, formate, glycine, asparagine, formate, acetate, phenylalanine, succinate, pantothenate, fumarate, acetoacetate, acetone, lysine
[85]	RA	GC/TOF-MS	Human synoviocytes	↑ Inosine, urate, guanine, behenic acid, palmitoleic acid, arachidic acid, oleic acid, glucose-6-phosphate, phosphogluconic acid, aspartate, adipate, asparagine ↓ Isoleucine, leucine, leucine, histidine, valine, ornithine, lysine, methionine sulfoxide, tryptophan, mannitol, xylose
[104]	RA	LCMS	Human plasma	↑ Kynurenine, indolelactic acid, hypoxanthine, cholesterol, triglyceride, lysophospatidylcholines ↓ Tryptophan, fatty acids, acylcarnitines
[105]	OA	MALDI-MSI	Human bone marrow MSCs	↑ Arachidonic acid, oleic acid, stearic acid, dihydroxyacetone phosphate, phosphatidylglycerol, phosphatidylinositol ↓ Myoinositol, phosphatidic acid, lysophosphatidic acid, glutamine
[90]	OS	UHPLC-QE-MS	Human osteosarcoma stem cells	↑ Aspartic acid, asparagine, glutamine, arginine, ornithine, methionine, methylthioadenosine ↓ succinic acid, citric acid, aconitic acid, oxoglutaric acid, ureidosuccinic acid
[106]	OS	UHPLC-HRMS	Human serum	↑ Adenosine monophosphate, inosinic acid, guanosine monophosphate, hypoxanthine, lactic acid ↓ Uric acid, 4-hydroxybenzoic acid, testosterone sulfate, iminodiacetic acid, 3-carboxy-4-methyl-5-propyl-2-furanpropionic acid, decanoylcarnitine
[107]	OS	GC-MS	Human serum and urine	↑ Cystine, 2-hydroxybutyrate, inosine, creatinine, putrescine, aspartate, proline, galactopyranose ↓ Malate, fumarate, pyruvate, lactate, sucrose, dodecanoate, glycerol phosphate, creatinine
[62]	Bone Injuries	UPLC-MS/MS	Trauma patient plasma	↑ Myristoleate, hexadecadienoate, octadecadienedioate, choline phosphate, phosphoethanolamine, pregnenolone sulfate, cortisol, glycerol 3-phosphate, beta-citrylglutamate, trans-urocanate, kynurenate, cysteine, spermidine, cysteinyl glycine ↓ Decanoyl carnitine, 2-hydroxyheptanoate, 4-hydroxynonenal, glycerophosphoethanolamine, palmitoyl-linoleoyl-glycerol, stearoyl-linoleoyl-glycerol, cholate, n-acetylglutamine, pyroglutamine, tryptophan, cysteine s-sulfate
[108]	Bone Injuries	LC-MS/MS	Human bone marrow plasma	↑ Kynurenine

POP = postmenopausal osteoporosis; DOP = diabetic osteoporosis; RA = rheumatoid arthritis; OA = osteoarthritis; OS = osteosarcoma.

4. Metabolomics for Development of Bone Disease Treatment Methods

Metabolite measurements can provide valuable information to evaluate the response and progress of cells or organism to treatment methods. In the field of bone disease treatment development, currently, it has been employed in two main fields: osteoporosis therapeutics and biomaterials.

4.1. Osteoporosis Therapeutics

Metabolomics can be applied to assess the therapeutic effect of drugs or dietary supplements on the recovery of an OP disorder. The effect of dietary Vitamin D on the bone metabolism of cats and dogs has been well reviewed [109]. The Icariin (IC) potential, a Chinese herbal bioactive molecule, in inducing bone differentiation has been proved previously [110,111]. It was reported that oral administration of IC to OP-induced 54-week-old

hens as a supplement eventually leads to an increase in the BMD level of both femur and tibia by inducing changes in pyrimidine, taurine, and lipid metabolism. Furthermore, untargeted metabolomics of serum from hens treated with icariin helped identify eight altered metabolites: uridine, taurine, palmitic acid, adrenic acid, 30 fexofenadine, lysoPC, lysoPE, and 3-acetyl-11-keto-beta-boswellic acid, which can be considered markers for the early diagnosis of OP [112]. Similarly, yak bone collagen peptides (YBPs) showed the ability to induce bone differentiation in vitro. The enhanced effect of the intragastric administration of YBP on bone recovery in OVX rats was reported. The UPLC/Q-TOF-MS metabolomics of post-treated serum identified 41 potential biomarkers, mostly unsaturated fatty acids, the positive effects of which on postmenopausal OP have been proven. Indicatively, YBP supplementation demonstrated an increased DHA, arachidonic acid, taurine, citrulline, and a reduced serotonin metabolite concentration [113]. Osthole (OS) is the main bioactive integrant of Cnidium, which exhibited excellent treatment potential for OP. The ability of osthole to be introduced as an effective drug for postmenopausal OP (POP) was investigated. To this end, UPLC-Q-TOF/MS revealed that OS treatment leads to POP recovery by the regulation of 19 of the 28 highlighted metabolites related to the OVX-OP model (listed in Table 1). Osthole treatments revealed metabolic perturbations in amino acid, lipid, carbohydrate, bile acid, purine metabolism, and TCA cycle [102]. Bone-protective effects of lignin-rich fraction (SWR) as a Chinese herbal medicine were also reported. Serum LC/MS metabolomics of OVX rats was performed following 12 weeks post-treatment of SWR. The results proved that SWR administration leads to bone recovery by restoring the levels of 26 metabolites corresponding to estrogen deficiency which are involved in lipids, amino acids, tryptophan metabolisms, and anti-oxidative systems. In particular, upon SWR treatment, upregulation of superoxide dismutase and catalase was observed while serotonin was downregulated [70,114]. Additionally, metabolomics can provide valuable data to determine bone tissue treatment a gents' side effect. A serum metabolomics study was performed to evaluate the side effects of long-term dexamethasone therapy in rats, and abnormal bone metabolism along with weight loss was observed, which was consistent with the reduced total ALP of serum. In detail, the dexamethason-treated rats exhibited six-fold downregulation of phenylalanine, lysine, and arginine and an increased tyrosine, hydroxyproline, and protein catabolism [115].

4.2. Biomaterials

Biomaterials are frequently used in surgical remediation of bone defects, especially for critical defects caused by traumatic fractures and bone tumor resection. Cell–material interactions play a critical role after the implantation of orthopaedic biomaterials. In recent years, few studies have demonstrated that metabolomics is a promising strategy to study that interaction and evaluate the implanted materials' performance.

Poly-L-lactic acid (PLLA) has been used as implantable fracture fixation devices (bone screws and plates) for decades [116]. To study the role of PLLA in osteanagenesis, Araújo et al. employed NMR-based metabolomics to assess changes in metabolic processes in osteoblasts cultured on PLLA [117]. The decrease in glucose and triglycerides suggested that the energy metabolism was upregulated upon the interaction of PLLA. Furthermore, an increased lactate level followed by polymer breakdown can decrease the amount of intracellular radical oxygen species, reducing the intracellular redox state [6]. Though biocompatible, with its long degradation period, chronic inflammation is still observed with PLLA with the appearance of pro-inflammation cytokines (IL-1β, TNF and MCP-1) [118,119], even though the metabolism study of this chronic inflammation is still lacking.

Alginate hydrogel, a polysaccharide hydrophilic polymer with high water content, is another material that has been widely studied in biomedicine. As a highly tailorable polymer, the studies on alginate hydrogel scaffolds are usually performed in the context of the changed material composition by incorporating additives such as ions, acids, and peptides [120]. Oxidized alginate hydrogel functionalized by glycine-histidine-lysine, a peptide fragment of osteonectin [121], was developed by Klontzas et al. [122], and the

osteogenesis properties were studied employing metabolome analysis. The reduction of lipid precursors, TCA cycle intermediates, and amino acid pools were observed in MSCs cultured with the modified hydrogel. Physical properties such as topography and stiffness of the material surfaces can also impact cell metabolism. Micro/nano surface structure has been an attractive topic in tissue engineering [6]. Researchers from two studies, conducted on titanium and polydimethylsiloxane, respectively, explored how the material surfaces impacted the metabolome with pillars in a pike shape [123,124].

Enhanced mitochondrial activity and lower ATP levels were identified in adherent cells, suggesting that macro pillars cause extra energy costs. The possible reason could be the cytophagy of the spires; however, further studies are needed to elucidate the underlying mechanisms. Additionally, material stiffness plays a role in adjusting cell behavior. Alakpa et al. synthesized hydrogels with different stiffness and studied the metabolome of cultured MSCs [125]. The steroid biosynthesis was enhanced in MSCs on hydrogel with a higher Young's modulus (higher stiffness), while elevated glycerolipid biosynthesis level was enhanced on the lower Young's modulus one. These findings indicate that MSCs tend to be osteogenically differentiated on rigid surfaces and chondrogenic differentiated on elastic or soft ones. Mechanical signals can also alter cell metabolism, as shown by Villaseñor et al. Metabolite analysis of cell medium samples obtained from mechanically stimulated osteocytes revealed a high citrate excretion and a decreased level of aspartate [126]. These alternations pointed to increased activity of the TCA cycle.

5. Conclusions and Outlook

Despite the overall maturity and broad application of metabolomics, it is still an emerging technique in bone research. However, it has become apparent that metabolism has a crucial role in bone homeostasis and disease at cellular and tissue levels. The metabolites profiling and metabolism pathway analysis can be combined with gene analysis, enzymatic activity assay, and biomaterial engineering to understand cell behavior at the molecular level. Metabolomics clarifies molecular mechanisms that are involved in the process of stem cell differentiation into bone-specific cells. This opens therapeutic possibilities to use metabolites directly or activating them indirectly, helping small molecules accelerate in vitro differentiation into bone cells and prevent unwanted differentiation. Despite the excellent understanding of the metabolic landscape of individual cell types involved in bone homeostasis, the interplay between these cells is currently understudied. It is apparent that cell–cell interactions have a crucial role, and future metabolomics studies are needed in this area. This could lead to new findings of metabolite signaling functions and the role of the metabolic microenvironment on cell functions.

Metabolomics has been successfully used to study disease-induced metabolic changes in vitro and in vivo and identify the potential biomarkers. Awareness of metabolic changes in the patient can lead to early diagnosis of bone-related diseases. Metabolomics can also accommodate a design of appropriate drugs to control the progress of the disease by following the decrease or increase in an effective biomarker in a disease. Additionally, as demonstrated by multiple animal model studies, metabolomics is a valuable tool to predict the therapeutic effect of a bone-protective agent on the recovery of bone diseases or their side effect on the normal function of bone. So far, several drugs have been designed to improve bone function, whereas their effectiveness can be challenged in further metabolomics studies. Furthermore, future metabolomics studies could be helpful to pinpoint the molecular targets for therapeutic agents.

The development and evaluation of biomaterials for bone regeneration is a fascinating and novel application area for metabolomics. As demonstrated in the available literature, biomaterial cues such as ions, oxygen, and regulatory metabolites affect cell metabolism and may cause changes in metabolic pathways and regeneration scenarios. The metabolic landscape of biomaterial–cell interactions appears to be uncharted territory. Although plenty of studies have been conducted on how biomaterials' physiochemical properties can impact different cell behaviors, few of them were combined with metabolites profiling

or metabolomics analysis. A combination of metabolomics and osteogenesis confirmation assays such as bone marker expression via a polymerase chain reaction, immunohistochemistry, and bone matrix mineralization could be a robust tool to guide the development and evaluate the performance of engineered biomaterials with desirable properties.

Altogether, metabolomics in the bone study is a promising area for interdisciplinary researchers, including material engineers, biologists, and clinicians.

Author Contributions: Conceptualization and methodology, J.F. and K.K.; writing—original draft preparation, J.F., V.J., review and editing, J.F. and K.K. All authors have read and agreed to the published version of the manuscript.

Funding: The authors acknowledge financial support from European Union's Horizon 2020 research and innovation programme under the Marie Sklodowska-Curie grant agreement No. 898858 and European Union's Horizon 2020 research and innovation programme under the grant agreement No. 857287.

Conflicts of Interest: The authors declare no conflict of interest.

References

1. Kemmak, A.R.; Rezapour, A.; Jahangiri, R.; Nikjoo, S.; Farabi, H.; Soleimanpour, S. Economic Burden of Osteoporosis in the World: A Systematic Review. *Med. J. Islam. Repub. Iran.* **2020**, *2020*, 1–8. [CrossRef]
2. Wade, S.W.; Strader, C.; Fitzpatrick, L.A.; Anthony, M.S.; O'Malley, C.D. Estimating prevalence of osteoporosis: Examples from industrialized countries. *Arch. Osteoporos.* **2014**, *9*, 182. [CrossRef] [PubMed]
3. Tian, L.; Yang, R.; Wei, L.; Liu, J.; Yang, Y.; Shao, F.; Ma, W.; Li, T.; Wang, Y.; Guo, T. Prevalence of osteoporosis and related lifestyle and metabolic factors of postmenopausal women and elderly men. *Medicine* **2017**, *96*. [CrossRef] [PubMed]
4. Guijas, C.; Montenegro-Burke, J.R.; Warth, B.; Spilker, M.E.; Siuzdak, G. Metabolomics activity screening for identifying metabolites that modulate phenotype. *Nat. Biotechnol.* **2018**, *36*, 316–320. [CrossRef]
5. Armiento, A.R.; Hatt, L.P.; Sanchez Rosenberg, G.; Thompson, K.; Stoddart, M.J. Functional Biomaterials for Bone Regeneration: A Lesson in Complex Biology. *Adv. Funct. Mater.* **2020**, *30*, 1–41. [CrossRef]
6. Ma, C.; Kuzma, M.L.; Bai, X.; Yang, J. Biomaterial-Based Metabolic Regulation in Regenerative Engineering. *Adv. Sci.* **2019**, *6*. [CrossRef]
7. Kubatzky, K.F.; Uhle, F.; Eigenbrod, T. From macrophage to osteoclast—How metabolism determines function and activity. *Cytokine* **2018**, *112*, 102–115. [CrossRef]
8. Liang, S.T.; Chen, J.R.; Tsai, J.J.; Lai, Y.H.; Hsiao, C. Der Overexpression of notch signaling induces hyperosteogeny in zebrafish. *Int. J. Mol. Sci.* **2019**, *20*, 3613. [CrossRef]
9. Mohammadalipour, A.; Dumbali, S.P.; Wenzel, P.L. Mitochondrial Transfer and Regulators of Mesenchymal Stromal Cell Function and Therapeutic Efficacy. *Front. Cell Dev. Biol.* **2020**, *8*, 1–22. [CrossRef]
10. Guntur, A.R.; Le, P.T.; Farber, C.R.; Rosen, C.J. Bioenergetics during calvarial osteoblast differentiation reflect strain differences in bone mass. *Endocrinology* **2014**, *155*, 1589–1595. [CrossRef]
11. Yao, Y.; Deng, Q.; Song, W.; Zhang, H.; Li, Y.; Yang, Y.; Fan, X.; Liu, M.; Shang, J.; Sun, C.; et al. MIF Plays a Key Role in Regulating Tissue-Specific Chondro-Osteogenic Differentiation Fate of Human Cartilage Endplate Stem Cells under Hypoxia. *Stem Cell Rep.* **2016**, *7*, 249–262. [CrossRef]
12. Shum, L.C.; White, N.S.; Mills, B.N.; De Mesy Bentley, K.L.; Eliseev, R.A. Energy Metabolism in Mesenchymal Stem Cells during Osteogenic Differentiation. *Stem Cells Dev.* **2016**, *25*, 114–122. [CrossRef]
13. Pattappa, G.; Heywood, H.K.; de Bruijn, J.D.; Lee, D.A. The metabolism of human mesenchymal stem cells during proliferation and differentiation. *J. Cell. Physiol.* **2011**, *226*, 2562–2570. [CrossRef]
14. Lee, W.C.; Ji, X.; Nissim, I.; Long, F. Malic Enzyme Couples Mitochondria with Aerobic Glycolysis in Osteoblasts. *Cell Rep.* **2020**, *32*, 108108. [CrossRef]
15. Lee, S.Y.; Abel, E.D.; Long, F. Glucose metabolism induced by Bmp signaling is essential for murine skeletal development. *Nat. Commun.* **2018**, *9*, 1–11. [CrossRef]
16. Kim, J.; Jeong, D.; Kang, H.K.; Jung, S.Y.; Kang, S.S.; Min, B. Cellular Physiology and Biochemistr y Biochemistry Osteoclast Precursors Display Dynamic Metabolic Shifts toward Accelerated Glucose Metabolism at an Early Stage of RANKL-Stimulated Osteoclast Differentiation. *Cell Physiol. Biochem.* **2007**, *749*, 935–946. [CrossRef]
17. Indo, Y.; Takeshita, S.; Ishii, K.A.; Hoshii, T.; Aburatani, H.; Hirao, A.; Ikeda, K. Metabolic regulation of osteoclast differentiation and function. *J. Bone Miner. Res.* **2013**, *28*, 2392–2399. [CrossRef]
18. Arnett, T.R.; Orriss, I.R. Metabolic properties of the osteoclast. *Bone* **2018**, *115*, 25–30. [CrossRef]
19. McDonald, M.M.; Khoo, W.H.; Ng, P.Y.; Xiao, Y.; Zamerli, J.; Thatcher, P.; Kyaw, W.; Pathmanandavel, K.; Grootveld, A.K.; Moran, I.; et al. Osteoclasts recycle via osteomorphs during RANKL-stimulated bone resorption. *Cell* **2021**, *184*, 1330–1347. [CrossRef]

20. Manolagas, S.C. Birth and death of bone cells: Basic regulatory mechanisms and implications for the pathogenesis and treatment of osteoporosis. *Endocr. Rev.* **2000**, *21*, 115–137. [CrossRef]
21. Jacome-Galarza, C.E.; Percin, G.I.; Muller, J.T.; Mass, E.; Lazarov, T.; Eitler, J.; Rauner, M.; Yadav, V.K.; Crozet, L.; Bohm, M.; et al. Developmental origin, functional maintenance and genetic rescue of osteoclasts. *Nature* **2019**, *568*, 541–545. [CrossRef]
22. Kasonga, A.E.; Deepak, V.; Kruger, M.C.; Coetzee, M. Arachidonic Acid and Docosahexaenoic Acid Suppress Osteoclast Formation and Activity in Human CD14 + Monocytes, In vitro. *PLoS ONE* **2015**, 1–19. [CrossRef]
23. Ryu, J.; Kim, H.; Chang, E.J.; Kim, H.J.; Lee, Y.; Kim, H.H. Proteomic analysis of osteoclast lipid rafts: The role of the integrity of lipid rafts on V-ATPase activity in osteoclasts. *J. Bone Miner. Metab.* **2010**, *28*, 410–417. [CrossRef]
24. Liu, X.; Liu, Y.; Cheng, M.; Zhang, X.; Xiao, H. A metabolomics study of the inhibitory effect of 17-beta-estradiol on osteoclast proliferation and differentiatio. *Mol. Biosyst.* **2015**, *11*, 635–646. [CrossRef]
25. Van Gastel, N.; Stegen, S.; Eelen, G.; Schoors, S. Lipid availability determines skeletal progenitor cell fate via SOX9. *Nature* **2020**, *579*, 111–117. [CrossRef]
26. Dar, H.Y.; Azam, Z.; Anupam, R.; Mondal, R.K.; Srivastava, R.K. Osteoimmunology: The Nexus between bone and immune system. *Front. Biosci. Landmark* **2018**, *23*, 464–492. [CrossRef]
27. Rath, M.; Müller, I.; Kropf, P.; Closs, E.I.; Munder, M. Metabolism via arginase or nitric oxide synthase: Two competing arginine pathways in macrophages. *Front. Immunol.* **2014**, *5*. [CrossRef]
28. Viola, A.; Munari, F.; Sánchez-Rodríguez, R.; Scolaro, T.; Castegna, A. The metabolic signature of macrophage responses. *Front. Immunol.* **2019**, *10*, 1–16. [CrossRef]
29. Rodriguez, P.C.; Ochoa, A.C.; Al-Khami, A.A. Arginine metabolism in myeloid cells shapes innate and adaptive immunity. *Front. Immunol.* **2017**, *8*. [CrossRef]
30. Climaco-Arvizu, S.; Domínguez-Acosta, O.; Cabañas-Cortés, M.A.; Rodríguez-Sosa, M.; Gonzalez, F.J.; Vega, L.; Elizondo, G. Aryl hydrocarbon receptor influences nitric oxide and arginine production and alters M1/M2 macrophage polarization. *Life Sci.* **2016**, *155*, 76–84. [CrossRef]
31. Chen, Z.; Klein, T.; Murray, R.Z.; Crawford, R.; Chang, J.; Wu, C.; Xiao, Y. Osteoimmunomodulation for the development of advanced bone biomaterials. *Mater. Today* **2016**, *19*, 304–321. [CrossRef]
32. Lu, L.Y.; Loi, F.; Nathan, K.; Lin, T.H.; Pajarinen, J.; Gibon, E.; Nabeshima, A.; Cordova, L.; Jämsen, E.; Yao, Z.; et al. Pro-inflammatory M1 macrophages promote Osteogenesis by mesenchymal stem cells via the COX-2-prostaglandin E2 pathway. *J. Orthop. Res.* **2017**, *35*, 2378–2385. [CrossRef] [PubMed]
33. Wang, F.; Zhang, S.; Vuckovic, I.; Jeon, R.; Lerman, A.; Folmes, C.D.; Dzeja, P.P.; Herrmann, J. Glycolytic Stimulation Is Not a Requirement for M2 Macrophage Differentiation. *Cell Metab.* **2018**, *28*, 463–475. [CrossRef] [PubMed]
34. Jha, A.K.; Huang, S.C.C.; Sergushichev, A.; Lampropoulou, V.; Ivanova, Y.; Loginicheva, E.; Chmielewski, K.; Stewart, K.M.; Ashall, J.; Everts, B.; et al. Network integration of parallel metabolic and transcriptional data reveals metabolic modules that regulate macrophage polarization. *Immunity* **2015**, *42*, 419–430. [CrossRef]
35. Muñoz, J.; Akhavan, N.S.; Mullins, A.P.; Arjmandi, B.H. Macrophage polarization and osteoporosis: A review. *Nutrients* **2020**, *12*, 2999. [CrossRef]
36. Lv, H.; Jiang, F.; Guan, D.; Lu, C.; Guo, B.; Chan, C.; Peng, S.; Liu, B.; Guo, W.; Zhu, H.; et al. Metabolomics and Its Application in the Development of Discovering Biomarkers for Osteoporosis Research. *Int. J. Mol. Sci.* **2018**, *17*, 2018. [CrossRef]
37. Zhang, A.h.; Ma, Z.m.; Sun, H.; Zhang, Y.; Liu, J.h.; Wu, F.f.; Wang, X.j. High-throughput metabolomics evaluate the efficacy of total lignans from Acanthophanax senticosus stem against ovariectomized osteoporosis rat. *Front. Pharmacol.* **2019**, *10*. [CrossRef]
38. Jiang, Y.; Li, Y.; Zhou, L.; Zhang, D. UPLC-MS metabolomics method provides valuable insights into the effect and underlying mechanisms of Rhizoma Drynariae protecting osteoporosis. *J. Chromatogr. B* **2020**, *1152*, 122262. [CrossRef]
39. Longo, A.B.; Ward, W.E. PUFAs, bone mineral density, and fragility fracture: Findings from human studies. *Adv. Nutr.* **2016**, *7*, 299–312. [CrossRef]
40. Xia, T.; Dong, X.; Lin, L.; Jiang, Y.; Ma, X.; Xin, H.; Zhang, Q.; Qin, L. Metabolomics profiling provides valuable insights into the underlying mechanisms of Morinda officinalis on protecting glucocorticoid-induced osteoporosis. *J. Pharm. Biomed. Anal.* **2019**, *166*, 336–346. [CrossRef]
41. Lee, N.K.; Choi, Y.G.; Baik, J.Y.; Han, S.Y.; Jeong, D.W.; Bae, Y.S.; Kim, N.; Lee, S.Y. A crucial role for reactive oxygen species in RANKL-induced osteoclast differentiation. *Blood* **2005**, *106*, 852–859. [CrossRef]
42. Kim, H.J.; Ohk, B.; Yoon, H.J.; Kang, W.Y.; Seong, S.J.; Kim, S.Y.; Yoon, Y.R. Docosahexaenoic acid signaling attenuates the proliferation and differentiation of bone marrow-derived osteoclast precursors and promotes apoptosis in mature osteoclasts. *Cell. Signal.* **2017**, *29*, 226–232. [CrossRef]
43. Liu, X.H.; Kirschenbaum, A.; Weinstein, B.M.; Zaidi, M.; Yao, S.; Levine, A.C. Prostaglandin E2 modulates components of the Wnt signaling system in bone and prostate cancer cells. *Biochem. Biophys. Res. Commun.* **2010**, *394*, 715–720. [CrossRef]
44. Garcia, C.; Boyce, B.F.; Gilles, J.; Dallas, M.; Qiao, M.E.; Mundy, G.R.; Bonewald, L.F. Leukotriene B, Stimulates Osteoclastic Bone Resorption. *J. Bone Miner. Res.* **1996**, 1619–1627. [CrossRef]
45. Qi, H.; Bao, J.; An, G.; Ouyang, G.; Zhang, P.; Wang, C.; Ying, H.; Ouyang, P.; Ma, B.; Zhang, Q. Association between the metabolome and bone mineral density in pre- and post-menopausal Chinese women using GC-MS. *Mol. Biosyst.* **2016**, *12*, 2265–2275. [CrossRef]

46. Ma, B.; Liu, J.; Zhang, Q.; Ying, H.; Jiye, A.; Sun, J.; Wu, D.; Wang, Y.; Li, J.; Liu, Y. Metabolomic Profiles Delineate Signature Metabolic Shifts during Estrogen Deficiency-Induced Bone Loss in Rat by GC-TOF/MS. *PLoS ONE* **2013**, *8*, 1–10. [CrossRef]
47. Ma, B.; Li, X.; Zhang, Q.; Wu, D.; Wang, G.; Jiye, A.; Sun, J.; Li, J.; Liu, Y.; Wang, Y.; et al. Metabonomic profiling in studying anti-osteoporosis effects of strontium fructose 1,6-diphosphate on estrogen deficiency-induced osteoporosis in rats by GC/TOF-MS. *Eur. J. Pharmacol.* **2013**, *718*, 524–532. [CrossRef]
48. Almeida, M.; Ambrogini, E.; Han, L.; Manolagas, S.C.; Jilka, R.L. Increased lipid oxidation causes oxidative stress, increased peroxisome proliferator-activated receptor-γ expression, and diminished pro-osteogenic Wnt signaling in the skeleton. *J. Biol. Chem.* **2009**, *284*, 27438–27448. [CrossRef]
49. Kawai, M.; Rosen, C.J. PPARγ: A circadian transcription factor in adipogenesis and osteogenesis. *Nat. Rev. Endocrinol.* **2010**, *6*, 629–636. [CrossRef]
50. Li, Y.; Jin, D.; Xie, W.; Wen, L.; Chen, W.; Xu, J.; Ding, J.; Ren, D. PPAR-γ and Wnt Regulate the Differentiation of MSCs into Adipocytes and Osteoblasts Respectively. *Curr. Stem Cell Res. Ther.* **2017**, *13*, 185–192. [CrossRef]
51. Casado-Díaz, A.; Santiago-Mora, R.; Dorado, G.; Quesada-Gómez, J.M. The omega-6 arachidonic fatty acid, but not the omega-3 fatty acids, inhibits osteoblastogenesis and induces adipogenesis of human mesenchymal stem cells: Potential implication in osteoporosis. *Osteoporos. Int.* **2013**, *24*, 1647–1661. [CrossRef]
52. Coetzee, M.; Haag, M.; Kruger, M.C. Effects of arachidonic acid, docosahexaenoic acid, prostaglandin E2 and parathyroid hormone on osteoprotegerin and RANKL secretion by MC3T3-E1 osteoblast-like cells. *J. Nutr. Biochem.* **2007**, *18*, 54–63. [CrossRef]
53. Zhao, H.; Li, X.; Zhang, D.; Chen, H.; Chao, Y.; Wu, K.; Dong, X.; Su, J. Integrative Bone Metabolomics—Lipidomics Strategy for Pathological Mechanism of Postmenopausal Osteoporosis Mouse Model. *Sci. Rep.* **2018**, *8*, 1–11. [CrossRef]
54. Choi, Y.J.; Song, I.; Jin, Y.; Jin, H.S.; Ji, H.M.; Jeong, S.Y.; Won, Y.Y.; Chung, Y.S. Transcriptional profiling of human femoral mesenchymal stem cells in osteoporosis and its association with adipogenesis. *Gene* **2017**, *632*, 7–15. [CrossRef]
55. Duque, G.; Troen, B.R. Understanding the mechanisms of senile osteoporosis: New facts for a major geriatric syndrome. *J. Am. Geriatr. Soc.* **2008**, *56*, 935–941. [CrossRef]
56. Abuna, R.P.F.; Almeida, L.O.; Souza, A.T.P.; Fernandes, R.R.; Sverzut, T.F.V.; Rosa, A.L.; Beloti, M.M. Osteoporosis and osteoblasts cocultured with adipocytes inhibit osteoblast differentiation by downregulating histone acetylation. *J. Cell. Physiol.* **2020**, 1–12. [CrossRef]
57. Wu, Y.; Zhang, M.; Chen, X.; Zhou, Y.; Chen, Z. Metabolomic analysis to elucidate the change of the n-3 polyunsaturated fatty acids in senescent osteoblasts. *Biosci. Biotechnol. Biochem.* **2021**, *85*, 611–620. [CrossRef]
58. Zhang, X.; Xu, H.; Li, G.H.Y.; Long, M.T.; Cheung, C.; Vasan, R.S.; Hsu, Y.; Kiel, D.P.; Liu, C. Metabolomics insights into osteoporosis through association with bone mineral density. *J. Bone Miner. Res.* **2021**, *36*, 729–738. [CrossRef]
59. Kuo, T.R.; Chen, C.H. Bone biomarker for the clinical assessment of osteoporosis: Recent developments and future perspectives. *Biomark. Res.* **2017**, *5*, 5–13. [CrossRef]
60. Miyamoto, T.; Hirayama, A.; Sato, Y.; Koboyashi, T.; Katsuyama, E.; Kanagawa, H.; Miyamoto, H.; Mori, T.; Yoshida, S.; Fujie, A.; et al. A serum metabolomics-based profile in low bone mineral density postmenopausal women. *Bone* **2017**, *95*, 1–4. [CrossRef]
61. Jagtap, V.R.; Ganu, J.V. Effect of antiresorptive therapy on urinary hydroxyproline in postmenopausal osteoporosis. *Indian J. Clin. Biochem.* **2012**, *27*, 90–93. [CrossRef] [PubMed]
62. Ibrahim, H.; Alnachoukati, O.; Baxter, B.A.; Chapin, T.; Schroeppel, T.; Dunn, J.; Ryan, E.P. Non-Targeted Metabolomics Signature in the Plasma and Bone Marrow of Patients with Long Bone Injuries. *Curr. Metab. Syst. Biol.* **2019**, *7*, 51–66. [CrossRef]
63. Calder, P.C. Fatty acids: Long-chain fatty acids and inflammation. *Proc. Nutr. Soc.* **2012**, *71*, 284–289. [CrossRef] [PubMed]
64. Ghezzi, P. Role of glutathione in immunity and inflammation in the lung. *Int. J. Gen. Med.* **2011**, *4*, 105–113. [CrossRef]
65. Kayoko, S.; Chian, J.J.; Kyoko, T.; Schaffer, S.W. Role of ROS Production and Turnover in the Antioxidant Activity of Taurine. *Adv. Exp. Med. Biol.* **2015**, *803*. [CrossRef]
66. Poli, G.; Schaur, R.J. 4-Hydroxynonenal in the pathomechanisms of oxidative stress. *IUBMB Life* **2000**, *50*, 315–321. [CrossRef]
67. Almadi, T.; Cathers, I.; Chow, C.M. Associations among work-related stress, cortisol, inflammation, and metabolic syndrome. *Psychophysiology* **2013**, *50*, 821–830. [CrossRef]
68. Dinçel, E.; Özkan, Y.; Şüküroğlu, M.; Özsoy, H.; Sepici Dinçel, A. Evaluation of tryptophan/kynurenine pathway relevance with immune system biomarkers of low energy trauma hip fractures in osteoporotic patients. *Arch. Rheumatol.* **2017**, *32*, 203–208. [CrossRef]
69. Chen, Y.; Guillemin, G.J. Kynurenine Pathway Metabolites in Humans: Disease and Healthy States. *Int. J. Tryptophan. Res.* **2010**, *61*, 1–19. [CrossRef]
70. Wolf, A.M.; Wolf, D.; Rumpold, H.; Moschen, A.R.; Kaser, A.; Obrist, P.; Fuchs, D.; Brandacher, G.; Winkler, C.; Geboes, K.; et al. Overexpression of indoleamine 2,3-dioxygenase in human inflammatory bowel disease. *Clin. Immunol.* **2004**, *113*, 47–55. [CrossRef]
71. Jasperson, L.K.; Bucher, C.; Panoskaltsis-Mortari, A.; Taylor, P.A.; Mellor, A.L.; Munn, D.H.; Blazar, B.R. Indoleamine 2,3-dioxygenase is a critical regulator of acute graft-versus-host disease lethality. *Blood* **2008**, *111*, 3257–3265. [CrossRef]
72. Westbrook, A.M.; Wei, B.; Hacke, K.; Xia, M.; Braun, J.; Schiestl, R.H. The role of tumour necrosis factor-α and tumour necrosis factor receptor signalling in inflammation-associated systemic genotoxicity. *Mutagenesis* **2012**, *27*, 77–86. [CrossRef]
73. Yoon, B.-H.; Yu, W. Clinical Utility of Biochemical Marker of Bone Turnover: Fracture Risk Prediction and Bone Healing. *J. Bone Metab.* **2018**, *25*, 73. [CrossRef]

74. Veitch, S.W.; Findlay, S.C.; Hamer, A.J.; Blumsohn, A.; Eastell, R.; Ingle, B.M. Changes in bone mass and bone turnover following tibial shaft fracture. *Osteoporos. Int.* **2006**, *17*, 364–372. [CrossRef]
75. Sousa, C.P.; Lopez-Peña, M.; Guzón, F.M.; Abreu, H.V.D.; Luís, M.R.; Viegas, C.A.; Camassa, J.; Azevedo, J.T.D.; Cabrita, A.S.; Reis, R.L.; et al. Evaluation of bone turnover markers and serum minerals variations for predicting fracture healing versus non-union processes in adult sheep as a model for orthopedic research. *Injury* **2017**, *48*, 1768–1775. [CrossRef]
76. McInnes, I.B.; Schett, G. The Pathogenesis of Rheumatoid Arthritis. *N. Engl. J. Med.* **2011**, *365*, 2205–2219. [CrossRef]
77. Innes, J.K.; Calder, P.C. Omega-6 fatty acids and inflammation. *Prostaglandins Leukot. Essent. Fat. Acids* **2018**, *132*, 41–48. [CrossRef]
78. Calder, P.C. Fatty acids and inflammation: The cutting edge between food and pharma. *Eur. J. Pharmacol.* **2011**, *668*, S50–S58. [CrossRef]
79. Miles, E.A.; Calder, P.C. Influence of marine n-3 polyunsaturated fatty acids on immune function and a systematic review of their effects on clinical outcomes in rheumatoid arthritis. *Br. J. Nutr.* **2012**, *107*. [CrossRef]
80. Rosser, E.C.; Piper, C.J.M.; Matei, D.E.; Blair, P.A.; Rendeiro, A.F.; Orford, M.; Alber, D.G.; Krausgruber, T.; Catalan, D.; Klein, N.; et al. Microbiota-Derived Metabolites Suppress Arthritis by Amplifying Aryl-Hydrocarbon Receptor Activation in Regulatory B Cells. *Cell Metab.* **2020**, *31*, 837–851. [CrossRef]
81. Mizuno, M.; Noto, D.; Kaga, N.; Chiba, A.; Miyake, S. The dual role of short fatty acid chains in the pathogenesis of autoimmune disease models. *PLoS ONE* **2017**, *12*, 1–15. [CrossRef]
82. Hui, W.; Yu, D.; Cao, Z.; Zhao, X. Butyrate inhibit collagen-induced arthritis via Treg/IL-10/Th17 axis. *Int. Immunopharmacol.* **2019**, *68*, 226–233. [CrossRef]
83. Narasimhan, R.; Coras, R.; Rosenthal, S.B.; Sweeney, S.R.; Lodi, A.; Tiziani, S.; Boyle, D.; Kavanaugh, A.; Guma, M. Serum metabolomic profiling predicts synovial gene expression in rheumatoid arthritis. *Arthritis Res. Ther.* **2018**, *20*, 1–11. [CrossRef]
84. Weyand, C.M.; Wu, B.; Goronzy, J.J. The metabolic signature of T cells in rheumatoid arthritis. *Curr. Opin. Rheumatol.* **2020**, *32*, 159–167. [CrossRef]
85. Kyong, J.; Kim, S.; Hwang, J.; Kim, J.; Heon, K.; Cha, H. Original article GC / TOF-MS-based metabolomic profiling in cultured fibroblast-like synoviocytes from rheumatoid arthritis. *Jt. Bone Spine* **2016**, *83*, 707–713. [CrossRef]
86. Quintero Escobar, M.; Costa, T.B.B.C.; Martins, L.G.; Costa, S.S.; van Helvoort Lengert, A.; Boldrini, E.; Morini da Silva, S.R.; Lopes, L.F.; Vidal, D.O.; Krepischi, A.C.V.; et al. Insights in Osteosarcoma by Proton Nuclear Magnetic Resonance Serum Metabonomics. *Front. Oncol.* **2020**, *10*, 1–9. [CrossRef]
87. Tandon, R. Future directions in the treatment of schizophrenia. *Pharmacol. Treat. Schizophr.* **2012**, 67–79. [CrossRef]
88. Hauben, E.I.; Weeden, S.; Pringle, J.; Van Marck, E.A. Does the histological subtype of high-grade central osteosarcoma influence the response to treatment with chemotherapy and does it affect overall survival ? A study on 570 patients of two consecutive trials of the European Osteosarcoma Intergroup. *Eur. J. Cancer* **2002**, *38*, 1218–1225. [CrossRef]
89. Song, J.; Wu, X.; Liu, F.; Li, M.; Sun, Y.; Wang, Y.; Wang, C.; Zhu, K.; Jia, X.; Wang, B.; et al. Long non-coding RNA PVT1 promotes glycolysis and tumor progression by regulating miR-497/HK2 axis in osteosarcoma. *Biochem. Biophys. Res. Commun.* **2017**, *490*, 217–224. [CrossRef]
90. Zhong, Z.; Mao, S.; Lin, H.; Li, H.; Lin, J.; Lin, J.M. Alteration of intracellular metabolome in osteosarcoma stem cells revealed by liquid chromatography-tandem mass spectrometry. *Talanta* **2019**, *204*, 6–12. [CrossRef]
91. Chen, K.; Zhu, C.; Cai, M.; Fu, D. Integrative metabolome and transcriptome profiling reveals discordant glycolysis process between osteosarcoma and normal osteoblastic cells. *J. Cancer Res. Clin.* **2014**. [CrossRef] [PubMed]
92. Ren, L.; Dowdy, T.; Huang, S.; Issaq, S.H.; Beck, J.; Wang, H.; Hoang, C.T.; Lita, A.; Larion, M.; Leblanc, A.K. Glutaminase-1 (GLS1) inhibition limits metastatic progression in osteosarcoma. *Cancer Metab.* **2020**, *8*, 1–13. [CrossRef] [PubMed]
93. Jackson, M.; Serada, N.; Sheehan, M.; Srinivasan, S.; Mason, N.; Id, M.G.; Avadhani, N. Mitochondrial genome and functional defects in osteosarcoma are associated with their aggressive phenotype. *PLoS ONE* **2018**, *13*, 1–20. [CrossRef] [PubMed]
94. Pang, Z.; Chong, J.; Zhou, G.; Anderson, D.; Morais, D.L.; Chang, L.; Barrette, M.; Gauthier, C.; Etienne, P.; Li, S.; et al. MetaboAnalyst 5.0: Narrowing the gap between raw spectra and functional insights. *Nucleic Acids Res.* **2021**, 1–9. [CrossRef]
95. Bronte, V.; Zanovello, P. Regulation of immune responses by L-arginine metabolism. *Nat. Rev. Immunol.* **2005**, *5*, 641–654. [CrossRef] [PubMed]
96. Yao, P.; Fox, P.L. Aminoacyl-tRNA synthetases in medicine and disease. *EMBO Mol. Med.* **2013**, *5*, 332–343. [CrossRef] [PubMed]
97. Wu, Y.; Streijger, F.; Wang, Y.; Lin, G.; Christie, S.; Mac-Thiong, J.M.; Parent, S.; Bailey, C.S.; Paquette, S.; Boyd, M.C.; et al. Parallel Metabolomic Profiling of Cerebrospinal Fluid and Serum for Identifying Biomarkers of Injury Severity after Acute Human Spinal Cord Injury. *Sci. Rep.* **2016**, *6*, 1–14. [CrossRef]
98. Phang, J.M.; Liu, W.; Zabirnyk, O. Proline metabolism and microenvironmental stress. *Annu. Rev. Nutr.* **2010**, *30*, 441–463. [CrossRef]
99. Ganapathy-kanniappan, S.; Geschwind, J.-F. Tumor glycolysis as a target for cancer therapy. *Mol. Cancer* **2013**, *12*, 1–11. [CrossRef]
100. Chen, J.Q.; Russo, J. Dysregulation of glucose transport, glycolysis, TCA cycle and glutaminolysis by oncogenes and tumor suppressors in cancer cells. *Biochim. Biophys. Acta Rev. Cancer* **2012**, *1826*, 370–384. [CrossRef]
101. Liu, S.; Yuan, X.; Ma, C.; Zhao, J.; Xiong, Z. 1H-NMR-based urinary metabolomic analysis for the preventive effects of gushudan on glucocorticoid-induced osteoporosis rats. *Anal. Biochem.* **2020**, *610*, 113992. [CrossRef]

102. Si, Z.; Zhou, S.; Shen, Z.; Luan, F. High-Throughput Metabolomics Discovers Metabolic Biomarkers and Pathways to Evaluating the Efficacy and Exploring Potential Mechanisms of Osthole Against Osteoporosis Based on UPLC/Q-TOF-MS Coupled With Multivariate Data Analysis. *Front. Pharmacol.* **2020**, *11*, 1–15. [CrossRef]
103. Liang, W.D.; Huang, P.J.; Xiong, L.H.; Zhou, S.; Ye, R.Y.; Liu, J.R.; Wei, H.; Lai, R.Y. Metabolomics and its application in the mechanism analysis on diabetic bone metabolic abnormality. *Eur. Rev. Med. Pharmacol. Sci.* **2020**, *24*, 9591–9600. [CrossRef]
104. Rantapa, S.; Surowiec, I.; Lisbeth, A. Metabolite and Lipid Profiling of Biobank Plasma Samples Collected Prior to Onset of Rheumatoid Arthritis. *PLoS ONE* **2016**, 1–14. [CrossRef]
105. Rocha, B.; Cillero-pastor, B.; Eijkel, G.; Calamia, V.; Fernandez-puente, P.; Paine, M.R.L.; Ruiz-romero, C.; Heeren, R.M.A.; Blanco, F.J.; Rocha, B.; et al. Integrative Metabolic Pathway Analysis Reveals Novel Therapeutic Targets in Osteoarthritis Authors Integrative Metabolic Pathway Analysis. *J. Title Mol. Cell. Proteomics* **2020**, *19*, 574–588. [CrossRef]
106. Lv, D.; Zou, Y.; Zeng, Z.; Yao, H.; Ding, S.; Bian, Y.; Wen, L.; Xie, X. Comprehensive metabolomic profiling of osteosarcoma based on UHPLC-HRMS. *Metabolomics* **2020**, *16*, 1–11. [CrossRef]
107. Zhang, Z.; Qiu, Y.; Hua, Y.; Wang, Y.; Chen, T.; Zhao, A.; Chi, Y.; Pan, L.; Hu, S.; Li, J.; et al. Serum and urinary metabonomic study of human osteosarcoma. *J. Proteome Res.* **2010**, *9*, 4861–4868. [CrossRef]
108. Le, A.R.T.I.C.; Metabolism, B.; Kim, B.; Hamrick, M.W.; Yoo, H.J.; Lee, S.H.; Kim, S.J.; Koh, J.; Isales, C.M.; Kim, O.B. The Detrimental Effects of Kynurenine, a Tryptophan Metabolite, on Human Bone Metabolism. *J. Clin. Endocrinol. Metab.* **2019**, *104*, 2334–2342. [CrossRef]
109. Zafalon, R.V.A.; Ruberti, B.; Rentas, M.F.; Amaral, A.R.; Vendramini, T.H.A.; Chacar, F.C.; Kogika, M.M.; Brunetto, M.A. The role of vitamin D in small animal bone metabolism. *Metabolites* **2020**, *10*, 496. [CrossRef]
110. Wu, J.Z.; Liu, P.C.; Liu, R.; Cai, M. Icariin Restores Bone Structure and Strength in a Rat Model of Chronic High-Dose Alcohol-Induced Osteopenia. *Cell. Physiol. Biochem.* **2018**, *46*, 1727–1736. [CrossRef]
111. Zhao, J.; Ohba, S.; Komiyama, Y.; Shinkai, M.; Chung, U.I.; Nagamune, T. Icariin: A potential osteoinductive compound for bone tissue engineering. *Tissue Eng. Part A* **2010**, *16*, 233–243. [CrossRef]
112. Huang, J.; Hu, Y.; Tong, X.; Zhang, L.; Yu, Z.; Zhou, Z. Untargeted metabolomics revealed therapeutic mechanisms of icariin on low bone mineral density in older caged laying hens. *Food Funct.* **2020**, *11*, 3201–3212. [CrossRef]
113. Ye, M.; Zhang, C.; Jia, W.; Shen, Q.; Qin, X.; Zhang, H.; Zhu, L. Metabolomics strategy reveals the osteogenic mechanism of yak (: Bos grunniens) bone collagen peptides on ovariectomy-induced osteoporosis in rats. *Food Funct.* **2020**, *11*, 1498–1512. [CrossRef]
114. Xiao, H.; Sham, T.; Chan, C.; Li, M.; Chen, X.; Mok, D.K. A Metabolomics Study on the Bone Protective Effects of a Lignan-Rich Fraction From Sambucus Williamsii Ramulus in Aged Rats. *Front. Pharmacol.* **2018**, *9*. [CrossRef]
115. Malkawi, A.K.; Alzoubi, K.H.; Jacob, M.; Matic, G.; Ali, A.; Al Faraj, A.; Almuhanna, F.; Dasouki, M.; Rahman, A.M.A. Metabolomics based profiling of Dexamethasone side effects in rats. *Front. Pharmacol.* **2018**, *9*, 1–14. [CrossRef]
116. Middleton, J.C.; Tipton, A.J. Synthetic biodegradable polymers as orthopedic devices. *Biomaterials* **2000**, *21*, 2335–2346. [CrossRef]
117. Araújo, R.; Carneiro, T.J.; Marinho, P.; da Costa, M.M.; Roque, A.; da Cruz e Silva, O.A.B.; Fernandes, M.H.; Vilarinho, P.M.; Gil, A.M. NMR metabolomics to study the metabolic response of human osteoblasts to non-poled and poled poly (L-lactic) acid. *Magn. Reson. Chem.* **2019**, *57*, 919–933. [CrossRef]
118. Yang, N.; Tan, R.P.; Chan, A.H.P.; Lee, B.S.L.; Santos, M.; Hung, J.; Liao, Y.; Bilek, M.M.M.; Fei, J.; Wise, S.G.; et al. Immobilized Macrophage Colony-Stimulating Factor (M-CSF) Regulates the Foreign Body Response to Implanted Materials. *ACS Biomater. Sci. Eng.* **2020**, *6*, 995–1007. [CrossRef] [PubMed]
119. Scislowska-Czarnecka, A.; Pamula, E.; Kolaczkowska, E. Impact of poly(L-lactide) versus poly(L-Lactide-co-Trimethylene Carbonate) on biological characteristics of fibroblasts and osteoblasts. *Folia Biol.* **2013**, *61*, 11–24. [CrossRef] [PubMed]
120. Hernández-González, A.C.; Téllez-Jurado, L.; Rodríguez-Lorenzo, L.M. Alginate hydrogels for bone tissue engineering, from injectables to bioprinting: A review. *Carbohydr. Polym.* **2020**, *229*, 115514. [CrossRef] [PubMed]
121. Jose, S.; Hughbanks, M.L.; Binder, B.Y.K.; Ingavle, G.C.; Leach, J.K. Enhanced trophic factor secretion by mesenchymal stem/stromal cells with Glycine-Histidine-Lysine (GHK)-modified alginate hydrogels. *Acta Biomater.* **2014**, *10*, 1955–1964. [CrossRef]
122. Klontzas, M.E.; Reakasame, S.; Silva, R.; Morais, J.C.F.; Vernardis, S.; MacFarlane, R.J.; Heliotis, M.; Tsiridis, E.; Panoskaltsis, N.; Boccaccini, A.R.; et al. Oxidized alginate hydrogels with the GHK peptide enhance cord blood mesenchymal stem cell osteogenesis: A paradigm for metabolomics-based evaluation of biomaterial design. *Acta Biomater.* **2019**, *88*, 224–240. [CrossRef]
123. Moerke, C.; Mueller, P.; Nebe, B. Attempted caveolae-mediated phagocytosis of surface-fixed micro-pillars by human osteoblasts. *Biomaterials* **2016**, *76*, 102–114. [CrossRef]
124. Singh, A.V.; Raymond, M.; Pace, F.; Certo, A.; Zuidema, J.M.; McKay, C.A.; Gilbert, R.J.; Lu, X.L.; Wan, L.Q. Astrocytes increase ATP exocytosis mediated calcium signaling in response to microgroove structures. *Sci. Rep.* **2015**, *5*, 1–8. [CrossRef]
125. Alakpa, E.V.; Lampel, A.; Pe, B.; Dalby, M.J.; Alakpa, E.V.; Jayawarna, V.; Lampel, A.; Burgess, K.V.; West, C.C.; Bakker, S.C.J.; et al. Tunable Supramolecular Hydrogels for Selection of Lineage-Guiding Metabolites in Stem Cell Cultures Tunable Supramolecular Hydrogels for Selection of Lineage-Guiding Metabolites in Stem Cell Cultures. *Chem* **2016**, 298–319. [CrossRef]
126. Villaseñor, A.; Aedo-Martín, D.; Obeso, D.; Erjavec, I.; Rodríguez-Coira, J.; Buendía, I.; Ardura, J.A.; Barbas, C.; Gortazar, A.R. Metabolomics reveals citric acid secretion in mechanically–stimulated osteocytes is inhibited by high glucose. *Sci. Rep.* **2019**, *9*, 2295. [CrossRef]

polymers

MDPI

Review

A Review of Recent Advances in Natural Polymer-Based Scaffolds for Musculoskeletal Tissue Engineering

Jingzhi Fan [1,2], Keyvan Abedi-Dorcheh [3], Asma Sadat Vaziri [3], Fereshteh Kazemi-Aghdam [3], Saeed Rafieyan [3], Masoume Sohrabinejad [3], Mina Ghorbani [3], Fatemeh Rastegar Adib [3], Zahra Ghasemi [3], Kristaps Klavins [1,2,*] and Vahid Jahed [1,2,*]

[1] Rudolfs Cimdins Riga Biomaterials Innovations and Development Centre of RTU, Institute of General Chemical Engineering, Faculty of Materials Science and Applied Chemistry, Riga Technical University, Pulka St 3, LV-1007 Riga, Latvia; jingzhi.fan@rtu.lv

[2] Baltic Biomaterials Centre of Excellence, Headquarters at Riga Technical University, Pulka St 3, LV-1007 Riga, Latvia

[3] Biomedical Engineering Division, Faculty of Chemical Engineering, Tarbiat Modares University, Tehran 14117-13116, Iran; keyvan.abedi@modares.ac.ir (K.A.-D.); asma.vaziri86@gmail.com (A.S.V.); fereshtehkazemiaghdam@gmail.com (F.K.-A.); saeed21041374@gmail.com (S.R.); m.sohrabinejad@modares.ac.ir (M.S.); mina.ghorbani2020@gmail.com (M.G.); rastegar.ft@gmail.com (F.R.A.); ghasemi.zh@yahoo.com (Z.G.)

* Correspondence: kristaps.klavins_3@rtu.lv (K.K.); vahid.jahedzomorrodi@rtu.lv (V.J.)

Abstract: The musculoskeletal (MS) system consists of bone, cartilage, tendon, ligament, and skeletal muscle, which forms the basic framework of the human body. This system plays a vital role in appropriate body functions, including movement, the protection of internal organs, support, hematopoiesis, and postural stability. Therefore, it is understandable that the damage or loss of MS tissues significantly reduces the quality of life and limits mobility. Tissue engineering and its applications in the healthcare industry have been rapidly growing over the past few decades. Tissue engineering has made significant contributions toward developing new therapeutic strategies for the treatment of MS defects and relevant disease. Among various biomaterials used for tissue engineering, natural polymers offer superior properties that promote optimal cell interaction and desired biological function. Natural polymers have similarity with the native ECM, including enzymatic degradation, bio-resorb and non-toxic degradation products, ability to conjugate with various agents, and high chemical versatility, biocompatibility, and bioactivity that promote optimal cell interaction and desired biological functions. This review summarizes recent advances in applying natural-based scaffolds for musculoskeletal tissue engineering.

Keywords: natural polymers; biomaterials; biodegradable scaffolds; musculoskeletal tissue; tissue engineering

check for updates

Citation: Fan, J.; Abedi-Dorcheh, K.; Sadat Vaziri, A.; Kazemi-Aghdam, F.; Rafieyan, S.; Sohrabinejad, M.; Ghorbani, M.; Rastegar Adib, F.; Ghasemi, Z.; Klavins, K.; et al. A Review of Recent Advances in Natural Polymer-Based Scaffolds for Musculoskeletal Tissue Engineering. *Polymers* **2022**, *14*, 2097. https://doi.org/10.3390/polym14102097

Academic Editors: Iolanda De Marco, Hernane S. Barud, Cristiano Legnani and Agnieszka Terçjak

Received: 15 April 2022
Accepted: 17 May 2022
Published: 20 May 2022

Publisher's Note: MDPI stays neutral with regard to jurisdictional claims in published maps and institutional affiliations.

1. Introduction

The musculoskeletal (MS) system consists of bone, cartilage, tendon, ligament, and skeletal muscle, which form the basic framework of the human body. The damage or loss of MS-related tissues significantly affects the quality of life. MS disorders can be caused by old age, traumatic events, autoimmune and degenerative diseases. According to the WHO report, between one in three and one in five people worldwide suffer from the mentioned disorders, which have the most persistent pain in non-cancerous cases [1–4].

The self-healing potential of MS-related tissues during injury depends on tissue type and the degree of damage and inflammation. Whereas bones and skeletal muscles have an adequate intrinsic ability for self-healing in minor injuries, the self-repair of severe injuries and injuries to other MS-related tissues needs clinical interventions for complete healing [5–7]. In these cases, donor grafting, a conventional clinical treatment, is limited

due to prolonged recovery time, risk of infection, immunological rejection, and donor site morbidity. To address these challenges, MS tissue engineering has emerged and developed as an alternative therapeutic option to fully recover the patient by boosting the spontaneously healing potential of the native tissues [8–10].

Tissue engineering provides an efficient approach for repairing damaged or lost tissues by combining scaffolds, cells, and signaling molecules. To this end, a scaffold is an essential part that can accommodate stem cells and biological cues such as small molecules and growth factors. A scaffold-based strategy can be applied as a local tool to accelerate the regeneration process [11,12]. Ideally, tissue-engineered scaffolds must be biocompatible and non-immunogenic, and their degradation rate is commensurate with the re-formation of new tissue. Additionally, these scaffolds should have the appropriate surface chemistry for cell adhesion and the desired porosity for the transport of oxygen, nutrients, and metabolic wastes. Furthermore, their mechanical properties should correspond to the host tissue strength to sustain the regeneration of tissue during the healing process and induce targeted stem cell differentiation to the host cells [13,14].

The fabrication of an artificial microenvironment with a suitable polymer should mimic the host tissue's native extracellular matrix (ECM) to guarantee successful tissue regeneration. ECM is a dynamic three-dimensional structure composed of glycoproteins and glycosaminoglycans, which have a tissue-specific proportion of these components and architecture. This non-cellular component acts as a physical scaffold for cells and controls cellular behavior such as homeostasis, adherent, proliferation, and cell differentiation through biochemical and biomechanical signals. Therefore, host ECM simulation becomes the most crucial part of scaffold design, especially for the scaffolds with incorporated cells [15].

Natural polymers are desirable among various biomaterials used for scaffolding, such as alloys, ceramics, and polymers. Figure 1 shows the natural-based polymers applied for tissue engineering and their extraction source. Recently, various types of natural-based polymer scaffolds with different architectures, including hydrogel, fibrous, solid porous, and a composite with decellularized tissue, have been developed for MS tissue engineering applications [5,16–19]. They offer superior biocompatibility, bioactivity, and high chemical versatility for desired biological function. Based on their sources, natural polymers can be classified into two main categories: (i) non-mammalian, which includes Marine algae (Carrageenans, Agarose, Alginate), crustacean (chitosan/chitin), insects (silk fibrin), plants (starch), microorganisms (xanthan gum, gellan gum, dextran), (ii) mammalian-based, including proteins (collagen, fibrin, elastin) and glycosaminoglycans (chondroitin sulfate, hyaluronan, and heparin). The basic structures of these polymers include proteins, polypeptides, and polysaccharides, which can mimic their various functions in the native ECM when registered as an engineered scaffold.

Hydrogels are hydrophilic three-dimensional networks made of physically associated or chemically crosslinked polymer chains that can uptake high amounts of water and biological fluids. A key feature of hydrogels is the structural similarities to the ECM due to their soft and flexible nature. Their physicochemical properties can be easily tailored, allowing them to be used in various tissue reconstruction applications [20,21].

Fiber scaffolds with a high length-to-width ratio are among the most attractive polymeric constructions in the tissue engineering field due to resembling the fibrous microstructure of muscles and connective tissues cartilage, bone, ligament, and tendon. This fibril architecture in various nano- and microscales plays an essential role in the mechanical properties and regulation of cell differentiation behavior [22,23].

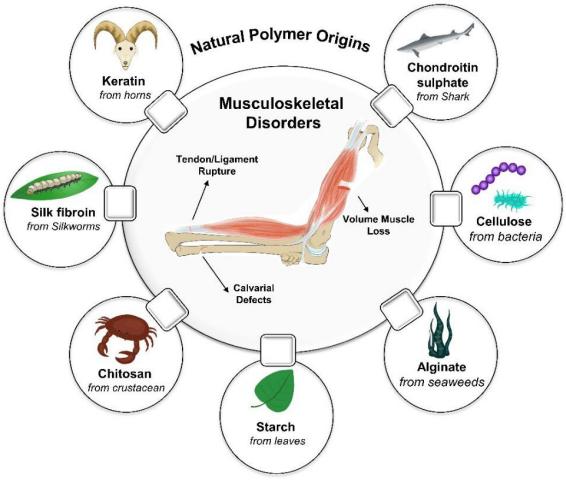

Figure 1. Schematic diagram of natural sources of natural polymers and their application in musculoskeletal tissue disorders.

Decellularized scaffolds prepared by removing cellular contents from native tissues or organs provide an ideal scaffold by preserving the architecture, components, and ligands of native ECM. Tissue-engineered grafts can be ex vivo re-cellularized with stem cells and applied for organ transplantation to reduce immune rejection [8,24].

Solid porous scaffolds serve as a three-dimensional matrix with interconnected pores and high porosity. This interconnected porous structure is essential for high-cell density culture and tissue growth, especially for organ angiogenesis and bone formation. Furthermore, their surface-to-volume ratio, crystallinity, porosity, and the size, shape, and interconnection of pores can be controlled to adapt to different application requirements in engineering various tissue types [25,26].

In this review, we describe the ECM structure corresponding to every distinct part of musculoskeletal tissue, which is followed by short explanations of what disorders are associated with them. We provide a concise review of recent advancements in natural-based scaffolds for each musculoskeletal tissue type and shortly discuss challenges and future directions.

It should be pointed out that the discussion about cartilage requires a separate article due to the diversity of cartilage types (including hyaline, fibrocartilage, and elastic cartilage) involved in the musculoskeletal tissue. Hence, this manuscript focuses on recent bone, tendon, ligament, and skeletal muscle tissue engineering advances. The key properties of these natural polymers are summarized in Table 1.

Table 1. Characterizations of the natural polymers used in tissue engineering.

Materials	Structure	Sources	Key Features	Ref
Chitosan	Linear polysaccharide	The shell of crustaceans (crabs, lobsters, shrimps, crayfish, and king crabs) as well as mollusks (e.g., squids), cuticles of insects, and cell walls of fungi	Second most abundant natural polymer, Biocompatible, Biodegradable, Bioadhesive, Biologically renewable, Antimicrobial, Hemostatic nature, Non-antigenic, Antioxidant, pH-sensitive	[27–29]
Alginate	Linear polysaccharide	Seaweeds and typically extracted from brown algae	Biocompatible, Biodegradable, Cytocompatible, Non-immunogenic, Mucoadhesive, Source abundance, Low cost, Water-soluble, pH-sensitive, in situ gelation	[30–33]
Starch	Composed of two kinds of polysaccharides, amylose, and amylopectin	The leaves of all green plants and in the seeds, fruits, stems, roots, and tubers of most plants and also in algae	Biocompatible, Biodegradable, Biorenewable, Low cost, Semicrystalline, High mechanical strength	[34–36]
Hyaluronic acid	Linear polysaccharide	A major macromolecular component of the ECM in the most connective tissues	Biocompatible, Biodegradable, Bioresorbable, Limited immunogenicity, Recognized by cell surface receptors, Flexible, Unique viscoelasticity	[37–40]
Chondroitin sulfate	Unbranched polysaccharide	A major component of ECM	Biocompatible, Biodegradable, Easily available, Immune-enhancing activity, Anti-inflammatory, Antioxidant, Antitumor, Anti-coagulation	[41]
Agarose	Liner polysaccharide	Marine red algae and also found as a support structure of cell wall for marine algae	Biocompatible, Non-immunogenic, Water solubility, pH-sensitive, Electro-responsive activity, Thermoreversible gelation behavior	[42,43]
Bacterial Cellulose	Linear polysaccharide	Microorganisms belonging to the Gluconacetobacter xylinum	Biocompatible, Biodegradable, High water-holding capacity, High mechanical strength, Porous structure, High crystallinity	[44–48]
Dextran	Branched polysaccharide	Lactic-acid bacteria	Biocompatible, Low cost, Easy to modify, Stable under mild acidic/basic conditions, Slowly degraded	[49–51]
Carrageenans	Linear polysaccharide	Marine red algae	Viscoelastic and gelling properties, Anti-inflammatory, Antitumor	[52]
Gellan gum	Linear polysaccharide	Sphingomonas elodea or Pseudomonas elodea bacteria	Minimal cytotoxicity, Ability to form hard and translucent gels which are stable at low pH, Thermally reversible gel in the presence of metallic ions	[53–55]
Xanthan gum	Branched polysaccharide	Xanthomonas bacteria	Biocompatible, Non-toxicity, Biodegradable, Stabile under a broad spectrum of pH, Shear-thinning	[56]
Heparin	Linear polysaccharide	Mucosal tissues such as the porcine intestine or bovine lungs	Antitumor, Anti-viral, Angiogenesis regulatory activities	[57,58]
Collagen	Fibrous protein	A major ECM component of most connective tissues within the mammalian body	Biocompatible, Biodegradable, Low-immunogenic, Hemostatic, High swelling ability, Low antigenicity, Capacity to facilitate cellular attachment	[59–62]
Gelatin	Protein	A hydrolysis derivative of collagen	Biocompatible, Biodegradable, Non-immunogenic, Elastic, Lower antigenicity, More accessible functional groups	[63–66]
Silk fibroin	Protein	Silkworms and spiders	Biocompatible, Biodegradable, Great mechanical properties, Versatile processability	[67–71]
Keratin	Polypeptide	A major component in nail, skin, hair, horns hooves, wool, feathers	Biocompatible, Biodegradable, Possesses cellular interaction sites Low-immunogenic, Intrinsic ability to self-assemble into three-dimensional structures	[72–75]
Fibrin	Glycoprotein	Fibrinogen	Biocompatible, Biodegradable, Ability of monomers to self-assemble into a gel	[76–79]
Elastin	Structural protein	A component in the ECMs of connective tissues (e.g., blood vessels, esophagus, skin)	Biocompatible, Biodegradable, Elasticity, Self-assembly, Long-term stability	[80,81]

2. Bone

Bone tissue consists of different types of cells and an extracellular matrix, which is mainly composed of collagen proteins. The major functions of bone include structural support, mechanical movement, hemopoiesis, and organ protection; it also acts as a body resource of calcium and phosphate ions [82,83]. The resorption and formation of bone are tightly regulated and orchestrated under bone homeostasis to keep skeletal integrity [84]. Bone tissue contains different types of cells, including osteoblasts, osteoclasts, and osteocytes. Osteoblasts and osteocytes originate from mesenchymal stem cells (MSCs), while osteoclasts are derived from hematopoietic stem cells. Ninety percent (90%) of the bone cell population includes osteocytes, which act as the primary cells for bone formation, mineralization, and regulating cell signaling. During the physiological process of bone remodeling, the damaged bone is resorbed by osteoclasts, and new bone, which is generated by osteoblasts, is replaced [84]. There is a balance between osteoclast-mediated bone resorption and osteoblast-mediated bone formation in healthy bone, which is controlled by several coordinated signaling mechanisms. However, under certain pathological conditions, an imbalance between these two processes may occur, leading to bone diseases.

2.1. Bone Extracellular Matrix

Type I collagen makes up most of the ECM in bone, and its orientation directly impacts its mechanical properties. Collagen fibers arranged in a uniform and parallel pattern reinforce the bone [85]. Apatite mineral crystallites comprise 65% of the total bone mass as the inorganic part of the ECM [86]. The direction of collagen fibrils and apatite crystals in ECM creates diverse mechanical properties in different bone types, e.g., being co-aligned in a direction makes the bone stiff and tight [87,88]. Other important non-cellular components of bone ECM are glycosaminoglycans, proteoglycans, cell adhesion cytokines, and key growth factors [89].

2.2. Bone Structure

The complex and hierarchical bone structure is divided into different parts based on macroscale (cancellous bone and cortical bone), microscale (Haversian canals, osteons), sub-microscale (single layer of lamella with collagen fibers), nanoscale (collagen fibrils), and sub-nanoscale (minerals, collagen molecule) (Figure 2). Spongy cancellous bone, which is distributed on the surface of the bone, is made up of intertwined bone trabeculae. Cortical bone (compact bone) is strong in compression and distortion due to its high density. Osteons, which are cylinders that contain osteocytes, are placed parallel to the shaft of the bone tube. Each osteon consists of lamellas surrounding the Haversian canal, containing blood vessels and fiber arrays as its subunits, containing mineralized collagen fibrils made of adjacent blocks adhered by crosslinkers. Collagen molecules comprise triple helix chains that coil each other and are stabilized by internal bonds. Crystallized apatite, the inorganic substance, is located between collagen fibrils [90].

The hierarchical structure in the cortical bone can be divided into six levels: (1) Macrostructure level (>10 mm), which consists of cortical and trabecular bone types, (2) Mesostructure level (0.5–10 mm), where osteons array together, (3) Microstructure level (10–500 μm), where a single osteon contains interstitial lamella, (4) Sub-microstructural level (1–10 μm), which is also a single lamella, (5) Nanostructure level (10–1000 nm), which is a multiphase nanocomposite consisting of an organic phase, inorganic phase, and water, and (6) Sub-nanostructure (<10 nm) in which molecules can be analyzed separately.

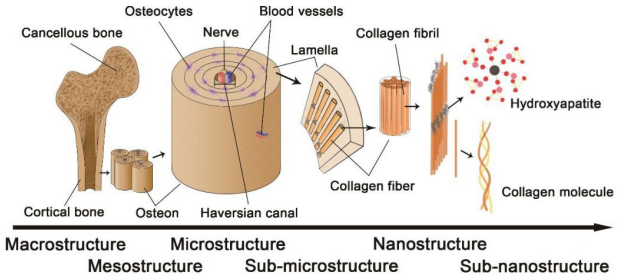

Figure 2. The hierarchical structure of bone.

2.3. Bone Diseases

There are many bone diseases, usually leading to fractures and defects. Osteogenesis imperfecta is generated by a defect in collagen and results in less organized bone; therefore, the bone fails as it is faced with only minimal amounts of tension. Osteoporosis, the most common bone disease, is characterized by decreased bone mass and deterioration of bone structure [91]. The defects in osteoclastic bone resorption cause osteopetrosis disease, which, despite increasing bone mass, will be followed by skeletal fragility. Osteosarcoma is a common bone tumor that mainly occurs in the large bones and the knee [92].

Conventional clinical therapies for bone filling, such as autologous and allogeneic bone grafts, suffer from several shortcomings, i.e., immune rejection, infection, insufficient or missing osseointegration, and lack of a donor. Bone tissue engineering has emerged as a novel method to hinder the mentioned risks. The new approaches for regenerating damaged bone are developed using the tissue engineering triangle: signaling molecules, cells, and scaffolds. Below, we summarize recent examples of natural-based polymers that have been used for bone tissue engineering.

2.4. Natural-Based Scaffolds for Bone Tissue Engineering

2.4.1. Collagen

As the main organic matrix of bone, type I collagen has superior bioactivity and biocompatibility as implants. However, the mechanical properties of collagen are not ideal for hard tissue engineering. As a result, many studies of collagen-based scaffolds have focused on improving strength, osteogenesis, and bioavailability.

Ceramics are usually used as enhancers to improve the strength of collagen-based material owing to their great mechanical strength. Among these, hydroxyapatite (HA), β-tricalcium phosphate (β-TCP), and bioactive glasses (BGs) are mainly employed with collagen for bone scaffolds. HA and β-TCP can also provide essential elements such as calcium and phosphorus for the bone matrix. Combining collagen–TCP composites with other materials has been evaluated as a biomimicking matrix and delivery vehicle of growth factors to improve their structural and biological properties [93]. β-TCP can provide good osteoconductivity and accelerate the degradation rate of the scaffold, which eventually can be replaced by a newly formed bone. The optimal β-TCP concentration should be 5–10 wt% to control the rapid release of Ca^{2+} [94]. HA is the original component of the bone matrix; therefore, its application for bone implants is widely studied. Although HA has superiorities with non-reactivity, osteoconductivity, and outstanding strength to composite collagen, the shortcomings such as the low degradation rate of HA still inhibit the development of HA/collagen materials. As a result, biphasic calcium phosphate (BCP) provides both the stability of HA and the biodegradability of β-TCP and has emerged as a promising future direction [95].

Bioactive glasses (BGs) are silica-based biomaterials that contain SiO_2-CaO-P_2O_5 networks. The release of Na^+, Ca^{2+}, and Si^{4+} can trigger osteoblast proliferation and differentiation by stimulating osteogenesis. More importantly, due to the formation of silanol active sites, it has been used for tissue binding and mineralization [96]. BGs offer higher bioavailability and bioactivity due to their higher surface reactivity than HA and β-TCP [97,98]. Ferreira et al. took advantage of the bioglass and carbonate apatite composite mineralized collagen scaffold to promote human osteoblast differentiation [98]. The composites could stimulate osteoblast differentiation and mineralization in vitro without osteogenic dopants [99].

Synthetic polymers are also applied to enhance the mechanical properties of collagen. Polymers such as polylactic acid (PLA) [100], poly lactic-co-glycolic acid (PLGA) [101], and polycaprolactone (PCL) [102] are often used for collagen composites.

Nowadays, 3D printing is commonly used for polymer processing due to the rapid development of this technology. The osteoconductive and osteoinductive properties of a 3D-printed PLA/collagen scaffold were proved by in vitro biomineralization tests [100]. Dewey et al. utilized fluffy-PLGA to reinforce mineralized collagen scaffolds to form a bone mesh [101]. The in vitro tests showed that this composite could increase hMSC osteogenesis and locally inhibit osteoclast activity to accelerate bone regeneration.

The biomimetically inspired approach is a promising strategy for forming osteogenic and hematopoietic niches and shows considerable osteoinductivity by the expression of cells and bone marrow stromal cell markers. Proteins and ions are frequently applied as dopants to achieve biological purposes. Tadalafil is a phosphodiesterase (PDE) enzyme inhibitor that benefits angiogenesis by upregulating the expression of VEGF and CYR61 as well as increasing the effect of nitrous oxide (NO) and the level of cGMP. The Tadalafil/β-TCP/collagen scaffold was prepared and further implanted in vivo in a rabbit critical-size calvarial defect, and it led to accelerating osteogenesis following 6 weeks [103]. The substitution of magnesium ions (Mg^{2+}) can induce angiogenesis through nitric acid production [104–106]. A recent study utilized magnesium as the primary material cooperated with collagen and HA to achieve a better degradation rate [107]. Copper ions (Cu^{2+}) are also available for bone implants. Culturing of pre-osteoblast cells on a porous collagen/copper-doped bioactive glass scaffold showed enhanced osteogenesis and angiogenesis [108]. Furthermore, when implanted in a chick embryo ex vivo model, it exhibited potential for osteomyelitis treatment by limiting infection while enhancing angio- and osteogenesis effect [108]. Other essential trace elements in the body play important roles in bone metabolism's anabolic and catabolic aspects. A collagen/HA porous scaffold incorporated with carboxyl-functionalized carbon nanotube (CNT) was developed to transplant MSCs in Sprague–Dawley rats with parietal bone defects [109]. After 12 weeks of implanting collagen/HA/CNT scaffold in a rat critical-sized calvarial defect model, favorable biocompatibility and biodegradability were observed. Furthermore, the utilization of CNT enhanced the mechanical strength and osteogenesis of the scaffold [109].

To offset the weaknesses of collagen, the reinforcement with ceramics and synthetic/natural-based polymers is a promising solution for bone tissue engineering.

2.4.2. Gelatin

Gelatin is a hydrolyzed form of collagen derived from acid and alkali pre-treatments of bovine and porcine collagen [65]. Gelatin has significant biocompatibility due to Arg-Gly-Asp (RGD), which is available in its structure, promoting cell attachment, spreading, and proliferation. However, the poor mechanical properties prohibit its direct usage for bone defect treatments. Several studies focus on gelatin-based scaffolds incorporated with other materials to evaluate mechanical stability and the osteogenic differentiation of osteoblasts. Micro and nano-additives such as silica nanoparticles, polymer microparticles, and nano-HA can be employed to improve mechanical strength and are additionally used as controlled delivery systems for osteogenesis, angiogenesis, and drug agents [110,111]. The dopants for biological functions usually aim at improved osteoinductivity, anti-inflammatory, and

antibacterial ability. A study of an alginate–TCP–gelatin porous scaffold loaded with dimethyloxalylglycine demonstrated an upregulation of angiogenesis markers [112]. Furthermore, in vivo tracking of stem cells seeded on the scaffold demonstrated considerable osteogenesis and angiogenesis potential. However, the sample's mechanical properties from this study lacked adequate strength to regenerate large-sized bone defects fully [112]. Although incorporating bioceramics can result in osteoconduction and mechanical strength, the balance between porosity and strength is still a challenge for researchers. The strategies to solve this contradiction include improving compositions, microstructures, and processing methods. One such illustration is the gelatin–PCL–nanoHA composite scaffold prepared by electrospinning [113]. The effect of several processing parameters such as porosity, fiber diameter, pore size, and HA concentration was investigated. Three-dimensional (3D) printing is more precise than electrospinning when a complex porous structure is needed. A graphene/gelatin/chitosan/TCP composite was recently fabricated by Lu et al. through additive manufacturing [114]. The combination of various materials and 3D printing provides scaffolds with a complex 3D structure and antibacterial properties.

With many functional groups in gelatin, chemical modification is also an attractive approach to developing gelatin-based scaffolds. Gelatin methacryloyl (GelMA), a photocrosslinkable gelatin, is one of the most studied. A recent study loaded metformin into mesoporous silica nanospheres and then composited it with GelMA through UV light crosslinking to form hydrogels [115]. Such a method can provide a stable release of loaded drugs. In addition, Ca^{2+} from HA can create a bridge with the hydroxyl group in GelMA, forming a weak bonding between gelatin and HA [116]. Such composites' cell viability and biocompatibility are superior, and they are easier for in situ curing simultaneously.

2.4.3. Chitosan

There are various forms of chitosan-based scaffolds in bone tissue engineering, including films, particles, hydrogels, fibers, and sponges [117]. Chitosan is introduced as a linear polysaccharide and has favorable biocompatibility, bioactivity, and biodegradability features. More importantly, chitosan contains free amino groups that can be protonated, making chitosan modifiable with biochemical groups. The protonated amino groups allow the electrostatic interaction with DNA, proteins, lipids, or negatively charged synthetic polymers [118]. A study grafted GRGDSPK (RGD) or FRHRNRKGY (HVP) sequences on chitosan and tested the sample with osteoblasts [119]. The functional groups improved cell adhesion and proliferation. Despite this, the main drawback of chitosan is their low mechanical strength for load-bearing defects. Making a composite with mechanical enhancers is usually applied to overcome this limitation. For example, a PCL fibrous scaffold was introduced for the inclusion of chitosan nanoparticles for a rat model of the critical-sized calvarial bone defect [120]. The hydrophilic nature of chitosan reduced the hydrophobic nature of PCL nanofibers. The presence of chitosan also regulated cellular functions by increasing protein adsorption, fluid uptake, and ALP activity. In another study, the incorporation of bioceramic into the chitosan matrix was evaluated [121]. The histopathological and microbiological results of the composite in an osteomyelitis animal model revealed the ability of chitosan and the calcium phosphate scaffold to induce cellular differentiation and augment the osteoconductive and mechanical properties. The superiority of modification and antibacterial properties make chitosan an excellent choice for functional bone implants, while the suitable mechanical properties demand a prompt solution.

2.4.4. Alginate

Alginate, a natural and anionic polysaccharide, has a great potential for bone tissue engineering due to its biocompatibility, gel-forming ability, and modifying capacity [31]. The studies of alginate scaffolds focus on improving biodegradability, strength, gelation property, and cell affinity. Recently, palygorskite, bioactive glass, graphene oxide, and PCL have been used to prepare composites with alginate for bone scaffolds [122–125]. Developing injectable alginate-based hydrogels with proper adhesivity and osteogenic

activity for utilization in filling bone defects and cavities has always been a tempting goal for researchers. Since complex chemical compositions usually cause difficulties in batch productions, developing a binary component multifunctional alginate-based hydrogel for bone regeneration was investigated. First, using an amidation reaction, dopamine (DA) was grafted to alginate. Then, mixing strontium ions with Alg-DA solution resulted in an injectable hydrogel with proper adhesivity due to catechol groups on Alg-DA. In addition, over 8 weeks of in vivo studies on rats, the enhanced osteogenic activity of strontium containing hydrogel scaffolds was indicated compared to hydrogels without strontium [126]. Tunable void-forming alginate-based hydrogels are excellent choices for filling bone cavities. Another study investigated the potential of alginate-based hydrogels containing rat mesenchymal stromal cells for bone regeneration for critical-sized femoral defects in rats. After 6 weeks post-surgery, the bone and tissue mineral density in the defect site that filled with MSCs encapsulated hydrogel were much higher than the non-cell seeded scaffold. However, none of the hydrogels could repair the defects completely [127]. Despite the benefits, the absence of regulated biodegradability can have undesirable consequences. It should be combined with other biodegradable polymers to eliminate this limitation. One instance of these combinations is chitosan–alginate to repair the physical injury in rats. The proposed hydrogel demonstrated significant controllable degradation that would inhibit bone growth deformities, and also it showed the ability for loading chondrogenic factors. Therefore, this scaffold can be a promising platform that improves physical injury repair [128]. To sum up, alginate has excellent biocompatibility and devisable potential with its functional groups; the limitations such as the strength and degradation of alginate are still the research priorities in this field.

2.4.5. Silk Fibroin

Compared to other natural polymers, silk fibroin (SF) possesses several significant advantages such as excellent biocompatibility, outstanding mechanical properties, and biodegradability [129]. The fibrous structure is the typical characteristic of SF. SF scaffolds with low porosity and thinner fibers can inhibit the immune activation of macrophages and T cells. Yang et al. fabricated an SF-based scaffold with different porosity and fiber thickness through electrospinning [130] and confirmed that the inflammatory response could be regulated through different silk fibroin architectures.

Functionality for biomedicine has been one of the research focuses for SF. Recently, the literature aimed to investigate SF's cell adhesion, drug-loading capacity, and osteoinductivity [131–135]. Some materials are usually applied to composite SF in hard tissue engineering to improve the biological properties. For example, HA is frequently used to coordinate SF for bone tissue scaffolds. The durability of silk fibroin can precisely make up for the shortcoming of HA to form a scaffold with the ideal mechanical properties. The HA-SF slurry demonstrated shear thinning behavior characteristics, making flow-based injection more clinically convenient [136]. The mechanical study showed that injection and compression molding could provide favorable strength for SF-based scaffolds. A compatible combination between SF and HA has been studied in hard tissue engineering [137]. Similar to HA, bioactive glasses (BGs) are also suitable for mixing with SF to improve biocompatibility and osteoconductivity. In a study, a composite scaffold comprised of SF/BG was constructed by the 3D printing fabrication technique. Bone marrow stem cells were seeded before transplanting into the back of nude mice [138]. The osteogenic ability of the scaffolds was confirmed with enhanced osteogenesis-related genes (COL-1, OCN, BSP, and BMP-2) expression. Synthetic polymers are also applied with SF for fiber scaffolds. An SF-coated PCL scaffold developed by Xiao et al. could improve tissue arrangement and remodeling and support a faster regeneration rate in the rat model [139]. The scaffold's porosity with electrospinning and gas-foaming technology was much higher than traditional nanofiber mats.

The summary of natural polymer based materials for bone regeneration shown in Table 2.

Table 2. Summary of recent studies using natural polymers in bone tissue engineering.

Ref	Applied Materials	Cell Type	Structure/Production Method	Benefits
[140]	HA/gelatin/chitosan	Human osteoblast-like cell line (MG-63)	Core–shell nanofibers/freeze-drying method and calcium ion crosslinking	Biomimetic porous 3D scaffold with gradient and layered microstructure
[141]	Gelatin–alginate graphene oxide	Human osteoblast-like cell line (MG-63)	Nanocomposite scaffold/freeze drying technique	Enhanced compressive strength, 700% swelling ratio, slow biodegradation (≈30% in 28 days)
[142]	Gelatin-bioactive glass-ceramic	Human osteoblast-like cell line (MG-63)	Macroporous composite/lyophilization	Controlled degradation of gelatin scaffold and enhanced mechanical strength by incorporation of bioactive glass particles
[143]	Carboxymethyl chitosan/PCL	Human osteoblast-like cell line (MG-63)	Nanofibrous scaffold/electrospinning	Ultrafine and splitting fibers, reduced water contact angle
[144]	Chitosan/honeycomb porous carbon/HA	Bone marrow mesenchymal stem cells	Hierarchical porous structures/vacuum freeze-dried	Suitable pore size and high porosity for cell viability, mineralization, proliferation, and osteoinduction
[145]	Alginate/chitosan-HA	Human chondrocytes and fibroblasts	Porous gradient scaffold/freeze-drying and crosslinking by calcium ions	High compression modules and porosity
[146]	Gelatin/alginate/ polyvinyl alcohol	MC3T3-E1 pre-osteoblast cells	Macroporous 3D spongy scaffold/cryogelation technique	Anti-bacterial scaffold for bone regeneration
[147]	Gelatin	L-929 fibroblasts, D1 MSC and MG63 osteoblasts	Fiber scaffold/freeze-dried	Enzymatically crosslinked scaffold for bone regeneration
[148]	Gelatin/PLLA	L929 fibroblasts	Multifunctional layered scaffold/electrospinning and 3D printing	Nasal cartilages and subchondral bonereconstruction
[149]	Strontium-Substituted HA/Gelatin	Coculture of osteoblasts and osteoclasts	Porous 3D scaffold/freeze-drying	Useful for local delivery of strontium and excessive bone resorption ability
[150]	Gelatin/PCL/nanoHA/ vitamin D3	Human adipose-derived stem cells	Nanocomposite scaffold/electrospinning	nHA and vitamin D3 have a synergistic effect on the osteogenic differentiation of hADSCs
[151]	Collagen/silica	Lymphocytes	Collagen fibrils with deposition of intrafibrillar amorphous silica	Promoting bone regeneration and angiogenesis via monocyte immunomodulation. Differentiation of blood-derived monocytes into TRAP-positive cells due to sustained release of silicic acid
[152]	Fibroin/poly(lactide-co-ε-caprolactone)	Human adipose-derived stem cells	Hybrid nanofibrous scaffold	Inducing cell adhesion and proliferation, favorable tensile strength, and surface roughness
[153]	Fibroin/PLGA	Rat bone marrow mesenchymal stem cells	Core–shell nanofibers	Enhancing cell adhesion, diffusion, and proliferation, promoting the osteogenic differentiation
[154]	SF/cellulose/chitosan	Human osteoblast cell line	Composite Porous scaffold	Supporting cell proliferation and promoting biomineralization
[155]	Fibroin/gelatin	Rat mesenchymal stem cell	Composite microcarrier	Supporting cell adhesion, proliferation, and elastic modulus
[156]	Alginate/nano-HA	Rat calvaria osteoblast	Composites	Good bioactivity, high biocompatibility, antibacterial activity
[157]	Silk/calcium silicate/sodium alginate	Bone marrow stromal cells	Hydrogel	Good biodegradation, cytocompatibility, bioactivity, and the proliferation of bone marrow stromal cells
[158]	Alginate/calcium phosphate paste	Stem cells	Injectable microbeads	Enhancing cell viability, proliferation, osteogenic differentiation, and bone regeneration
[159]	Alginate/gelatin/ apatite coating	Rat bone marrow stem cells	3D printed composite scaffold	Higher proliferation, osteogenic differentiation, surface protein adsorption, and Young's modulus for apatite-coated scaffold

3. Skeletal Muscle

The skeletal muscle connects to the bones by tendons and forms nearly 40% of the total body mass. Skeletal muscles play a significant role in skeletal support and movement, regulation of metabolism, and temperature. Muscle fibers are composed of many myofibrils, and myofibrils contain many myofilaments. Myofibrils are arranged in a unique pattern to form sarcomeres [160], which is the basic contraction unit of skeletal muscle. The two most essential filaments are actin and myosin, which are arranged uniquely to form various bands on skeletal muscle. Skeletal muscle consists of multinucleated single muscle cells called myofibers. Muscle stem cells are distributed at the periphery of the myofibers, making up 1 to 5% of total muscle cells [161]. These cells multiply in response to mechanical and chemical damage and cause growth, replacement, and repair of the tissue [162–167]. Skeletal muscles are joined to the nervous system for activation and contraction and the blood vessels for the diffusion of nutrients and oxygen and waste effusion.

3.1. Skeletal Muscle ECM Structure

Skeletal muscle tissue's extracellular matrix (ECM) is complex with a highly organized structure [168]. The ECM plays a vital role in the growth, development, repair, muscle elasticity, regeneration, cell function, and force transmission in the muscle [169]. In addition to mechanical support for cells, the ECM also plays a host of signaling cascades [166]. The main components of the ECM structure are collagen, glycoproteins, proteoglycans, and elastin. The most abundant collagen types in skeletal muscle tissue are collagen type I and III [170]. Skeletal muscle tissue has two separate parts of the ECM structure: the basal lamina, which has a sheet-like structure, and intramuscular connective tissue, with an organized structure consisting of three major parts, as shown in Figure 3 described below [166,171].

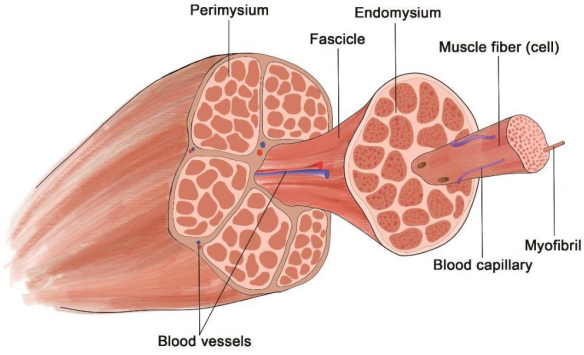

Figure 3. Structure of Skeletal Muscle.

The muscle is composed of myocytes arranged in bundles. The length of each cell varies, and the cells are closely spaced and complementary in length. Each cell is wrapped with a thin reticular membrane, which is called the endomysium; each muscle bundle is enfolded with a connective tissue membrane mixed with glial and elastic fibers, which is called the fascicle membrane; outside of each muscle, there is a thicker layer of connective tissue, which is called the epimysium. The connective tissues of each membrane are continuous, and the blood vessels and nerves distributed to the muscles enter along the connective tissue membrane [165,166,168].

3.2. Disorders

Injuries and disorders such as traumatic injuries, surgical procedures, and congenital and acquired diseases that result in complete and irrecoverable loss of skeletal muscle function have been known as volume muscle loss (VML). The standard VML treatment is autologous transplantation of skeletal muscle from a cadaver or a donor. However, this approach is costly and time-consuming, and it is associated with immune response and donor site morbidity. Tissue engineering approaches have been developed as an alternative to overcome these complications. Many scaffolds combined with cells, drugs, small molecules, or growth factors have been used in tissue engineering applications [172–174].

3.3. Natural-Based Scaffold for Skeletal Muscle Tissue Engineering

3.3.1. Keratin

Keratin is known as a carrier for the primary fibroblasts growth factor (bFGF or FGF-2), insulin-like growth factor 1 (IGF-1), and vascular endothelial growth factor (VEGF) [172]. bFGF directly regenerates muscles by enhancing the proliferation of the satellite cells. Similarly, IGF-1 plays an essential role in muscle maintenance and regeneration. VEGF is a protein that plays a positive effective role in angiogenesis, which increases the longevity of tissue-engineered skeletal muscle [172–174]. Keratin contains growth factors that significantly elevate the formation of new muscle tissue, myofibers, and blood vessels and reduce fibrosis [173]. The binding between those cytokines and keratin can prevent rapid degradation and achieve controlled release [175]. The in vivo implantation of keratin hydrogel in combination with IGF-1, bFGF, or muscle progenitor cell (MPCs) as a scaffold in rat tibialis anterior muscle VML injury model demonstrated significant improvement in the regeneration of skeletal muscle tissue. In another in vivo study, the scaffold and MPCs, VEGF, IGF-1, and bFGF were examined. This study proved a diminished inflammatory response and an enhanced muscle re-formation [174]. These studies suggested that keratin hydrogel, along with growth factors, improves treatment performance in VML injury.

Keratin is also frequently mixed with synthetic polymers, especially PCL [176,177]. Commonly, the keratin composite scaffolds for muscle tissue are prepared by electrospinning. Keratin contains a large amount of nitrogen that produces NO, which is one of the metabolism products of keratin [177]. Due to the catalytic generation of NO, the PCL/keratin composite scaffold can accelerate endothelial cell growth and reduce smooth muscle cell proliferation [178]. Such keratin-based scaffolds are a NO donor in the blood, benefiting vascular tissue regeneration.

3.3.2. Collagen

Collagen is the central part of ECM, which increases the formation of new blood vessels and muscular tissue [179]. The application of murine muscle-derived stem cells (MDSCs) and collagen for the regeneration of muscle defects has been reported. The results demonstrated better skeletal muscle regeneration, higher cell proliferation, and reduction in fibrotic scar formation in the collagen scaffolds with MDSCs compared to only collagen scaffolds [180]. In an in vivo study, a mice VML injury model was used to screen different scaffolds. It was reported that collagen type I and an ECM hydrogel demonstrated better cell viability and VML treatment. The following indicated that the ECM-based scaffold (in comparison with the collagen type I hydrogel) led to the highest number of myofibers [181].

Collagen and glycosaminoglycan (GAG) (chondroitin 6-sulfate) were applied as a scaffold to regenerate a mice VML injury model. Chondroitin sulfate is one of the most critical components in cartilage structure and plays a vital role in the formation of skeletal muscle tissue and the regeneration of muscular tissue [179]. The collagen–GAG scaffold led to elevated expression levels of growth factors related to muscle tissue. A mice VML model treated with the scaffold also showed a reduction in fibrosis compared to untreated VML [179]. The research on collagen composites for muscle tissue engineering often contains synthetic materials. PCL, polypyrrole (PPy), and polyvinyl alcohol (PVA) have been recently used with collagen for skeletal muscle tissue engineering [182–184]. These combi-

nations can reinforce collagen and provide various functions for the scaffolds. For instance, collagen mixed with conductive PPy nanoparticles promoted cell adhesion, growth, and proliferation [182]. Furthermore, enhanced myotube formation and maturation were found in another collagen/PPy implantation study [185].

Muscle is well-aligned tissue with fibrous structures at various levels. Therefore, the scaffolds for skeletal muscle tissue should be aligned. A murine model used collagen-aligned scaffolds comprising mouse myoblast and human microvascular endothelial cells to treat VML injury. The results indicated that collagen-aligned nanofibrillar scaffolds promote the regeneration of skeletal muscle and angiogenesis in comparison with randomly oriented ones [186]. Lotus-root-like collagen scaffolds prepared by Hwangbo et al. showed a more bio-stimulating structure than conventional collagen struts [183]. The aligned hierarchical microtubular collagen niche can enhance cell adhesion and promote myogenic differentiation and maturation. Such a porous structure is also necessary for angiogenesis in soft tissue regeneration.

3.3.3. Alginate

This abundant biopolymer is not only biocompatible and has low toxicity but also exhibits a temperature-independent gelation process in the presence of divalent cations, making it an excellent candidate for tissue engineering [187]. The partial oxidation of alginate is a common way of controlling biodegradability, and it is mainly used for tissue regeneration purposes [188]. The wet-spun fabrication of alginate fibers containing muscle precursor cells is reported to be efficient for muscle recovery based on an in vivo study on a mouse model [187]. Another work used an injectable 3D RGD-coupled alginate scaffold to deliver gingival mesenchymal stem cells for muscle regeneration and confirmed effective muscle regeneration in mice [189]. Oxidized alginate-gelatin bioink was also used for 3D printing of mouse myoblast cells (C2C12). The results showed that the proper selection of nozzle size extrusion pressure could affect cell orientation and migration in the printed scaffold for muscle regeneration [190]. A new approach was also reported for muscle regeneration exploiting the interplay between specific cell membrane receptors. This research utilized borax-loaded alginate hydrogels to stimulate the borate transporter, NaBC1. In vivo studies of this approach on mice showed a successful acceleration of the muscle regeneration process [190].

3.3.4. Laminin, Fibrin, and Gelatin

Laminins are heterotrimeric glycoproteins that are naturally formed by the muscle and localized in ECM consequently. A new hydrogel consisting of fibrinogen and laminin-111 (laminin-111 enriched with fibrin) was applied to treat a murine model of VML injury. The different properties of laminin trimers allow cell receptors to regulate different cellular pathways [191]. The LM-111 scaffold significantly improved muscle weight and increased the penetration of satellite, endothelial, hematopoietic, and immune cells [192]. Adipose-derived stem cells (ASCs) can be used in muscle tissue engineering applications. The combination of ASCs and electrospun fibrin fibers can mimic the native tissue. Following in vivo implantation, the ASCs seeded on a fibrin scaffold did not significantly enhance muscle regeneration [193].

In situ bioprinting of GelMA hydrogel was employed to treat VML injury. The use of encapsulated cells in this study led to the formation of multinucleated myotubes [194]. The most attractive part of this study is the direct-printing technology used in the defect area. In situ crosslinking allows surgeons to fill VLM injury rapidly and adequately, significantly improving tissue regeneration and functional recovery.

Recently, Hwangbo et al. used an in situ UV crosslinking hydrogel to treat VML by two different bio-inks, GelMa and C2C12 or GelMa and human adipose-derived stem cells (hASCs). They optimized printer parameters such as barrel temperature, number of UV light sources, UV exposure dose, and wall shear stresses at the first step. Next, bio-printed structures laden with hASCs were implanted into mice as in vivo tests and

showed a significant improvement in muscle regeneration. Based on the reported result, they developed a promising in situ crosslink GelMa construct for treating VML [195].

Natural polymers alone are not suitable for treating injuries such as VML due to their poor mechanical properties. Thus, combining hydrogels, growth factors, and cells increases skeletal muscle regeneration.

The summary of natural polymer based biomaterials for skeletal muscle regeneration is shown in Table 3.

Table 3. Summary of recent studies using natural polymers in skeletal muscle tissue engineering.

Ref	Applied Materials	Cell Type	Structure/Production Method	Advantages
[196]	Collagen/PPy	C2C12 mouse myoblast	3D, highly aligned, and electrically conductive collagen scaffold via directional lyophilization of a polypyrrole-doped collagen suspension	Increasing electrical conductivity by using polypyrrole (PPy)
[197]	Collagen	C2C12 murine skeletal muscle myoblast cell	Fused deposition modeling (FDM)	Increased IGF1 mRNA and, Akt, p70S6K, and 4EBP1 phosphorylation, along with myotube hypertrophy and improved designed muscle functionality
[198]	Alginate/Gelatin/ Heparin	Human skeletal muscle progenitor cells (hSMPCs)	Hydrogel	Cost-effective and an alternative for commercial biomaterials
[199]	Alginate	Mesenchymal stromal cells (MSCs)	Hydrogel	IGF-1 and VEGF165 had significant effects on muscle progenitor cells
[188]	Alginate/Gelatin	C2C12	Extrusion-bioprinting of hydrogel	Alginate–gelatin hydrogel is a simple and cost-efficient biodegradable bio-ink
[200]	Gelatin/Hyaluronic acid	C2C12	Hydrogel	Myotube production was established throughout the hydrogel when both gelatin and hyaluronic acid were present, and no shrinkage occurred
[201]	Fibrin/Polyethylene oxide (PEO)	C2C12	C2C12s are encapsulated and electrospun into fibrin/polyethylene oxide (PEO) microfiber bundles with aqueous solution electrospinning.	Loading C2C12s as cellular aggregates increasing cell viability
[202]	Fibrin	Muscle progenitor cells (MPCs) adipogenic	Hydrogel	Adipogenic differentiation was decreased by myogenic differentiation but not prevented, and MPCs produced from diabetic animals had a higher capacity for adipogenic differentiation.
[203]	Fibrin/Laminin	C2C12	Hydrogel	Integrating laminin-111 into fibrin hydrogels is possible
[204]	Fibrin/Alginate	C2C12	Three-dimensional engineering of skeletal muscle tissue using electrospun fibrin microfiber bundles	To promote tissue formation, myoblasts should undergo biophysical stimulation
[205]	Fibrin/Thrombin	C2C12	3D printing, co-extruding fibrinogen and thrombin	Enhancing the regeneration of functional muscle tissue by tuning the topographic features of scaffolds
[206]	Fibrin/Collagen	Primary human skeletal muscle cells	Hydrogels	The Young's modulus increased twofold, maximum strain decreased 2.5 times, and collagen deposition increased 1.6 times
[207]	Gelatin methacrylate (GelMA)	C2C12	Under single UV exposure, silicone tubes-based coagulant produces cell-laden GelMA microfibers	Increased uniaxial strain ratio of up to 35–45% and significantly improved myotube contractility
[208]	Fibrin + Alginate	Primary human myoblasts	Injectable gel	Optimization of myoblast transplantation can include consideration of cell state

Table 3. *Cont.*

Ref	Applied Materials	Cell Type	Structure/Production Method	Advantages
[209]	Fibrin/Alginate/Collagen	Human umbilical vein endothelial cells (HUVEC)	The use of 3D printing to create scaffolds composed of multiple gel layers and hollow channels	They developed a very cost-effective 3D printing system
[210]	Fibrin/Collagen-I	Mesenchymal stem cells (MSCs)	Parallel nanofiber electrospinning	When myogenic differentiation occurs, IGFBPs play a role, varying based on culture and stimulation conditions.
[211]	Fibrin	Muscle-derived stem cells (MDSCs)	Gel	SW033291 increased MDSC myogenic differentiation and myotube creation in a significant way.
[212]	Gelatin	C2C12	Cell-based 3D bioprinting	The dECM components accelerated myogenic differentiation, while topographical cues caused cellular alignment
[213]	Gelatin	C2C12	Cryogel	Myoblasts organize themselves around this pore structure and colonize the entire three-dimensional structure
[214]	Gelatin/Chitosan	L929 fibroblasts cell line	Hydrogel–3D printing	Increased cell viability
[215]	Gelatin/Alginate	C2C12	Hydrogel–3D printing	Adding calcium peroxide (CPO) as an oxygen-generating source to bio-ink can improve cell metabolic activity in Gelma bio-ink
[216]	Gelatin	C2C12	Hydrogel	Soft substrates can support longer-term cell culture
[217]	Fibrin	Bovine satellite cells (BSCs)	Hydrogel	Up to a 15-fold increase in myoglobin expression in vascular smooth muscle cells
[218]	Gelatin	C2C12	Hydrogel	An increase in sarcomere formation in myotube cultures using micropatterned gelatin hydrogels

4. Tendon and Ligament

Despite having essential and unique functions in the musculoskeletal system, research on tendons and ligaments is not as advanced as the rest of skeletal tissues [219]. Tendons and ligaments are very similar but still distinct connective tissues. According to this, tendons are fibrous tissues that join skeletal muscle to bone, making movements possible through force transmission from muscles to bones [220]. At the same time, ligaments are the dense fibrous connective tissue that connects bone to bone [221]. The transmission of these tensile forces by tendons and ligaments makes them susceptible to tearing or complete rupture, depending on the amount of the force [222].

The use of natural and synthetic polymers for tendon and ligament tissue engineering has been investigated for years, and obviously, each has its pros and cons. For example, better cell attachment to synthetic scaffolds with dense, fine, and aligned fibers and a tendon-like cellular phenotype on synthetic scaffolds have been reported. On the other hand, biological scaffolds promote better cell proliferation and the expression of collagen genes, the most abundant molecular component in tendon and ligament [223]. Hence, using both natural and synthetic polymers to maintain both biological and mechanical requirements simultaneously seems logical.

4.1. Tendon and Ligament ECM Structure

Tendons and ligaments have very similar ECM components and structures. At the microscale, they both have wave-form patterns with fibers oriented parallel to the stress axis. They are straightened when put under tension and reconverted when released. They both have a hierarchical structure, beginning with collagen molecules, fibrils, fiber bundles, fascicles (considered the basic functional unit of the tissue), and ultimately tendon and ligament units [224,225] (Figure 4). The tensile strength of the tendon is reported to be

about 50–150 MPa, and its elastic modulus is about 1200–1800 MPa, while the ligament has a tensile strength of about 50 MPa and elastic modulus of about 150–355 MPa. They both have a certain degree of plasticity for adaption to changing stresses [225]. They both follow the elastic model up to a certain amount of strain. Afterward, they will undergo microscopic failure, and further strain may lead to a total rupture of the tissue [226].

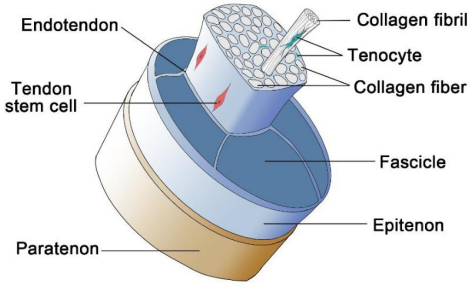

Figure 4. The hierarchical structure of tendon and ligament.

The chemical composition of the tendon and ligament is very similar, with a slight difference in the number of components. The main component of both tendon and ligament is water, 60% to 80% in weight [220,221]. They contain a protein phase (collagen) and a polysaccharide phase (proteoglycans). Collagen type I is the most abundant protein in the tendon and ligament [225]. It constitutes about 60% of the tendon's dry weight and corresponds to 95% of the total tendon collagen. The other 5% involves mainly collagen types III and V. There are minimal amounts of collagen types II, VI, IX, X, and XI. On the other hand, ligaments contain more protein, less total collagen, and greater amounts of type III collagen and GAGs [221]. While many of these collagen types' full biological and biophysical roles are still unclear, some specific functions of each type have been identified [224]. Elastin is another important component of both tendon and ligament, which is responsible for recovering the native configuration after stretching [226]. The proteoglycans found in tendons and ligaments, including decorin, aggrecan, tenascin C, fibronectin, fibromodulin, biglycan, and lumican, have specific functions mainly to organize and lubricate collagen fiber bundles [219,226].

Tenoblasts and tenocytes are the two main cell types present in tendons. Tenoblasts are very active spindle-shaped immature tendon cells that can be found as clusters in some areas of tendons. They are the predominant cell type in the tendon that can mature into tenocytes with fibroblastic morphology and low metabolic activity. Other types of cells present in the tendon are progenitor cells, synovial cells, endothelial cells, and even chondrocytes [221]. The primary cell type of ligament is fibroblasts, and these cells help in the production of collagen and matrix remodeling by the degradation of the pre-existing collagen [225].

4.2. Disorders

Lesions of tendon and ligament account for over 40% of musculoskeletal injuries [227]. These injuries are widespread in the elderly and very physically active persons such as athletes. Half (50%) of all sports injuries are related to lesions of tendons and ligaments [228]. Two of the most common ligaments exposed to the risk of injury are the Anterior Cruciate Ligament (ACL) and Deltoid Ligament (DL) of the ankle. Ankle sprains or sports accidents are the leading cause of injury to ACL and DL [229,230]. The most common tendons exposed to the risk of injury are the Achilles tendon, Flexor/Extensor tendons of the hand,

and the rotator cuff shoulder tendons [231]. The hypocellularity and hypervascularity of these tissues reduce their natural intrinsic healing ability. Thus, full recovery is relatively difficult [232]. The healing process follows three typical steps: inflammatory, proliferative, and remodeling phase. The latter is characterized by the alignment of collagen fibers parallel to the axis of muscle force direction, which plays an important role in the recovery of biomechanical properties of the tissue. Natural healing typically forms scar-like tissue with poor biomechanical properties that cannot have the proper functionality. The most common mode of surgical repair for these injuries involves using different suture techniques for reattachment. However, this method's high chance of failure and re-rupture provides excellent room for improvement. Crosslinking agents, bio-patch, or grafts to cover the ruptured area and the sutures for strengthening the repair of ruptured connective tissue have been proposed to overcome the failure and re-rupture [233]. The gold standard for surgical procedures is autografts, which have several limitations. As alternative commercialized allografts and xenografts are available, these have the risk of rejection and disease transmission. None of these approaches is considered the best [234]. However, using these tissue engineering techniques is necessary because an aberrant natural wound healing would result in excessive collagen synthesis and the formation of scar-like tissue (fibrosis) with poor biomechanical functionality [235]. Therefore, a sound understanding of the production and assembly of type I collagen fibrils is fundamental for tendon and ligament biomaterials engineering [236].

4.3. Natural-Based Scaffold for Tendon and Ligament Tissue Engineering

Despite all the valuable research in tissue engineering for tendons and ligaments in recent years, there are still many material and method selection challenges. Multiple factors should be considered when developing new therapies: on the one hand, perfect biocompatibility, proper biodegradability, and the ability to mimic the native ECM of the targeted tissue. On the other hand, having good functionality and biomechanical properties have made it difficult for researchers to agree on one biopolymer. Recently, collagen and silk have attracted much interest in this research area.

4.3.1. Collagen

The first material that has been considered for tendon and ligament implants is collagen type I, as it is the most abundant polymer in the structure of the tendon and ligament. However, natural polymers alone usually lack the required strength and biomechanical properties. A common way to increase the mechanical properties of natural polymers is to use them along with synthetic polymers. In 2021, the use of hybrid material of poly-L-lactic acid (PLLA)-based copolymers with collage/chondroitin sulfate was investigated [236]. After implantation in rats, it was observed that the collagen/chondroitin sulfate/PLLA rod enhanced cell proliferation and in vivo collagen fibrillation, suggesting benefits for tendon regeneration. In another study, electrospun PCL fiber was composited with collagen to fabricate the ligament scaffolds. With its outstanding elasticity, PCL is a perfect match with natural polymer for tendon and ligament repair [236]. The porous core-shell scaffolds were also doped with proteoglycans and glycosaminoglycans (GAG). Both are essential components of ECM, allowing cells a more appropriate space for migration. At the same time, growth factors can be applied to improve the performance of collagen scaffolds. One recent study confirmed that collagen sponge scaffolds with TGF-β1 and GDF-7 can promote tenogenic differentiation [237].

4.3.2. Silk

Silk attracts much interest from researchers to fabricate artificial scaffolds for tendons. As a linear material, the mechanical properties of silk fibroin are anisotropy, leading to the possibility of anisotropic functionalization. Chen et al. fabricated a gradient biomineralized silk fibroin nanofibrous scaffold [238]. The combination of silk fibroin and synthetic polymer has also been investigated. For example, nano-yarn scaffolds made of

PLLA/PCL/silk fibroin for ACL reconstruction in rabbit were reported [239]. In this study, both sufficient cellularity and higher modulus and stiffness are reported after 12 weeks of implantation compared to the control group due to collagen and silk.

In recent years, there have also been other studies using other natural biopolymers such as chitosan, alginate, cellulose, and fibrin [240–244]. Hybrid natural polymers like alginate–chitin scaffold that improved supraspinatus tendon-to-bone healing in vivo is also reported [245]. These studies are summarized in Table 4.

Table 4. Summary of recent studies using natural polymers in tendon/ligament tissue engineering.

Ref.	Applied Materials	Cell Type	Structure/Production Method	Advantages
[241]	Silk/Collagen Polyurethane	L929 fibroblast cell line	Knitted silk covered by electrospun collagen/polyurethane	___
[240]	Collagen/Silk	Tendon stem progenitor cells (TSPCs)	Knitted silk scaffold dipped in collagen solution (in vivo study)	Macroporous structure
[242]	Alginate/Polyacrylamide Silica Microparticles	____	Hydrogel scaffolds dried under stretch	Scaffold production under tension
[243]	Alginate/Cellulose	____	Aligned fibrous hydrogels dried under stretch	Scaffold production under tension
[244]	Fibrin	Rabbit bone marrow-derived mesenchymal stem cells (BMSCs)	2D and 3D fiber based structures	Use of different growth factors
[245]	Collagen/Nanocarbon fibers	___	Electrospun collagen/nanocarbon fibers	Use of nanocarbon fibers
[246]	Bacterial Cellulose	Human mesenchymal stem cells (hMSCs)	Bacterial cellulose sheets	Use of invaluable bacterial cellulose
[247]	PCL/CHT/CNC (Cellulose Nanocrystals)	Tendon-derived cells and adipose stem cells	Aligned electrospun nanofiber threads, braided and woven scaffolds	Reinforcement of mechanical properties by CNC
[248]	PCL/CHT CNCs	Human tendon-derived cells (hTDCs)	Electrospun nanofibrous scaffolds	Reinforcement of mechanical properties by CNC
[249]	PLLA/Collagen	___	Electrospun fibrous structure	CT scans of fiber to compare the morphology with native tendon
[250]	Collagen/PCL	C2C12 cells	Scaffold production using solvent casting and freeze drying including a subsequent crosslinking	Highly interconnected porous scaffold
[251]	Collagen–GAG	Equine tenocytes	Directional solidification of scaffolds	Investigation of scaffold pore size and crosslinking density

5. Conclusions

Current natural polymer scaffold research for MS tissue engineering focuses on improving existing materials and preparation processes and exploring novel naturally inspired materials. The number of studies using only one natural polymer for MS tissue engineering is declining in recent years, while compositing different materials together is becoming more popular. A single polymer cannot satisfy all the expectations and requirements for a perfect scaffold for MS tissue engineering purposes. However, a combination of polymers may contribute to the structure's cellular and mechanical aspects. An ideal strategy is to take advantage of each type of material and combine them. The development of natural

polymer scaffolds has become a hot spot in the research field. Moreover, it has shown excellent application prospects, giving various possibilities for developing artificial organs, injury repair, and disease treatments. It will promote tissue engineering research forward to a mature stage.

Considering recent research, natural polymers have many merits as implantable materials for MS tissue engineering. However, natural polymer-based implants have specific issues that need to be addressed: (1) Natural source polymers are uncontrollable from the initial production phase. As a result, each batch of natural biomaterials might have a varied quality. Therefore, it is necessary to harmonize the quality standards of materials, strictly control their quality, and strengthen the research of fundamental theories such as the properties and structure of materials. (2) There is a contradiction in mechanical properties, degradation speed, and permeability between biopolymers. Polymers with high molecular weight or stable structure usually have higher strength, and their degradation speed and permeability are challenging to meet the requirements in tissue engineering, especially in in vivo and clinical studies. Advanced strategies to break through this barrier are promising in polymer science (3) The development of composited biomaterials to meet the requirements of different tissues works very well. However, more research should be completed with different compositing methods instead of simple mechanical mixing. The more complex chemical and/or physical structures would enable accomplishing the regeneration mission compared with a widely used homogeneous structure. (4) The adhesion of cells on natural polymers needs to be further studied. Physically speaking, topology, hydrophilicity, nano/micro pattern, macromolecular structure adjusting, and other polymer characteristics can cater to the cells' requirements. From a biological point of view, the superior biocompatibility of natural-origin polymers makes them stand out among other materials. Taking natural polymers as one of the first considerations when facing the challenge of inflammation is reasonable. Chemically speaking, the ability of grafting is the most significant advantage of natural biopolymers and should attract widespread attention. The functional groups, such as carboxyl, hydroxyl, and amidogen, provide potential for design, modification, and functionalization. Apart from this, the metabolites of degraded polymers might have a functional contribution to tissue regeneration and have not been researched extensively. Other study methods such as drug or micro/macro-molecular doping are also the research focuses. In addition to these obstacles, existing natural biological materials, including their derivatives, have tremendous potential for further research and development, such as the chemical modification of chitin and hyaluronic acid to produce a variety of derivatives, making it more suitable as a scaffold material in musculoskeletal tissue for clinical application.

Author Contributions: Conceptualization and methodology, V.J.; writing—original draft preparation, J.F. and V.J.; review and editing, J.F., K.K. and V.J.; writing—contribution, K.A.-D., M.S., A.S.V., F.K.-A., M.G., S.R., F.R.A. and Z.G. All authors have read and agreed to the published version of the manuscript.

Funding: The authors acknowledge financial support from the European Union's Horizon 2020 research and innovation program under the Marie Sklodowska-Curie grant agreement No. 898858 and European Union's Horizon 2020 research and innovation program under the grant agreement No. 857287.

Institutional Review Board Statement: Not applicable.

Informed Consent Statement: Not applicable.

Data Availability Statement: Not applicable.

Conflicts of Interest: The authors declare no conflict of interest.

References

1. Loebel, C.; Burdick, J.A. Engineering Stem and Stromal Cell Therapies for Musculoskeletal Tissue Repair. *Cell Stem Cell* **2018**, *22*, 325–339. [CrossRef] [PubMed]
2. Zumwalt, M.; Reddy, A.P. Stem Cells for Treatment of Musculoskeletal Conditions—Orthopaedic/Sports Medicine Applications. *Biochim. Biophys. Acta Mol. Basis Dis.* **2020**, *1866*, 165624. [CrossRef] [PubMed]
3. Bai, M.; Cai, L.; Li, X.; Ye, L.; Xie, J. Stiffness and Topography of Biomaterials Dictate Cell-Matrix Interaction in Musculoskeletal Cells at the Bio-Interface: A Concise Progress Review. *J. Biomed. Mater. Res. Part B Appl. Biomater.* **2020**, *108*, 2426–2440. [CrossRef]
4. Madrigal, J.L.; Stilhano, R.; Silva, E.A. Biomaterial-Guided Gene Delivery for Musculoskeletal Tissue Repair. *Tissue Eng. Part B Rev.* **2017**, *23*, 347–361. [CrossRef]
5. Ma, D.; Wang, Y.; Dai, W. Silk Fibroin-Based Biomaterials for Musculoskeletal Tissue Engineering. *Mater. Sci. Eng. C* **2018**, *89*, 456–469. [CrossRef]
6. Gonzalez-Fernandez, T.; Sikorski, P.; Leach, J.K. Bio-Instructive Materials for Musculoskeletal Regeneration. *Acta Biomater.* **2019**, *96*, 20–34. [CrossRef] [PubMed]
7. Narayanan, N.; Jiang, C.; Uzunalli, G.; Thankappan, S.K.; Laurencin, C.T.; Deng, M. Polymeric Electrospinning for Musculoskeletal Regenerative Engineering. *Regen. Eng. Transl. Med.* **2016**, *2*, 69–84. [CrossRef]
8. Nie, X.; Wang, D.A. Decellularized Orthopaedic Tissue-Engineered Grafts: Biomaterial Scaffolds Synthesised by Therapeutic Cells. *Biomater. Sci.* **2018**, *6*, 2798–2811. [CrossRef]
9. Ferrigno, B.; Bordett, R.; Duraisamy, N.; Moskow, J.; Arul, M.R.; Rudraiah, S.; Nukavarapu, S.P.; Vella, A.T.; Kumbar, S.G. Bioactive Polymeric Materials and Electrical Stimulation Strategies for Musculoskeletal Tissue Repair and Regeneration. *Bioact. Mater.* **2020**, *5*, 468–485. [CrossRef]
10. Qazi, T.H.; Mooney, D.J.; Pumberger, M.; Geißler, S.; Duda, G.N. Biomaterials Based Strategies for Skeletal Muscle Tissue Engineering: Existing Technologies and Future Trends. *Biomaterials* **2015**, *53*, 502–521. [CrossRef]
11. Bayrak, E.; Yilgor Huri, P. Engineering Musculoskeletal Tissue Interfaces. *Front. Mater.* **2018**, *5*, 24. [CrossRef]
12. Abalymov, A.; Parakhonskiy, B.; Skirtach, A.G. Polymer-and Hybrid-Based Biomaterials for Interstitial, Connective, Vascular, Nerve, Visceral and Musculoskeletal Tissue Engineering. *Polymers* **2020**, *12*, 620. [CrossRef]
13. Jiménez, M.; Abradelo, C.; San Román, J.; Rojo, L. Bibliographic Review on the State of the Art of Strontium and Zinc Based Regenerative Therapies. Recent Developments and Clinical Applications. *J. Mater. Chem. B* **2019**, *7*, 1974–1985. [CrossRef] [PubMed]
14. Wheelton, A.; Mace, J.S.; Khan, W.; Anand, S. Biomaterials and Fabrication to Optimise Scaffold Properties for Musculoskeletal Tissue Engineering. *Curr. Stem Cell Res. Ther.* **2016**, *11*, 578–584. [CrossRef]
15. Lim, W.L.; Liau, L.L.; Ng, M.H.; Chowdhury, S.R.; Law, J.X. Current Progress in Tendon and Ligament Tissue Engineering. *Tissue Eng. Regen. Med.* **2019**, *16*, 549–571. [CrossRef] [PubMed]
16. Filippi, M.; Born, G.; Chaaban, M.; Scherberich, A. Natural Polymeric Scaffolds in Bone Regeneration. *Front. Bioeng. Biotechnol.* **2020**, *8*, 474. [CrossRef] [PubMed]
17. Malafaya, P.B.; Silva, G.A.; Reis, R.L. Natural-Origin Polymers as Carriers and Scaffolds for Biomolecules and Cell Delivery in Tissue Engineering Applications. *Adv. Drug Deliv. Rev.* **2007**, *59*, 27–207. [CrossRef]
18. Del Bakhshayesh, A.R.; Asadi, N.; Alihemmati, A.; Tayefi Nasrabadi, H.; Montaseri, A.; Davaran, S.; Saghati, S.; Akbarzadeh, A.; Abedelahi, A. An Overview of Advanced Biocompatible and Biomimetic Materials for Creation of Replacement Structures in the Musculoskeletal Systems: Focusing on Cartilage Tissue Engineering. *J. Biol. Eng.* **2019**, *13*, 85. [CrossRef]
19. Roberts, J.J.; Martens, P.J. Engineering Biosynthetic Cell Encapsulation Systems. In *Biosynthetic Polymers for Medical Applications*; Elsevier Ltd.: Amsterdam, The Netherlands, 2016; pp. 205–239, ISBN 9781782421139.
20. Spicer, C.D. Hydrogel Scaffolds for Tissue Engineering: The Importance of Polymer Choice. *Polym. Chem.* **2020**, *11*, 184–219. [CrossRef]
21. Bao, W.; Li, M.; Yang, Y.; Wan, Y.; Wang, X.; Bi, N.; Li, C. Advancements and Frontiers in the High Performance of Natural Hydrogels for Cartilage Tissue Engineering. *Front. Chem.* **2020**, *8*, 53. [CrossRef]
22. Bhattarai, D.P.; Aguilar, L.E.; Park, C.H.; Kim, C.S. A Review on Properties of Natural and Synthetic Based Electrospun Fibrous Materials for Bone Tissue Engineering. *Membranes* **2018**, *8*, 62. [CrossRef] [PubMed]
23. Tan, G.Z.; Zhou, Y. Electrospinning of Biomimetic Fibrous Scaffolds for Tissue Engineering: A Review. *Int. J. Polym. Mater. Polym. Biomater.* **2020**, *69*, 947–960. [CrossRef]
24. Robb, K.P.; Shridhar, A.; Flynn, L.E. Decellularized Matrices as Cell-Instructive Scaffolds to Guide Tissue-Specific Regeneration. *ACS Biomater. Sci. Eng.* **2018**, *4*, 3627–3643. [CrossRef] [PubMed]
25. Bose, S.; Koski, C.; Vu, A.A. Additive Manufacturing of Natural Biopolymers and Composites for Bone Tissue Engineering. *Mater. Horiz.* **2020**, *7*, 2011–2027. [CrossRef]
26. Dhandayuthapani, B.; Yoshida, Y.; Maekawa, T.; Kumar, D.S. Polymeric Scaffolds in Tissue Engineering Application: A Review. *Int. J. Polym. Sci.* **2011**, *2011*, 290602. [CrossRef]
27. Lavanya, K.; Chandran, S.V.; Balagangadharan, K.; Selvamurugan, N. Temperature- and PH-Responsive Chitosan-Based Injectable Hydrogels for Bone Tissue Engineering. *Mater. Sci. Eng. C* **2020**, *111*, 110862. [CrossRef]
28. Islam, S.; Bhuiyan, M.A.R.; Islam, M.N. Chitin and Chitosan: Structure, Properties and Applications in Biomedical Engineering. *J. Polym. Environ.* **2017**, *25*, 854–866. [CrossRef]

29. Ahmed, S.; Annu; Ali, A.; Sheikh, J. A Review on Chitosan Centred Scaffolds and Their Applications in Tissue Engineering. *Int. J. Biol. Macromol.* **2018**, *116*, 849–862. [CrossRef]
30. Hernández-González, A.C.; Téllez-Jurado, L.; Rodríguez-Lorenzo, L.M. Alginate Hydrogels for Bone Tissue Engineering, from Injectables to Bioprinting: A Review. *Carbohydr. Polym.* **2020**, *229*, 115514. [CrossRef]
31. Venkatesan, J.; Bhatnagar, I.; Manivasagan, P.; Kang, K.-H.; Kim, S.-K. Alginate Composites for Bone Tissue Engineering: A Review. *Int. J. Biol. Macromol.* **2015**, *72*, 269–281. [CrossRef]
32. Rajesh, R.; Dominic Ravichandran, Y.; Kuo, Y.C. Alginate in Bone Tissue Engineering. In *Seaweed Polysaccharides: Isolation, Biological and Biomedical Applications*; Venkatesan, J., Anil, S., Kim, S.-K., Eds.; Elsevier: Amsterdam, The Netherlands, 2017; pp. 349–368, ISBN 9780128098172.
33. Farokhi, M.; Shariatzadeh, F.J.; Solouk, A.; Mirzadeh, H. Alginate Based Scaffolds for Cartilage Tissue Engineering: A Review. *Int. J. Polym. Mater. Polym. Biomater.* **2020**, *69*, 230–247. [CrossRef]
34. Roslan, M.R.; Nasir, N.F.F.M.; Cheng, E.M.; Amin, N.A.M. Tissue Engineering Scaffold Based on Starch: A Review. In Proceedings of the International Conference on Electrical, Electronics, and Optimization Techniques, ICEEOT 2016, Chennai, India, 3–5 March 2016; IEEE: Chennai, India; pp. 1857–1860.
35. Robyt, J.F. Starch: Structure, Properties, Chemistry, and Enzymology. In *Glycoscience*; Springer: Berlin/Heidelberg, Germany, 2008; pp. 1437–1472.
36. Hemamalini, T.; Giri Dev, V.R. Comprehensive Review on Electrospinning of Starch Polymer for Biomedical Applications. *Int. J. Biol. Macromol.* **2018**, *106*, 712–718. [CrossRef] [PubMed]
37. Fakhari, A.; Berkland, C. Applications and Emerging Trends of Hyaluronic Acid in Tissue Engineering, as a Dermal Filler and in Osteoarthritis Treatment. *Acta Biomater.* **2013**, *9*, 7081–7092. [CrossRef] [PubMed]
38. Hemshekhar, M.; Thushara, R.M.; Chandranayaka, S.; Sherman, L.S.; Kemparaju, K.; Girish, K.S. Emerging Roles of Hyaluronic Acid Bioscaffolds in Tissue Engineering and Regenerative Medicine. *Int. J. Biol. Macromol.* **2016**, *86*, 917–928. [CrossRef] [PubMed]
39. Chircov, C.; Grumezescu, A.M.; Bejenaru, L.E. Hyaluronic Acid-Based Scaffolds for Tissue Engineering. *Rom. J. Morphol. Embryol.* **2018**, *59*, 71–76. [PubMed]
40. Collins, M.N.; Birkinshaw, C. Hyaluronic Acid Based Scaffolds for Tissue Engineering—A Review. *Carbohydr. Polym.* **2013**, *92*, 1262–1279. [CrossRef] [PubMed]
41. Yang, J.; Shen, M.; Wen, H.; Luo, Y.; Huang, R.; Rong, L.; Xie, J. Recent Advance in Delivery System and Tissue Engineering Applications of Chondroitin Sulfate. *Carbohydr. Polym.* **2020**, *230*, 115650. [CrossRef]
42. Zarrintaj, P.; Manouchehri, S.; Ahmadi, Z.; Saeb, M.R.; Urbanska, A.M.; Kaplan, D.L.; Mozafari, M. Agarose-Based Biomaterials for Tissue Engineering. *Carbohydr. Polym.* **2018**, *187*, 66–84. [CrossRef]
43. Khang, G.; Lee, S.J.; Kim, M.S.; Lee, H.B. Biomaterials: Tissue Engineering and Scaffolds. In *Encyclopedia of Medical Devices and Instrumentation*; Major Reference Works; John Wiley & Sons, Inc.: Hoboken, NJ, USA, 2006; pp. 366–383, ISBN 9780471732877.
44. Eslahi, N.; Mahmoodi, A.; Mahmoudi, N.; Zandi, N.; Simchi, A. Processing and Properties of Nanofibrous Bacterial Cellulose-Containing Polymer Composites: A Review of Recent Advances for Biomedical Applications. *Polym. Rev.* **2020**, *60*, 144–170. [CrossRef]
45. Torgbo, S.; Sukyai, P. Bacterial Cellulose-Based Scaffold Materials for Bone Tissue Engineering. *Appl. Mater. Today* **2018**, *11*, 34–49. [CrossRef]
46. Halib, N.; Ahmad, I.; Grassi, M.; Grassi, G. The Remarkable Three-Dimensional Network Structure of Bacterial Cellulose for Tissue Engineering Applications. *Int. J. Pharm.* **2019**, *566*, 631–640. [CrossRef] [PubMed]
47. Pang, M.; Huang, Y.; Meng, F.; Zhuang, Y.; Liu, H.; Du, M.; Ma, Q.; Wang, Q.; Chen, Z.; Chen, L.; et al. Application of Bacterial Cellulose in Skin and Bone Tissue Engineering. *Eur. Polym. J.* **2020**, *122*, 109365. [CrossRef]
48. Hickey, R.J.; Pelling, A.E. Cellulose Biomaterials for Tissue Engineering. *Front. Bioeng. Biotechnol.* **2019**, *7*, 45. [CrossRef]
49. Sun, G.; Mao, J.J. Engineering Dextran-Based Scaffolds for Drug Delivery and Tissue Repair. *Nanomedicine* **2012**, *7*, 1771–1784. [CrossRef] [PubMed]
50. Maia, J.; Evangelista, M.; Gil, H.; Ferreira, L. Dextran-Based Materials for Biomedical Applications. In *Carbohydrates Applications in Medicine*; Research Signpost: Kerala, India, 2014; Volume 2, pp. 31–53, ISBN 978-81-308-0523-8.
51. Varshosaz, J. Dextran Conjugates in Drug Delivery. *Expert Opin. Drug Deliv.* **2012**, *9*, 509–523. [CrossRef] [PubMed]
52. Zia, K.M.; Tabasum, S.; Nasif, M.; Sultan, N.; Aslam, N.; Noreen, A.; Zuber, M. A Review on Synthesis, Properties and Applications of Natural Polymer Based Carrageenan Blends and Composites. *Int. J. Biol. Macromol.* **2017**, *96*, 282–301. [CrossRef]
53. Zia, K.M.; Tabasum, S.; Khan, M.F.; Akram, N.; Akhter, N.; Noreen, A.; Zuber, M. Recent Trends on Gellan Gum Blends with Natural and Synthetic Polymers: A Review. *Int. J. Biol. Macromol.* **2018**, *109*, 1068–1087. [CrossRef] [PubMed]
54. Stevens, L.R.; Gilmore, K.J.; Wallace, G.G.; In het Panhuis, M. Tissue Engineering with Gellan Gum. *Biomater. Sci.* **2016**, *4*, 1276–1290. [CrossRef]
55. Mohammadinejad, R.; Kumar, A.; Ranjbar-Mohammadi, M.; Ashrafizadeh, M.; Han, S.S.; Khang, G.; Roveimiab, Z. Recent Advances in Natural Gum-Based Biomaterials for Tissue Engineering and Regenerative Medicine: A Review. *Polymers* **2020**, *12*, 176. [CrossRef]
56. Kumar, A.; Rao, K.M.; Han, S.S. Application of Xanthan Gum as Polysaccharide in Tissue Engineering: A Review. *Carbohydr. Polym.* **2018**, *180*, 128–144. [CrossRef]

57. del Rodriguez-Torres, M.P.; Acosta-Torres, L.S.; Diaz-Torres, L.A. Heparin-Based Nanoparticles: An Overview of Their Applications. *J. Nanomater.* **2018**, *2018*, 9780489. [CrossRef]
58. Liang, Y.; Kiick, K.L. Heparin-Functionalized Polymeric Biomaterials in Tissue Engineering and Drug Delivery Applications. *Acta Biomater.* **2014**, *10*, 1588–1600. [CrossRef] [PubMed]
59. Dong, C.; Lv, Y. Application of Collagen Scaffold in Tissue Engineering: Recent Advances and New Perspectives. *Polymers* **2016**, *8*, 42. [CrossRef] [PubMed]
60. Parenteau-Bareil, R.; Gauvin, R.; Berthod, F. Collagen-Based Biomaterials for Tissue Engineering Applications. *Materials* **2010**, *3*, 1863–1887. [CrossRef]
61. Marques, C.F.; Diogo, G.S.; Pina, S.; Oliveira, J.M.; Silva, T.H.; Reis, R.L. Collagen-Based Bioinks for Hard Tissue Engineering Applications: A Comprehensive Review. *J. Mater. Sci. Mater. Med.* **2019**, *30*, 32. [CrossRef] [PubMed]
62. Silver, F.H.; Jaffe, M.; Shah, R.G. Structure and Behavior of Collagen Fibers. In *Handbook of Properties of Textile and Technical Fibres*, 2nd ed.; Bunsell, A.R., Ed.; Elsevier: Amsterdam, The Netherlands, 2018; pp. 345–365, ISBN 9780081012727.
63. Afewerki, S.; Sheikhi, A.; Kannan, S.; Ahadian, S.; Khademhosseini, A. Gelatin-Polysaccharide Composite Scaffolds for 3D Cell Culture and Tissue Engineering: Towards Natural Therapeutics. *Bioeng. Transl. Med.* **2018**, *4*, 96–115. [CrossRef]
64. Hoque, M.; Nuge, T.; Yeow, T.; Nordin, N.; Prasad, R. Gelatin Based Scaffolds for Tissue Engineering—A Review. *Polym. Res. J.* **2015**, *9*, 15.
65. Kuttappan, S.; Mathew, D.; Nair, M.B. Biomimetic Composite Scaffolds Containing Bioceramics and Collagen/Gelatin for Bone Tissue Engineering—A Mini Review. *Int. J. Biol. Macromol.* **2016**, *93*, 1390–1401. [CrossRef]
66. Tungkavet, T.; Pattavarakorn, D.; Sirivat, A. Bio-Compatible Gelatins (Ala-Gly-Pro-Arg-Gly-Glu-4Hyp-Gly-Pro-) and Electromechanical Properties: Effects of Temperature and Electric Field. *J. Polym. Res.* **2012**, *19*, 9759. [CrossRef]
67. Melke, J.; Midha, S.; Ghosh, S.; Ito, K.; Hofmann, S. Silk Fibroin as Biomaterial for Bone Tissue Engineering. *Acta Biomater.* **2016**, *31*, 1–16. [CrossRef]
68. Koh, L.-D.; Cheng, Y.; Teng, C.-P.; Khin, Y.-W.; Loh, X.-J.; Tee, S.-Y.; Low, M.; Ye, E.; Yu, H.-D.; Zhang, Y.-W.; et al. Structures, Mechanical Properties and Applications of Silk Fibroin Materials. *Prog. Polym. Sci.* **2015**, *46*, 86–110. [CrossRef]
69. Wang, Y.; Kim, H.-J.; Vunjak-Novakovic, G.; Kaplan, D.L. Stem Cell-Based Tissue Engineering with Silk Biomaterials. *Biomaterials* **2006**, *27*, 6064–6082. [CrossRef] [PubMed]
70. Nguyen, T.P.; Nguyen, Q.V.; Nguyen, V.-H.; Le, T.-H.; Huynh, V.Q.N.; Vo, D.-V.N.; Trinh, Q.T.; Kim, S.Y.; Le, Q. Van Silk Fibroin-Based Biomaterials for Biomedical Applications: A Review. *Polymers* **2019**, *11*, 1933. [CrossRef] [PubMed]
71. Kasoju, N.; Bora, U. Silk Fibroin in Tissue Engineering. *Adv. Healthc. Mater.* **2012**, *1*, 393–412. [CrossRef]
72. Shavandi, A.; Silva, T.H.; Bekhit, A.A.; Bekhit, A.E.D.A. Keratin: Dissolution, Extraction and Biomedical Application. *Biomater. Sci.* **2017**, *5*, 1699–1735. [CrossRef]
73. Lu, T.-Y.; Huang, W.-C.; Chen, Y.; Baskaran, N.; Yu, J.; Wei, Y. Effect of Varied Hair Protein Fractions on the Gel Properties of Keratin/Chitosan Hydrogels for the Use in Tissue Engineering. *Colloids Surf. B Biointerfaces* **2020**, *195*, 111258. [CrossRef]
74. Costa, F.; Silva, R.; Boccaccini, A.R. Fibrous Protein-Based Biomaterials (Silk, Keratin, Elastin, and Resilin Proteins) for Tissue Regeneration and Repair. In *Peptides and Proteins as Biomaterials for Tissue Regeneration and Repair*; Barbosa, M.A., Cristina, M., Martins, L., Eds.; Elsevier: Amsterdam, The Netherlands, 2018; pp. 175–204, ISBN 978-0-08-100803-4.
75. Rouse, J.G.; Van Dyke, M.E. A Review of Keratin-Based Biomaterials for Biomedical Applications. *Materials* **2010**, *3*, 999–1014. [CrossRef]
76. Chiti, M.C.; Dolmans, M.M.; Donnez, J.; Amorim, C.A. Fibrin in Reproductive Tissue Engineering: A Review on Its Application as a Biomaterial for Fertility Preservation. *Ann. Biomed. Eng.* **2017**, *45*, 1650–1663. [CrossRef]
77. Bujoli, B.; Scimeca, J.-C.; Verron, E. Fibrin as a Multipurpose Physiological Platform for Bone Tissue Engineering and Targeted Delivery of Bioactive Compounds. *Pharmaceutics* **2019**, *11*, 556. [CrossRef]
78. Li, Y.; Meng, H.; Liu, Y.; Lee, B.P. Fibrin Gel as an Injectable Biodegradable Scaffold and Cell Carrier for Tissue Engineering. *Sci. World J.* **2015**, *2015*, 685690. [CrossRef]
79. de la Puente, P.; Ludeña, D. Cell Culture in Autologous Fibrin Scaffolds for Applications in Tissue Engineering. *Exp. Cell Res.* **2014**, *322*, 1–11. [CrossRef] [PubMed]
80. Yeo, G.C.; Mithieux, S.M.; Weiss, A.S. The Elastin Matrix in Tissue Engineering and Regeneration. *Curr. Opin. Biomed. Eng.* **2018**, *6*, 27–32. [CrossRef]
81. Daamen, W.F.; Veerkamp, J.H.; van Hest, J.C.M.; van Kuppevelt, T.H. Elastin as a Biomaterial for Tissue Engineering. *Biomaterials* **2007**, *28*, 4378–4398. [CrossRef] [PubMed]
82. Karpiński, R.; Jaworski, Ł.; Czubacka, P. The Structural and Mechanical Properties of the Bone. *J. Technol. Exploit. Mech. Eng.* **2017**, *3*, 43–50. [CrossRef]
83. Miller, M.D.; Thompson, S.R. *Miller's Review of Orthopaedics*; Elsevier: Amsterdam, The Netherlands, 2016; Volume 53, ISBN 9788578110796.
84. Khurana, J.S. *Bone Pathology*; Humana Press: Totowa, NJ, USA, 2009; ISBN 9781588297662.
85. Zhang, D.; Wu, X.; Chen, J.; Lin, K. The Development of Collagen Based Composite Scaffolds for Bone Regeneration. *Bioact. Mater.* **2018**, *3*, 129–138. [CrossRef]
86. Ishimoto, T.; Sato, B.; Lee, J.W.; Nakano, T. Co-Deteriorations of Anisotropic Extracellular Matrix Arrangement and Intrinsic Mechanical Property in c-Src Deficient Osteopetrotic Mouse Femur. *Bone* **2017**, *103*, 216–223. [CrossRef]

87. Viswanath, B.; Raghavan, R.; Ramamurty, U.; Ravishankar, N. Mechanical Properties and Anisotropy in Hydroxyapatite Single Crystals. *Scr. Mater.* **2007**, *57*, 361–364. [CrossRef]
88. Tanaka, Y.; Kubota, A.; Matsusaki, M.; Duncan, T.; Hatakeyama, Y.; Fukuyama, K.; Quantock, A.J.; Yamato, M.; Akashi, M.; Nishida, K. Anisotropic Mechanical Properties of Collagen Hydrogels Induced by Uniaxial-Flow for Ocular Applications. *J. Biomater.Sci. Polym. Ed.* **2011**, *22*, 1427–1442. [CrossRef]
89. Fan, J.; Jahed, V.; Klavins, K. Metabolomics in Bone Research. *Metabolites* **2021**, *11*, 434. [CrossRef]
90. Qu, H.; Fu, H.; Han, Z.; Sun, Y. Biomaterials for Bone Tissue Engineering Scaffolds: A Review. *RSC Adv.* **2019**, *9*, 26252–26262. [CrossRef]
91. *U.S. Department of HHS Bone Health and Osteoporosis: A Report of the Surgeon General. US Health Human Service*; Office of the Surgeon General (US): Washington, DC, USA, 2004; p. 437. [CrossRef]
92. Monterde-Cruz, L.; Ramírez-Salazar, E.G.; Rico-Martínez, G.; Linares-González, L.M.; Guzmán-González, R.; Delgado-Cedillo, E.; Estrada-Villaseñor, E.; Valdés-Flores, M.; Velázquez-Cruz, R.; Hidalgo-Bravo, A. MicroRNA Expression in Relation with Clinical Evolution of Osteosarcoma. *Pathol. Res. Pract.* **2020**, *216*, 153038. [CrossRef]
93. Lu, Y.; Li, M.; Long, Z.; Yang, D.; Guo, S.; Li, J.; Liu, D.; Gao, P.; Chen, G.; Lu, X.; et al. Collagen/β-TCP Composite as a Bone-Graft Substitute for Posterior Spinal Fusion in Rabbit Model: A Comparison Study. *Biomed. Mater.* **2019**, *14*, 045009. [CrossRef] [PubMed]
94. Zheng, H.; Bai, Y.; Shih, M.S.; Hoffmann, C.; Peters, F.; Waldner, C.; Hübner, W.D. Effect of a β-TCP Collagen Composite Bone Substitute on Healing of Drilled Bone Voids in the Distal Femoral Condyle of Rabbits. *J. Biomed. Mater. Res. Part B Appl. Biomater.* **2014**, *102*, 376–383. [CrossRef] [PubMed]
95. Guerrero-Gironés, J.; Alcaina-Lorente, A.; Ortiz-Ruiz, C.; Ortiz-Ruiz, E.; Pecci-Lloret, M.P.; Ortiz-Ruiz, A.J.; Rodríguez-Lozano, F.J.; Pecci-Lloret, M.R. Biocompatibility of a Ha/B-tcp/c Scaffoldas a Pulp-capping Agent for Vital Pulp Treatment: An in Vivo Study in Rat Molars. *Int. J. Environ. Res. Public Health* **2021**, *18*, 3936. [CrossRef] [PubMed]
96. Ebrahimi, M.; Botelho, M.G.; Dorozhkin, S.V. Biphasic Calcium Phosphates Bioceramics (HA/TCP): Concept, Physicochemical Properties and the Impact of Standardization of Study Protocols in Biomaterials Research. *Mater. Sci. Eng. C* **2017**, *71*, 1293–1312. [CrossRef] [PubMed]
97. Mohamed, N.; Rahamana; Daya, D.E.; Balb, B.S.; Fuc, Q.; Junga, S.B.; Lynda, F.; Bonewalde, A.P.T. Bioactive Glass in Tissue Engineering. *Acta Biomater.* **2011**, *7*, 2355–2373. [CrossRef]
98. Gerhardt, L.C.; Boccaccini, A.R. Bioactive Glass and Glass-Ceramic Scaffolds for Bone Tissue Engineering. *Materials* **2010**, *3*, 3867–3910. [CrossRef]
99. Ferreira, S.A.; Young, G.; Jones, J.R.; Rankin, S. Bioglass/Carbonate Apatite/Collagen Composite Scaffold Dissolution Products Promote Human Osteoblast Differentiation. *Mater. Sci. Eng. C* **2021**, *118*, 111393. [CrossRef]
100. Hamzah, M.S.A.; Ng, C.; Zulkarnain, N.I.S.; Majid, H.A.; Razak, S.I.A.; Nayan, N.H.M. Entrapment of Collagen on Polylactic Acid 3D Scaffold Surface as a Potential Artificial Bone Replacement. *Mater. Today Proc.* **2021**, *46*, 1668–1673. [CrossRef]
101. Dewey, M.J.; Nosatov, A.V.; Subedi, K.; Shah, R.; Jakus, A.; Harley, B.A.C. Inclusion of a 3D-Printed Hyperelastic Bone Mesh Improves Mechanical and Osteogenic Performance of a Mineralized Collagen Scaffold. *Acta Biomater.* **2021**, *121*, 224–236. [CrossRef]
102. Oh, G.W.; Nguyen, V.T.; Heo, S.Y.; Ko, S.C.; Kim, C.S.; Park, W.S.; Choi, I.W.; Jung, W.K. 3D PCL/Fish Collagen Composite Scaffolds Incorporating Osteogenic Abalone Protein Hydrolysates for Bone Regeneration Application: In Vitro and in Vivo Studies. *J. Biomater. Sci. Polym. Ed.* **2021**, *32*, 355–371. [CrossRef] [PubMed]
103. Soufdoost, R.S.; Yazdanian, M.; Tahmasebi, E.; Yazdanian, A.; Tebyanian, H.; Karami, A.; Nourani, M.R.; Panahi, Y. In Vitro and in Vivo Evaluation of Novel Tadalafil/β-TCP/Collagen Scaffold for Bone Regeneration: A Rabbit Critical-Size Calvarial Defect Study. *Biocybern. Biomed. Eng.* **2019**, *39*, 789–796. [CrossRef]
104. Maier, J. High Concentrations of Magnesium Modulate Vascular Endothelial Cell Behaviour In Vitro. *Biochim. Et Biophys. Acta BBA Mol. Basis Dis.* **2004**, *1689*, 6–12. [CrossRef] [PubMed]
105. Lin, K.; Zhou, Y.; Zhou, Y.; Qu, H.; Chen, F.; Zhu, Y.; Chang, J. Biomimetic Hydroxyapatite Porous Microspheres with Co-Substituted Essential Trace Elements: Surfactant-Free Hydrothermal Synthesis, Enhanced Degradation and Drug Release. *J. Mater. Chem.* **2011**, *21*, 16558–16565. [CrossRef]
106. Minardi, S.; Taraballi, F.; Cabrera, F.J.; Van Eps, J.; Wang, X.; Gazze, S.A.; Fernandez-Mourev, J.S.; Tampieri, A.; Francis, L.; Weiner, B.K.; et al. Biomimetic Hydroxyapatite/Collagen Composite Drives Bone Niche Recapitulation in a Rabbit Orthotopic Model. *Mater. Today Bio* **2019**, *2*, 100005. [CrossRef]
107. Antoniac, I.V.; Antoniac, A.; Vasile, E.; Tecu, C.; Fosca, M.; Yankova, V.G.; Rau, J.V. In Vitro Characterization of Novel Nanostructured Collagen-Hydroxyapatite Composite Scaffolds Doped with Magnesium with Improved Biodegradation Rate for Hard Tissue Regeneration. *Bioact. Mater.* **2021**, *6*, 3383–3395. [CrossRef]
108. Ryan, E.J.; Ryan, A.J.; González-Vázquez, A.; Philippart, A.; Ciraldo, F.E.; Hobbs, C.; Nicolosi, V.; Boccaccini, A.R.; Kearney, C.J.; O'Brien, F.J. Collagen Scaffolds Functionalised with Copper-Eluting Bioactive Glass Reduce Infection and Enhance Osteogenesis and Angiogenesis Both In Vitro and In Vivo. *Biomaterials* **2019**, *197*, 405–416. [CrossRef]
109. Jing, Z.; Wu, Y.; Su, W.; Tian, M.; Jiang, W.; Cao, L.; Zhao, L.; Zhao, Z. Carbon Nanotube Reinforced Collagen/Hydroxyapatite Scaffolds Improve Bone Tissue Formation In Vitro and In Vivo. *Ann. Biomed. Eng.* **2017**, *45*, 2075–2087. [CrossRef]

110. Ju, T.; Zhao, Z.; Ma, L.; Li, W.; Li, S.; Zhang, J. Cyclic Adenosine Monophosphate-Enhanced Calvarial Regeneration by Bone Marrow-Derived Mesenchymal Stem Cells on a Hydroxyapatite/Gelatin Scaffold. *ACS Omega* **2021**, *6*, 13684–13694. [CrossRef]
111. Rezaei, H.; Shahrezaee, M.; Jalali Monfared, M.; Ghorbani, F.; Zamanian, A.; Sahebalzamani, M. Mussel-Inspired Polydopamine Induced the Osteoinductivity to Ice-Templating PLGA–Gelatin Matrix for Bone Tissue Engineering Application. *Biotechnol. Appl. Biochem.* **2021**, *68*, 185–196. [CrossRef]
112. Jahangir, S.; Hosseini, S.; Mostafaei, F.; Sayahpour, F.A.; Eslaminejad, M.B. 3D-Porous β-Tricalcium Phosphate–Alginate–Gelatin Scaffold with DMOG Delivery Promotes Angiogenesis and Bone Formation in Rat Calvarial Defects. *J. Mater. Sci. Mater. Med.* **2019**, *30*, 1. [CrossRef] [PubMed]
113. Gautam, S.; Sharma, C.; Purohit, S.D.; Singh, H.; Dinda, A.K.; Potdar, P.D.; Chou, C.F.; Mishra, N.C. Gelatin-Polycaprolactone-Nanohydroxyapatite Electrospun Nanocomposite Scaffold for Bone Tissue Engineering. *Mater. Sci. Eng. C* **2021**, *119*, 111588. [CrossRef] [PubMed]
114. Lu, H.; Pan, X.; Hu, M.; Zhang, J.; Yu, Y.; Hu, X.; Jiang, K. Fabrication of Graphene/Gelatin/Chitosan/Tricalcium Phosphate 3D Printed Scaffolds for Bone Tissue Regeneration Applications. *Appl. Nanosci.* **2021**, *11*, 335–346. [CrossRef]
115. Qu, L.; Dubey, N.; Ribeiro, J.S.; Bordini, E.A.F.; Ferreira, J.A.; Xu, J.; Castilho, R.M.; Bottino, M.C. Metformin-Loaded Nanospheres-Laden Photocrosslinkable Gelatin Hydrogel for Bone Tissue Engineering. *J. Mech. Behav. Biomed. Mater.* **2021**, *116*, 104293. [CrossRef]
116. Wang, Y.; Cao, X.; Ma, M.; Lu, W.; Zhang, B.; Guo, Y. A GelMA-PEGDA-NHA Composite Hydrogel for Bone Tissue Engineering. *Materials* **2020**, *13*, 3735. [CrossRef]
117. Ramírez Rodríguez, G.; Patrício, T.; Delgado López, J. Natural Polymers for Bone Repair. In *Bone Repair Biomaterials*; Woodhead: Cambridge, UK, 2019; pp. 199–232.
118. Aguilar, A.; Zein, N.; Harmouch, E.; Hafdi, B.; Bornert, F.; Damien, O.; Clauss, F.; Fioretti, F.; Huck, O.; Benkirane-jessel, N.; et al. Application of Chitosan in Bone and Dental Engineering. *Biodental Eng. V* **2019**, *24*, 3009. [CrossRef]
119. Brun, P.; Zamuner, A.; Battocchio, C.; Cassari, L.; Todesco, M.; Graziani, V.; Iucci, G.; Marsotto, M.; Tortora, L.; Secchi, V.; et al. Bio-Functionalized Chitosan for Bone Tissue Engineering. *Int. J. Mol. Sci.* **2021**, *22*, 5916. [CrossRef]
120. Balagangadharan, K.; Trivedi, R.; Vairamani, M.; Selvamurugan, N. Sinapic Acid-Loaded Chitosan Nanoparticles in Polycaprolactone Electrospun Fibers for Bone Regeneration in Vitro and in Vivo. *Carbohydr. Polym.* **2019**, *216*, 1–16. [CrossRef]
121. Radwan, N.H.; Nasr, M.; Ishak, R.A.H.; Abdeltawab, N.F.; Awad, G.A.S. Chitosan-Calcium Phosphate Composite Scaffolds for Control of Post-Operative Osteomyelitis: Fabrication, Characterization, and In Vitro–In Vivo Evaluation. *Carbohydr. Polym.* **2020**, *244*, 116482. [CrossRef]
122. Bari, E.; Scocozza, F.; Perteghella, S.; Sorlini, M.; Auricchio, F.; Torre, M.L.; Conti, M. 3d Bioprinted Scaffolds Containing Mesenchymal Stem/Stromal Lyosecretome: Next Generation Controlled Release Device for Bone Regenerative Medicine. *Pharmaceutics* **2021**, *13*, 515. [CrossRef]
123. Zhang, J.; Eyisoylu, H.; Qin, X.H.; Rubert, M.; Müller, R. 3D Bioprinting of Graphene Oxide-Incorporated Cell-Laden Bone Mimicking Scaffolds for Promoting Scaffold Fidelity, Osteogenic Differentiation and Mineralization. *Acta Biomater.* **2021**, *121*, 637–652. [CrossRef] [PubMed]
124. Keshavarz, M.; Alizadeh, P. On the Role of Alginate Coating on the Mechanical and Biological Properties of 58S Bioactive Glass Scaffolds. *Int. J. Biol. Macromol.* **2021**, *167*, 947–961. [CrossRef] [PubMed]
125. Zhou, W.; Li, Q.; Ma, R.; Huang, W.; Zhang, X.; Liu, Y.; Xu, Z.; Zhang, L.; Li, M.; Zhu, C. Modified Alginate-Based Hydrogel as a Carrier of the CB2 Agonist JWH133 for Bone Engineering. *ACS Omega* **2021**, *6*, 6861–6870. [CrossRef] [PubMed]
126. Zhang, H.; Cai, Q.; Zhu, Y.; Zhu, W. A Simple Hydrogel Scaffold with Injectability, Adhesivity and Osteogenic Activity for Bone Regeneration. *Biomater. Sci.* **2021**, *9*, 960–972. [CrossRef] [PubMed]
127. Garske, D.S.; Schmidt-Bleek, K.; Ellinghaus, A.; Dienelt, A.; Gu, L.; Mooney, D.J.; Duda, G.N.; Cipitria, A. Alginate Hydrogels for In Vivo Bone Regeneration: The Immune Competence of the Animal Model Matters. *Tissue Eng. Part A* **2020**, *26*, 852–862. [CrossRef]
128. Erickson, C.B.; Newsom, J.P.; Fletcher, N.A.; Feuer, Z.M.; Yu, Y.; Rodriguez-Fontan, F.; Hadley Miller, N.; Krebs, M.D.; Payne, K.A. In Vivo Degradation Rate of Alginate–Chitosan Hydrogels Influences Tissue Repair Following Physeal Injury. *J. Biomed. Mater. Res. Part B Appl. Biomater.* **2020**, *108*, 2484–2494. [CrossRef]
129. Ke, X.; Dong, Z.; Tang, S.; Chu, W.; Zheng, X.; Zhen, L.; Chen, X.; Ding, C.; Luo, J.; Li, J. A Natural Polymer Based Bioadhesive with Self-Healing Behavior and Improved Antibacterial Properties. *Biomater. Sci.* **2020**, *8*, 4346–4357. [CrossRef]
130. Yang, N.; Moore, M.J.; Michael, P.L.; Santos, M.; Lam, Y.T.; Bao, S.; Ng, M.K.C.; Rnjak-Kovacina, J.; Tan, R.P.; Wise, S.G. Silk Fibroin Scaffold Architecture Regulates Inflammatory Responses and Engraftment of Bone Marrow-Mononuclear Cells. *Adv. Healthc. Mater.* **2021**, *2100615*, e2100615. [CrossRef]
131. Teramoto, H.; Shirakawa, M.; Tamada, Y. Click Decoration of Bombyx Mori Silk Fibroin for Cell Adhesion Control. *Molecules* **2020**, *25*, 4106. [CrossRef]
132. Akrami-Hasan-Kohal, M.; Eskandari, M.; Solouk, A. Silk Fibroin Hydrogel/Dexamethasone Sodium Phosphate Loaded Chitosan Nanoparticles as a Potential Drug Delivery System. *Colloids Surf. B Biointerfaces* **2021**, *205*, 111892. [CrossRef]
133. Zheng, H.; Zuo, B. Functional Silk Fibroin Hydrogels: Preparation, Properties and Applications. *J. Mater. Chem. B* **2021**, *9*, 1238–1258. [CrossRef] [PubMed]

134. Wu, M.; Han, Z.; Liu, W.; Yao, J.; Zhao, B.; Shao, Z.; Chen, X. Silk-Based Hybrid Microfibrous Mats as Guided Bone Regeneration Membranes. *J. Mater. Chem. B* **2021**, *9*, 2025–2032. [CrossRef] [PubMed]
135. Zheng, X.; Ke, X.; Yu, P.; Wang, D.; Pan, S.; Yang, J.; Ding, C.; Xiao, S.; Luo, J.; Li, J. A Facile Strategy to Construct Silk Fibroin Based GTR Membranes with Appropriate Mechanical Performance and Enhanced Osteogenic Capacity. *J. Mater. Chem. B* **2020**, *8*, 10407–10415. [CrossRef] [PubMed]
136. McNamara, S.L.; McCarthy, E.M.; Schmidt, D.F.; Johnston, S.P.; Kaplan, D.L. Rheological Characterization, Compression, and Injection Molding of Hydroxyapatite-Silk Fibroin Composites. *Biomaterials* **2021**, *269*, 120643. [CrossRef] [PubMed]
137. Saleem, M.; Rasheed, S.; Yougen, C. Silk Fibroin/Hydroxyapatite Scaffold: A Highly Compatible Material for Bone Regeneration. *Sci. Technol. Adv. Mater.* **2020**, *21*, 242–266. [CrossRef] [PubMed]
138. Du, X.; Wei, D.; Huang, L.; Zhu, M.; Zhang, Y.; Zhu, Y. 3D Printing of Mesoporous Bioactive Glass/Silk Fibroin Composite Scaffolds for Bone Tissue Engineering. *Mater. Sci. Eng. C* **2019**, *103*, 109731. [CrossRef] [PubMed]
139. Xiao, L.; Wu, M.; Yan, F.; Xie, Y.; Liu, Z.; Huang, H.; Yang, Z.; Yao, S.; Cai, L. A Radial 3D Polycaprolactone Nanofiber Scaffold Modified by Biomineralization and Silk Fibroin Coating Promote Bone Regeneration In Vivo. *Int. J. Biol. Macromol.* **2021**, *172*, 19–29. [CrossRef]
140. Chen, P.; Liu, L.; Pan, J.; Mei, J.; Li, C.; Zheng, Y. Biomimetic Composite Scaffold of Hydroxyapatite/Gelatin-Chitosan Core-Shell Nanofibers for Bone Tissue Engineering. *Mater. Sci. Eng. C* **2019**, *97*, 325–335. [CrossRef]
141. Purohit, S.D.; Bhaskar, R.; Singh, H.; Yadav, I.; Gupta, M.K.; Mishra, N.C. Development of a Nanocomposite Scaffold of Gelatin–Alginate–Graphene Oxide for Bone Tissue Engineering. *Int. J. Biol. Macromol.* **2019**, *133*, 592–602. [CrossRef]
142. Thomas, A.; Bera, J. Preparation and Characterization of Gelatin-Bioactive Glass Ceramic Scaffolds for Bone Tissue Engineering. *J. Biomater. Sci. Polym. Ed.* **2019**, *30*, 561–579. [CrossRef]
143. Sharifi, F.; Atyabi, S.M.; Norouzian, D.; Zandi, M.; Irani, S.; Bakhshi, H. Polycaprolactone/Carboxymethyl Chitosan Nanofibrous Scaffolds for Bone Tissue Engineering Application. *Int. J. Biol. Macromol.* **2018**, *115*, 243–248. [CrossRef]
144. Dai, C.; Li, Y.; Pan, W.; Wang, G.; Huang, R.; Bu, Y.; Liao, X.; Guo, K.; Gao, F. Three-Dimensional High-Porosity Chitosan/Honeycomb Porous Carbon/Hydroxyapatite Scaffold with Enhanced Osteoinductivity for Bone Regeneration. *ACS Biomater. Sci. Eng.* **2020**, *6*, 575–586. [CrossRef]
145. Shi, D.; Shen, J.; Zhang, Z.; Shi, C.; Chen, M.; Gu, Y.; Liu, Y. Preparation and Properties of Dopamine-Modified Alginate/Chitosan–Hydroxyapatite Scaffolds with Gradient Structure for Bone Tissue Engineering. *J. Biomed. Mater. Res. Part A* **2019**, *107*, 1615–1627. [CrossRef]
146. Saini, R.K.; Bagri, L.P.; Bajpai, A.K. Nano-Silver Hydroxyapatite Based Antibacterial 3D Scaffolds of Gelatin/Alginate/Poly (Vinyl Alcohol) for Bone Tissue Engineering Applications. *Colloids Surf. B Biointerfaces* **2019**, *177*, 211–218. [CrossRef]
147. Echave, M.C.; Pimenta-Lopes, C.; Pedraz, J.L.; Mehrali, M.; Dolatshahi-Pirouz, A.; Ventura, F.; Orive, G. Enzymatic Crosslinked Gelatin 3D Scaffolds for Bone Tissue Engineering. *Int. J. Pharm.* **2019**, *562*, 151–161. [CrossRef]
148. Rajzer, I.; Kurowska, A.; Jabłoński, A.; Jatteau, S.; Śliwka, M.; Ziąbka, M.; Menaszek, E. Layered Gelatin/PLLA Scaffolds Fabricated by Electrospinning and 3D Printing- for Nasal Cartilages and Subchondral Bone Reconstruction. *Mater. Des.* **2018**, *155*, 297–306. [CrossRef]
149. Panzavolta, S.; Torricelli, P.; Casolari, S.; Parrilli, A.; Fini, M.; Bigi, A. Strontium-Substituted Hydroxyapatite-Gelatin Biomimetic Scaffolds Modulate Bone Cell Response. *Macromol. Biosci.* **2018**, *18*, e1800096. [CrossRef]
150. Sattary, M.; Rafienia, M.; Kazemi, M.; Salehi, H.; Mahmoudzadeh, M. Promoting Effect of Nano Hydroxyapatite and Vitamin D3 on the Osteogenic Differentiation of Human Adipose-Derived Stem Cells in Polycaprolactone/Gelatin Scaffold for Bone Tissue Engineering. *Mater. Sci. Eng. C* **2019**, *97*, 141–155. [CrossRef]
151. Sun, J.L.; Jiao, K.; Niu, L.-N.; Jiao, Y.; Song, Q.; Shen, L.-J.; Tay, F.R.; Chen, J.-H. 5Intrafibrillar Silicified Collagen Scaffold Modulates Monocyte to Promote Cell Homing, Angiogenesis and Bone Regeneration. *Biomaterials* **2017**, *113*, 203–216. [CrossRef]
152. Wang, Z.; Lin, M.; Xie, Q.; Sun, H.; Huang, Y.; Zhang, D.D.; Yu, Z.; Bi, X.; Chen, J.; Wang, J.; et al. Electrospun Silk Fibroin/Poly(Lactide-Co-ε-Caprolactone) Nanofibrous Scaffolds for Bone Regeneration. *Int. J. Nanomed.* **2016**, *11*, 1483–1500. [CrossRef]
153. Yao, J.; Wang, Y.; Ma, W.; Dong, W.; Zhang, M.; Sun, D. Dual-Drug-Loaded Silk Fibroin/PLGA Scaffolds for Potential Bone Regeneration Applications. *J. Nanomater.* **2019**, *2019*, 8050413. [CrossRef]
154. He, J.X.; Tan, W.L.; Han, Q.M.; Cui, S.Z.; Shao, W.; Sang, F. Fabrication of Silk Fibroin/Cellulose Whiskers–Chitosan Composite Porous Scaffolds by Layer-by-Layer Assembly for Application in Bone Tissue Engineering. *J. Mater. Sci.* **2016**, *51*, 4399–4410. [CrossRef]
155. Luetchford, K.A.; Chaudhuri, J.B.; De Bank, P.A. Silk Fibroin/Gelatin Microcarriers as Scaffolds for Bone Tissue Engineering. *Mater. Sci. Eng. C* **2020**, *106*, 110116. [CrossRef]
156. Benedini, L.; Laiuppa, J.; Santillán, G.; Baldini, M.; Messina, P. Antibacterial Alginate/Nano-Hydroxyapatite Composites for Bone Tissue Engineering: Assessment of Their Bioactivity, Biocompatibility, and Antibacterial Activity. *Mater. Sci. Eng. C* **2020**, *115*, 111101. [CrossRef]
157. Zheng, A.; Cao, L.; Liu, Y.; Wu, J.; Zeng, D.; Hu, L.; Zhang, X.; Jiang, X. Biocompatible Silk/Calcium Silicate/Sodium Alginate Composite Scaffolds for Bone Tissue Engineering. *Carbohydr. Polym.* **2018**, *199*, 244–255. [CrossRef]
158. Wang, P.; Song, Y.; Weir, M.D.; Sun, J.; Zhao, L.; Simon, C.G.; Xu, H.H.K. A Self-Setting IPSMSC-Alginate-Calcium Phosphate Paste for Bone Tissue Engineering. *Dent. Mater.* **2016**, *32*, 252–263. [CrossRef]

159. Luo, Y.; Li, Y.; Qin, X.; Wa, Q. 3D Printing of Concentrated Alginate/Gelatin Scaffolds with Homogeneous Nano Apatite Coating for Bone Tissue Engineering. *Mater. Des.* **2018**, *146*, 12–19. [CrossRef]
160. Scott, W.; Stevens, J.; Binder-Macleod, S.A. Human Skeletal Muscle Fiber Type Classifications. *Phys. Ther.* **2001**, *81*, 1810–1816. [CrossRef]
161. Relaix, F.; Bencze, M.; Borok, M.J.; Der Vartanian, A.; Gattazzo, F.; Mademtzoglou, D.; Perez-Diaz, S.; Prola, A.; Reyes-Fernandez, P.C.; Rotini, A.; et al. Perspectives on Skeletal Muscle Stem Cells. *Nat. Commun.* **2021**, *12*, 692. [CrossRef]
162. Ostrovidov, S.; Salehi, S.; Costantini, M.; Suthiwanich, K.; Ebrahimi, M.; Sadeghian, R.B.; Fujie, T.; Shi, X.; Cannata, S.; Gargioli, C.; et al. 3D Bioprinting in Skeletal Muscle Tissue Engineering. *Small* **2019**, *15*, e1805530. [CrossRef]
163. Fischer, K.M.; Scott, T.E.; Browe, D.P.; McGaughey, T.A.; Wood, C.; Wolyniak, M.J.; Freeman, J.W. Hydrogels for Skeletal Muscle Regeneration. *Regen. Eng. Transl. Med.* **2020**, *7*, 353–361. [CrossRef]
164. Liu, J.; Saul, D.; Böker, K.O.; Ernst, J.; Lehman, W.; Schilling, A.F. Current Methods for Skeletal Muscle Tissue Repair and Regeneration. *BioMed Res. Int.* **2018**, *2018*, 1984879. [CrossRef]
165. Gholobova, D.; Terrie, L.; Gerard, M.; Declercq, H.; Thorrez, L. Vascularization of Tissue-Engineered Skeletal Muscle Constructs. *Biomaterials* **2020**, *235*, 119708. [CrossRef]
166. Zhuang, P.; An, J.; Chua, C.K.; Tan, L.P. Bioprinting of 3D in Vitro Skeletal Muscle Models: A Review. *Mater. Des.* **2020**, *193*, 108794. [CrossRef]
167. del Carmen Ortuño-Costela, M.; García-López, M.; Cerrada, V.; Gallardo, M.E. IPSCs: A Powerful Tool for Skeletal Muscle Tissue Engineering. *J. Cell. Mol. Med.* **2019**, *23*, 3784–3794. [CrossRef]
168. Gillies, A.R.; Lieber, R.L. Structure and Function of the Skeletal Muscle Extracellular Matrix. *Muscle Nerve* **2011**, *44*, 318–331. [CrossRef]
169. Csapo, R.; Gumpenberger, M.; Wessner, B. Skeletal Muscle Extracellular Matrix—What Do We Know About Its Composition, Regulation, and Physiological Roles? A Narrative Review. *Front. Physiol.* **2020**, *11*, 253. [CrossRef]
170. Takala, T.E.; Virtanen, P. Biochemical Composition of Muscle Extracellular Matrix: The Effect of Loading. *Scand. J. Med. Sci. Sports* **2000**, *10*, 321–325. [CrossRef]
171. Thorsteinsdottir, S.; Deries, M.; Cachaço, A.S.; Bajanca, F. The Extracellular Matrix Dimension of Skeletal Muscle Development. *Dev. Biol.* **2011**, *354*, 191–207. [CrossRef]
172. Baker, H.B.; Passipieri, J.A.; Siriwardane, M.; Ellenburg, M.D.; Vadhavkar, M.; Bergman, C.R.; Saul, J.M.; Tomblyn, S.; Burnett, L.; Christ, G.J. Cell and Growth Factor-Loaded Keratin Hydrogels for Treatment of Volumetric Muscle Loss in a Mouse Model. *Tissue Eng. Part A* **2017**, *23*, 572–581. [CrossRef]
173. Tomblyn, S.; Kneller, E.L.P.; Walker, S.J.; Ellenburg, M.D.; Kowalczewski, C.J.; Van Dyke, M.; Burnett, L.; Saul, J.M. Keratin Hydrogel Carrier System for Simultaneous Delivery of Exogenous Growth Factors and Muscle Progenitor Cells. *J. Biomed. Mater. Res. Part B Appl. Biomater.* **2016**, *104*, 864–879. [CrossRef]
174. Passipieri, J.A.; Baker, H.B.; Siriwardane, M.; Ellenburg, M.D.; Vadhavkar, M.; Saul, J.M.; Tomblyn, S.; Burnett, L.; Christ, G.J. Keratin Hydrogel Enhances In Vivo Skeletal Muscle Function in a Rat Model of Volumetric Muscle Loss. *Tissue Eng. Part A* **2017**, *23*, 556–571. [CrossRef]
175. Wan, X.; Li, P.; Jin, X.; Su, F.; Shen, J.; Yuan, J. Poly(ε-Caprolactone)/Keratin/Heparin/VEGF Biocomposite Mats for Vascular Tissue Engineering. *J. Biomed. Mater. Res. Part A* **2020**, *108*, 292–300. [CrossRef]
176. Dou, J.; Wang, Y.; Jin, X.; Li, P.; Wang, L.; Yuan, J.; Shen, J. PCL/Sulfonated Keratin Mats for Vascular Tissue Engineering Scaffold with Potential of Catalytic Nitric Oxide Generation. *Mater. Sci. Eng. C* **2020**, *107*, 110246. [CrossRef]
177. Li, P.; Wang, Y.; Jin, X.; Dou, J.; Han, X.; Wan, X.; Yuan, J.; Shen, J. Fabrication of PCL/Keratin Composite Scaffolds for Vascular Tissue Engineering with Catalytic Generation of Nitric Oxide Potential. *J. Mater. Chem. B* **2020**, *8*, 6092–6099. [CrossRef]
178. Korniłowicz-Kowalska, T.; Bohacz, J. Biodegradation of Keratin Waste: Theory and Practical Aspects. *Waste Manag.* **2011**, *31*, 1689–1701. [CrossRef]
179. Panayi, A.C.; Smit, L.; Hays, N.; Udeh, K.; Endo, Y.; Li, B.; Sakthivel, D.; Tamayol, A.; Neppl, R.L.; Orgill, D.P.; et al. A Porous Collagen-GAG Scaffold Promotes Muscle Regeneration Following Volumetric Muscle Loss Injury. *Wound Repair Regen.* **2020**, *28*, 61–74. [CrossRef]
180. Wang, H.D.; Lough, D.M.; Kurlander, D.E.; Lopez, J.; Quan, A.; Kumar, A.R. Muscle-Derived Stem Cell-Enriched Scaffolds Are Capable of Enhanced Healing of a Murine Volumetric Muscle Loss Defect. *Plast. Reconstr. Surg.* **2019**, *143*, 329e–339e. [CrossRef]
181. Quarta, M.; Cromie, M.; Chacon, R.; Blonigan, J.; Garcia, V.; Akimenko, I.; Hamer, M.; Paine, P.; Stok, M.; Shrager, J.B.; et al. Bioengineered Constructs Combined with Exercise Enhance Stem Cell-Mediated Treatment of Volumetric Muscle Loss. *Nat. Commun.* **2017**, *8*, 15613. [CrossRef]
182. Zarei, M.; Samimi, A.; Khorram, M.; Abdi, M.M.; Golestaneh, S.I. Fabrication and Characterization of Conductive Polypyrrole/Chitosan/Collagen Electrospun Nanofiber Scaffold for Tissue Engineering Application. *Int. J. Biol. Macromol.* **2021**, *168*, 175–186. [CrossRef]
183. Hwangbo, H.; Kim, W.J.; Kim, G.H. Lotus-Root-Like Microchanneled Collagen Scaffold. *ACS Appl. Mater. Interfaces* **2021**, *13*, 12656–12667. [CrossRef]
184. Perez-Puyana, V.; Wieringa, P.; Yuste, Y.; de la Portilla, F.; Guererro, A.; Romero, A.; Moroni, L. Fabrication of Hybrid Scaffolds Obtained from Combinations of PCL with Gelatin or Collagen via Electrospinning for Skeletal Muscle Tissue Engineering. *J. Biomed. Mater. Res. Part A* **2021**, *109*, 1600–1612. [CrossRef]

185. Basurto, I.M.; Mora, M.A.; Christ, G.J.; Caliari, S.R. Aligned and Conductive 3D Collagen Scaffolds for Skeletal Muscle Tissue Engineering. In Proceedings of the Transactions of the Annual Meeting of the Society for Biomaterials and the Annual International Biomaterials Symposium, Seattle, WA, USA, 3–6 April 2019; Volume 40, p. 370.
186. Nakayama, K.H.; Quarta, M.; Paine, P.; Alcazar, C.; Karakikes, I.; Garcia, V.; Abilez, O.J.; Calvo, N.S.; Simmons, C.S.; Rando, T.A.; et al. Treatment of Volumetric Muscle Loss in Mice Using Nanofibrillar Scaffolds Enhances Vascular Organization and Integration. *Commun. Biol.* **2019**, *2*, s42003–s42019. [CrossRef]
187. Quigley, A.F.; Cornock, R.; Mysore, T.; Foroughi, J.; Kita, M.; Razal, J.M.; Crook, J.; Moulton, S.E.; Wallace, G.G.; Kapsa, R.M.I. Wet-Spun Trojan Horse Cell Constructs for Engineering Muscle. *Front. Chem.* **2020**, *8*, 18. [CrossRef]
188. Distler, T.; Solisito, A.A.; Schneidereit, D.; Friedrich, O.; Detsch, R.; Boccaccini, A.R. 3D Printed Oxidized Alginate-Gelatin Bioink Provides Guidance for C2C12 Muscle Precursor Cell Orientation and Differentiation via Shear Stress During Bioprinting. *IOP Publ. Biofabr. J. Biofabr.* **2020**, *12*, 045005. [CrossRef]
189. Ansari, S.; Chen, C.; Xu, X.; Annabi, N.; Zadeh, H.H.; Wu, B.M.; Khademhosseini, A.; Shi, S.; Moshaverinia, A. Muscle Tissue Engineering Using Gingival Mesenchymal Stem Cells Encapsulated in Alginate Hydrogels Containing Multiple Growth Factors. *Ann. Biomed. Eng.* **2016**, *44*, 1908–1920. [CrossRef]
190. Ciriza, J.; Rodríguez-Romano, A.; Nogueroles, I.; Gallego-Ferrer, G.; Cabezuelo, R.M.; Pedraz, J.L.; Rico, P. Borax-Loaded Injectable Alginate Hydrogels Promote Muscle Regeneration in Vivo after an Injury. *Mater. Sci. Eng. C* **2021**, *123*, 112003. [CrossRef]
191. Pęziński, M.; Daszczuk, P.; Pradhan, B.S.; Lochmüller, H.; Prószyński, T.J. An Improved Method for Culturing Myotubes on Laminins for the Robust Clustering of Postsynaptic Machinery. *Sci. Rep.* **2020**, *10*, 4524. [CrossRef]
192. Marcinczyk, M.; Dunn, A.; Haas, G.; Madsen, J.; Scheidt, R.; Patel, K.; Talovic, M.; Garg, K. The Effect of Laminin-111 Hydrogels on Muscle Regeneration in a Murine Model of Injury. *Tissue Eng. Part A* **2019**, *25*, 1001–1012. [CrossRef]
193. Gilbert-Honick, J.; Ginn, B.; Zhang, Y.; Salehi, S.; Wagner, K.R.; Mao, H.Q.; Grayson, W.L. Adipose-Derived Stem/Stromal Cells on Electrospun Fibrin Microfiber Bundles Enable Moderate Muscle Reconstruction in a Volumetric Muscle Loss Model. *Cell Transplant.* **2018**, *27*, 1644–1656. [CrossRef]
194. Russell, C.S.; Mostafavi, A.; Quint, J.P.; Panayi, A.C.; Baldino, K.; Williams, T.J.; Daubendiek, J.G.; Sánchez, V.H.; Bonick, Z.; Trujillo-Miranda, M.; et al. In Situ Printing of Adhesive Hydrogel Scaffolds for the Treatment of Skeletal Muscle Injuries. *ACS Appl. Bio Mater.* **2020**, *3*, 1568–1579. [CrossRef]
195. Hanjun, H.; Hyeongjin, L.; Eun-Ju, J.; JaeYoon, L.; Yunju, J.; Dongryeol, R.; GeunHyung, K. Bio-printing of aligned GelMa-based cell-laden structure for muscle tissue regeneration. *Bioact. Mater.* **2022**, *8*, 57–70. [CrossRef]
196. Basurto, I.M.; Mora, M.A.; Christ, G.J.; Caliari, S.R. Aligned and Conductive 3D Collagen Scaffolds for Skeletal Muscle Tissue Engineering. *Trans. Annu. Meet. Soc. Biomater. Annu. Int. Biomater. Symp.* **2019**, *40*, 370. [CrossRef]
197. Aguilar-Agon, K.W.; Capel, A.J.; Martin, N.R.W.; Player, D.J.; Lewis, M.P. Mechanical Loading Stimulates Hypertrophy in Tissue-Engineered Skeletal Muscle: Molecular and Phenotypic Responses. *J. Cell. Physiol.* **2019**, *234*, 23547–23558. [CrossRef]
198. Yi, H.; Forsythe, S.; He, Y.; Liu, Q.; Xiong, G.; Wei, S.; Li, G.; Atala, A.; Skardal, A.; Zhang, Y. Tissue-Specific Extracellular Matrix Promotes Myogenic Differentiation of Human Muscle Progenitor Cells on Gelatin and Heparin Conjugated Alginate Hydrogels. *Acta Biomater.* **2017**, *62*, 222–233. [CrossRef]
199. Pumberger, M.; Qazi, T.H.; Ehrentraut, M.C.; Textor, M.; Kueper, J.; Stoltenburg-Didinger, G.; Winkler, T.; von Roth, P.; Reinke, S.; Borselli, C.; et al. *Synthetic Niche to Modulate Regenerative Potential of MSCs and Enhance Skeletal Muscle Regeneration*; Elsevier Ltd.: Amsterdam, The Netherlands, 2016; Volume 99, ISBN 4930450659.
200. Poveda-Reyes, S.; Moulisova, V.; Sanmartín-Masiá, E.; Quintanilla-Sierra, L.; Salmerón-Sánchez, M.; Ferrer, G.G. Gelatin—Hyaluronic Acid Hydrogels with Tuned Stiffness to Counterbalance Cellular Forces and Promote Cell Differentiation. *Macromol. Biosci.* **2016**, *16*, 1311–1324. [CrossRef]
201. Guo, Y.; Gilbert-Honick, J.; Somers, S.M.; Mao, H.Q.; Grayson, W.L. Modified Cell-Electrospinning for 3D Myogenesis of C2C12s in Aligned Fibrin Microfiber Bundles. *Biochem. Biophys. Res. Commun.* **2019**, *516*, 558–564. [CrossRef]
202. Acosta, F.M.; Jia, U.T.A.; Stojkova, K.; Pacelli, S.; Brey, E.M.; Rathbone, C. Divergent Effects of Myogenic Differentiation and Diabetes on the Capacity for Muscle Precursor Cell Adipogenic Differentiation in a Fibrin Matrix. *Biochem. Biophys. Res. Commun.* **2020**, *526*, 21–28. [CrossRef]
203. Marcinczyk, M.; Elmashhady, H.; Talovic, M.; Dunn, A.; Bugis, F.; Garg, K. Laminin-111 Enriched Fibrin Hydrogels for Skeletal Muscle Regeneration. *Biomaterials* **2017**, *141*, 233–242. [CrossRef]
204. Somers, S.M.; Zhang, N.Y.; Morrissette-McAlmon, J.B.F.; Tran, K.; Mao, H.Q.; Grayson, W.L. Myoblast Maturity on Aligned Microfiber Bundles at the Onset of Strain Application Impacts Myogenic Outcomes. *Acta Biomater.* **2019**, *94*, 232–242. [CrossRef]
205. Carnes, M.E.; Pins, G.D. Etching Anisotropic Surface Topography onto Fibrin Microthread Scaffolds for Guiding Myoblast Alignment. *J. Biomed. Mater. Res. Part B Appl. Biomater.* **2020**, *108*, 2308–2319. [CrossRef]
206. Thorrez, L.; DiSano, K.; Shansky, J.; Vandenburgh, H. Engineering of Human Skeletal Muscle with an Autologous Deposited Extracellular Matrix. *Front. Physiol.* **2018**, *9*, 1076. [CrossRef]
207. Chen, X.; Du, W.; Cai, Z.; Ji, S.; Dwivedi, M.; Chen, J.; Zhao, G.; Chu, J. Uniaxial Stretching of Cell-Laden Microfibers for Promoting C2C12 Myoblasts Alignment and Myofibers Formation. *ACS Appl. Mater. Interfaces* **2020**, *12*, 2162–2170. [CrossRef]
208. Hejbøl, E.K.; Sellathurai, J.; Nair, P.D.; Schrøder, H.D. Injectable Scaffold Materials Differ in Their Cell Instructive Effects on Primary Human Myoblasts. *J. Tissue Eng.* **2017**, *8*, 2041731417717677. [CrossRef]

209. Attalla, R.; Puersten, E.; Jain, N.; Selvaganapathy, P.R. 3D Bioprinting of Heterogeneous Bi- and Tri-Layered Hollow Channels within Gel Scaffolds Using Scalable Multi-Axial Microfluidic Extrusion Nozzle. *Biofabrication* **2019**, *11*, 015012. [CrossRef]
210. Witt, R.; Weigand, A.; Boos, A.M.; Cai, A.; Dippold, D.; Boccaccini, A.R.; Schubert, D.W.; Hardt, M.; Lange, C.; Arkudas, A.; et al. Mesenchymal Stem Cells and Myoblast Differentiation under HGF and IGF-1 Stimulation for 3D Skeletal Muscle Tissue Engineering. *BMC Cell Biol.* **2017**, *18*, 15. [CrossRef]
211. Dong, Y.; Li, Y.; Zhang, C.; Chen, H.; Liu, L.; Chen, S. Effects of SW033291 on the Myogenesis of Muscle-Derived Stem Cells and Muscle Regeneration. *Stem Cell Res. Ther.* **2020**, *11*, 76. [CrossRef]
212. Kim, W.J.; Lee, H.; Lee, J.U.; Atala, A.; Yoo, J.J.; Lee, S.J.; Kim, G.H. Efficient Myotube Formation in 3D Bioprinted Tissue Construct by Biochemical and Topographical Cues. *Biomaterials* **2020**, *230*, 119632. [CrossRef]
213. Williams, N.P.; Rhodehamel, M.; Yan, C.; Smith, A.S.T.; Jiao, A.; Murry, C.E.; Scatena, M.; Kim, D.H. Engineering Anisotropic 3D Tubular Tissues with Flexible Thermoresponsive Nanofabricated Substrates. *Biomaterials* **2020**, *240*, 119856. [CrossRef]
214. Fischetti, T.; Celikkin, N.; Negrini, N.C.; Farè, S.; Swieszkowski, W. Tripolyphosphate-Crosslinked Chitosan/Gelatin Biocomposite Ink for 3D Printing of Uniaxial Scaffolds. *Front. Bioeng. Biotechnol.* **2020**, *8*, 400. [CrossRef]
215. Seyedmahmoud, R.; Çelebi-Saltik, B.; Barros, N.; Nasiri, R.; Banton, E.; Shamloo, A.; Ashammakhi, N.; Dokmeci, R.M.; Ahadian, S. Three-Dimensional Bioprinting of Functional Skeletal Muscle Tissue Using Gelatin. *Micromachines* **2019**, *10*, 679. [CrossRef]
216. Jensen, J.H.; Cakal, S.D.; Li, J.; Pless, C.J.; Radeke, C.; Jepsen, M.L.; Jensen, T.E.; Dufva, M.; Lind, J.U. Large-Scale Spontaneous Self-Organization and Maturation of Skeletal Muscle Tissues on Ultra-Compliant Gelatin Hydrogel Substrates. *Sci. Rep.* **2020**, *10*, 13305. [CrossRef]
217. Simsa, R.; Yuen, J.; Stout, A.; Rubio, N.; Fogelstrand, P.; Kaplan, D.L. Extracellular Heme Proteins Influence Bovine Myosatellite Cell Proliferation and the Color of Cell-Based Meat. *Foods* **2019**, *8*, 521. [CrossRef]
218. Denes, L.T.; Riley, L.A.; Mijares, J.R.; Arboleda, J.D.; McKee, K.; Esser, K.A.; Wang, E.T. Culturing C2C12 Myotubes on Micromolded Gelatin Hydrogels Accelerates Myotube Maturation. *Skelet. Muscle* **2019**, *9*, 17. [CrossRef]
219. Asahara, H.; Inui, M.; Lotz, M.K. Tendons and Ligaments: Connecting Developmental Biology to Musculoskeletal Disease Pathogenesis. *J. Bone Miner. Res.* **2017**, *32*, 1773–1782. [CrossRef]
220. Beldjilali-Labro, M.; Garcia Garcia, A.; Farhat, F.; Bedoui, F.; Grosset, J.-F.; Dufresne, M.; Legallais, C. Biomaterials in Tendon and Skeletal Muscle Tissue Engineering: Current Trends and Challenges. *Materials* **2018**, *11*, 1116. [CrossRef]
221. Uquillas, J.A.; Pacelli, S.; Kobayashi, S.; Uquillas, S. Musculoskeletal Tissue Engineering: Tendon, Ligament, and Skeletal Muscle Replacement and Repair. In *Tissue Engineering for Artificial Organs*; Wiley-VCH Verlag GmbH & Co. KGaA: Weinheim, Germany, 2017; Volume 2, pp. 465–523, ISBN 9783527689934.
222. Govoni, M.; Muscari, C.; Lovecchio, J.; Guarnieri, C.; Giordano, E. Mechanical Actuation Systems for the Phenotype Commitment of Stem Cell-Based Tendon and Ligament Tissue Substitutes. *Stem Cell Rev. Rep.* **2016**, *12*, 189–201. [CrossRef]
223. Smith, R.; Carr, A.; Dakin, S.; Snelling, S.; Yapp, C.; Hakimi, O. The Response of Tenocytes to Commercial Scaffolds Used for Rotator Cuff Repair. *Eur. Cells Mater.* **2016**, *31*, 107–118. [CrossRef]
224. Wunderli, S.L.; Blache, U.; Snedeker, J.G. Tendon Explant Models for Physiologically Relevant In Vitro Study of Tissue Biology—A Perspective. *Connect. Tissue Res.* **2020**, *61*, 262–277. [CrossRef]
225. Liu, W.; Webster, T.J. Toxicity and Biocompatibility Properties of Nanocomposites for Musculoskeletal Tissue Regeneration. In *Nanocomposites for Musculoskeletal Tissue Regeneration*; Elsevier: Amsterdam, The Netherlands, 2016; pp. 95–122, ISBN 9781782424758.
226. Anjana, J.; Deepthi, S.; Shalumon, K.T.; Mony, U.; Chen, J.P.; Jayakumar, R. Nanoengineered Biomaterials for Tendon/Ligament Regeneration. In *Nanoengineered Biomaterials for Regenerative Medicine*; Elsevier: Amsterdam, The Netherlands, 2018; pp. 73–93, ISBN 9780128133552.
227. Sensini, A.; Gualandi, C.; Focarete, M.L.; Belcari, J.; Zucchelli, A.; Boyle, L.; Reilly, G.C.; Kao, A.P.; Tozzi, G.; Cristofolini, L. Multiscale Hierarchical Bioresorbable Scaffolds for the Regeneration of Tendons and Ligaments. *Biofabrication* **2019**, *11*, 35026. [CrossRef]
228. Gereke, T.; Döbrich, O.; Aibibu, D.; Nowotny, J.; Cherif, C. Approaches for Process and Structural Finite Element Simulations of Braided Ligament Replacements. *J. Ind. Text.* **2017**, *47*, 408–425. [CrossRef]
229. Higashiyama, R.; Sekiguchi, H.; Takata, K.; Endo, T.; Takamori, Y.; Takaso, M. Arthroscopic Reconstruction of the Anterior Tibiotalar Ligament Using a Free Tendon Graft. *Arthrosc. Tech.* **2020**, *9*, e541–e547. [CrossRef]
230. Lee, K.I.; Lee, J.S.; Kang, K.T.; Shim, Y.B.; Kim, Y.S.; Jang, J.W.; Moon, S.H.; D'Lima, D.D. In Vitro and In Vivo Performance of Tissue-Engineered Tendons for Anterior Cruciate Ligament Reconstruction. *Am. J. Sports Med.* **2018**, *46*, 1641–1649. [CrossRef]
231. Pauly, H.M.; Kelly, D.J.; Popat, K.C.; Trujillo, N.A.; Dunne, N.J.; McCarthy, H.O.; Haut Donahue, T.L. Mechanical Properties and Cellular Response of Novel Electrospun Nanofibers for Ligament Tissue Engineering: Effects of Orientation and Geometry. *J. Mech. Behav. Biomed. Mater.* **2016**, *61*, 258–270. [CrossRef]
232. Chen, C.-H.; Chen, S.-H.; Kuo, C.-Y.; Li, M.-L.; Chen, J.-P. Response of Dermal Fibroblasts to Biochemical and Physical Cues in Aligned Polycaprolactone/Silk Fibroin Nanofiber Scaffolds for Application in Tendon Tissue Engineering. *Nanomaterials* **2017**, *7*, 219. [CrossRef]
233. Sundararaj, S.; Slusarewicz, P.; Brown, M.; Hedman, T. Genipin Crosslinker Releasing Sutures for Improving the Mechanical/Repair Strength of Damaged Connective Tissue. *J. Biomed. Mater. Res. Part B Appl. Biomater.* **2017**, *105*, 2199–2205. [CrossRef]

234. Atluri, K.; Chinnathambi, S.; Mendenhall, A.; Martin, J.A.; Sander, E.A.; Salem, A.K. Targeting Cell Contractile Forces: A Novel Minimally Invasive Treatment Strategy for Fibrosis. *Ann. Biomed. Eng.* **2020**, *48*, 1850–1862. [CrossRef]
235. Gaut, L.; Duprez, D.; Gaut, L.; Duprez, D.; Reviews, I. Tendon Development and Diseases. *Wiley Interdiscip. Rev. Dev. Biol.* **2016**, *5*, 5–23. [CrossRef]
236. Gouveia, P.J.; Hodgkinson, T.; Amado, I.; Sadowska, J.M.; Ryan, A.J.; Romanazzo, S.; Carroll, S.; Cryan, S.A.; Kelly, D.J.; O'Brien, F.J. Development of Collagen-Poly (Caprolactone)-Based Core-Shell Scaffolds Supplemented with Proteoglycans and Glycosaminoglycans for Ligament Repair. *Mater. Sci. Eng. C* **2021**, *120*, 111657. [CrossRef]
237. Zhang, B.Y.; Xu, P.; Luo, Q.; Song, G. Bin Proliferation and Tenogenic Differentiation of Bone Marrow Mesenchymal Stem Cells in a Porous Collagen Sponge Scaffold. *World J. Stem Cells* **2021**, *13*, 115–127. [CrossRef]
238. Chen, P.; Li, L.; Dong, L.; Wang, S.; Huang, Z.; Qian, Y.; Wang, C.; Liu, W.; Yang, L. Gradient Biomineralized Silk Fibroin Nanofibrous Scaffold with Osteochondral Inductivity for Integration of Tendon to Bone. *ACS Biomater. Sci. Eng.* **2021**, *7*, 841–851. [CrossRef]
239. Chen, S.; Wang, J.; Chen, Y.; Mo, X.; Fan, C. Tenogenic Adipose-Derived Stem Cell Sheets with Nanoyarn Scaffolds for Tendon Regeneration. *Mater. Sci. Eng. C* **2021**, *119*, 111506. [CrossRef]
240. Mredha, M.T.I.; Guo, Y.Z.; Nonoyama, T.; Nakajima, T.; Kurokawa, T.; Gong, J.P. A Facile Method to Fabricate Anisotropic Hydrogels with Perfectly Aligned Hierarchical Fibrous Structures. *Adv. Mater.* **2018**, *30*, 1704937. [CrossRef]
241. Laranjeira, M.; Domingues, R.M.A.; Costa-Almeida, R.; Reis, R.L.; Gomes, M.E. 3D Mimicry of Native-Tissue-Fiber Architecture Guides Tendon-Derived Cells and Adipose Stem Cells into Artificial Tendon Constructs. *Small* **2017**, *13*, 1700689. [CrossRef]
242. Zheng, Z.; Ran, J.; Chen, W.; Hu, Y.; Zhu, T.; Chen, X.; Yin, Z.; Heng, B.C.; Feng, G.; Le, H.; et al. Alignment of Collagen Fiber in Knitted Silk Scaffold for Functional Massive Rotator Cuff Repair. *Acta Biomater.* **2017**, *51*, 317–329. [CrossRef]
243. Choi, S.; Choi, Y.; Kim, J. Anisotropic Hybrid Hydrogels with Superior Mechanical Properties Reminiscent of Tendons or Ligaments. *Adv. Funct. Mater.* **2019**, *29*, 1904342. [CrossRef]
244. Bottagisio, M.; Lopa, S.; Granata, V.; Talò, G.; Bazzocchi, C.; Moretti, M.; Barbara Lovati, A. Different Combinations of Growth Factors for the Tenogenic Differentiation of Bone Marrow Mesenchymal Stem Cells in Monolayer Culture and in Fibrin-Based Three-Dimensional Constructs. *Differentiation* **2017**, *95*, 44–53. [CrossRef]
245. Younesi, M.; Akkus, A.; Akkus, O. Microbially-Derived Nanofibrous Cellulose Polymer for Connective Tissue Regeneration. *Mater. Sci. Eng. C* **2019**, *99*, 96–102. [CrossRef]
246. Domingues, R.M.A.; Chiera, S.; Gershovich, P.; Motta, A.; Reis, R.L.; Gomes, M.E. Enhancing the Biomechanical Performance of Anisotropic Nanofibrous Scaffolds in Tendon Tissue Engineering: Reinforcement with Cellulose Nanocrystals. *Adv. Healthc. Mater.* **2016**, *5*, 1364–1375. [CrossRef]
247. Green, E.C.; Zhang, Y.; Li, H.; Minus, M.L. Gel-Spinning of Mimetic Collagen and Collagen/Nano-Carbon Fibers: Understanding Multi-Scale Influences on Molecular Ordering and Fibril Alignment. *J. Mech. Behav. Biomed. Mater.* **2017**, *65*, 552–564. [CrossRef]
248. Sensini, A.; Cristofolini, L.; Focarete, M.L.; Belcari, J.; Zucchelli, A.; Kao, A.; Tozzi, G. High-Resolution X-Ray Tomographic Morphological Characterisation of Electrospun Nanofibrous Bundles for Tendon and Ligament Regeneration and Replacement. *J. Microsc.* **2018**, *272*, 196–206. [CrossRef]
249. Sharifi-Aghdam, M.; Faridi-Majidi, R.; Derakhshan, M.A.; Chegeni, A.; Azami, M. Preparation of Collagen/Polyurethane/Knitted Silk as a Composite Scaffold for Tendon Tissue Engineering. *Proc. Inst. Mech. Eng. Part H J. Eng. Med.* **2017**, *231*, 652–662. [CrossRef]
250. Mozafari, M.; Kargozar, S.; de Santiago, G.T.; Mohammadi, M.R.; Milan, P.B.; Koudehi, M.F.; Aghabarari, B.; Nourani, M.R. Synthesis and Characterisation of Highly Interconnected Porous Poly(ε-Caprolactone)-Collagen Scaffolds: A Therapeutic Design to Facilitate Tendon Regeneration. *Mater. Technol.* **2018**, *33*, 29–37. [CrossRef]
251. Grier, W.K.; Iyoha, E.M.; Harley, B.A.C. The influence of pore size and stiffness on tenocyte bioactivity and transcriptomic stability in collagen-GAG scaffolds. *J. Mech. Behav. Biomed. Mater.* **2017**, *65*, 295–305. [CrossRef]

Chemical Research in Toxicology

pubs.acs.org/crt
Communication

Cell via Cell Viability Assay Changes Cellular Metabolic Characteristics by Intervening with Glycolysis and Pentose Phosphate Pathway

Published as part of Chemical Research in Toxicology virtual special issue "Chemical Biology Approaches for Investigating Toxicological Mechanisms".

Jingzhi Fan, Theresa Schiemer, Annija Vaska, Vahid Jahed, and Kristaps Klavins*

Cite This: https://doi.org/10.1021/acs.chemrestox.3c00339
Read Online

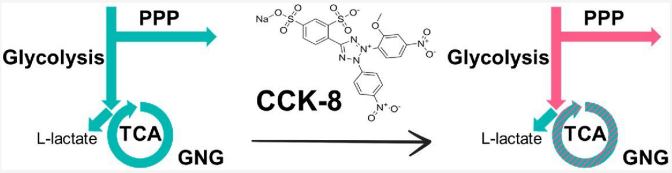

ABSTRACT: The Cell Counting Kit-8 (CCK-8) cell viability assay, also known as WST-8, is widely recognized for its nontoxic nature, making it suitable for further studies on treated cells. This practice is commonly observed in the field of tissue engineering. While live/dead imaging may not readily reveal macroscopic differences, our investigation has uncovered significant intracellular metabolic changes. Notably, we observed substantial down-regulation of metabolites within the glycolysis and pentose phosphate pathways. These metabolic alterations predominantly affect energy metabolism and may potentially impact the cellular redox environment. In light of these findings, we strongly recommend that researchers exercise caution when using cells treated with CCK-8 in subsequent experiments.

The Cell Counting Kit-8 (CCK-8) assay has been widely used in the assessment of cell viability and cytotoxicity. While CCK-8 is commonly employed as an end point assay, it is also frequently applied multiple times within the same experimental group, particularly in the fields of tissue engineering and material research (Figure S1).[1] Researchers frequently conduct multiple characterization experiments on the same sample in succession, often including the use of CCK-8, as a practical means of conserving both time and resources. The minimal toxicity exhibited by CCK-8 facilitates its application in treating cells for successive cell proliferation assays, including crystal violet assay, neutral red assay, or DNA fluorometric assay. However, it is important to acknowledge that uniform viability across different living cells might not precisely portray their cellular conditions. Moreover, the specific intracellular molecular changes induced by this assay in the treated cells remain uncertain.

The quantification of the cell metabolic activity is crucial for assessing cell viability. In the case of the CCK-8 assay, it relies on the detection of high NAD(P)H levels using tetrazolium salt. NAD(P)H levels directly correspond to dehydrogenase activity, thereby providing a measure of cellular metabolic activity.[2] As NAD(P)H is closely linked to metabolism, assays that rely on the depletion of NADPH are theorized to affect cellular metabolism, which, in turn, can affect cellular phenotype or function.

In this work, we employed a liquid chromatography−mass spectrometry (LC−MS)-based metabolomics workflow to identify metabolism pathways affected by CCK-8 treatments. In parallel to the CCK-8 assay, a live/dead staining assay and LDH assay were conducted to compare the status of the cells. The comparison of staining images between the CCK-8 treated group (named CCK) with the control group (named CNT) did not show a significant difference between them (Figure 1a and Figure S2). These results exemplify why researchers

Received: October 25, 2023
Revised: December 7, 2023
Accepted: December 14, 2023

https://doi.org/10.1021/acs.chemrestox.3c00339
Chem. Res. Toxicol. XXXX, XXX, XXX−XXX

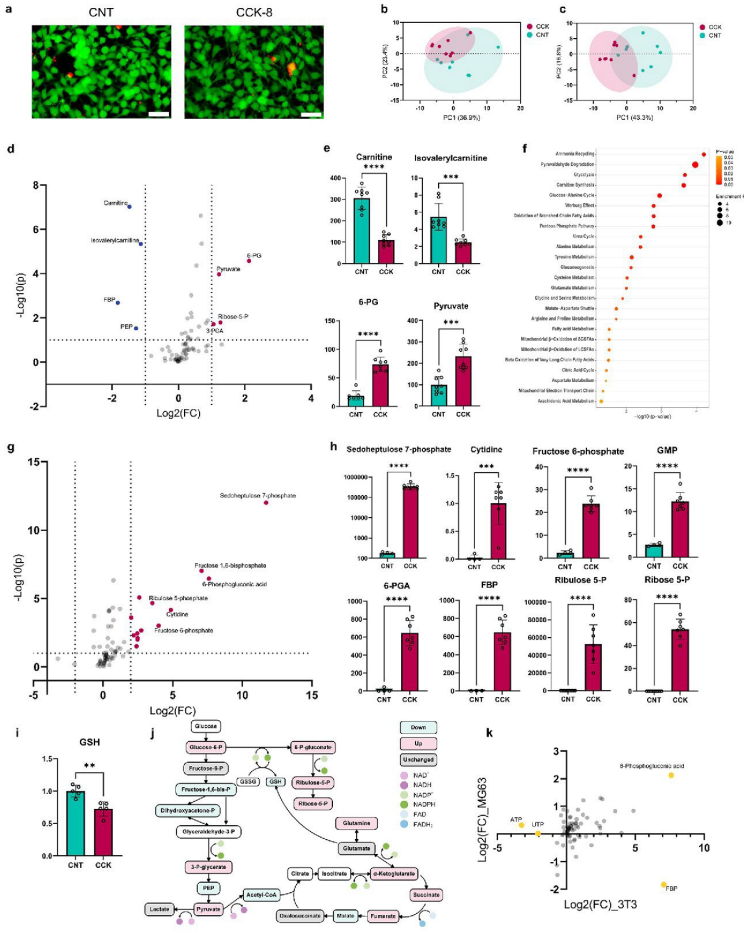

Figure 1. The changes of cells after treatment with Cell Counting Kit-8. (a) LIVE/DEAD staining of NIH/3T3 cells. Scale bar = 100 μm. (b, c) The PCA of MG-63 and NIH/3T3. (d) Volcano plots representing the significantly changed metabolites of MG-63 (Threshold FC > 2 or FC < 0.5, $p < 0.1$). (e) 4 metabolites that were significantly up-regulated and 4 that were down-regulated in MG-63 (unit pmol). (f) Pathway enrichment analysis was based on the metabolomic result of MG-63. The graph shows the top 25 pathways with significant alterations. (g) Volcano plots representing the significantly changed metabolites of 3T3. (h) The most significantly changed metabolites in NIH/3T3 cells. (i) GSH level of MG-63 cells treated with CCK-8 (unit pmol). (j) The metabolism map presented the mostly relevant pathways in energy production (MG-63, threshold Log2(FC) > 0.263034 was up-regulated, Log2(FC) < −0.263034 was down-regulated, 0.263034 > Log2(FC) > −0.263034 was considered as unchanged). (k) The comparison between the fold changes of MG-63 sarcoma cells and 3T3 fibroblasts (**$P < 0.01$; ***$P < 0.001$; ****$P < 0.0001$).

https://doi.org/10.1021/acs.chemrestox.3c00339
Chem. Res. Toxicol. XXXX, XXX, XXX−XXX

typically deem cells treated with CCK-8 suitable for subsequent studies

Using LC−MS-based targeted metabolomics profiling, we obtained results for 74 metabolites from osteosarcoma (MG-63) cells and 78 metabolites from fibroblast (NIH/3T3) cells. MG-63 cells are commonly used as an osteoblastic or osteosarcoma models for tissue engineering studies, and NIH/3T3 cells are often used as a normal, noncancerous models in biomedical research.[3,4] Using these cells in our study provides information about the influence of CCK-8 on cancerous and normal cells.

These metabolites included amino acids, nucleotides, nucleosides, carboxylic acids, carnitines, and other organic acids (Figure S3). Principal component analysis (PCA) indicated the differences between CCK-8 treated cells and the controls (Figure 1b,c). In osteosarcoma cell lines, 8 metabolites were significantly changed (Figure 1d): 6 of them were relevant to glycolysis, and the other 2 were from the carnitine family (Figure 1d,e). In fibroblast cell lines, 14 metabolites were upregulated, of which mostly belong to glycolysis and pentose phosphate pathway (PPP) (Figure 1d).

The enrichment analysis (Figure 1e) highlighted that CCK-8 significantly impacted energy metabolism, particularly glycolysis, modifying cellular energy production. It also disrupted cellular homeostasis, influencing ammonia recycling and carnitine synthesis. Notably, the altered metabolites in the 3T3 cells were primarily linked to downstream glucose metabolism (Figure 1g).

The production of NAD(P)H is directly related to glucose metabolism pathways. This suggests that the glycolysis-relevant metabolism was influenced by CCK-8, while NAD(P)H plays the role of an intermediary here. Coenzymes $NADP^+$/NADPH and NAD^+/NADH are central to the glucose metabolism pathways: NAD^+/NADH is primarily involved in energy-yielding glycolysis and the citric acid cycle, while $NADP^+$/NADPH participates in biosynthetic processes and antioxidant defense, the PPP.[5] These coenzymes shuttle electrons between metabolic reactions, facilitating the transfer of energy and maintaining the redox balance within cells. Carnitine and its derivatives participate in fatty acid metabolism, which involves NAD^+ and NADH in beta-oxidation, as well as $NAD(P)^+$ and NAD(P)H in redox reactions. Carnitine facilitates the transport of fatty acids into the mitochondria, so the decreasing of carnitine can disturb the supply of fatty acids in mitochondria.[6] Furthermore, the enzyme carnitine palmitoyltransferase 1, which plays a central role in fatty acid transport, is regulated by the ratio of NADH to NAD^+ and NADPH to $NADP^+$.[7] The regulation of enzymes involved in carnitine metabolism and fatty acid transport can be influenced by the cellular redox state and the NAD^+/NADH and $NADP^+$/NADPH ratios.

NADPH is a key cofactor required for the enzymatic reduction of oxidized glutathione (GSSG) back to its reduced form, GSH, through the action of the enzyme glutathione reductase.[3] Therefore, we sought to scrutinize the redox state by detecting the GSH changes in MG-63, and as expected, the GSH level was decreased (Figure 1i). The shift toward oxidation disrupts the GSH-GSSG balance, decreasing the cellular GSH pool due to reduced NADPH levels. The alteration in GSH levels impacts the cellular redox state and its defense against oxidants.[8] As a result, if the cells treated with CKK-8 were continued to be applied to other biological evaluations, the result could be misled by this redox state change.

NADPH plays a crucial role as a component of the cellular antioxidant defense system. Utilizing an assay that depletes NADPH could have detrimental effects on studies that rely on these reduced cofactors. For example, the emerging cell death mechanism known as disulfidptosis, which occurs due to inadequate NADPH supply.[9] Consequently, relying on an assay that depletes NADPH may compromise the accuracy of the obtained results associated with disulfidptosis.

Next, we integrated enrichment analysis and pathway topology analysis from the metabolomics data. The metabolism pathways directly related to energy production were significantly influenced (Figure 1f, Figures S4 and S5). The supply of reduced cofactors is ensured by the mitochondrial oxidation of substrates derived from glucose, fatty acids, and amino acids via different metabolic pathways. Therefore, the disruption of homeostasis can cause changes in many cellular functions, such as innate immune responses.[10] It should not be ignored, although the impact could be small. Oxidative phosphorylation is a complex process regulated by interactions between mitochondrial and cytosolic metabolism. These interactions can lead to changes in cellular respiration, influencing cell reactions.[11] As a result, CCK-8 can impact the continued experimental results of the same cells, especially the cell function evaluation relevant to mitochondrial and cytosolic metabolism. Changes were not limited to metabolites directly involved in reduced cofactors; both upstream and downstream metabolites were also altered (Figure 1j).

In our study, we utilized two distinct cell lines, and the findings revealed that CCK-8 can affect the metabolic processes of both cell types. When we compared the fold changes between these two cell types, we observed a significant increase in the level of 6-phosphogluconic acid in both cell lines. However, FBP, ATP, and UTP exhibited changes in opposite directions (see Figure 1k). Notably, the fibroblast cell line displayed greater sensitivity to the depletion of NAD(P)H compared with the osteosarcoma cell line (refer to Figure 1).

The depletion or low regulation of reduced cofactors in cells by CCK-8 can have significant implications of metabolites level. Therefore, the antioxidant defense, biosynthesis, cellular metabolism, detoxification processes, and redox homeostasis are altered.[12] It is essential to note that even when both the experimental and control groups receive the same treatment, the accuracy of results may be compromised by potential synergistic interactions between CCK-8 and the tested drugs or materials. This alteration could significantly influence the results, especially in the color changes, because CCK-8 is a colorimetric method.[13] These interactions have also the potential to induce cellular death and trigger immune-inflammatory responses[14,15] These effects can ultimately impact cell functionality and even the long-term overall cellular state. To conclude, the usage of cells after the CCK-8 kit assay for any subsequent experiment or assay should be approached with caution and consideration of possible implications.

■ ASSOCIATED CONTENT

Supporting Information

The Supporting Information is available free of charge at https://pubs.acs.org/doi/10.1021/acs.chemrestox.3c00339.

https://doi.org/10.1021/acs.chemrestox.3c00339
Chem. Res. Toxicol. XXXX, XXX, XXX−XXX

User manual for CCK-8; influence of the CCK-8 assay on cell viability; pathways influenced by CCK-8; Enrichment Network of Metabolite Correlation; materials and methods utilized in the manuscript (PDF)

AUTHOR INFORMATION

Corresponding Author

Kristaps Klavins − *Rudolfs Cimdins Riga Biomaterials Innovations and Development Centre, Institute of General Chemical Engineering, Faculty of Materials Science and Applied Chemistry, Riga Technical University, Riga LV-1007, Latvia; Baltic Biomaterials Centre of Excellence, Headquarters at Riga Technical University, Riga LV-1048, Latvia*; Email: kristaps.klavins_3@rtu.lv

Authors

Jingzhi Fan − *Rudolfs Cimdins Riga Biomaterials Innovations and Development Centre, Institute of General Chemical Engineering, Faculty of Materials Science and Applied Chemistry, Riga Technical University, Riga LV-1007, Latvia; Baltic Biomaterials Centre of Excellence, Headquarters at Riga Technical University, Riga LV-1048, Latvia*; orcid.org/0000-0002-3736-0275

Theresa Schiemer − *Rudolfs Cimdins Riga Biomaterials Innovations and Development Centre, Institute of General Chemical Engineering, Faculty of Materials Science and Applied Chemistry, Riga Technical University, Riga LV-1007, Latvia; Baltic Biomaterials Centre of Excellence, Headquarters at Riga Technical University, Riga LV-1048, Latvia; Medical University of Innsbruck, Innsbruck 6020, Austria*

Annija Vaska − *Rudolfs Cimdins Riga Biomaterials Innovations and Development Centre, Institute of General Chemical Engineering, Faculty of Materials Science and Applied Chemistry, Riga Technical University, Riga LV-1007, Latvia; Baltic Biomaterials Centre of Excellence, Headquarters at Riga Technical University, Riga LV-1048, Latvia*

Vahid Jahed − *Rudolfs Cimdins Riga Biomaterials Innovations and Development Centre, Institute of General Chemical Engineering, Faculty of Materials Science and Applied Chemistry, Riga Technical University, Riga LV-1007, Latvia; Baltic Biomaterials Centre of Excellence, Headquarters at Riga Technical University, Riga LV-1048, Latvia*

Complete contact information is available at: https://pubs.acs.org/10.1021/acs.chemrestox.3c00339

Author Contributions

J.F. and K.K. conceptualized and designed the study. J.F. conducted cell experiments, metabolites collection, data analysis, and prepared the manuscript. T.S. and V.J. conducted LIVE/DEAD imaging. A.V. performed LC−MS analysis. K.K. provided supervision, and reviewed and edited the manuscript.

Notes

The authors declare no competing financial interest.

ACKNOWLEDGMENTS

The authors acknowledge financial support from the EU research and innovation program under the grant agreement No. 857287 (BBCE − Baltic Biomaterials Centre of Excellence) and the Ministry of Economics Republic of Latvia project "State research project in the field of biomedicine, medical technologies, and pharmacy", Project No. VPP-EM-BIOMEDICĪNA-2022/1-0001.

ABBREVIATIONS

CCK-8, Cell Counting Kit-8; NAD(P)H, nicotinamide adenine dinucleotide (phosphate) hydrogen; GSSG, oxidized glutathione; GSH, glutathione; FBP, fructose-1,6-bisphosphatase; GNG, gluconeogenesis

REFERENCES

(1) Dojindo Laboratories. *Technical Manual - Cell Counting Kit-8* **2016**, *8*, 1−2.

(2) Chamchoy, K.; Pakotiprapha, D.; Pumirat, P.; Leartsakulpanich, U.; Boonyuen, U. Application of WST-8 Based Colorimetric NAD(P)H Detection for Quantitative Dehydrogenase Assays. *BMC Biochem.* **2019**, *20* (1), 1−14.

(3) Jiang, T.; Xu, G.; Chen, X.; Huang, X.; Zhao, J.; Zheng, L. Impact of Hydrogel Elasticity and Adherence on Osteosarcoma Cells and Osteoblasts. *Adv. Healthc. Mater.* **2019**, *8* (9), 1−11.

(4) Rahimi, A. M.; Cai, M.; Hoyer-Fender, S. Heterogeneity of the NIH3T3 Fibroblast Cell Line. *Cells* **2022**, *11* (17), 2677.

(5) Navas, L. E.; Carnero, A. NAD+ Metabolism, Stemness, the Immune Response, and Cancer. *Signal Transduct. Target. Ther.* **2021**, *6* (1), 2 DOI: 10.1038/s41392-020-00354-w.

(6) Geier, D. A.; Geier, M. R. L-Carnitine Exposure and Mitochondrial Function in Human Neuronal Cells. *Neurochem. Res.* **2013**, *38* (11), 2336−2341.

(7) Ju, H. Q.; Lin, J. F.; Tian, T.; Xie, D.; Xu, R. H. NADPH Homeostasis in Cancer: Functions, Mechanisms and Therapeutic Implications. *Signal Transduct. Target. Ther.* **2020**, *5* (1), 1−12.

(8) Xiong, Y.; Xiao, C.; Li, Z.; Yang, X. Engineering Nanomedicine for Glutathione Depletion-Augmented Cancer Therapy. *Chem. Soc. Rev.* **2021**, *50* (10), 6013−6041.

(9) Liu, X.; Nie, L.; Zhang, Y.; Yan, Y.; Wang, C.; Colic, M.; Olszewski, K.; Horbath, A.; Chen, X.; Lei, G.; Mao, C.; Wu, S.; Zhuang, L.; Poyurovsky, M. V.; James You, M.; Hart, T.; Billadeau, D. D.; Chen, J.; Gan, B. Actin Cytoskeleton Vulnerability to Disulfide Stress Mediates Disulfidptosis. *Nat. Cell Biol.* **2023**, *25*, 404.

(10) Song, Y.; Zhou, Y.; Zhou, X. The Role of Mitophagy in Innate Immune Responses Triggered by Mitochondrial Stress. *Cell Commun. Signal.* **2020**, *18* (1), 1−14.

(11) Jouaville, L. S.; Pinton, P.; Bastianutto, C.; Rutter, G. A.; Rizzuto, R. Regulation of Mitochondrial ATP Synthesis by Calcium: Evidence for a Long-Term Metabolic Priming. *Proc. Natl. Acad. Sci. U. S. A.* **1999**, *96* (24), 13807−13812.

(12) Ying, W. NAD+/NADH and NADP+/NADPH in Cellular Functions and Cell Death: Regulation and Biological Consequences. *Antioxidants Redox Signal.* **2008**, *10* (2), 179−206.

(13) Cai, L.; Qin, X.; Xu, Z.; Song, Y.; Jiang, H.; Wu, Y.; Ruan, H.; Chen, J. Comparison of Cytotoxicity Evaluation of Anticancer Drugs between Real-Time Cell Analysis and CCK-8 Method. *ACS Omega* **2019**, *4* (7), 12036−12042.

(14) Zhang, L.; Virgous, C.; Si, H. Synergistic Anti-Inflammatory Effects and Mechanisms of Combined Phytochemicals. *J. Nutr. Biochem.* **2019**, *69*, 19−30.

(15) Lee, C. S.; Kim, Y. J.; Lee, M. S.; Han, E. S.; Lee, S. J. 18β-Glycyrrhetinic Acid Induces Apoptotic Cell Death in SiHa Cells and Exhibits a Synergistic Effect against Antibiotic Anti-Cancer Drug Toxicity. *Life Sci.* **2008**, *83* (13−14), 481−489.

Heliyon 10 (2024) e39753

Contents lists available at ScienceDirect

Heliyon

journal homepage: www.cell.com/heliyon

Research article

Exploring the impact of calcium phosphate biomaterials on cellular metabolism

Jingzhi Fan [a,b], Theresa Schiemer [a,b], Vita Steinberga [a], Annija Vaska [a,b], Anastasija Metlova [b,c], Antons Sizovs [b,c], Janis Locs [a,b], Kristaps Klavins [a,b,*]

[a] Institute of Biomaterials and Bioengineering, Faculty of Natural Sciences and Technology, Riga Technical University, Riga, Latvia
[b] Baltic Biomaterials Centre of Excellence, Headquarters at Riga Technical University, Riga, Latvia
[c] Latvian Institute of Organic Synthesis, Riga, Latvia

ARTICLE INFO

Keywords:
Glycolysis
Calcium phosphate
Hydroxyapatite
β-tricalcium phosphate
Metabolism

ABSTRACT

Calcium phosphate (CaP) biomaterials have been widely used in hard tissue engineering, but their impact on cell metabolism is unclear. We synthesized and characterized hydroxyapatite, β-tricalcium phosphate, and biphasic calcium phosphate composites to investigate material effects on NIH/3T3 cell metabolism. The intracellular metabolites were analyzed employing LC-MS metabolomics, and cell metabolic status was assessed comparatively. Our results revealed that CaPs adsorb metabolites, particularly amino acids. Furthermore, CaP biomaterials significantly influence amino acid and energy metabolism pathways. Specifically, we observed glycolysis and TCA cycle activity stimulation, resulting in higher energy consumption in cells adhered to CaP surfaces. Our findings suggest that CaPs composed of different ratios of hydroxyapatite (HAp) and β-tricalcium phosphate (β-TCP) have a similar impact on cell metabolism alterations. Moreover, we observed that the metabolism alterations gradually decreased over time. Our study enhances understanding of cell-CaP interplay, paving the way for metabolic regulation biomaterials and improving efficacy in tissue engineering and regenerative medicine.

1. Introduction

Bone is distinguished by its unique, organic matrix composition (35 %) and inorganic components (65 %) [1]. Calcium phosphate

Abbreviations: HAp, hydroxyapatite; CaP, calcium phosphate; β-TCP, β-tricalcium phosphate; BCP, biphasic calcium phosphates; XRD, X-ray diffraction; ANOVA, analysis of variance; F6P, fructose 6-phosphate; FBP, fructose 1,6-bisphosphate; PCA, principal component analysis; AMP, adenosine monophosphate; ADP, adenosine diphosphate; ATP, adenosine tri-phosphate; UMP, uridine monophosphate; UDP, Uridine diphosphate; UTP, uridine triphosphate; CMP, cytidine monophosphate; CDP, cytidine diphosphate; CTP, cytidine triphosphate; OMP, orotidine monophosphate; His, Histidine; Trp, Tryptophan; Tyr, Tyrosine; Phe, Phenylalanine; Gly, Glycine; Gln, Glutamine; Asp, Aspartate; Tau, Taurine; Cys, Cystine; Met, Methionine; Ser, Serine; Val, Valine; Leu, Leucine; Ile, Isoleucine; Ala, Alanine; Arg, Arginine; Pro, Proline; Cr, Creatinine; PCr, Phosphocreatine; Glucose-6P, Glucose-6-phosphate; Ribulose-6P, Ribulose-6-phosphate; Erythrose-4P, Eythrose-4-phosphate; Fructose-6P, Fuctose-6-phosphate; Sedoheptulose-1,7P2, Sedoheptulose-1,7-bisphosphate; R5P, Ribose-5-phosphate; PRPP, Phosphoribosyl pyrophosphate; DHAP, Dihydroxyacetone phosphate; GA3P, Glyceraldehyde-3-phosphate; Acetyl-CoA, Acetyl coenzyme A; PEP, Phosphoenolpyruvate; NAD, Nicotinamide adenine dinucleotide; FAD, Flavin adenine dinucleotide; GMP, Guanosine monophosphate; IMP, Inositol monophosphate; Ura, Uracil; Urd, uridine.

* Corresponding author. Institute of Biomaterials and Bioengineering, Faculty of Natural Sciences and Technology, Riga Technical University, Riga, Latvia.
E-mail address: kristaps.klavins_3@rtu.lv (K. Klavins).

https://doi.org/10.1016/j.heliyon.2024.e39753
Received 2 April 2024; Received in revised form 18 July 2024; Accepted 22 October 2024
Available online 26 October 2024

(CaP) makes up most of the bone's inorganic substance. In bone, it exists in a form analogous to the mineral hydroxyapatite (HAp) and deposits on the collagen matrix [2]. CaP ceramics are similar in composition to bone minerals, giving them excellent biological properties that stimulate osteoconduction and osteoinduction [3]. Using CaPs as implanted biomaterials has benefited countless hard tissue repairs [4]. Hydroxyapatite and β-tricalcium phosphate (β-TCP) are the most used and potent synthetic bone graft substitutes among the many calcium phosphate materials. Both are biodegradable with excellent bioactivity [5]. CaP ceramics exhibit osteoconductivity through partial dissolution in body fluids, facilitating the reprecipitation of biological apatite on their surface. This phenomenon promotes osteoblast cell adhesion, facilitating the production of the bone matrix. Nevertheless, these materials still present distinct clinical challenges, including chronic inflammation and degradation rates that do not align with tissue growth rates [6]. To achieve a better therapeutic outcome, significant efforts are dedicated to improving the physical, chemical, and biological properties of CaPs. The current focus of CaP biomaterial development is mainly on crystallography, morphology, organic/inorganic composite, and advanced preparation methods. At the same time, a deeper understanding of the biological mechanism behind CaP interactions with organisms is still in demand.

Cell-material interaction is a crucial bridge between biology and materials engineering. Gene expression, protein characterization, cell imaging, and histology, from in vitro to in vivo, are mature and widely applied to evaluate a new biomaterial [7]. However, the studies about crosstalk at the cell-material interface mainly focus on macromolecules, while the building blocks of living systems, the small molecules – metabolites - are belittled aside. Metabolites, including amino acids, lipids, sugars, and organic acids, are constantly consumed and formed in the anabolism or catabolism process to maintain cell functions [8]. The catabolic and anabolic cell activities altered by contacted materials or cellular microenvironments are directly linked to cell behaviors [9]. Therefore, metabolite profiling can be an efficient strategy for analyzing cell-material interaction. The metabolic clues can benefit the understanding and development of tissue engineering strategies [10]. On the flip side, the measurement of metabolite changes in the cellular environment has a considerable potential to directly or indirectly assess cell adhesion, differentiation, functionalization, and other cell activities. The role of metabolites in cell behaviors is getting more and more attention in biomaterial studies. Mass spectrometry-based metabolomics can acquire accurate quantitative information on metabolites and their diversity [10,11]. Mass spectrometry enables the simultaneous detection and measurement of several hundreds of metabolites, providing characteristic chemical fingerprints and offering cutting-edge technology for novel diagnostic and prognostic approaches in contemporary health and medical science research [12]. The measured cellular metabolite profiles provide information about catabolic and anabolic regulation in cell health, accurately reflecting cellular phenotype [10]. In recent years, metabolomics has become crucial in clinical research, drug discovery, nutritional science, and toxicology. Metabolomics studies are widely applied to investigate various human diseases, improve diagnosis, and design therapeutic strategies [13]. Similarly, metabolomics could be a powerful tool in advanced biomaterial research and development. The influence of CaPs on cell metabolism has not yet been fully understood. Such knowledge about cell-material interaction can aid the development of advanced bio-functional materials. Combining metabolomics with other material evaluation techniques can provide a comprehensive understanding of complex biomolecular processes.

In this study, we selected calcium phosphate-based bioceramics to study their influence on cell metabolism as they are clinically relevant and widely used biomaterials. For this purpose, bioceramics were synthesized via wet precipitation and characterized by X-ray diffraction (XRD), contact angle, and cell viability tests. The investigated materials were hydroxyapatite (HAp), β-tricalcium phosphate (β-TCP), and biphasic calcium phosphate (BCP) composites with HAp/β-TCP ratios of 95/5 w/w (named H95) and 58/42 w/w (named H58). The two HAp/β-TCP ratios have been approved on the market and clinically applied (e.g., Calciresorb™ and CellCeram™) [14]. Different ratios were included to verify whether BCP composition affects metabolism.

We selected the NIH/3T3 fibroblasts cell line for the model cell culture as these cells are commonly used as cell-material interaction models to characterize biomaterials [15]. Cells were cultured on calcium phosphate (CaP) materials for 5 days. Quantitative metabolite profiles were determined using LC-MS-based workflow, and statistical analysis was applied to compare the metabolite profiles between different groups. Besides the intracellular metabolite profile, the metabolite adsorption on CaP materials was also investigated.

We were able to demonstrate that CaPs can adsorb metabolites. Moreover, CaPs altered cellular amino acid metabolism and accelerated energy metabolism, and the CAP's influence on cell metabolism decreased over time. The results expand the current understanding of CaP-based bioceramic interactions with cells and demonstrate the applicability of metabolomics in biomaterials research.

2. Material and methods

2.1. CaP materials preparation

Calcium phosphate powders were synthesized via the wet precipitation synthesis described by Sokolova1 et al. [16] In brief, calcium oxide (CaO, Fluka, from marble, ≥97 %), orthophosphoric acid (H_3PO_4, Sigma-Aldrich, 85 % w/w), and deionized water were used in the wet precipitation reaction. The pH of the reaction media varied between 5.0 and 7.6, depending on the desired phase composition of the product. Generally, an acidic pH for the β-TCP phase and an alkaline pH for the HAp phase were set. The precipitates were washed, vacuum-filtered, and dried. Detailed description of procedures is available in supporting information (Synthesis of CaPs). The obtained powders were pressed into CaP discs under the pressure of 30 KPa and further sintered with high temperatures to produce disks that fit the 24-well plate for cell culture. The temperatures for sintering were as follows: HAP: 990 °C; H95: 1030 °C; H58: 1135 °C; TCP: 1100 °C. The materials were sterilized by autoclaving at 121 °C for 20 min. A contact angle test was applied to the sintered CaPs to assess the surface hydrophobicity. 10 ml of deionized water was dropped onto material surfaces and captured by a

camera. The angles were measured using ImageJ software.

2.2. The pH and ion release test

The pH test and calcium and phosphate ion release test from the materials were conducted using Dulbecco's Modified Eagle's medium (DMEM, Gibco) by immersing CaPs disks for 24 h (1 ml/disk). The pH was measured by pH meter (WTW inoLab pH 7110). The calcium level in media was measured by calcium colorimetric assay kit (Sigma). 50 μL conditioned media was taken into the 96-well plate (Tecan), followed by 90 μL of the chromogenic reagent to each well. 60 μL calcium assay from buffer supplied from the assay kits. The plate was incubated at room temperature for 15 min, protected from light, and then immediately measured by the plate reader (Tecan), with the absorbance at 575 nm. The phosphate level in media was measured by phosphate assay kit (Sigma). 50 μL conditioned media was taken into the 96-well plate (Tecan), followed by 100 μL of the malachite green reagent to each well. The plate was incubated for 30 min at room temperature, avoiding light interference. The plate reader (Tecan) set to the absorbance at 620 nm was employed for measurements.

2.3. Scanning electron microscope (SEM) imaging

After incubation for 24 h, the NIH/3T3 cells were rinsed with phosphate-buffered saline (PBS). Samples were washed twice with PBS (37 °C) and fixed in 4 % paraformaldehyde solution for 40 min at room temperature. Then, cells were washed three times with cold PBS and dehydrated with gradual ethanol dehydration (25 %, 50 %, 75 %, 90 %, 100 %; 5 min each) and dried for 20 min after adding one drop of hexamethyldisilane (Sigma Aldrich, ≥99 %) on top of the material. The original CaP materials were imaged together with the cells on materials by SEM. Dried materials were mounted on sample holders with double-sided carbon tape and sputter coated with carbon (LEICA EM ACE200, Flash, 20 pulses), and one connective line was drawn with silver paint. SEM images were acquired at 5 keV, 1 uS scanning speed, and a distance of 3.03 mm (Tescan Vega SEM) using frame averaging with 50 frames.

2.4. Specific surface area analysis

The results were calculated using the Brunner-Emmett-Teller (BET) specific surface area theory. The surface area was measured with the N_2 adsorption system QuadraSorb SI (Quantachrome Instruments, USA). All material tablet samples were broken into pieces to fit the container. Excess moisture and vapors were removed at room temperature for 24 h.

2.5. X-Ray diffraction (XRD) characterization of CaPs

The crystalline phase of all sintered CaP discs was determined by XRD (PANalytical Aeris, Netherlands) to verify the composition of CaPs. The characterization analysis was performed with X'Pert Data Collector, X'Pert Data Viewer, X'PertHighScore, and the International Centre for Diffraction Data PDF-2 (ICDD). XRD patterns were recorded using 40 kV and 15 mA, K-α1,2 wavelengths 1.541, step size 0.0435°, within range 2θ from 10° to 70°, time per step 147.39 ms, for crystalline phase identification succeeding ICDD entries were used. The crystallographic patterns and corresponding peaks of HAp (ICDD 09-0432) and β-TCP (ICDD 09-0169) were identified using X'PertHighScore software (Malvern Panalytical, Worcestershire, UK), based on data from the International Center for Diffraction Data (ICDD) database. Detailed instrument settings are given in Table S3. Crystallographic identification of the synthesized phases was accomplished by comparing the experimental XRD patterns to ICDD.

2.6. Cell culture and viability tests

NIH/3T3 cell line (ATCC CRL-1658, ECACC 93061524), (6×10^4 cells/ml) were cultured in Dulbecco's Modified Eagle's medium (DMEM, Gibco) supplemented with 10 % calf serum (Sigma-Aldrich) and 1 % Penicillin-Streptomycin (Gibco). The cells were incubated at 37 °C in a 5 % CO_2 environment. The cells at passage 7 were seeded on material surfaces in a 24-well culture plate with 4 replicates of each group. The cells seeded in wells without materials were used as control groups. Metabolite extraction was performed for all the cells on days 1, 3, and 5 for 4 replicates per group and time point. Cell Counting Kit-8 (CCK-8, Sigma-Aldrich) was used to determine cell viability in parallel with 4 replicates in each group. Mycoplasma from culture media was tested by Rapid Mycoplasma Detection Kit (AssayGenie) and shown negative.

2.7. Cell attachment analysis

Materials were placed in a 24-well plate, and 3×10^4 cells were seeded in 100 μl and left to attach. The culture medium (supernatant) and the cells on the materials were pipetted out for further cell viability tests. Per the manufacturer's instructions, viability was assessed in duplicates using CellTiter-Blue (Promega).

2.8. Metabolite extraction

The methanol-based protocol was employed for the metabolite extraction. It was essential to extract cells directly from the material to avoid changes in cell metabolism during detaching. Before the extraction, cell culture media was removed, and cells were washed

with ammonium bicarbonate (NH_4HCO_3, Sigma-Aldrich, ≥99.5 %) solution (75 mM, 37 °C). Cells were then quenched in cold 80 % v/v methanol (CH_3OH, Sigma-Aldrich, ≥99.9 %) and harvested by scraping. The harvested samples were centrifuged at 600 RCF at room temperature for 5 min, and the supernatant was collected. The collected supernatant was dried by vacuum centrifuge. Afterward, 10 μL of the isotopically labeled internal standard mix was added to dried samples, followed by 90 μL of methanol. Reconstituted samples were transferred to glass vials and used for liquid chromatography-mass spectrometry (LC-MS) analysis.

The same metabolite extraction procedure was also applied to the CaPs without cultured cells to verify the adsorption of metabolites by materials. 1 ml complete media was filled in well plates with and without materials for 24 h, and 3 replicates were set for each group. The media was removed, the wells were washed with ammonium bicarbonate solution, and cold 80 % v/v methanol was added. The methanol solution was collected by pipetting and scraping. The extracts were dried by vacuum centrifuge, and 10 μL of the isotopically labeled internal standard mix was added to dried samples, followed by 90 μL of methanol. Reconstituted samples were transferred to glass vials and used for liquid chromatography-mass spectrometry (LC-MS) analysis.

2.9. Metabolite analysis

Targeted quantitative metabolite analysis was conducted using HILIC-based liquid chromatography combined with mass spectrometric detection employing a triple quadrupole mass spectrometer. Metabolites were separated on an ACQUITY UPLC BEH Amide 1.7 μm 2.1 × 100 mm analytical column (Waters). The gradient elution was carried out using 0.15 % formic acid and 10 mM ammonium formate in water as mobile phase A and a solution of 0.15 % formic acid and 10 mM ammonium formate in 85 % acetonitrile as mobile phase B. The initial conditions were set to 100 % mobile phase A. After 6 min, a 0.1 min gradient (6.0–6.1 min) was started, and the mobile phase A level was reduced to 94.1 %. From 6.1 to 10 min, mobile phase A was set to 82.4 %, and from 10 to 12 min, mobile phase A was set to 70.6 %. The column was then equilibrated for 6 min at initial conditions. The total analysis time was 18 min. The mobile phase flow rate was 0.4 mL/min; the injection volume was 2 μL, and the column temperature was 40 °C. For MS detection, a TSQ Quantis (Thermos Fisher Scientific) triple quadrupole mass spectrometer was used. The MS analysis was performed in ESI positive and ESI negative modes using MRM detection (MRM settings are provided in Supplement Information). The ESI spray

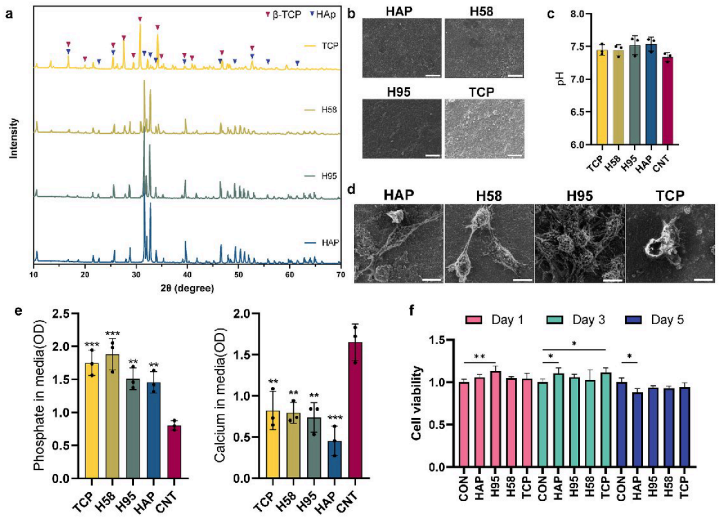

Fig. 1. a) The XRD analysis of CaP disk crystal structure. Red arrows indicate characteristic peaks of β-TCP, and blue arrows indicate distinct peaks of HAp. The composites had both patterns, and the peak values varied by the compositions. The intensity and pattern of corresponding peaks changed according to the relative composition ratio of HAp/β-TCP. Peaks at 27.80° (214), 31.07° (210), and 32.42° (128), 34.23° (220), indicating the increase of the HAp phase proportion. b) SEM images of prepared CaP disks. Scale bar = 10 μm c) pH of media immersed with materials. d) The SEM images of cells attached to CaP material surfaces. Scale bar = 10 μm. e) Phosphate and calcium ion level of media immersed with materials. $^{**}P < 0.01$, $^{***}P < 0.001$ v CON. f) The cell viability was tested by CCK-8 on days 1, 3, and 5. Cell viability is normalized to control samples. Synthesized CaPs significantly increased cell viability compared to controls (one-way ANOVA followed Tukey's multiple comparisons tests, $^{*}P < 0.05$, $^{**}P < 0.01$ vs. CON).

voltage was set to 3.5 kV in positive mode and 2.5 kV in negative mode, the gas heater temperature was set to 400 °C, the capillary temperature was set to 350 °C, the auxiliary gas flow rate was set to 12 arbitrary units, and nebulizing gas flow rate was set to 50 arbitrary units. For quantitative analysis, seven-point calibration curves with internal standardization were used. Tracefinder 51.1 General Quan (Thermofisher Scientific) software was used for LC-MS data processing and quantification. Detailed information of detected metabolites is shown in Table S4. The metabolite concentration was normalized for further data analysis versus cell counting results.

2.10. Data analysis

The metabolomics data analysis was performed with MetaboAnalyst 5.0 [17]. The total amount of metabolites was normalized based on the number of cells according to the cell proliferation data. For data preprocessing, obtained concentrations were log-transformed and scaled by mean-centering, and each variable was divided by the standard deviation. GraphPad Prism 9 was used for statistical analysis. The metabolites with a high adsorption rate (fold change over 0.1 compared to the cell results) were excluded from the group comparison. Analysis of variance (ANOVA) was applied for multi-group data. Pathway enrichment analysis used The Small Molecule Pathway Database as the pathway library. Fold-change and p-value were calculated for two-group comparisons to find significantly changed metabolites. The two-group comparison data was analyzed using the *t*-test. The cluster analysis was performed by principal component analysis (PCA). The machine learning method to rank the metabolite contributions to classification accuracy was done by random forest, with 500 trees and 7 predictors.

3. Results

3.1. Characterization of CaP materials

The hydrophilicity test was conducted and presented by the contact angle (Supplemental information, Fig. S1). The angles were 91.781 (TCP), 92.278 (HAP), 95.020 (H95), and 90.944 (H58). The samples had a mild hydrophobicity, which was acceptable for cell cultures, and no significant difference between different CaP samples was observed.

XRD was used to determine the composition of sintered CaP discs (Fig. 1a). Pattern fitting was carried out between 10° and 70°. The diffraction patterns showed sharp diffraction peaks, indicating the presence of different crystalline species in CaP discs, including β-TCP and HAp. The materials were verified as pure HAp, β-TCP, and BCP with HAp/β-TCP ratios of 95/5 and 58/42. The Ca/P ratio of prepared CaPs are presented in Table 1.

$$\text{Overall Ca / P ratio} = \omega_{\beta-TCP} \times 1.5 + \omega_{HAp} \times 1.67$$

SEM was used to characterize the morphology of 4 types of CaP disks (Fig. 1b). The material had a slightly rough but relatively flat surface. Ceramic materials sintered at high temperatures had a high degree of sealing on the surface. Cells (about 10 μm) cannot enter the material's interior but can only grow on the surface.

The material did not cause pH changes in the culture medium (Fig. 1c). In the absence of cells, immersion for 24 h reduced the calcium concentration of the culture medium. On the contrary, the concentration of phosphate ions is increased by the biomaterial (Fig. 1e). The addition of CaPs could cause precipitation of calcium phosphate compounds. This lead to a decrease in the free calcium ion concentration in the media as calcium ions bind to phosphate ions and precipitate out of solution.

3.2. Cell viability and attachment

Cell viability responding to a biomaterial is a critical parameter commonly assessed during biomaterial evaluation. Furthermore, for quantitative metabolite analysis, different cell numbers can influence quantitative results; hence, it is crucial to normalize obtained data to the cell numbers. The CCK-8 measures the metabolic activity of cells by reacting with NAD(H) and NADP(H), therefore reflecting the total number of viable cells. The cell viability for material groups was similar to the surface-treated culture plate (Fig. 1f). As expected, CaPs showed good biocompatibility, and cell viability was not affected when seeded directly on material surfaces. SEM images and cell attachment analysis showed attachment and cell spreading (Fig. 1d and Fig. S2.). The cell viability and attachment results confirmed the quality of the synthesized CaP materials in this study.

Table 1
Ca/P ratio. The crystal form ratio is calculated from the XRD analysis results using the formula: Overall Ca/P ratio=ωβ−TCP×1.5+ωHAp×1.67.

Materials	Overall Ca/P ratio
HAp	1.67
H95	1.66
H58	1.60
TCP	1.50

3.3. Intracellular metabolic profiling

We employed a targeted quantitative metabolomics approach in this study and analyzed 58 metabolites. Broadly, those metabolites fall into 6 related categories: TCA cycle, glycolysis, pentose phosphate pathway, nucleotide synthesis, fatty acid oxidation, and amino acid metabolism. The downstream analysis of obtained metabolite data was divided into three parts: in-between CaP materials, between CaPs and the control group, and analysis of longitudinal metabolism changes. The obtained quantitative metabolite values were log-transformed, scaled by mean-centering and presented in a heatmap (Fig. 2).

3.4. Metabolites adsorption by CaPs

Understanding the influence of metabolite adsorption is vital as it can alter the cellular microenvironment. Moreover, considering the potential adsorption of metabolites onto biomaterial surfaces from cell culture media is essential to address experimental biases, as co-extraction with intracellular metabolites may compromise the accuracy of the results. In this study, we focused on intercellular metabolite measurements. Therefore, evaluating if the experimental condition could introduce bias in metabolite measurements was essential to ensure accurate data interpretation. The experimental procedure included immersion of the cap disk in cell culture media, seeding the cell directly on the material, and extracting the intercellular metabolites. Typical cell culture media contains a plethora of metabolites to ensure proper cellular functions. These small molecules can adhere to biomaterial surfaces and could be co-extracted with intercellular metabolites, resulting in inaccurate metabolite data. To assess the metabolite affinity for adsorption on material surface and thus potential interferences when analyzing intercellular metabolite levels, we performed metabolite extraction for CaP disks immersed in complete media containing 90 % DMEM and 10 % calf serum without cells. 29 metabolites were found to adsorb onto the CaP surface even after washing with PBS (Fig. 2). Compared to the control (cell culture plate), more metabolites were adsorbed onto CaP surfaces. CaPs showed a higher affinity with the positively charged amino acids (basic side chains). Lactic acid was adsorbed on both CaP and control groups, while the lactic acid level on the CaP surface was almost 4 times lower than the control (on the plate). Sulfur-containing amino acids (methionine, taurine, and cystine) had the highest adsorption affinity on CaP surfaces. Both CaP and culture plate showed attraction to arginine.

To assess the impact of adsorption on extracted metabolite levels, the quantities of adsorbed metabolites were compared with intracellular metabolite levels. This analysis aimed to determine how much adsorption influenced the measured metabolite levels. For this purpose, the average concentration of metabolites from the biomaterials group on day 1 was used as a reference to calculate fold changes of the CAP group, and the control group was calculated with the intracellular metabolites of the control group (without biomaterial) from day 1. 26 metabolites had a high adsorption rate (fold change over 0.1 compared to the cell results) (see Fig. 3).

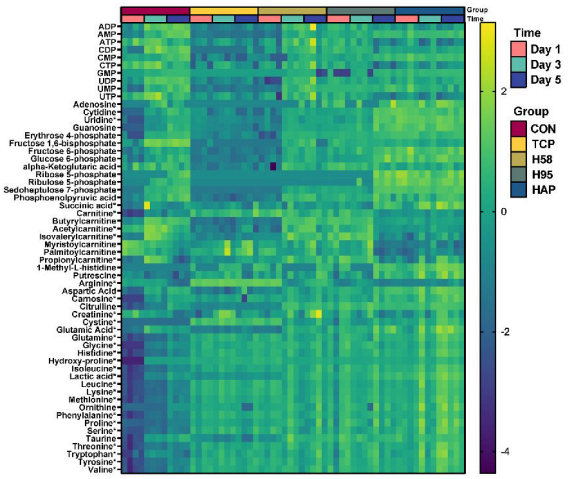

Fig. 2. The heatmap of the complete metabolite profile for 5 groups at 3 different time points. Metabolites are nucleosides, sugar metabolites, carnitine family, and amino acids. Metabolites that adsorbed on CaP surfaces are labeled by *.

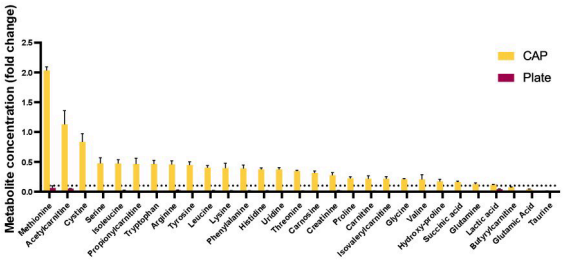

Fig. 3. The level of metabolites adsorbed onto calcium phosphate surfaces and culture plate surfaces. The levels were compared to intracellular metabolite levels and expressed as fold change. The group to compare was a 24-well culture plate (Purple color, material PS, surface treated), and for intracellular metabolite levels, average values for the materials group collected on day 1 were used. Metabolites with a high adsorption rate (a fold change greater than 0.1 compared to the intracellular results) were excluded from further analysis.

3.5. CaP material phase composition influence on cell metabolism

We used PCA and ANOVA to investigate if CaP phase composition influenced metabolite levels. No distinct clusters for CaP samples with various phase compositions were observed with PCA. (Fig. 4). With ANOVA, in all 3 days the residuals presented a normal distribution (Supplemental information, Fig. S3). To follow up on a potential correlation with hydroxyapatite content, we performed the pattern search between CaPs (Supplemental information, Fig. S5), i.e., correlate metabolite changes to HAP phase content (0, 58 %, 95 %, and 100 %). Although few metabolites were found to increase or decrease with the changes in HAp content, the correlation coefficients were too low to draw any conclusions.

3.6. CaP biomaterials influence cell metabolism

Glycolysis was the most significantly changed one from pathway enrichment analysis, followed by other energy metabolism pathways and gluconeogenesis fructose and mannose degradation (Fig. 5a). Statistical data analysis, including PCA and *t*-test, was performed to identify metabolites with significant changes induced by CaP bioceramics. PCA score plots revealed a close clustering of the CaP materials group and a substantial separation between the materials group and the control group (Fig. 5d). The metabolite levels at the earlier time point had significantly higher variation compared with the later time points, suggesting a more substantial distinction between CaPs and control groups at the initial phase of biomaterials exposure (Fig. 5c). Proline level was up to 5 times higher in CaP groups over all 3 time points. Notably, the reduction of any amino acid was not observed with CaP groups. On the other hand, levels for compounds involved in energy metabolism were significantly lower upon exposure to CaPs (Fig. 5b). For example, ATP levels in material groups were 4 times lower than the control groups (Fig. 5e). At the same time, levels of fructose 1,6-bisphosphate (FBP), a critical molecule in the glycolysis metabolic pathway, were 10 times reduced in cells exposed to CaPs (Fig. 5e).

3.7. Analysis of metabolism changes over time

Metabolism is a dynamic process. Therefore, we extracted metabolites at 3-time points to obtain data about temporal CaP's influence on cell metabolism. PCA score plot (Fig. 6a) showed a clear separation of material and control groups for all time points. However, the distance between the groups on the PC1 axis diminishes over time.

We found compounds of energy metabolism (G6P, F6P, FBP, and lactic acid) and nucleotides (ATP and ADP) significantly altered with prolonged CaP exposure time. The level of nucleobase adenosine was rapidly increased, whereas the taurine level was gradually reduced, and fold change compared to control decreased from 4 on day 1–1.2 times on day 3.

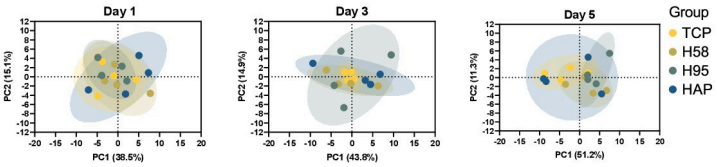

Fig. 4. PCA plots of all 4 types of CaPs on Day 1, Day 3, and Day 5.

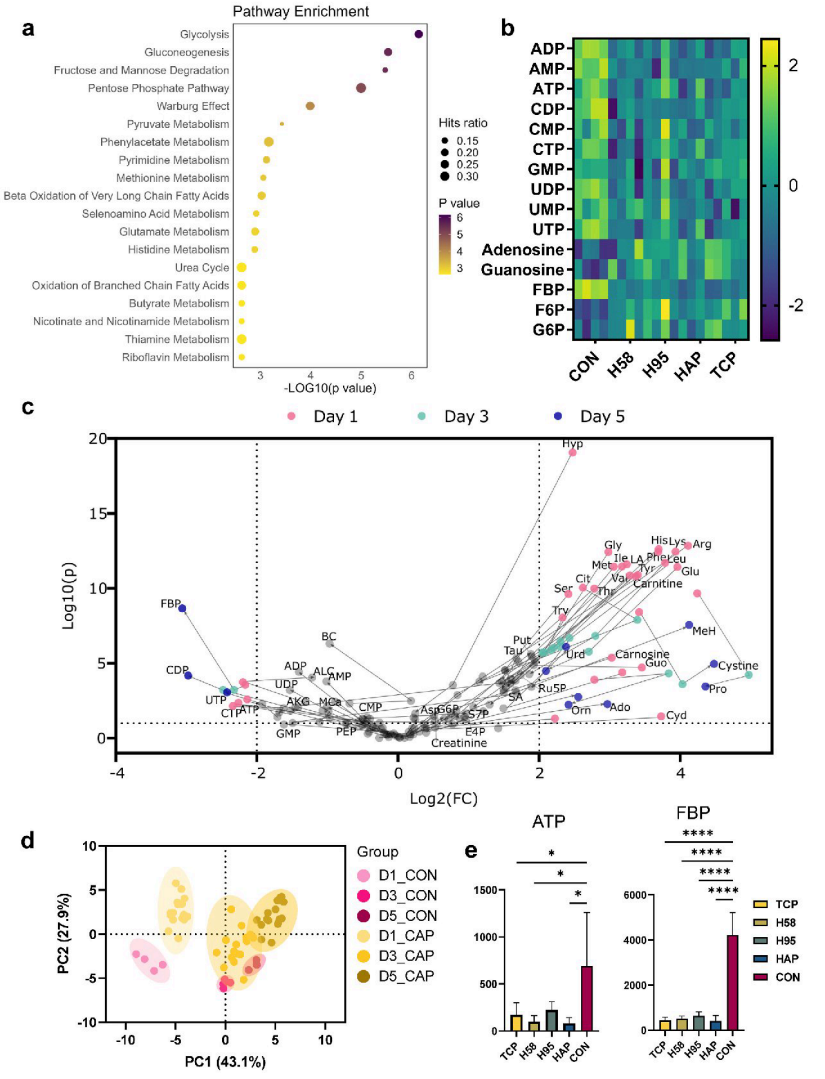

(caption on next page)

Fig. 5. a) Pathway enrichment analysis b) The heatmap of nucleotides and pentose phosphate pathway/glycolysis metabolites on day 1. c) The volcano plot of metabolites. Lines in the volcano plot link the significant metabolites on different days. The lines provided clues about the direction of changes and the metabolite's ability to distinguish between the material and control groups. Thresholds: log2 (fold change) > 2 or < -2, and -log10(p) > 1. Fold change was calculated from CON for each metabolite, fold change = (metabolite level in CaP)/(metabolite level in CON). d) PCA for all CaP and control groups from days 1, 3, and 5 (n = 4). e) The metabolite level of ATP and FBP from each group on day 1. *$P < 0.05$, & $P < 0.0001$ (n = 4).

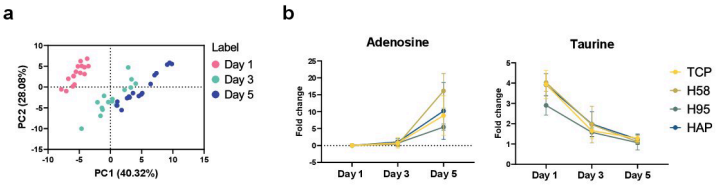

Fig. 6. a) The PCA plot scores of intracellular metabolites from material groups on days 1, 3, and 5. b) The fold changes of adenosine and taurine over time. n = 4.

The metabolic alteration caused by CaPs during the 3-time points was compound-specific. Some metabolites indicated a trend toward narrowing the disparities between CaP groups and control groups, approaching that of the control groups (Figs. 6b and 7). Among these, the difference in carbohydrate metabolism was more profound (Fig. 7). Levels of G6P and F6P initially were close to the control and increased over time. FBP was exhausted on the first day. Although FBP increased over time, the level was still lower than

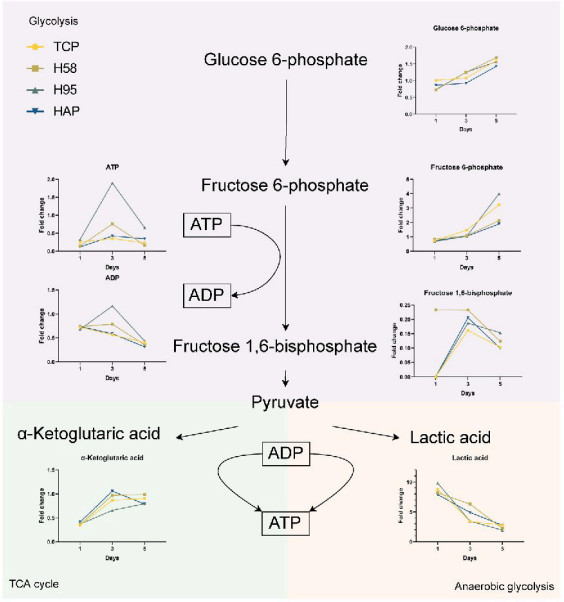

Fig. 7. The changes of metabolite levels in glucose metabolism.

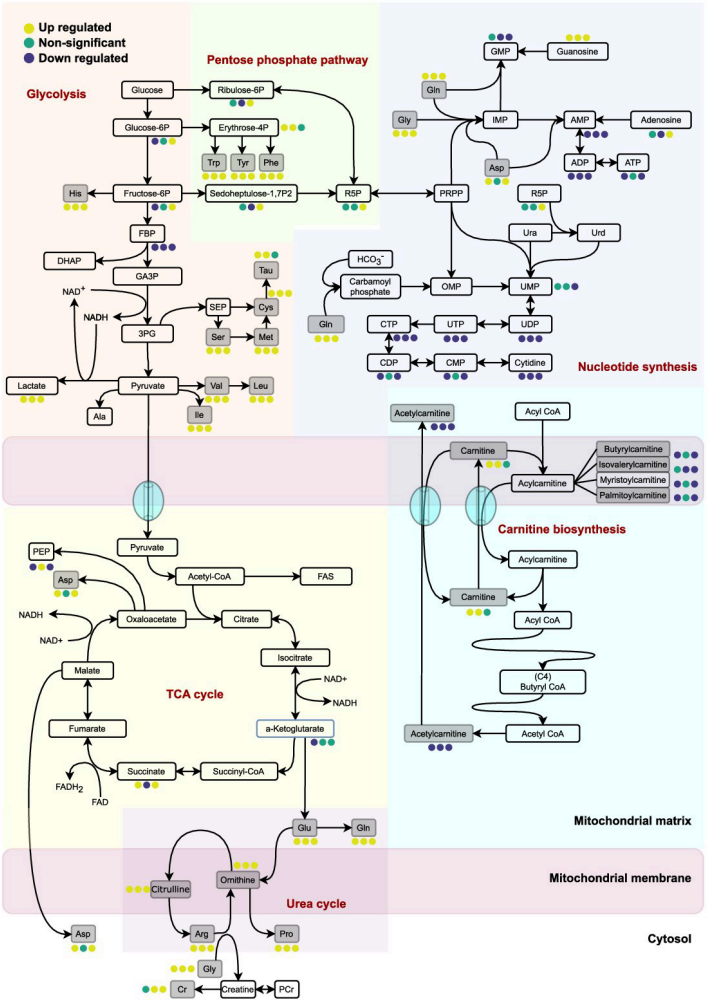

Fig. 8. The metabolic pathway map of detected metabolites. Metabolites were marked as up/down regulated or non-significant changes by color code. The covered pathways include glycolysis, the pentose phosphate pathway, nucleotide synthesis, the TCA cycle, carnitine biosynthesis, and the urea cycle.

the control. ATP had dynamic changes, and ADP slightly decreased over time. Also, on the first day, α-Ketoglutaric acid was about half the amount of the control, and lactic acid was 9 times higher than the control. Both of these subsequent metabolites were steadily approaching the control. α-Ketoglutaric acid, a key metabolite in the TCA cycle, was increasing, while lactic acid, a final product of anaerobic glycolysis, was decreasing (see Fig. 8).

4. Discussion

Despite the prevalent use of CaP-based biomaterials in clinical applications, their impact on cell metabolism remains understudied. We aimed to explore the cellular perturbations induced by calcium phosphates. In this study, we focused on three aspects: (I) metabolite adsorption on biomaterials, (II) biomaterial influence on cell metabolism, and (III) longitudinal changes in cell metabolism.

Metabolite adsorption on biomaterials is crucial in metabolism studies, as it can impact measured intracellular concentrations due to co-extraction with cellular metabolites. Adsorbed metabolites on material surfaces enhance their availability to cells, potentially modulating microenvironment and cellular functions. Our results showed an increased affinity of several compounds toward CaPs. Cystine is excessively adsorbed on CaP ceramics. Cystine is the oxidized and predominant form of cysteine in non-reducing environments, such as the extracellular space [18]. Our results suggest that the CaP ceramic surfaces provide a reducing extracellular environment to cells via the adsorption of oxidized metabolites. This aligns with numerous reports noting high cell viability on CaPs, suggesting that their physicochemical properties mitigate oxidative stress. Besides cysteine, other amino acids were adsorbed by CaPs. Notably, the amino acids with basic side chains (His, Lys, and Arg) adsorbed to CaPs at a higher level. The hydroxyl group from CaPs attracts the amino acids by interacting with the amino groups (Gln) or carboxy (Ser, Trp, and Tyr). Carnitine and its metabolites are also adsorbed on CaP surfaces utilizing similar interactions. Carnitine's function in cells is to transport fatty acids into the mitochondria, indicating that cells that come into contact with CaPs have altered energy metabolism [19]. Taurine, a sulfur amino acid with diverse biological functions, adsorbs on CaP surfaces by its amino group, and there was no trace of taurine on the culture plate surface. Taurine substantially impacts energy metabolisms [20]. The ability of biomaterials to adsorb small molecules can be utilized in future research to develop advanced biomaterials that modulate cellular phenotypes by altering the microenvironment.

Our results showed that the intracellular metabolite profiles did not significantly differ for materials with various CaP compositions. For decades, CaPs such as HAp and β-TCP have been employed in bone tissue repair, demonstrating satisfactory clinical performance [21]. While differences in properties like degradation rates are well-documented, the impact of these CaP materials on cell metabolism at the molecular level appears comparable. The differences between materials, such as degradation and hard tissue regeneration rates, are usually reported over several weeks [22]. Here, we exposed cells to CaPs for 5 days, which might not be sufficient to capture material composition-induced differences in cell metabolism. Therefore, for further data analysis, we merged results obtained from CaP groups and focused on the general perturbations caused by the material.

The results showed that CaP strongly influenced central carbon metabolism and interconnected pathways, including amino acid metabolism, glycolysis, tricarboxylic acid (TCA) cycle, and nucleotide metabolism. Intracellular amino acid levels were increased upon exposure to CaPs, including the amino acids not adsorbed on material surfaces: citrulline, aspartic acid, and ornithine. This hints that the exposure to CaPs provided the stimulus for increased amino acid biosynthesis. Arginine, hydroxyproline, and proline levels were significantly increased at all investigated time points. These amino acids are interconnected with numerous metabolism pathways [23].

A substantial disturbance of energy metabolism and higher energy consumption of the cells caused by CaPs was presumed. The levels of G6P and F6P, two intermediates of the glycolysis pathway formed in the first and second steps, respectively, were higher than the control. In contrast, the FBP, formed at the sixth step of glycolysis, was significantly downregulated by CaPs (Fig. 7.). The enzyme that catalyzes the irreversible conversion of F6P, phosphofructokinase-1 (PFK-1), is the rate-limiting enzyme of glycolysis [24]. The significant reduction of FBP indicates that glycolysis and the following energy metabolisms are extensively enhanced. As a result, the depletion of FBP could be a signature of CaP biomaterials instructing the energy metabolism switch. FBP can also indirectly alter lactic acid production by influencing glucose metabolism, especially glycolysis [25,26]. A low FBP and high lactic acid levels can result from increased glycolysis. Consequently, in pathway analysis, the most prominent alterations were observed in glycolysis, indicating a potential shift in glucose utilization for energy production. Moreover, the impact extended to various interconnected pathways, including amino acid metabolism, suggesting a broad-reaching effect on cellular functions. The perturbations observed in gluconeogenesis and fructose degradation pathways hint at alterations in carbohydrate utilization and the potential rerouting of these substrates within the metabolic network.

Amino acids and sugars are essential raw materials for the synthesis of nucleotides. For example, purine synthesis requires glycine, aspartic acid, and one-carbon units from amino acid metabolism [27]. Despite the high substrate level, CaPs significantly impair nucleotide synthesis, particularly the purine nucleotide cycle, as evidenced by a drastic reduction in the total amount of nucleotides, despite the precursor fructose 6-phosphate (F6P) being metabolized to ribose 5-phosphate via the pentose phosphate pathway [28–30].

The chemical composition of CaPs themselves modulates the cellular microenvironment by releasing calcium and phosphate ions and affecting cellular functions [31]. Low calcium concentrations have been reported to enhance cellular energy transduction, modulating three TCA cycle dehydrogenases (pyruvate, isocitrate, and α-ketoglutarate) [32]. Simultaneously, phosphate ions contribute phosphoryl groups for various cellular processes, where phosphorylation, a reversible reaction, regulates protein activity [33]. Oxidative phosphorylation in ATP synthesis involves phosphate group participation, aligning with the enhanced phosphorylation induced by CaP biomaterials. ATP and other nucleotides store and transfer chemical energy within the cell, vital for cell proliferation [34]. Our results showed that the nucleotide concentrations were significantly decreased. Activated cells with a high

phosphorylation level consume more energy, while energy metabolism was notably regulated because of the interaction with CaP. Depleted ATP and glycolytic metabolite levels indicated the metabolic impact on energy consumption and pathway regulation.

We noted diminishing metabolic disparities between CaP and the control group over time (Fig. 6a). This trend is particularly notable for lactic acid and acetylcarnitine levels (Fig. 6c). A shift in cellular energy utilization was evident across the 5 days. Initially, lactic acid levels were approximately ninefold higher than the control, decreasing by nearly half on day 5 (Fig. 7). Which indicates that early exposure to CaPs heightened anaerobic glycolysis. Simultaneously, the α-ketoglutaric acid level was reduced by half compared to the control level but reached near equivalence by day 5. The enzymatic production and reduction of α-ketoglutarate are irreversible, making it a valuable indicator of TCA cycle activity [35–37]. α-ketoglutarate decarboxylase is a rate-limiting step of the TCA cycle [32]. The depletion of α-ketoglutarate on the first day indicated a high energy consumption requirement from the TCA cycle suggesting that the cells are actively dividing and proliferating; this phenomenon suggests enhanced anaerobic glycolysis, typically observed when the TCA cycle cannot meet energy demands or under limited oxygen supply conditions.

The initial exposure to CaPs resulted in a shock pressure on the cellular energy metabolism response to biomaterials with stronger glycolysis, presented by more extensive variability in metabolite profiles. At a later time point, the metabolic alteration diminished, tending towards cellular homeostasis, which demonstrated the ability of cells to adapt to a new environment caused by CaP.

5. Conclusion

We demonstrated that calcium phosphates significantly influenced cell metabolism and the cellular microenvironment. These synthesized CaPs absorbed small molecules, particularly amino acids, affecting amino acid levels and energy pathways, notably glycolysis. Different HAp and β-TCP ratios in CaPs showed similar impacts on cell metabolism. Cells interacting with CaP surfaces displayed increased energy consumption due to heightened glycolysis and TCA cycle activity, gradually declining over time. These insights deepen our understanding of cell interactions with CaPs, shedding light on their clinical performance and opening new avenues for novel biomaterials capable of regulating metabolism.

6. Limitations of the study

This study's primary limitation lies in using fibroblasts as the model cell line instead of bone-specific cells like osteocytes or osteoblasts, which would be more relevant for bioceramic materials research. Using bone cells could yield a more clinically relevant understanding of the molecular mechanism alterations induced by biomaterial. Additionally, expanding the number of analyzed metabolites could enhance the depth of analysis.

CRediT authorship contribution statement

Jingzhi Fan: Writing – original draft, Investigation, Formal analysis, Data curation, Conceptualization. **Theresa Schiemer:** Writing – original draft, Methodology, Investigation, Formal analysis. **Vita Steinberga:** Methodology, Investigation. **Annija Vaska:** Methodology, Investigation, Formal analysis, Data curation. **Anastasija Metlova:** Methodology, Investigation, Data curation. **Antons Sizovs:** Supervision, Data curation, Conceptualization. **Janis Locs:** Supervision, Methodology, Funding acquisition. **Kristaps Klavins:** Writing – review & editing, Supervision, Project administration, Methodology, Conceptualization.

Ethics approval and consent to participate

The manuscript does not include experiments on animal or human subjects such that no ethical approval is needed.

Data availability statement

Data will be made available on request.

Declaration of competing interest

The authors declare that they have no known competing financial interests or personal relationships that could have appeared to influence the work reported in this paper.

Acknowledgment

The authors acknowledge financial support from the European Union' Horizon 2020 research and innovation program under the grant agreement No. 857287 (BBCE – Baltic Biomaterials Centre of Excellence) and the Ministry of Economics Republic of Latvia project "State research project in the field of biomedicine, medical technologies, and pharmacy," project No. VPP-EM-BIOMEDICĪNA-2022/1-0001. The authors also acknowledge the help of Vahid Jahedzomorrodi in this study.

Appendix A. Supplementary data

Supplementary data to this article can be found online at https://doi.org/10.1016/j.heliyon.2024.e39753.

References

[1] S.V. Dorozhkin, M. Epple, Biological and medical significance of calcium phosphates, Angew. Chem. Int. Ed. 41 (2002) 3130–3146, https://doi.org/10.1002/1521-3773(20020902)41:17<3130::AID-ANIE3130>3.0.CO;2-1.

[2] J. Fan, K. Abedi-Dorcheh, A.S. Vaziri, F. Kazemi-Aghdam, S. Rafieyan, M. Sohrabinejad, M. Ghorbani, F.R. Adib, Z. Ghasemi, K. Klavins, et al., A review of recent advances in natural polymer-based scaffolds for musculoskeletal tissue engineering, Polymers 14 (2022), https://doi.org/10.3390/polym14102097.

[3] J.M. Bouler, P. Pilet, O. Gauthier, E. Verron, Biphasic calcium phosphate ceramics for bone reconstruction: a review of biological response, Acta Biomater. 53 (2017) 1–12, https://doi.org/10.1016/j.actbio.2017.01.076.

[4] M. Prakasam, J. Locs, K. Salma-Ancane, D. Loca, A. Largeteau, L. Berzina-Cimdina, Fabrication, properties and applications of dense hydroxyapatite: a review, J. Funct. Biomater. 6 (2015) 1099–1140, https://doi.org/10.3390/jfb6041099.

[5] S.J. Kalita, A. Bhardwaj, H.A. Bhatt, Nanocrystalline calcium phosphate ceramics in biomedical engineering, Mater. Sci. Eng. C 27 (2007) 441–449, https://doi.org/10.1016/j.msec.2006.05.018.

[6] P. Humbert, M. Brennan, N. Davison, P. Rosset, V. Trichet, F. Blanchard, P. Layrolle, Immune modulation by transplanted calcium phosphate biomaterials and human mesenchymal stromal cells in bone regeneration, Front. Immunol. 10 (2019) 1–15, https://doi.org/10.3389/fimmu.2019.00663.

[7] M. Ermis, E. Antmen, V. Hasirci, Micro and Nanofabrication methods to control cell-substrate interactions and cell behavior: a review from the tissue engineering perspective, Bioact. Mater. 3 (2018) 355–369, https://doi.org/10.1016/j.bioactmat.2018.05.005.

[8] I. Elia, M.C. Haigis, Metabolites and the tumour microenvironment: from cellular mechanisms to systemic metabolism, Nat. Metab. 3 (2021) 21–32, https://doi.org/10.1038/s42255-020-00317-z.

[9] P. Romani, L. Valcarcel-Jimenez, C. Frezza, S. Dupont, Crosstalk between mechanotransduction and metabolism, Nat. Rev. Mol. Cell Biol. 22 (2021) 22–38, https://doi.org/10.1038/s41580-020-00306-w.

[10] J. Fan, V. Jahed, K. Klavins, Metabolomics in bone research, Metabolites 11 (2021), https://doi.org/10.3390/metabo11070434.

[11] J.L. Ren, A.H. Zhang, L. Kong, X.J. Wang, Advances in mass spectrometry-based metabolomics for investigation of metabolites, RSC Adv. 8 (2018) 22335–22350, https://doi.org/10.1039/c8ra01574k.

[12] X.W. Zhang, Q.H. Li, Z. Di Xu, J.J. Dou, Mass spectrometry-based metabolomics in health and medical science: a systematic review, RSC Adv. 10 (2020) 3092–3104, https://doi.org/10.1039/c9ra08985c.

[13] D.S. Wishart, Emerging applications of metabolomics in drug discovery and precision medicine, Nat. Rev. Drug Discov. 15 (2016) 473–484, https://doi.org/10.1038/nrd.2016.32.

[14] M. Ebrahimi, M.G. Botelho, S.V. Dorozhkin, Biphasic calcium phosphates bioceramics (HA/TCP): concept, physicochemical properties and the impact of standardization of study protocols in biomaterials research, Mater. Sci. Eng. C 71 (2017) 1293–1312, https://doi.org/10.1016/j.msec.2016.11.039.

[15] R.T. Hannan, S.M. Peirce, T.H. Barker, Fibroblasts: diverse cells critical to biomaterials integration, ACS Biomater. Sci. Eng. 4 (2018) 1223–1232, https://doi.org/10.1021/acsbiomaterials.7b00244.

[16] M. Sokolova, A. Putnins, I. Kreicbergs, J. Locs, Scale-up of wet precipitation calcium phosphate synthesis, Key Eng. Mater. 604 (2014) 216–219, https://doi.org/10.4028/www.scientific.net/KEM.604.216.

[17] Z. Pang, G. Zhou, J. Ewald, L. Chang, O. Hacariz, N. Basu, J. Xia, Using MetaboAnalyst 5.0 for LC–HRMS spectra processing, multi-omics integration and covariate adjustment of global metabolomics data, Nat. Protoc. 17 (2022) 1735–1761, https://doi.org/10.1038/s41596-022-00710-w.

[18] A. Banjac, T. Perisic, H. Sato, A. Seiler, S. Bannai, N. Weiss, P. Kölle, K. Tschoep, R.D. Issels, P.T. Daniel, et al., The cystine/cysteine cycle: a redox cycle regulating susceptibility versus resistance to cell death, Oncogene 27 (2008) 1618–1628, https://doi.org/10.1038/sj.onc.1210796.

[19] L.Y. Li, S.M. Limbu, Q. Ma, L.Q. Chen, M.L. Zhang, Z.Y. Du, The metabolic regulation of dietary L-carnitine in aquaculture nutrition: present status and future research strategies, Rev. Aquacult. 11 (2019) 1228–1257, https://doi.org/10.1111/raq.12289.

[20] C. Wen, F. Li, L. Zhang, Y. Duan, Q. Guo, W. Wang, S. He, J. Li, Y. Yin, Taurine is involved in energy metabolism in muscles, adipose tissue, and the liver, Mol. Nutr. Food Res. 63 (2019) 1–11, https://doi.org/10.1002/mnfr.201800536.

[21] C.W. Cheah, N.M. Al-Namnam, M.N. Lau, G.S. Lim, R. Raman, P. Fairbairn, W.C. Ngeow, Synthetic material for bone, periodontal, and dental tissue regeneration: where are we now, and where are we heading next? Materials 14 (20) (2021) 6123, https://doi.org/10.3390/ma14206123.

[22] Pamela Habibovic, Moyo C. Kruyt, Maria V. Juhl, Stuart Clyens, Roberta Martinetti, Laura Dolcini, Naseem Theilgaard, Clemens A. van Blitterswijk, Comparative in vivo study of six hydroxyapatite-based bone graft substitutes, J. Orthop. Res. 26 (2008) 1363–1370, https://doi.org/10.1002/jor.20648.

[23] S. Hu, W. He, G. Wu, Hydroxyproline in animal metabolism, nutrition, and cell signaling, Amino Acids 54 (2022) 513–528, https://doi.org/10.1007/s00726-021-03056-x.

[24] J. Zuo, J. Tang, M. Lu, Z. Zhou, Y. Li, H. Tian, E. Liu, B. Gao, T. Liu, P. Shao, Glycolysis rate-limiting enzymes: novel potential regulators of rheumatoid arthritis pathogenesis, Front. Immunol. 12 (2021) 1–17, https://doi.org/10.3389/fimmu.2021.779787.

[25] J.A. Kelleher, P.H. Chan, T.Y.Y. Chan, G.A. Gregory, Energy metabolism in hypoxic astrocytes: protective mechanism of fructose-1,6-bisphosphate, Neurochem. Res. 20 (1995) 785–792, https://doi.org/10.1007/BF00969690.

[26] H. Li, J. Wang, H. Xu, R. Xing, Y. Pan, W. Li, J. Cui, H. Zhang, Y. Lu, Decreased fructose-1,6-bisphosphatase-2 expression promotes glycolysis and growth in gastric cancer cells, Mol. Cancer 12 (2013) 1–12, https://doi.org/10.1186/1476-4598-12-110.

[27] M.A. Razak, P.S. Begum, B. Viswanath, S. Rajagopal, Multifarious beneficial effect of nonessential amino acid, Glycine: a review, Oxid. Med. Cell. Longev. (2017), https://doi.org/10.1155/2017/1716701.

[28] E. Cheung, V. Olin-sandoval, N. Grüning, The return of metabolism: biochemistry and physiology of the pentose phosphate pathway, Biol. Rev. Camb. Phil. Soc. 90 (2015) 927–963, https://doi.org/10.1111/brv.12140.The.

[29] M.H. Soflaee, R. Kesavan, U. Sahu, A. Tasdogan, E. Villa, Z. Djabari, F. Cai, D.H. Tran, H.S. Vu, E.S. Ali, et al., Purine nucleotide depletion prompts cell migration by stimulating the serine synthesis pathway, Nat. Commun. 13 (2022) 1–14, https://doi.org/10.1038/s41467-022-30362-z.

[30] P.L. Ipata, R. Pesi, Metabolic interaction between purine nucleotide cycle and oxypurine cycle during skeletal muscle contraction of different intensities: a biochemical reappraisal, Metabolomics 14 (2018), https://doi.org/10.1007/s11306-018-1341-0, 0.

[31] D. Xu, Y. Wan, Z. Li, C. Wang, Q. Zou, C. Du, Y. Wang, Tailorable hierarchical structures of biomimetic hydroxyapatite micro/nanoparticles promoting endocytosis and osteogenic differentiation of stem cells, Biomater. Sci. 8 (2020) 3286–3300, https://doi.org/10.1039/d0bm00443j.

[32] G.E. Hansen, G.E. Gibson, The α-ketoglutarate dehydrogenase complex as a hub of plasticity in neurodegeneration and regeneration, Int. J. Mol. Sci. 23 (2022), https://doi.org/10.3390/ijms232012403.

[33] L. Zhang, Y. Yao, S. Zhang, Y. Liu, H. Guo, M. Ahmed, T. Bell, H. Zhang, G. Han, E. Lorence, et al., Metabolic reprogramming toward oxidative phosphorylation identifies a therapeutic target for mantle cell lymphoma, Sci. Transl. Med. 11 (2019) 1–17, https://doi.org/10.1126/scitranslmed.aau1167.

[34] M.P. Pandey, S. Sasidharan, V.A. Raghunathan, H. Khandelia, Molecular mechanism of hydrotropic properties of GTP and ATP, J. Phys. Chem. B (2022), https://doi.org/10.1021/acs.jpcb.2c06077.

[35] R.T. Stubbs, M. Yadav, R. Krishnamurthy, G. Springsteen, A plausible metal-free ancestral analogue of the Krebs cycle composed entirely of α-ketoacids, Nat. Chem. 12 (2020) 1016–1022, https://doi.org/10.1038/s41557-020-00560-7.
[36] B. Zdzisińska, A. Żurek, M. Kandefer-Szerszeń, Alpha-ketoglutarate as a molecule with pleiotropic activity: well-known and novel possibilities of therapeutic use, Arch. Immunol. Ther. Exp. 65 (2017) 21–36, https://doi.org/10.1007/s00005-016-0406-x.
[37] I. Martínez-Reyes, N.S. Chandel, Mitochondrial TCA cycle metabolites control physiology and disease, Nat. Commun. 11 (2020) 1–11, https://doi.org/10.1038/s41467-019-13668-3.

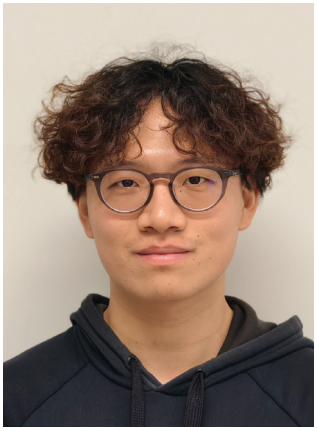

Jingzhi Fan dzimis 1995. gadā Ķīnā, Liaoninas provincē. Pekinas Ķīmijas tehnoloģijas universitātē ieguvis bakalaura grādu biomateriālos (2018), Dublinas Universitātes koledžā – maģistra grādu materiālzinātnē un inženierzinātnē (2019). Kopš 2020. gada studē Rīgas Tehniskās universitātes (RTU) doktorantūrā. 2021. gadā bijis *AO Research Institute Davos* viespētnieks. Patlaban ir RTU zinātniskais asistents. Pētniecības intereses saistītas ar biomedicīnas inženieriju un vielmaiņu.

Jingzhi Fan was born in 1995 in Liaoning, China. He obtained his Bachelor's degree in Biomaterials (2018) from Beijing University of Chemical Technology and a Master's degree in Materials Science and Engineering (2019) from University College Dublin. Since 2020, he has been a PhD student at Riga Technical University. In 2021, he was a visiting researcher at AO Research Institute Davos. He is currently a research assistant at Riga Technical University. His research interests are biomedical engineering and metabolism.